HYDRODYNAMIC CHARACTERISTICS OF A PLATE HEAT EXCHANGER

A Thesis Submitted

by

Abdul-Fattah Muhammad-Ali Fattah

for the degree of

Doctor of Philosophy

Department of Chemical Engineering,
The University of Aston in Birmingham

November, 1975

SUMMARY

This thesis describes a detailed investigation of the hydrodynamic characteristics of a commercially available three-dimensional plate heat exchanger. The literature on this topic was found to be scarce and misleading due, partly, to the problems inherent in experimentations with packs of plates and, partly, to the marked lack of a common basis for terminology. Because of the complex flow geometry of this type of heat exchanger, a large majority of work previously published has been carried out with packs of plates and an empirical approach has been adopted. However, a thorough understanding of fluid behaviour in the channels between plates is a prerequisite, prior to any meaningful heat transfer studies, in order to ultimately establish a generally acceptable design method for plate heat exchangers.

A model channel was developed to eliminate all the difficulties encountered in investigations of plate packs in addition to facilitating flow visualisation and pressure drop measurements of selected sections. The breakthrough was achieved by producing, for the first time, transparent plastic replicas of metal plates.

Four different channels were examined to establish the basic flow characteristics and the effects of the entrance, heat transfer section, and exit on the hydrodynamics. Special attention was paid to the effect of contact between the plates. Five different fluids were employed with viscosities ranging from one to about sixteen centipoises (at 20°C) and the overall Reynolds number range covered was between three and five thousand. The nature of this study necessitated an extensive examination of problems associated with existing and unconventional techniques

for accurately measuring small liquid differential pressures.

It was found that the basic resistance coefficient-Reynolds number interaction in this type of geometry is very similar to that between the drag coefficient and Reynolds number relevant to a disc with the flat side perpendicular to the direction of flow. Such an interaction has never been reported before. It was also found that, contrary to previous beliefs, a significant part of the pressure drop is unproductively lost in the port regions. The contributions of the heat transfer section and the two port regions to the channel total pressure drop were found to be dependent on the Reynolds number. The physical contact between the channel plates was found to be a major factor, influencing every aspect of the hydrodynamic characteristics. Severance of this contact would result in rapid fall-off in performance, especially in the transition and turbulent regions.

Owing to the basic nature of this work, the extensive programme of experimentation has resulted in a large amount of data, full account of which is given to augment and facilitate comparisons by future workers in this field of research.

ACKNOWLEDGEMENTS

The author wishes to express his profound appreciation and sincere gratitude to Mr.A.F.Price, the supervisor, for his help, encouragement, and assistance in surmounting all the difficulties throughout this research project from its initiation to completion and for critical review of the manuscript.

The author also wishes to thank Dr.B.Gay, the adviser, for guidance and constructive criticism.

Recognition is due to the following persons:

Professor G.V.Jeffreys, Head of Department, for providing the research facilities.

Dr.D.A.L.Wilson, of the Department of Mathematics, for his assistance in analysis of the data.

Mr.J.Kemp, of the Plastic Technology Laboratory, Department of Chemistry, for his assistance in early attempts to produce plastic plates.

Mr.F.A.Roberts, of the Departmental Workshop, for his assistance with the experimental equipment.

The author also acknowledges the assistance made available by the APV Co.Ltd. during the course of this work.

NOMENCLATURE

A	=	heat transfer area	m^2
A'	=	constant in equation (2.22)	—
B	=	constant in equation (2.22)	—
b	=	mean plate gap	m
Cp	=	specific heat	$J/Kg°C$
De	=	equivalent diameter	m
Eu	=	Euler number ($= \Delta P/\rho u^2$)	—
f	=	friction factor or resistance coefficient ($= \Delta P\ De/2\rho u^2 L$)	—
K	=	overall heat transfer coefficient	$W/m^2 °C$
K_c	=	coefficient of loss of head at inlet of channels, equation (2.29)	—
K_e	=	coefficient of loss of head at exit of channels	—
L	=	plate (channel) length	m
M	=	mass flow rate	Kg/s
ΔP	=	differential pressure (pressure drop)	N/m^2
q	=	volumetric flow rate	m^3/s
Re	=	Reynolds number ($= \rho\ De\ u/\mu$)	—
S_a	=	area of flow, equation (2.28)	m^2
Δt	=	temperature change	°C
$\Delta T_{\ell m}$	=	log mean temperature difference	°C
u	=	velocity	m/s
V_a	=	channel volume in equations (2.27) and (2.28)	m^3
W	=	plate width available for flow	m

Subscripts:

en	=	entrance
ex	=	exit

r	=	ribbed (heat transfer) section	
t	=	channel total (ribbed section + two port regions)	
a	=	air (equation (2.29)	

Greek:

α	=	film heat transfer coefficient	$W/m^2\,°C$
Γ	=	dimensionless parameter, equation (2.34)	—
θ	=	number of heat transfer units	—
λ	=	resistance coefficient ($\equiv 4f$), equations (2.35)-(2.38)	—
μ	=	dynamic viscosity	Ns/m^2
ξ	=	resistance coefficient ($\equiv \lambda \equiv 4f$), equations (2.29)-(2.32)	—
ρ	=	density	Kg/m^3
σ	=	ratio of channel flow area to pipe cross sectional area, equation (2.29)	—
ϕ	=	ratio of developed to projected area	—
ψ	=	angle between corrugations on adjacent plates, Fig.3.3	deg.or rad.

CONTENTS

LIST OF FIGURES

LIST OF TABLES

C H A P T E R 1

INTRODUCTION

1.1) GENERAL DESCRIPTION OF PLATE HEAT EXCHANGERS

The plate heat exchanger (PHE) was known and used originally extensively by food industries having rigorous hygienic requirements as in the dairy and brewing industries. There has been, however, an increasing use of the PHE in the chemical processing industries during the last 15 years.

The PHE is a simple heat transfer apparatus resembling a plate-and-frame filter press and is assembled from a number of parallel, generally identical, corrugated metal plates aligned top and bottom between horizontal carrier bars. The plates, gasketted around the edge, are clamped together between a stationary rigid head and a movable rigid follower, riding on the carrying bars, using either bolts or a compression device. Each pair of clamped plates therefore forms one channel through which one fluid flows while the second fluid flows through the two adjacent channels. The fluids are thus separated by the thin plate, pressed from metal sheet, so that there are four corner ports, one pair for each of the two fluid media. These ports are open or blind according to need. The plates are sealed at their outer edges and around the ports by elastomeric gaskets. This peripheral and port gasketting is so arranged that in addition to separating the plates it divides the plate pack into two separate systems of channels where the heating and cooling media flow in alternate interplate spaces. A double sealing system forming pockets open to the atmosphere prevents mixing of the two fluids in the event of a leakage past a gasket in the vicinity of the ports. The fluids enter and leave the exchanger by means of connections situated at the corners of the head and/or follower, which lead to the passages or manifolds formed by the plates corner ports. All wetted parts are accessible for inspection by removing the clamping bolts and rolling back the

movable cover.

By suitable blanking or unblanking of the corner ports, the plates can be easily and quickly arranged to give any number and size of pass arrangement for either of the two fluids. Three or more separate fluid streams can be accommodated in the plate pack by including intermediate separating/connecting plates so that multiple duties such as heating, cooling and recuperation can all take place in a single frame, e.g. in the sterilisation of gelatine[25]. Frames are usually free standing or, for smaller units, they are attached to structural steel work or wall mounted.

1.2) PLATE ARRANGEMENTS

1.2.1) LOOPED FLOW

In this arrangement each fluid divides into n streams and reunites after one pass through the exchanger, one fluid flowing in the upward direction, and the other fluid flowing downwards through the other n channels. This simple single pass counter-current flow arrangement could take one of two possible forms known as the "U" and "Z" arrangements. They are illustrated diagrammatically in Fig. 1.1 . In the U arrangement the inlet and outlet ports for the two fluid streams are on the same end of the pack; in the Z arrangement they are on opposite ends. It is also possible to have one fluid in the Z arrangement and the other in the U arrangement, in the same pack, in which case there will be three connections on one end cover and one connection on the other.

1.2.2) SERIES FLOW

In series flow, both fluids flow continuously through the exchanger with a change in direction after each pass, i.e. the total bulk of each fluid flows through the exchanger n times,

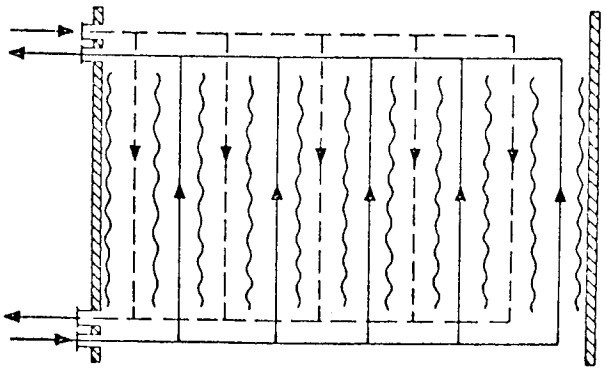

U arrangement

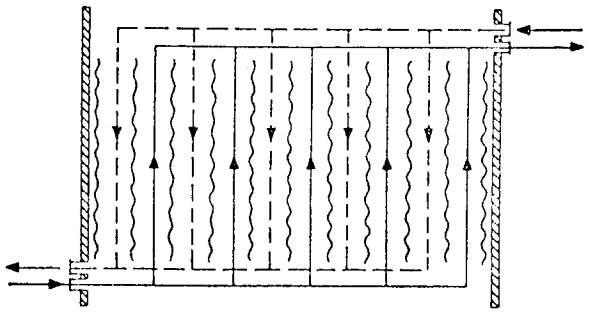

Z arrangement

Fig. 1.1 -*Single pass-flow arrangements*

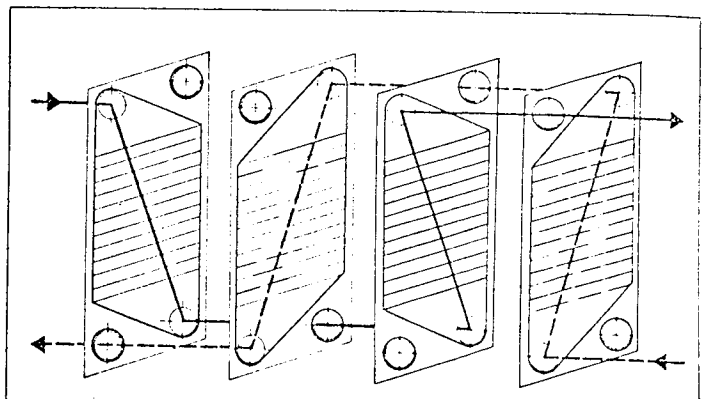

Fig. 1.2 - Series Flow

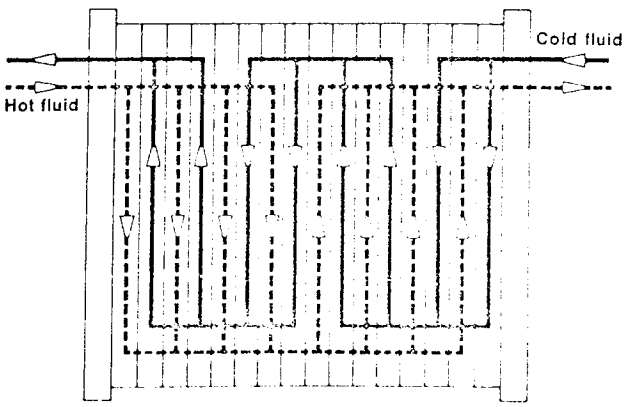

Fig. 1.3 – Complex Flow

n/2 times in an upward direction, and n/2 times in a downward direction, where n = (N-1)/2 (N is the total number of plates in the pack).

This plate arrangement is demonstrated in Fig. 1.2 . Fluid connections are required on both the head and follower in this case as could be deduced from inspection of the diagram.

1.2.3) COMPLEX FLOW

Complex flow arrangements consist of various combinations of looped and series flow arrangements. One arrangement is shown in Fig. 1.3 . The cold fluid is moving through the exchanger in 4 passes with 2 channels per pass; the hot fluid in 2 passes with 4 channels per pass. Complex flow arrangements, like series flow, requires fluid connections on both the stationary and movable covers.

1.2.4) PRACTICAL CONSIDERATIONS

Looped flow arrangement is used wherever possible because of the following reasons:

(a) In both series and complex flow arrangements some of the fluid pressure is being used to bring about flow reversal between the passes instead of using it to enhance heat transfer. Clearly, fewer passes means less pressure is lost in this respect and the pressure is used more effectively. With single pass operation no pressure will be wasted on flow reversal.

(b) Only looped flow arrangement offers counter-current condition between the two media throughout the plate pack as could be seen in Fig. 1.1 . Hence, this arrangement is more thermally efficient than the series or complex ones in which partial co-current conditions exist, bringing about sometimes substantial log mean temperature difference (LMTD) correction factor. Cooper[17] reports that with single pass operation, this factor is about 1

(b) contd.

except for plate packs of less than 20 plates when the end effect has a significant bearing on the calculation[5]. This is due to the fact that the channel at either end of the plate pack only transfers heat from one side and therefore the heat load is reduced. When the plate unit is arranged for multiple pass use, a further correction factor must be applied depending on the degree of parallel-flow and hence will cause an increase in the required heat transfer area.

(c) It has already been pointed out that in the single-pass U arrangement all fluid connections are on the same end cover. With all connections on the stationary cover, rather than the follower, connections do not have to be broken to move back the follower to give access to the plates when the exchanger is opened for inspection and/or cleaning or even extension. Cattell[14] explains that in the industrial market where flowrates are high, pipework diameters are large (25 cm diameter is not unusual) and it is therefore a difficult task to dismantle pipework from the follower of a PHE at the annual shutdown for inspection.

In spite of the aforementioned arguments it is sometimes necessary to select multiple/unequal passes such as when the thermal duty cannot be achieved in single pass or when unequal flow conditions are handled, i.e. high and low flow rates. In the latter case the required velocities can only be maintained with the low fluid flow rate by using an increased number of passes. Even though the plate unit is more efficient when the number of passes are equal because of the limited degree of parallel-flow or when the flow ratio between the two fluids is in the range 0.7-1.4, other flow ratios can be accommodated in unequal passes. This is achieved however, at the

expense of the LMTD factor[17].

1.3) THE PLATES

The gasketted plate is the basic heat transfer element in a PHE as against a tube in the tubular heat exchanger. It utilises the cheapest form of material supply, i.e. sheet, and to regain the strength lost in changing from tube to flat sheet, pressed corrugations are used. The tube is the best shape of flow conduit for withstanding pressure but it is entirely the wrong shape for optimum heat transfer performance since it has the smallest surface area per unit of cross sectional flow area.

1.3.1) EMBOSSING

The detailed configuration pressed into the plates produces the required characteristics by fulfilling the following functions:-

(a) The provision of a number of support points of contact with the adjacent plate in order to maintain the relative spacing by preventing deflection under the differential pressure that can exist between the two fluid media.

(b) To induce turbulence at low Reynolds numbers in both process fluids flowing in thin streams between the plates by imposing continual changes in velocity and direction on the fluids. This brings all parts of both media into repeated contact with the heat transfer surfaces, giving rise to high heat transfer coefficients to meet the required heat transfer and pressure drop characteristics.

(c) Boosting thermal performance by increasing the effective plate heat transfer area relative to a flat plate.

(d) The corrugations serve to increase the mechanical strength of the plate and reduce the metal sheet thickness needed, thereby

(d) contd.

saving material costs and minimising thermal resistance of the plate itself.

There are two basic forms of pressed plate:-

(1) The first, referred to as the "pipped" or "intermating trough" type consists of a number of fairly deep parallel corrugations, running transverse to the average direction of flow, which intermate with the corresponding ones on adjacent plates. These troughs carry pips or depressions at their crest which contact corresponding pips on troughs on adjacent plates thereby controlling the flow gap between the plates. The channels formed by such plates are two-dimensional and the plates themselves are described as having two-dimensional trough form. This type of plate is typical of the older generation of hygienic design where contact between adjacent plates is relatively infrequent (about every 6.452 cm^2 to 19.355 cm^2 of heat transfer area[5]) and the pressed shape consists of large scale lateral corrugations.

The majority of work reported in the literature has been concerned with plates of this design.

(2) The second and more recent type is based on relatively shallower and narrower series of parallel undulations which are inclined to the vertical axis of the plate. These corrugations are complementary to the corrugations on adjacent plates, i.e. with successive plates forming mirror images; thus, when the plates are clamped together, the peaks of the corrugations of one plate contact the peaks on the next plate; peaks which constitute valleys in the adjacent channel. In other words, the corrugations cross one another, instead of intermating, giving a high density of contact points between plates (for every 1.290 cm^2 to 6.452 cm^2 of heat transfer area[5]), a major advantage of this form. This type of plate is, therefore, self-supporting and

(2) contd.

the resulting lattice pattern of mutual support points brace the pack and allow thinner gauge plates to be used. Cattell[14] points out that the shallow, smooth pressed shape is easily pressable into the major corrosion resistant metals. Channels formed by these cross-corrugated plates are three-dimensional, their relatively complex geometry giving rise to higher levels of induced turbulence and higher heat transfer coefficients. The plates themselves are also referred to as three-dimensional trough form.

By far the most widely used of the three-dimensional trough form designs is the so-called "herringbone" or "chevron" plate which has been very successful for industrial applications and is the subject of this work.

1.3.2) THERMAL AND HYDRODYNAMIC INTERACTION

The performance of a heat exchange module may conveniently be expressed as the relationship between the number of heat transfer units θ, pressure drop, and flow rate. θ is the ratio of temperature change (duty to be achieved Δt) to effective mean temperature difference (driving force available $\Delta T_{\ell m}$):

$$\theta = \Delta t / \Delta T_{\ell m} \qquad (1.1)$$

this is a dimensionless quantity referred to also as thermal length and its value, clearly depends on the temperature programme only. θ serves to establish the character of a given heat exchange duty, since duties involving the same flow rates and θ values will be performed by similar exchangers, even though the actual temperature programmes may be very different.

Equation (1.1) could also be expressed as:

$$\theta = KA/\rho q C_p \qquad (1.2)$$

since $$KA\ \Delta T_{\ell m} = \rho q C_p \Delta t \qquad (1.3)$$

If the heat exchange module, through which a fluid is flowing, has fixed dimensions i.e. it represents a fixed area of heat transfer surface, there will within the module be developed a heat transfer coefficient α and a pressure drop. These will each be different functions of the flow rate. The following relationships are valid:

$$\alpha = \text{const. } q^m \qquad (1.4)$$

$$\Delta P = \text{const. } q^n \qquad (1.5)$$

the values of m and n in the above equations depend on the physical properties of the fluid, the geometrical characteristics of the module, and the nature of flow. Ahlstrom and Rylander[1] report that for PHE's (water/water, turbulent flow) typical values of m are 0.6-0.8 and for n 1.75-1.95.

Equation (1.3) could be rearranged as:

$$A = \rho\ C_p \left(\frac{q}{K}\right) \left(\frac{\Delta t}{\Delta T_{\ell m}}\right) \qquad (1.6)$$

now **A** is constant because the module has fixed dimensions. On the right-hand side of equation (1.6), if the heat load $\Delta T_{\ell m}$ remains constant, then the remaining interacting variables would be q, K, and Δt and the quantity $\left[\left(\frac{q}{K}\right) \Delta t\right]$ must be constant. For this purpose of investigating general effects, the overall heat transfer coefficient K is assumed to be related directly to the film heat transfer coefficient α since the metal wall of a heat exchanger plate is thin and the metal resistance low.

As q increases then α, and therefore K, will increase more slowly according to equation (1.4) because index m is less than one. Hence, the ratio $\left(\frac{q}{K}\right)$ will increase and in order that $\left[\left(\frac{q}{K}\right) \Delta t\right]$ remains constant then Δt must become smaller. Thus q is inversely related to Δt and from equation (1.1) it becomes evident that q is

inversely related to θ. This fact could also be established from equation (1.2) since q increases faster than K. Because pressure drop is a function of flow according to equation (1.5) and that index n is greater than one, the conclusion is that θ is more inversely related to ΔP. The final conclusion is that the heat exchange module considered will have a definite and fixed θ-ΔP relationship for any given fluid.

For a specific heat exchanger plate, as the liquid flow over the plate decreases the θ value increases and the maximum occurs at the lowest practicable plate flow below which air will not be completely removed from the plate channel accommodating downward flow. To avoid this situation the plate flow rate should correspond to a pressure drop which is not less than the static head between the ports of the plate. The minimum θ value attainable within a single pass will be determined by the maximum allowable pressure drop. Usher[36] points out that in general a 16-fold increase in pressure drop will halve the θ value. It is then only possible to operate within this range, or in whole number multiples of the range as the number of passes and hence heat transfer area increases.

Individual heat exchanger plates may differ widely in their θ-ΔP relationships according to the type of duty for which they are designed. This variation is not in the context of the aforementioned interaction between θ and ΔP in one specific plate, rather it is in the values and ranges of these two variables attained by different plate designs. Plates designed for high θ values are, by virtue of the trough pattern adopted, more suitable for higher pressure drops than low θ plates. Hence as a general rule, when considering different plate designs, high θ means high pressure drop and low θ, low pressure drop. Therefore, the low θ plate requires a restricted degree of artificial turbulence which calls for a relatively small number of wide-angle corrugations spaced fairly wide

apart, i.e. the two-dimensional design discussed in Section 1.3.1. A plate pack of low θ plates results in a unit suitable for high flows and small temperature change or duties where the temperature gradient is high and thus the exchanger is chosen for minimum pressure drop. Furthermore, because PHE's are easily arranged for complex (multipass) flow, a plate design with a low θ value will give the greatest degree of flexibility of pass arrangement in covering a wide range of θ duties.

Plates giving high θ values will call for a high degree of induced turbulence and this will require smaller, more closely pitched troughs, i.e. the three-dimensional design described in Section 1.3.1. Industrial duties call for single-pass arrangements where a plate of high thermal performance can be used to minimise the surface area required. Jones and Usher[25] point out that this requirement is most effectively achieved by the inclined cross-over trough pattern which gives a much greater number of changes of direction of liquid velocity than the plates pressed with the 2-dimensional transverse intermating troughs. Clark[15] indicates that high θ plates result in a unit suitable for heavy thermal duties, i.e. medium flow rate with large temperature change, typically heating from 30 to 90°C. Such units are also chosen for duties where the effective mean temperature differences are small.

1.4) DESIGN DIFFICULTIES

Unlike shell-and-tube heat exchangers, PHE plates are not custom built, as each type of plate is a standard, mass produced, mechanical pressing involving large capital expenditure in press tools. It is, therefore, important that each standard design is carefully specified so that its performance characteristics have the widest possible market potential[25]. As a result plates are produced in a limited number of standard designs.

Different thermal duties have different θ values. Each θ value requires a matching type of plate. Of course a specific plate design will attain different θ values with different fluids, e.g. a plate which gives a θ value of 2.0 on water would have a much lower value, about 0.6, when say cooling a mineral oil[15]. However, once a plate form for use in a PHE has been established, it is comparable to a fixed dimension heat exchange module, e.g. a tube of fixed diameter and length in a tubular heat exchanger, and therefore has one specific θ-ΔP relationship with practical limitations to these variables for any given fluid. The engineer designing a tubular heat exchanger is not limited to a tube of fixed diameter and length, he can instead select the nearest standard length and diameter to satisfy the heat transfer and pressure drop requirement of the duty considered. Obviously, the shell side presents more problems but these can be managed by suitable baffle systems. From this can be seen one of the difficulties encountered when rating PHE's, since it will be only occasionally that a plate design will be fully compatible with both the θ value required to perform a duty and the pressure drop available to perform it[6]. The result will be that many of the requirements cannot be met satisfactorily, i.e. either an excessive θ value is developed meaning excessive heat transfer surface is installed but correct pressure drop or correct θ and heat transfer surface but either the pressure drop available is not fully utilised or it has been exceeded. Hence the rating engineer cannot always trim his design as closely as he would wish.

For any specific duty, a tubular heat exchanger can be designed by choosing the dimensions of the tubes so that by using the correct empirical equations and performance data which are generally available for calculation and estimating purposes, the required heat transfer coefficient and pressure drop are obtained. Although the PHE is now widely used, there is only a limited amount

of information available. Correlations and data pertaining to commericial PHE's used by the manufacturers are not published for obvious commercial reasons. However, to counteract this lack of knowledge to some extent, two major manufacturers have provided confidential computer programs on commerical time sharing systems to enable potential customers to size and budget price their own exchanger[17]. Final designs are then carried out by the manufacturer if required. The multiplicity of plate forms and the lack of published data have so far prevented the development of a generalised design procedure.

Other problems arise when the plates are grouped together to form a pack. The assumption, frequently made, that the effect of port friction could be ignored and hence each channel in a pass is operating under exactly similar conditions is not really tenable. This is more so in units involving large platages and flow rates since the consequent high velocities in the passage formed by the ports of the plates coupled with the large length of the plate pack will result in appreciable extraneous losses in the ports. Usher[35] points out that these port losses are made up of two components (1) a frictional loss along the port manifold itself, and (2) an energy loss due to the change in direction of flow at the beginning and end of each pass. This pressure loss along the port will result in a considerable variation in flow to individual channels along the pack and will affect both the overall pressure drop and θ[35]. The flow distribution pattern will depend on whether the entry and exit are at the same or opposite ends of the pack. Usher[35] suggests that for simple plate arrangements one method of tackling this problem is to measure the friction factor f down the port passage experimentally. This is then written into a computer program which then tries different patterns of flow distribution until it eventually finds one in which the sum of the channel pressure

drops and extraneous pressure losses correspond to the stipulated operating conditions. The individual channel rates, flow ratios, and temperature conditions are computed and this leads to the overall effective number of heat transfer units θ.

Another factor is that a channel with an upward liquid flow will always run full; as mentioned earlier a channel accommodating downward flow may well run partially empty if the pressure loss is less than the static head between the plate ports. The effect of the extraneous losses on flow distribution may reduce the channel rate below this critical figure.

It is therefore important that the ports should be large enough to handle the maximum flow envisaged without involving excessive port velocities and pressure drop which is wasteful in pumping power and leads to unequal flow distribution. Usher[35], however, explains that plate design always lags behind operatonal requirements, and ports are never lage enough, so that there will always be a tendency to overload them because for commercial reasons sales engineers are bound to want to minimize the number of individual frames required. Cattell[14] points out that for large industrial units the tolerable maximum velocity is set at approximately 5 m/s to keep pressure losses in the manifolds to acceptable limits. Having set the port diameter accordingly, Cattell explains that the minimum possible plate width is set by the need to keep the two ports at each end of the plate sufficiently far apart to allow standard flanges to be connected without interference.

1.5) RECENT TRENDS

One of the design difficulties has been eased by employing a technique known as plate mixing in which 2 or more plate forms of different θ ranges are made to fit into a single pack. The mixing

of two types of plate within a single pass can achieve a compromise between the two plate characteristics and an exact fit with the duty requirements. According to Cattell[14] this is a revived concept and that the original system employed cast gun-metal plates with machined flow grooves which varied between plates, thus providing differing heat transfer characteristics. The modern counterpart consists of two plate designs which are mechanically compatible with each other and when combined in different ways these two plate forms develop 3 distinct and widely separated θ-ΔP relationships. Furthermore, the proportions of two of these three channel types incorporated in the same pack can be continuously varied so as to achieve, in a single pass unit, exactly the required θ value at the stipulated pressure drop, so long as this lies within the limits for the extreme channel types[6]. The 3-dimensional trough form known as the chevron or herringbone pattern, mentioned in Section 1.3.1, has gained substantial significance in this respect, for it was realised that with this type of plate form, the θ-ΔP relationship is affected not only by the pressing depth and the pitch of the corrugations, but also quite dramatically by the angle of the chevron. It was also discovered that if the angle the inclined corrugations make with the vertical axis of the plate on one type is x° and that on the other type is $(90-x^\circ)$, then the frequency of support points is the same for both types. Belcher[6] points out that by this simple method of varying only the chevron angle, it has been found possible and practical to vary θ values by a ratio of 6:1. The three different channels that could be formed from the two plate types are as follows:

(1) Channels formed by identical plates with corrugations running at an angle of about 70° with the vertical axis of the plate giving high θ values and high pressure loss because of high degree of induced turbulence.

(2) Channels made from identical plates with corrugations running

(2) contd.

at an angle of about 30° with the vertical axis of the plate resulting in low θ values and low pressure drop because of the relatively low level of turbulence.

(3) A plate of the first category and another from the second would result in the mixed channel with intermediate characteristics.

Clark[15] gives typical θ values for the three channels as 3.0, 0.5, and 1.5 respectively. He also indicates that prior to this development several manufacturers used to alter the gap between plates to change θ. The disadvantages with such a method are problems of support, removal of air pockets, and prediction of flow characteristics.

The practical advantage of the plate mixing technique is that it reduces the size and therefore the cost, of a PHE for a given duty. The average saving in total plate area is reported to be of the order of 20%[4]. However, Clark[15] indicates that the mixed θ units are more complex to rate due to the differing flow conditions in different channels and a very advanced computer program is used for rating and optimising these units. Cattell[14] points out that although mixing allows more freedom of choice in θ level, a mixed θ unit will always be more expensive than a unit made of exact-θ plates. The amount of the excess is a function of the difference between the two characteristics being mixed, i.e. as the range of θ covered by the mixing system is increased, excess areas increase. He concludes that it is essential to design a plate mixing system which for a majority of commercial cases operates near the characteristics of one of the two basic forms, and to keep the θ range covered within acceptable limits.

The inlet and outlet ports of any plate could be either on the same side of the plate e.g. the APV Junior used in this work, or they are on opposite sides of the plate, see Fig.1.2. The former is referred to as "vertical flow" and the latter "diagonal flow".

The diagonal flow pattern necessitates the manufacture of separate right-hand and left-hand plates. With the vertical flow type only one pattern is needed; alternate plates are rotated 180° to form the dual channel system. The loss of efficiency caused by having both inlet and outlet at the same side has been claimed, following experience, to be negligible[4]. Consequently vertical flow has been adopted with recent designs because of its obvious simplifying effect on production.

Usher[36] points out that the modern high pressure thin gauge plate is designed to have interplate contact points as close as possible to the peripheral gaskets not only inside but also outside the flow area so that the gasket can be regarded as a simply supported beam rather than a cantilever thereby permitting higher pressures to be used.

The aforementioned recent developments have brought the PHE nearer to a status equivalent to that of the tubular exchanger. It also highlights the necessity for basic understanding of fluid flow and heat transfer in 3-dimensional channels of the chevron type. This work represents a step in this direction.

1.6) APPLICATIONS AND LIMITATIONS

In order to appreciate the reasons for the increasing popularity of the PHE it may be useful to consider the following points:

(1) Normal assembly of a plate pack involves no welding so difficult-to-weld but pressable materials can be used at relatively low prices. Hence, economic use is made of expensive materials — in fact, the more expensive the material, the more economic the PHE becomes in comparison with other exchangers[28]. Ahlstrom and Rylander[1] indicate that this makes units in titanium highly competitive and able to handle any kind of

(1) contd.

natural water up to 110°C without corrosion risk.

(2) The compact nature allows it to be installed into odd spaces which could not otherwise be so productively used. No extra space is required for inspection and/or manual cleaning of the plates. Jones and Usher[25] point out that an example of this is in the marine field where, because of shortage of space, plate units are finding an increasing use for shipboard operations such as for cooling diesel oil and jacket water.

(3) This design achieves a much higher surface-to-volume ratio than is possible with tubes or other types of partition. By virtue of its narrow flow channels the PHE therefore has a low volumetric capacity meaning a short liquid residence time and this can be of major importance when processing expensive liquids where the priming volume must be kept to a minimum and also where product quality is affected by time and temperature.

(4) With high levels of induced turbulence even low flow rates give high heat transfer coefficients (values as high as 6.0 KW/m^2 °C have been reported[4]).

Dahlgren and Jenssen[18] point out that at a given pumping energy per unit heat transfer area, the PHE gives higher heat transfer than tubular exchangers. This means that the plate unit is a high efficiency machine which can operate economically, with a close temperature approach, at relatively low pumping powers. Jones and Usher[25] explain that the attainment of a high number of heat transfer units resulting from high heat transfer coefficients and counter-current-flow makes the plate unit ideally suited for recuperative duties and other heat recovery schemes. They report recuperative efficiencies of over 90% in the heating of

(4) contd.

turbine lubricating oils prior to centrifuging and heat recovery from industrial waste solutions such as dye and distillery effluents.

(5) Its flexibility in incorporating more than one duty within the same frame has already been discussed.

Basically there are 3 areas of application:

(a) Hygienic/heat-sensitive duties in the food, beverage and pharmaceutical industries.

(b) High-pressure/high-temperature duties in the chemical and metallurgical industries.

(c) High-capacity cooling duties in chemical plants, steelworks, nuclear power stations, etc.

The majority of these installations are used for turbulent liquid/liquid services because the high heat transfer of the plate is more pronounced under these conditions. However, Parrott[30] indicates that the PHE potential when applied to viscous non-aqueous products is only now being appreciated. Furthermore, the high shear rates generated in a PHE channel is of particular significance when considering non-Newtonian fluids, since in the case of Bingham plastic and pseudoplastic materials the effective viscosity is reduced, improving plate performance. As a result transition and laminar flow duties are becoming more important. Marriott[28] and Cooper[16] point out that boiling duties and condensation of vapour (including steam) at moderate pressures (41 KN/m^2 to 410 KN/m^2) are also economically handled by PHE's.

Such wide fields of application obviously require plates in a variety of materials. Fortunately, any material of reasonable ductility which can be cold formed may be used for heat exchanger plates. The use of plates made of mild steel does not appear to be economically justified[24]. The most commonly used material is

stainless steel either 18 Cr/10 Ni (AISI 304) or 18 Cr/12 Ni/2.5 Mo (AISI 316), preferably with carbon content of less than 0.07%, since this eliminates the need for titanium stabilisation[28]. Stainless steel is mandatory for hygienic reasons in food and beverage processing. Titanium (99.8%) and palladium stabilised (0.2%) titanium are used because of their outstanding corrosion resistance, e.g. in duties involving chloride solutions (including brackish cooling water) and cooling factory effluents using sea water[4]. Other materials used include the high nickel alloys (Monel 400, Incoloy 825, Inconel 600 and 625, Hastelloy B and C) and copper based alloys (Cu/Ni 70/30 and 90/10, aluminium brass 76/22/2, etc.) Pure metals such as copper, aluminium, nickel, silver, and tantalum are also used[28]. In order to eliminate electrochemical effects, liquid connections are usually made of the same material as the plates.

In spite of its advantages, the narrow gap represents a handicap to the use of plates for certain duties because of the risk of blockage where there are large quantities of solids in suspension or where there is heavy fouling[25].

Although a wide range of gasket materials is available including natural rubber, neoprene, styrene-butadiene, hypalon, Viton, resin-cured butyl, medium nitrile, ethylene-propylene, fluorocarbon rubber, silicone rubber, and compressed asbestos fibre, the fact that the PHE depends on elastomers as a sealing medium proved to be a distinct limitation on its use. Cooper[17] points out that even compressed asbestos fibre gaskets contain about 6% rubber. Marriott[28] indicates that usually it is the gasket that limits the maximum operating temperature for a PHE and suggests that the following table may serve as a rough guide in the absence of chemical attack:

Natural, styrene, neoprene max.	...	70°C
Nitrile, Viton	...	100°C
Resin-cured butyl	...	120°C
Ethylene/propylene, silicone	...	140°C
Compressed asbestos fibre	...	200°C

TABLE 1-I

Other information in this respect appeared in a recent APV Co. publication[5] and is as follows:

Gasket Material	Approx.Max. Operating temp.	Application
Paracril (Medium Nitrile)	135°C	Resistant to fatty materials
E.P.D.M.	150°C	High temp.resistance for a wide range of chemicals.
Paratherm (Resin-cured butyl)	150°C	Aldehydes, ketones and some esters
Paradur (Fluoro-carbon rubber base)	177°C	Mineral oils, fuels, vegetable and animal oils.
Paracaf (Compressed asbestos fibre).	260°C	Organic solvents such as chlorinated hydro-carbons.

TABLE 1-II

It seems therefore that the maximum operating temperature is limited usually to 260°C. It must be realised that operating temperatures may also be limited by plate corrosion effects, Marriott[28] indicates that refrigerant quality brine, for instance, can be handled by 18 Cr/12 Ni/2.5 Mo (AISI 316) stainless steel plates provided the surface temperature does not exceed 10°C.

The maximum allowable working pressure may be determined by frame strength, gasket retainment, or plate deformation resistance. All PHE's used in the chemical and allied industries are capable of

operating at 593 KN/m^2, most at 986 KN/m^2, many at 1593 KN/m^2 and some at pressures as high as 2085 KN/m^2[28].

Individual plate sizes range from 0.0258 m^2 (corresponding to the APV Junior which is the smallest commerically available PHE) to 1.6 m^2 (corresponding to Alfa-Laval A30 which is the biggest exchanger available at present). The A30 PHE with up to 400 plates has a total surface area of 640 m^2. It stands 2.8 m high, with 30 cm connections permitting water flows of up to 1500 m^3/h[4].

The present work is a detailed investigation of the hydrodynamic characteristics of a particular plate form, namely, the APV Junior Paraflow, as a first step in establishing a generalised design procedure for plate heat exchangers. A single channel was fabricated from transparent polymethylmethacrylate in order that visual observation could be made during the course of experimental runs and pressure measurements could be made at preselected positions.

A method was developed for casting the plastic plate to ensure a very close reproduction of the standard metal plate so that the results would be representative of a single channel in a pack of plates.

Although a range of viscosities of working fluids was used, the very low pressure drops encountered during viscous flow required the development of an accurate and reliable method for measuring such low pressure differentials. The difficulties encountered are discussed in Appendix A-2.0.

CHAPTER 2

LITERATURE REVIEW

2.0) LITERATURE REVIEW

The following is a critical survey of the available literature on 3-dimensional trough form plate heat exchangers.

Shaoul[34] investigated the hydrodynamic characteristics of an APV Junior PHE under isothermal and heat-transfer conditions. The plate arrangement was single pass for both fluids (1 pass/1 pass) with 10 channels per pass, 21 plates in all. The working fluids were aqueous glycerol and H_2O which flowed in a counter-current manner.

The equivalent diameter (see Section 5.1) was taken as twice the gap between plates (pitch minus thickness). However, it is not clear how the area of flow was calculated nor what length was considered for the pressure gradient. The values of these parameters were not given and therefore the significance of the quoted Reynolds numbers and friction factors is somewhat limited. The pressure drop across the complete pack for both fluids was measured by means of U-tube mercury manometers.

The range of Reynolds numbers covered by Shaoul was between 2.5 and 2500. He suggested three distinct regions of flow. Laminar flow extending up to Re of 90, a transition zone of unpredictable flow between Re of 90 and 600, and turbulent regime when Re becomes greater than 600. The,friction factor - Reynolds number, empirical equations are as follows:

$$f = 123.0 \ Re^{-0.86} \quad (Re < 90) \qquad (2.1)$$

$$f = 5.3 \ Re^{-0.178} \quad (Re > 600) \qquad (2.2)$$

The above equations were obtained utilising data obtained under isothermal and heat-transfer conditions. There is considerable scatter in the data, those under isothermal condition being below the lines described by equations (2.1) and (2.2), while data above correspond to the situation where heat-transfer was taking place.

Shaoul used the inlet fluid temperature to estimate the physical properties required to calculate f and Re when heat-transfer was taking place. He did not explain the reason behind this although he briefly discussed its effect on the correlations and pointed out that if the average temperature was used the equation for Re < 90 under heat transfer would be

$$f = 65.0\ Re^{-0.64} \qquad (2.3)$$

Shaoul misinterpreted the gradual and extensive transition region since it was unexpected at that time. For a substantial part of this zone it is now known that the slope of the PHE friction factor - Reynolds number plot experiences little and gradual variation. It is almost certain that the data used to obtain equation (2.1) represent laminar/transition flows. Hence a slope value of (-0.86) is not surprising whereas a slope of (-1.0) is expected for laminar conditions. The slope of the line best describing the turbulent regime compares reasonably with results of the present work. No experimental data were plotted by Shaoul in the Re range he considered transitional even though they were reported. Plotting these isothermal results with the others showed a definite trend in spite of the scatter. It is not clear why Shaoul ignored them.

Ellison [21] carried out isothermal pressure drop measurements on the APV Junior PHE making use of Shaoul's experimental set-up. He paid special attention to ensure that no pockets of air were trapped in the exchanger. The number of plates in the pack was varied to observe its effect on the hydrodynamics. Hence, packs of 21, 15, 11, 7, 5 and 3 plates were examined with the (1 pass/1 pass) arrangement maintained.

Considering the equivalent diameter to be twice the plate-gap, Ellison used the following definition for Re:

$$Re = \frac{(M)\ (2b)}{(Wb)(n)(\mu)} = \frac{2M}{Wn\ \mu} \qquad (2.4)$$

where M, b, W and n are the mass flow-rate, the plate gap, the plate width, and channels/pass respectively. Again no values were given for M,b,W or the plate length L. The range covered was $0.5 < Re \leq 2000$.

Ellison reported that laminar flow existed up to an Re of about 10. However, he indicated different correlations depending on the direction of flow as follows:

UP - Flow $\quad f = 67.1\ Re^{-1.12} \quad (Re < 10) \qquad (2.5)$

DOWN - Flow $\quad f = 96.2\ Re^{-1.38} \quad (Re < 10) \qquad (2.6)$

Equation (2.6) was subsequently rejected on the grounds that it may not be valid due to air occlusion in spite of the measures taken against it. The contradiction between a slope of more than (-1.0) and laminar flow theory was not discussed. A 21-plate pack was used to obtain data corresponding to $Re < 10$.

The next stage of Ellison's work covered the range $20 < Re < 300$. Packs of 15, 11, 7 and 5 plates were investigated. The results follow a definite trend, namely a gradually decreasing slope up to an Re of 160 beyond which f becomes constant and independent of Re. Data corresponding to 15-plate and 11-plate packs are comparable with each other, but they are noticeably higher than those corresponding to 7-plate and 5-plate packs. Ellison was surprised by these interesting aspects but did not attempt to correlate the data in this region. Instead he attributed their trend to air pockets in the exchanger.

Correlations referring to turbulent flow and the corresponding packs are as follows:

21-plate pack $f = 2.17\ Re^{-0.123}$ $(Re > 700)$ (2.7)

11 and 15-plate " $f = 1.98\ Re^{-0.123}$ $(Re > 600)$ (2.8)

7-plate " $f = 1.73\ Re^{-0.123}$ $(Re > 1000)$ (2.9)

Ellison concludes that the position of the correlation is a function of the number of plates in the pack. For packs of 5 or 3 plates the results did not follow the trend described by equations 2.7-9 and were not correlated.

Edwards et al.[20] carried out work at Bradford University on the APV Junior PHE. Two plate arrangements were considered

(a) 1 pass/1 pass with 12 channels per pass

(b) 2 pass/2 pass with 12 channels per pass

Newtonian and non-Newtonian fluids with widely ranging viscosities were used.

The equivalent diameter was defined as follows:

$$De = \frac{2b}{\phi} \qquad (2.10)$$

where b is the mean plate spacing (pitch minus thickness) and ϕ is the ratio of developed to projected area. This definition was suggested by Parrott [30] as suitable for 3-dimensional trough form PHE's. Application of equation (2.10) produced a value of 0.343 cm for the Junior. The fluid velocity was calculated from the following relationship:

$$u = \frac{q}{bW} \qquad (2.11)$$

where q is the volumetric flow-rate between two plates. The values of b and W were reported as 0.203 cm and 5.3 cm respectively. The plate length was taken as the projected distance between the edges of the two ports, namely 45 cm, rather than the one between their centres. The range covered corresponds to $0.04 < Re < 1000$.

Edwards et al. claim that under the conditions employed it is likely that port losses are negligible. They add, that if the port losses were significant then it is improbable that the data

for different pass arrangements would fall together and conclude that their results represent the flow between corrugated plates with reasonable accuracy.

The results of Edwards et al. indicate that laminar flow conditions exist up to a Re of about 10, followed by a very gradual transition to turbulent flow when f becomes weakly dependent upon Re. An analogy was drawn between the geometry of channels formed by chevron-type plates and packed beds of near-spherical particles. The Ergun equation[23] for packed beds was expressed in a form consistent with f and Re used for the PHE and the resulting relationship was compared with the data. Good agreement was observed. However, the tendency of the PHE data to lie above the Ergun equation was attributed to port losses thereby contradicting the earlier suggestion that these were negligible.

A single Ergun-type relationship was developed to describe the Junior PHE data over the entire Re range namely:

$$f = \frac{34.0}{Re} + 0.8 \qquad (2.12)$$

The first term on the right-hand side of equation (2.12) is the laminar contribution to the pressure drop which dominates at low Re and the second term is the turbulent contribution becoming important at higher Re.

Fig.2.1 shows the friction factor - Reynolds number relationship of two 3-dimensional trough form PHE's. The Alfa-Laval Chevron plot was first published in reference[2] and appeared again in a paper by Clark[15]. Alfa-Laval manufactures the following Chevron plates: P0, P2, P3, P4, and the recently introduced A10, A20, and A30 plates[3]. The Thermal Handbook[2] did not indicate to which Chevron plate the plot referred. However, Clark's paper suggests that it is relevant to P3 plates. No information was given about the plate arrangement in the exchanger used. Approximate correlations corresponding

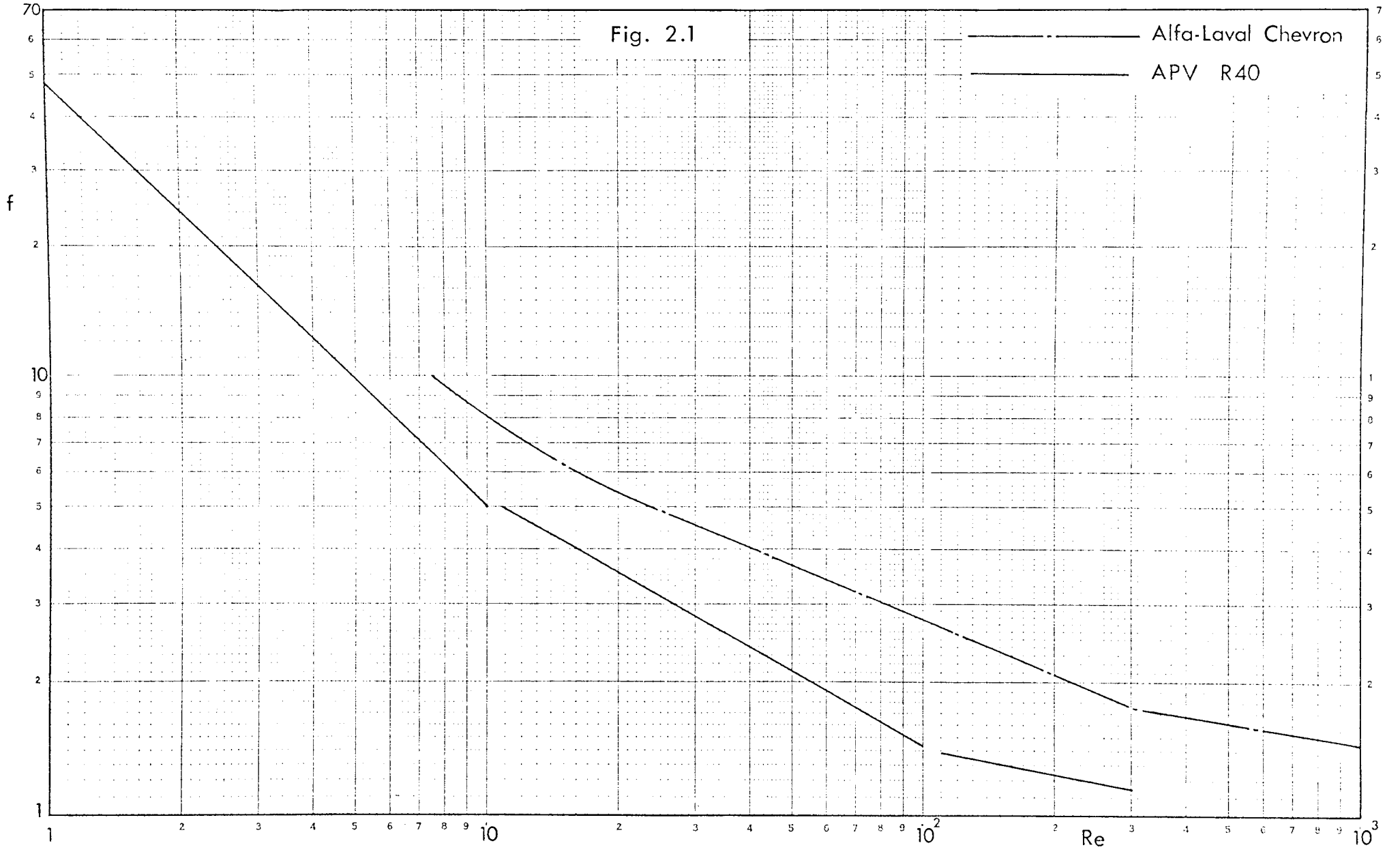
Fig. 2.1
Alfa-Laval Chevron
APV R40
f
Re
70
6
5
4
3
2
10
9
8
7
6
5
4
3
2
1
1
2
3
4
5
6
7
8
9
10
10^2
10^3

to it are as follows:

(Transition, $18 \leq Re < 300$) $\quad f = 18.5\ Re^{-0.42}$ (2.13)

(Turbulent, $\quad Re > 300$) $\quad f = 4.0\ Re^{-0.12}$ (2.14)

The APV R40 PHE f vs. Re relationship presented in Figure 2.1 was made available through private communication. It was obtained using 1 pass of 3 channels. The R40 PHE channels have similar geometries to those of the Junior PHE but are larger. The equivalent diameter and ratio of developed/projected area are both larger than those of the Junior, namely: 0.498 cm and 1.22 respectively compared to 0.386 cm and 1.18. The two ports are 13 cm in diameter (cf. 1.43 cm for the Junior), about $\frac{1}{3}$ the plate width available for flow, situated diagonally. Consequently the plot should reflect the hydrodynamics of this type of plate since the effects of the manifolds would be small because of the port size and the use of only 3 channels. The empirical equations pertaining to the R40 plot are as follows:

(Laminar , $Re < 10$) $\quad f = 47.0\ Re^{-0.965}$ (2.15)

(Transition, $10 < Re < 100$) $f = 19.0\ Re^{-0.559}$ (2.16)

(Turbulent, $Re > 100$) $\quad f = 3.3\ Re^{-0.184}$ (2.17)

Kovalenko[27] investigated the 3-dimensional trough form plates known as the Rosenblad 3S . These plates appear to be physically similar to the Alfa-Laval P3 plates described in reference[3]. The plate arrangement was (1 pass/1 pass) with 4 channels per pass. His results are very different from the Alfa-Laval Chevron plot in Fig.2.1 even if one assumes that Kovalenko used definitions for the relevant parameters related to flat plates. He suggested laminar flow up to Re of 200 followed by turbulent flow at higher Re with an almost insignificant transition in between. For the turbulent regime the following relationship was quoted

$(200 < Re < 16000) \quad Eu = 1843\ Re^{-0.25}$ (2.18)

Emerson[22] examined a Rosenblad PHE containing plates

of a 3-dimensional trough form and being very similar to Alfa-Laval's P2 plates. The plate arrangement in the exchanger was: (1 pass/ 1 pass) with 11 channels per pass. The Rosenblad exchanger was one of four different types investigated by Emerson, one of which consisted of flat plates. The latter was adopted as the reference to which the other three were compared. Hence, all parameters were defined relevant to the 2-dimensional flat-plate exchanger. The following relationships were proposed to describe the data for the Rosenblad exchanger:

$$(Re < 40) \qquad f = 40.9\ Re^{-0.74} \tag{2.19}$$

$$(Re > 40) \qquad f = 10.5\ Re^{-0.33} \tag{2.20}$$

Fortunately the geometrical characteristics of the Rosenblad plates were given by Emerson. These characteristics have been used by the author to transform f and Re to replot the data. Details of this transformation are given in Appendix A-1.0. Application of equation (2.10) produced an equivalent diameter of 0.482 cm for the Rosenblad plates and the ratio of developed/projected area was found to be 1.22. Fig.2.2 shows Emerson's transformed data compared with the R40 PHE plot discussed earlier. The important parameters pertaining to the Rosenblad and R40 PHE's are given in the table below:

	Rosenblad PHE	R40 PHE
Ratio developed/ projected area	1.22	1.22
Equivalent diameter	0.482 cm	0.498 cm
Developed heat transfer area/plate	1200 cm^2	3762 cm^2
Developed plate length	55.8 cm	92.6 cm
Plate width available for flow	21.5 cm	40.6 cm
Port diameter	7.0 cm	12.7 cm

TABLE 2-I

Although the R40 plates are larger than those of the Rosenblad, the fact that the ratio of developed to projected area is the same with the two PHE's having rather similar equivalent diameters indicates that the two channels should exhibit close hydrodynamic

characteristics. The agreement is striking as seen in Fig.2.2. Since it has already been pointed out that the R40 plot reflects flow between plates of this type: one of the two following possibilities arises:

1) The effect of the manifolds in the Rosenblad PHE is negligible.
2) The hydrodynamic characteristics of the two plate types are different and the observed agreement as seen in Fig.2.2 is coincidental, i.e. the combination of the manifolds and the channels in the Rosenblad pack is equivalent to the R40 behaviour.

It would seem that the first possibility is more likely.

Also included in Fig.2.2 is the plot pertaining to the Junior PHE developed by Edwards et al.[20] at Bradford University. The curve corresponds to equation (2.12) with slight modification of f, namely the replacement of the 45 cm port to port projected plate length by the 47.2 cm developed plate length, to ensure consistency. The number of channels per pass of the Rosenblad and Junior exchangers were almost the same (11 vs. 12).

The curves shown in Fig.2.3 have appeared in the literature referring to "typical" exchangers without mention of geometrical characteristics and dimensions. Manufacturers of PHE's are reluctant to release information, thus making comparisons and conclusions very difficult and in some cases impossible where supporting evidence cannot be found. The only certain aspect of these exchangers is that their plates have 3-dimensional trough forms.

Marriott[28] discussed his results comparing the value of the friction factor to that in a tube. Cattell[13] compared his data with those for a rectangular duct and a tube. Approximate relationships obtained from Cattell's plot are as follows:

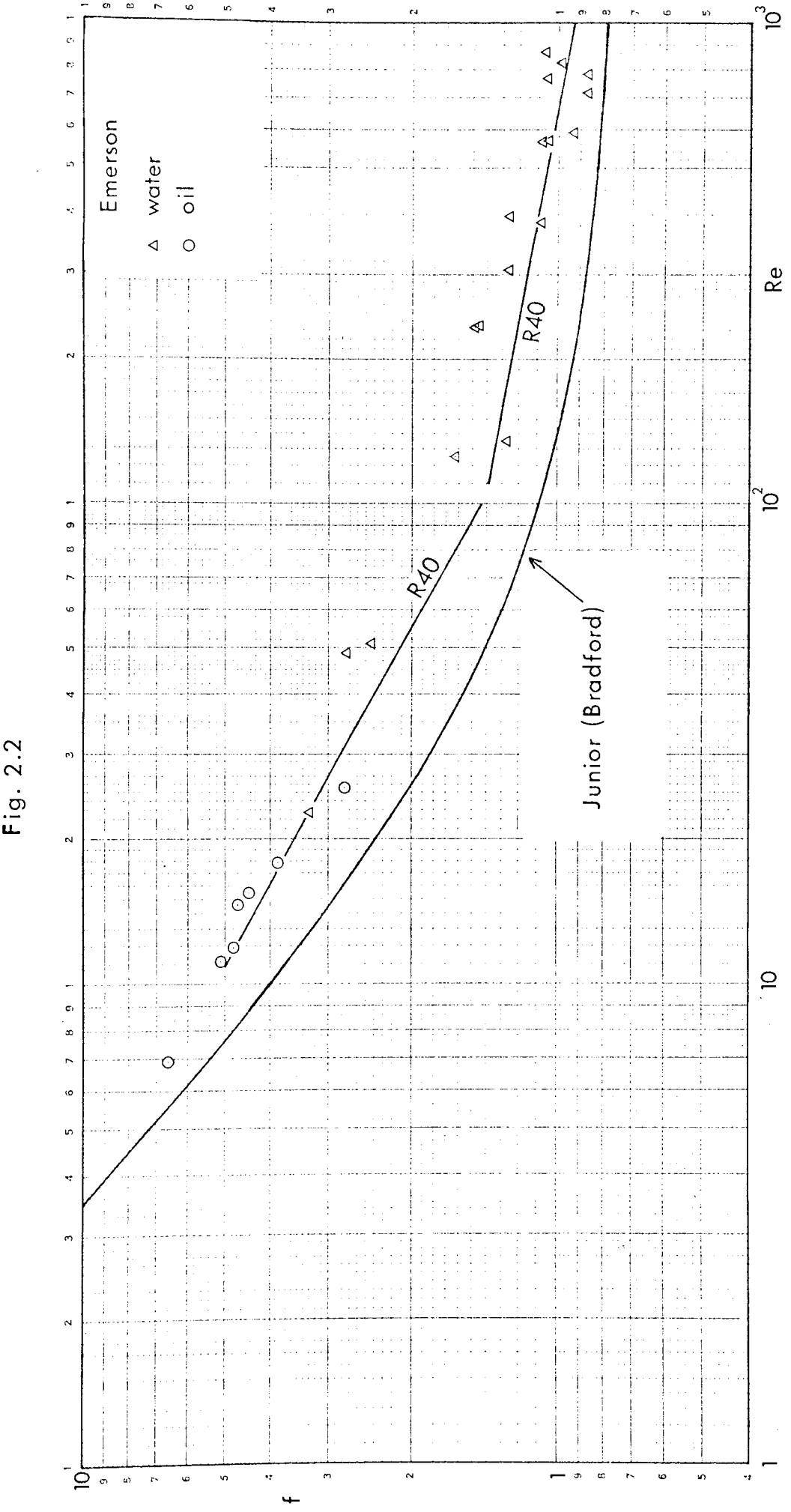

Fig. 2.2

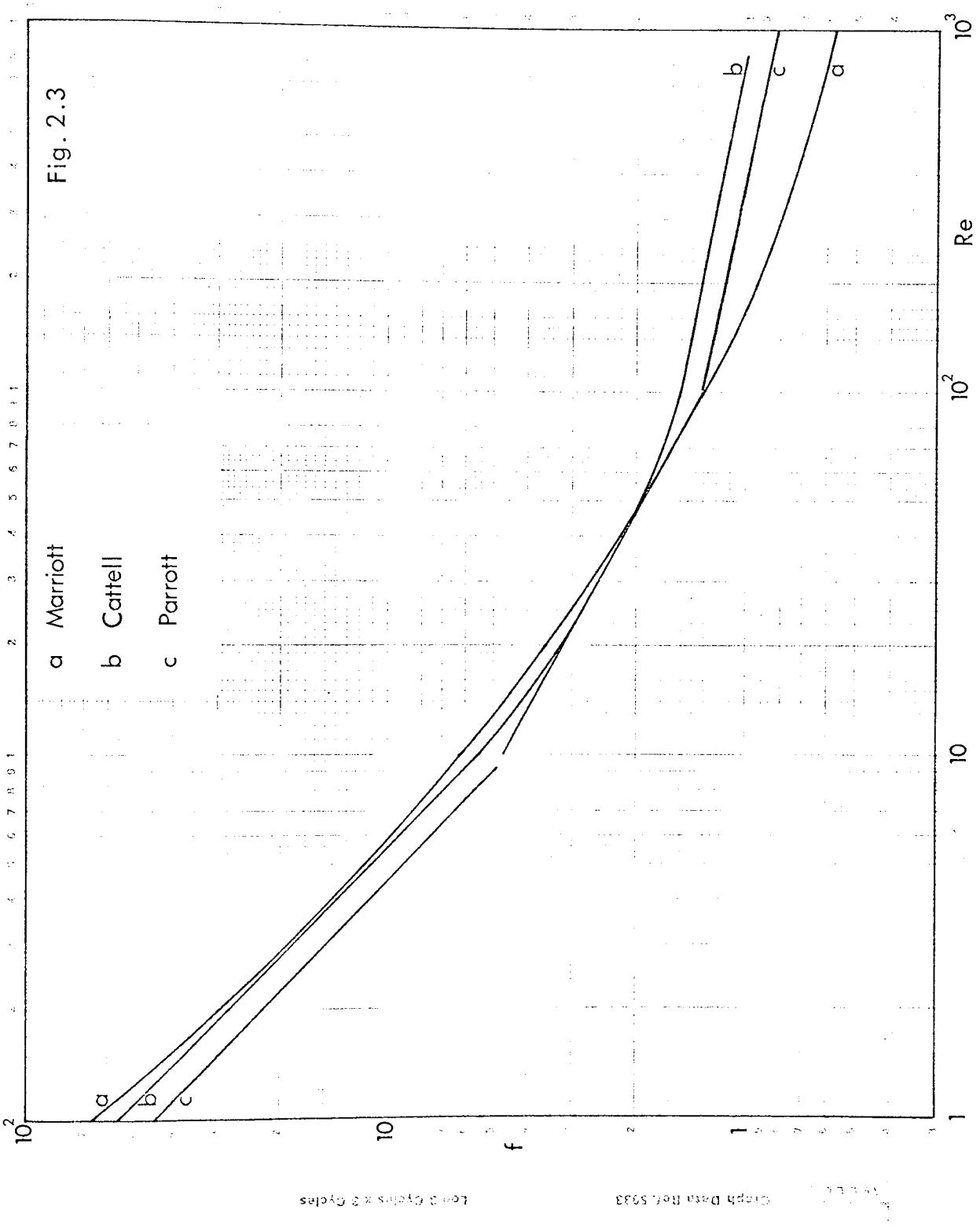
Fig. 2.3
a Marriott
b Cattell
c Parrott
a
b
c
f
Re
10^2
10
1
1
10
10^2
10^3

(Laminar, Re < 10) $f = 56\ Re^{-1.0}$ (2.21)

(Transition, 10 < Re < 100) $f = A' + \frac{B}{Re}$ (2.22)

(Turbulent, Re > 100) $f = 3.6\ Re^{-0.19}$ (2.23)

Parrott[30] put forward results as an example of a 3-dimensional trough form PHE f vs. Re relationship. Although an APV Junior plate was shown as an illustration in the paper, Parrott did not indicate whether the plot belonged to the Junior or some other exchanger. The corresponding empirical equations estimated from the plot are as follows:

(Laminar, Re < 10) $f = 44.5\ Re^{-0.99}$ (2.24)

(Transition, 10 < Re < 100) $f = 15.5\ Re^{-0.56}$ (2.25)

(Turbulent, Re > 100) $f = 3.4\ Re^{-0.20}$ (2.26)

A most interesting work was carried out in the Soviet Union by Savostin and Tikhonov[33]. The model considered was described as heat transfer elements of "Frenkel packing" type. This is a matrix of channels formed by corrugated plates with the undulations on adjacent sheets at an angle ψ to one another, Fig.3.3. The working media were air/water. The flow of the two fluids was in a cross-current manner. The cooling fluid (water) flowed over the external surfaces of the matrix and its pressure was maintained higher than the air pressure to ensure reliable contact of the plates in the matrix. However, the hydraulic characteristics were determined with isothermal air flow, i.e. without preheating the air and without supplying the cooling water.

The equivalent diameter was defined as:

$$De = 4\ V_a/F_a \qquad (2.27)$$

where V_a is the volume of the matrix occupied by air and F_a is the area of heat transfer surface, i.e. the developed rather than projected

area. The area of the passage section was calculated using the relationship:

$$S_a = V_a/L \tag{2.28}$$

where L is the nominal distance between the ends of the heat exchanger. The coefficient of hydraulic resistance suggested by Kays and London[26] for isothermal air flow was used, namely:

$$\xi = \left[\frac{\Delta P_a}{\rho u^2/2} - (K_c + 1 - \sigma^2) \right] \frac{De}{L} \tag{2.29}$$

where σ is the ratio of passage section S_a to cross section of the pipe and K_c is the coefficient of loss of head at the inlet of the channels. Savostin and Tickhonov claim that tests carried out at different distances of the pressure tappings from the end of the heat exchanger have shown the measured downstream pressure to be virtually equal to the static pressure at the outlet from the channels. Therefore in calculation of ξ the term $(1-\sigma^2-K_e)$ allowing for the influence of the outlet was assumed to be zero.

The first six types of plate investigated (B-1 to B-6) had approximately the same dimensions and shape of the cross section of the channels but the angle between the corrugations on adjacent plates (relative to the direction of flow) varied from 0° to 144°. Consequently their results should reflect the effect of the angle between the corrugations. The main geometrical characteristics of these specimens are given in the following table:

Specimen	ψ , deg.	De, mm	L/De	h, mm	t, mm
B-1	0°	1.72	46.4	1.19	2.57
B-2	20°	1.54	51.0	1.20	2.57
B-3	37°	1.54	52.9	1.19	2.57
B-4	66°	1.53	50.5	1.17	2.57
B-5	96°	1.54	49.2	1.19	2.57
B-6	144°	1.49	27.2	1.12	2.57

TABLE 2-II

h is the height of the corrugation and t is its base width.

Savostin and Tickhonov's results were presented in tabular form. They suggested that results of tests on specimens B-1 to B-4 could be approximated by the following relationships (angle ψ in the equations is in radians; depending on the value of ψ the value of $\cos\psi$ can be positive or negative):

at $200 < Re < 600$:

$$\xi = 25.0\ (1+0.95\ \psi^{1.72})/Re^{0.84} \tag{2.30}$$

at $600 < Re < 4000$:

$$\xi = 3.7(0.62+0.38\ \cos 2.6\psi)/Re^{0.53(0.58+0.42\cos 1.87\psi)} \tag{2.31}$$

Plotting the tabulated results of plates B-1 to B-6 is shown in Fig.2.4. The ordinate axis was considered $\xi/4$ since:

$$\xi = 4f \tag{2.32}$$

The plotted data clearly reveal a pronounced change in the hydrodynamic characteristics as the angle is increased to 66° (specimen B-4). It is also evident that as the angle ψ is increased the dependence of the resistance coefficient on Re becomes less, indicating higher degrees of turbulence. The other interesting feature of Savostin and Tickhonov's data is the magnitude by which the resistance coefficient increases as the angle ψ is increased.

Five additional specimens were examined by Savostin and Tickhonov. In these the angle ψ was fixed at 29°, but the

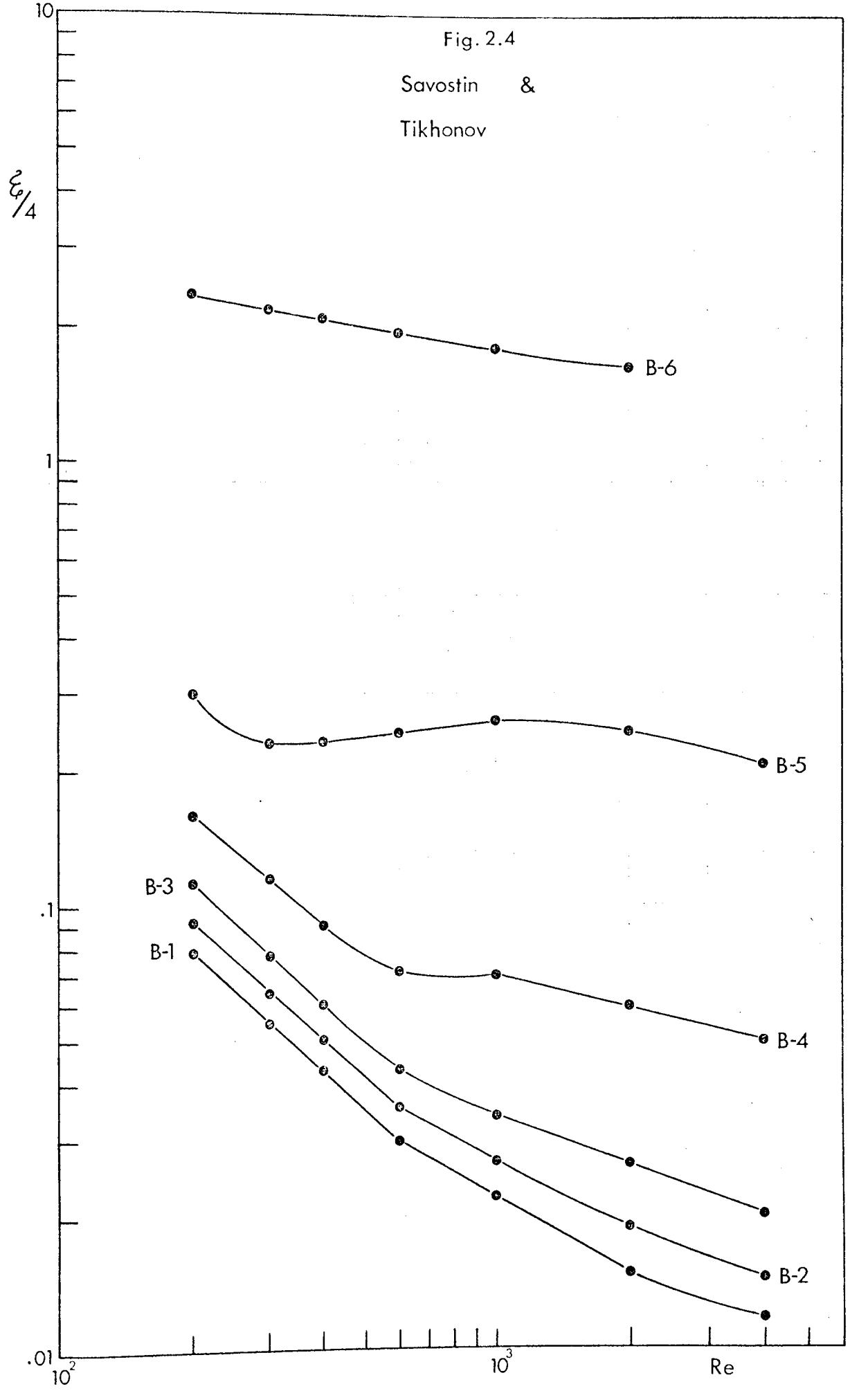
Fig. 2.4
Savostin &
Tikhonov
$\zeta_\varphi/4$
10
1
.1
.01
10^2
10^3
Re
B-6
B-5
B-4
B-3
B-2
B-1

height of the corrugations was varied, changing the channel cross section as a result. They discovered that increasing the depth of the corrugations decreased the resistance coefficient.

It may be useful to point out that the angle ψ between corrugations of adjacent plates is 120° (corrugations on individual plates run at an angle of 60° with the vertical axis of the plate) for almost all the existing Chevron (herring-bone) PHE's, e.g. APV Junior, Alfa-Laval's P0, P2 (Rosenblad), P3 (Rosenblad 3S) and P4 plates. Notable exceptions are the recently introduced Alfa-Laval's A10, A20, and A30 with angles of 140° (70° with the vertical axis) for 'high θ' plates and 60° (30° with the vertical axis) for 'low θ' and combination of the two angles for 'medium θ' (see Section 1.5). The high θ A20 plates seem to have an angle ψ of 128° (64° with the vertical axis).

The effect of the angle between corrugations of adjacent plates on heat transfer and resistance characteristics was examined in Japan by Okada et al.[29]. The ψ angles tested were 120°, 135°, 150°, and 165° (60°,67.5°, 75°, and 82.5° respectively relative to the vertical axis of the plate). The minimum Re encountered in some channels was 400, the maximum in others was about 10,000. The equivalent diameter was considered to be 4 times the ratio of the channel volume to the heat transfer area and the channel length was taken to be its developed length.

Unfortunately the results of Okada et al. were of little value to the present work because they were presented in the form of plots of the hydraulic gradient ($\Delta P/L$) - rather than resistance coefficient - versus Re without sufficient information to allow transformation into a form suitable for comparison. In addition, the plot corresponding to plates with 120°ψ angle between their undulations started from an Re of 2000. Nevertheless, the results illustrate the increase in the pressure gradient as the angle ψ between corrugations of adjacent plates increases. The effect of

the corrugation base width (wave pitch) on the pressure gradient for plates of 150°ψ angle was reported. At a given Re the smaller the wave pitch the greater is the pressure loss.

Beloborodov and Volgin published two papers about their work in the Soviet Union. Their first work[7] was a study of convectional heat exchange and resistance characteristics of narrow channels of sinuous and variable cross-section involving both 2-dimensional and 3-dimensional channels. The experimental set-up was based on a single hot water channel with a cold water channel on either side, 4 plates in all. Five different geometries were tested including flat plates. The other four channels used were different from each other by the mutual disposition of the corrugations on adjacent plates. The undulations of one model were arranged in a herringbone pattern at an angle ψ of 120°; the direction of the troughs of the opposite plate was inverted. It appears, however, that no contact occurred between the plates of any channel investigated including the one with the chevron pattern. This is contrary to current industrial practice where the majority of plates manufactured are assembled in such a way that there is metal to metal contact of adjacent plates.

The equivalent diameter adopted by Beloborodov and Volgin seems to be based on the average distance between the plates and the fluid velocity on the average cross-section. It is not clear whether the channel length used is apparent or developed.

Rather than being determined isothermally, the hydraulic resistances of the models were reported along with the heat transfer characteristics under the same conditions. They were related to a cold water channel across which a manometer was connected. The Re range covered was 4000 to 42,000 and the results were presented graphically in the form:

$$\frac{Eu}{\Gamma} = \phi\ (Re) \tag{2.33}$$

where ϕ stands for 'function of' and Γ is:

$$\Gamma = L/De \tag{2.34}$$

At Re > 10,000 all the models exhibit constant values of the resistance coefficient. The value of Eu/Γ corresponding to the herringbone model is 0.27. Only 3 points were reported in the range $4000 \leq Re < 10^4$ rendering assessment to be difficult.

In their more recent paper[8], Beloborodov and Volgin revealed the following relationship for the channel with the herringbone pattern mentioned in their previous paper:

$$(8000 < Re < 40{,}000) \qquad \lambda = \frac{1.05}{Re^{0.15}} \tag{2.35}$$

where $$\lambda = \frac{2Eu}{\Gamma} \tag{2.36}$$

Furthermore they reported the following equations when the herringbones on adjacent plates were parallel:

$$(4300 < Re < 11{,}000) \qquad \lambda \approx \frac{40.75}{Re^{0.45}} \tag{2.37}$$

$$(11{,}000 < Re < 38{,}000) \qquad \lambda \approx 0.6 \tag{2.38}$$

$$\text{or} \qquad \frac{Eu}{\Gamma} \approx 0.3 \tag{2.39}$$

This contradiction between the two papers when referring to the same channel appears to be due to a reference error in the second paper. The values of the heat transfer areas confirm this. Hence, at very high Re (> 10,000) the reversing of the direction of the herringbones on the adjacent plates (3-dimensional channel) results in the indepence of the resistance coefficient from Re whereas parallel herringbones (2-dimensional channel) retain the dependence of the resistance coefficient on Re. This could be attributed to the higher degrees of turbulence encountered in the 3-dimensional channel.

Wilkinson[39] examined the problem of flow distribution in PHE's. He considered single pass counter-current flow arrangements described as the U and Z arrangements (see Section 1.2.1 and Fig.1.1). The flow distribution through the channels in the pack was determined by the pressure profiles in the inlet and exit manifolds. These manifolds approximate to very rough pipes according to Wilkinson.

An APV Junior PHE was used for this study and the results indicate much less variation in channel flowrate with the Z arrangement than with the U arrangement. However, the accuracy of the results was not high and considerable scatter was evident. Wilkinson attributed this to the fact that the flowrate-pressure drop relationship for a pair of plates (single channel) is changed when the plates are assembled into a pack.

The equations governing the pressure profile in the manifolds of a PHE and the distribution of channel flowrate for the U and Z arrangements were developed by Wilkinson. Solutions to these equations were suggested.

It is to be noted that Wilkinson's findings of better flow distribution with the Z arrangement is unfortunate because of the U arrangement practical advantages (refer to Section 1.2.4 point (C)).

At this stage, it is not clear how the two different arrangements might affect the f vs. Re relationship in light of Wilkinson's findings since Shaoul[34] and Ellison[21] used the U arrangement whereas Edwards et al.[20] appear to have used the Z arrangement.

It is apparent that there is not a great deal of information published on the performance of plate heat exchangers. That which is published is confusing due to a lack of basic definitions of dimensions and terms used, rendering comparisons difficult. Additionally a great deal of the work reported applies

to high Reynolds number, highly turbulent operation, whereas there is a present tendency for the use of PHE's in low Reynolds number, viscous flow situations.

The present work is therefore intended to standardise the relevant definitions and to examine in detail the isothermal hydrodynamic characteristics of a particular commercial PHE channel. A clear understanding of the behaviour of flow in such channels is a basic necessity before the effects of heat flux can be studied.

CHAPTER 3

EXPERIMENTAL

3.0) EXPERIMENTAL

A series of studies on fluid flow in 2-dimensional PHE's were carried out during the last decade at the Northeastern University, Boston, Mass, USA, e.g.[12]. The experiments involved were based on transparent plastic channels fabricated from polymethylmethacrylate (better known as 'plexiglas' in the USA and 'perspex' in the UK). The plastic plates were prepared by cementing transverse ribs of various shapes (rectangular, triangular, trapezoidal, and semi-cylindrical) on flat sheets. The entrance and exit regions were left flat even though the corresponding metal plates being copied were not flat in these regions.

These models were therefore an approximation to the plates under consideration. They did, however, represent a significant improvement over the previous work of Watson et al.[37] who clamped a flat plastic sheet to a metal plate from a heat exchanger. The Northeastern University workers were the first to attempt a realistic simulation of commercial pressed plates for experimental investigations of PHE's channels.

In the present work investigating hydrodynamic behaviour in the three-dimensional APV Junior PHE it was intended that the plastic model should be as close a copy as possible of the metal plate. The results would then be more representative of a typical channel with the advantage of transparency allowing visual observation during experimental work. Therefore, instead of cementing ribs to flat sheets of perspex, the possibility of producing replicas by casting methyl methacrylate on a metal plate was investigated. Initial attempts to do this failed due to the complexities involved and the difficulty of obtaining suitable technical information. A different approach involving softening perspex slabs by heating in a press while in contact with a metal plate was partially successful.

Transparent plates of the same shape as the metal plates were produced but the depth of the corrugations was smaller than the commercial plates. Nevertheless, these plates proved useful in setting up the apparatus and establishing some familiarity with the experimental procedures.

It became apparent that a good replica of the metal plate would only be produced by casting perspex from a liquid form at low temperature. The former would ensure perfect following of the shape of the mould while the latter would minimise shrinkage during curing. The necessary expertise was eventually discovered at Stanley Plastics Ltd., Hambrook, Chichester where plastic reproductions were obtained with a depth of corrugation of 0.08432 inch. This is 2.1% smaller than the 0.08613 inch measured with the vertical pattern of a Microptic Measuring Machine on the metal plates. It is unlikely that a more accurate replica could be obtained in a transparent material. Fig.3.1 shows a metal plate alongside the perspex replica.

The model channel formed from plastic replicas in the present work is considered to have the following advantages:

a) Since the replicas are identical in shape and very similar in dimensions compared to the metal plates, the flow behaviour through the model channel should be similar to that in an actual channel.

b) The transparent nature of the plates allows visual observation of the flow patterns and an immediate indication of the formation of air pockets in any part of the channel. The latter has occasionally given rise to erroneous results when experimenting with metal channels.

c) It is possible to ensure with transparent plates that the tops of the ribs of both plates forming the channel are in contact under all conditions of flow.

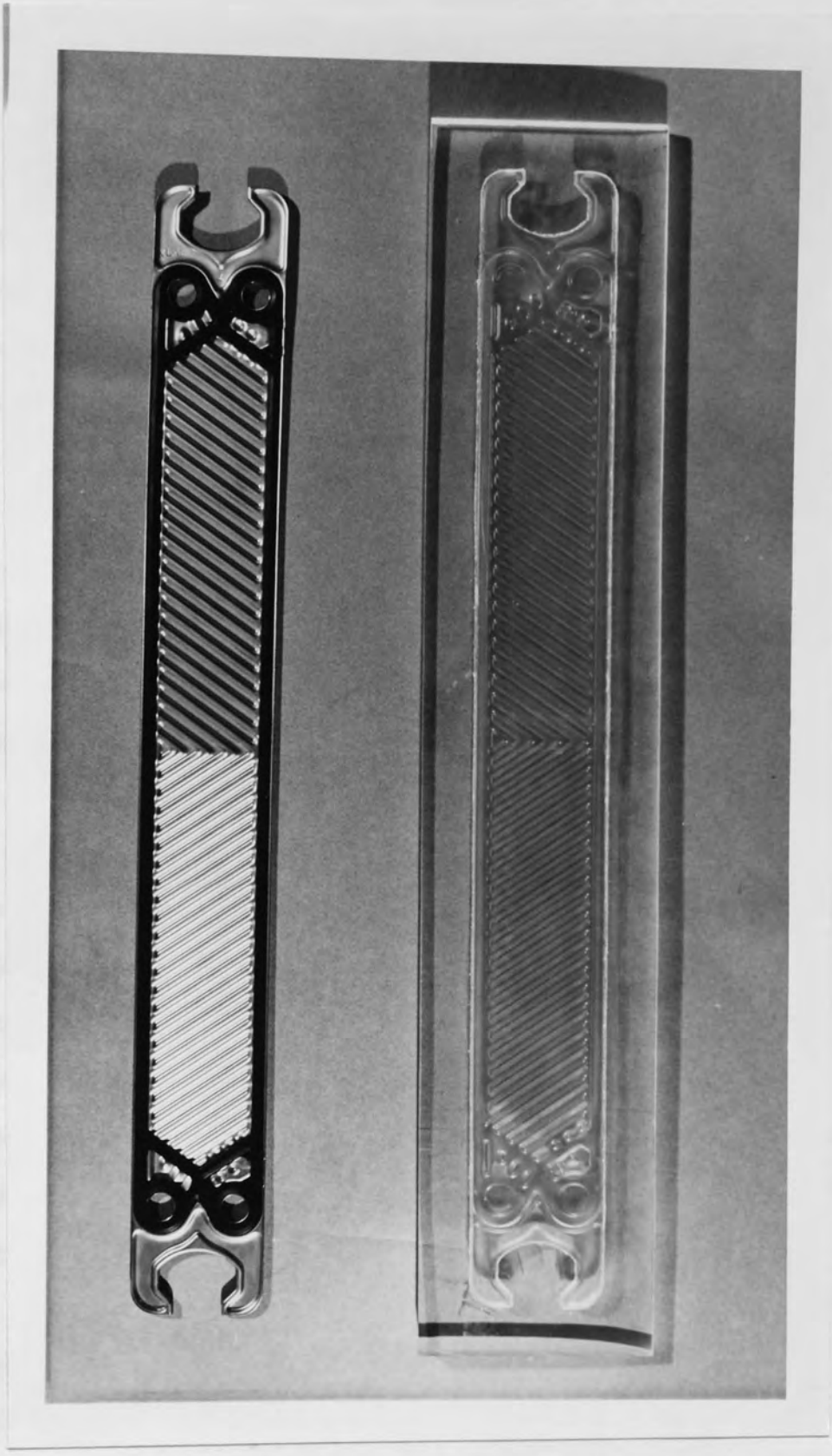

Fig. 3.1 — Metal Plate & Perspex Replica

In order to form a channel, the two perspex plates must be 'positive' and 'negative' reproductions, i.e. they are made by casting on the two opposite sides of a metal plate. Overall dimensions of the plastic moulding are 63 × 12 cm with a minimum thickness of 1.27 cm. The metal plates measure 57.8 × 7 cm. This leaves a 2.5 cm margin around the perspex plates. These margins were utilised in joining the plastic plates by drilling 10 holes of 6.35 mm diameter to accommodate bolts. Relatively large diameter washers were used, on both sides, in conjunction with the bolts and nuts to spread the sealing load. At the outset, more complicated methods were envisaged, e.g. steel grids. However, they proved unnecessary with respect to achieving contact between the plates and would have impeded flow visualization.

The gasket used with the metal plates was utilised along with the plastic plates to establish the "standard channel" representing a channel of an actual pack of plates. Thicker gaskets were obtained, and fitted, to increase the gap between plates so that there was no longer any contact between the plates. These neoprene gaskets were similar in every respect to the original gaskets apart from the thickness which was 3.175 mm for the 'Gap 1' channel and 4.7625 mm for the 'Gap 2' channel. The three respective gaskets are shown in Fig.3.2.

When assembling a channel, care was taken to tighten the bolts to similar stresses. In the case of Gap 1 or Gap 2 channels, when there was no contact between the plates, overtightening or unbalanced stresses could cause one of the mouldings to crack. This problem is non-existent in the case of the standard channel since the many points of contact act to spread the load supporting the two plates against each other. Indeed, this fact was one of the means by which the plates of the standard channel were ensured to be in contact. It was also possible to check the contact visually.

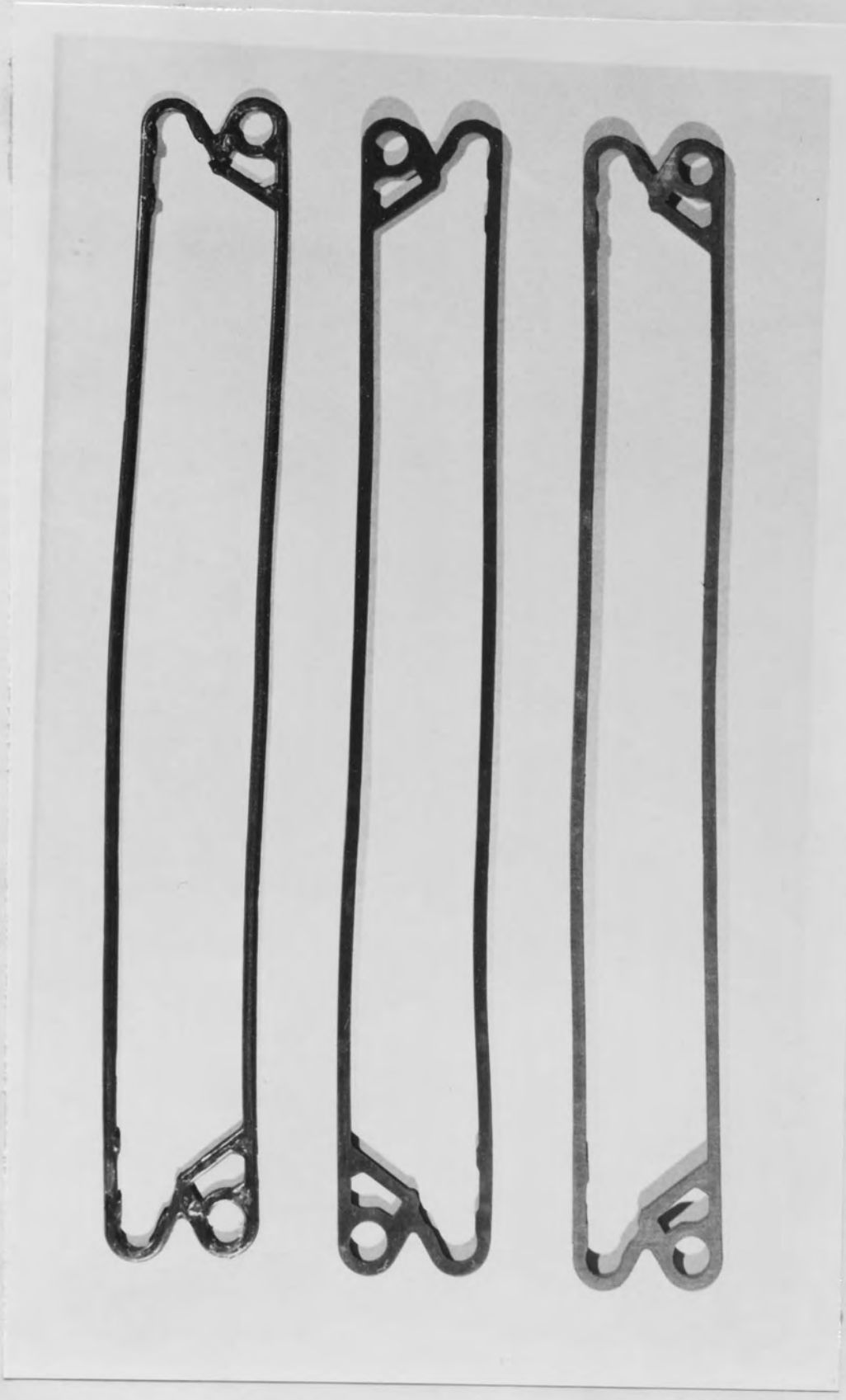

Fig. 3.2 — Original & 'New' Gaskets

The inlet and outlet ports are 15.875 mm in diameter and the perspex sections of the inlet and outlet pipes in contact with the channel, have an O.D. of 22.225 mm. These pipe sections were secured to the channel and to perspex flanges, at the other end, by 'perspex cement no.7'. Earlier attempts to apply the simpler 'perspex cement no.6' produced leaks. The no.6 cement is perspex (polymethylmethacrylate) dissolved in the monomer (methylmethacrylate) which sets by evaporation of the latter, whereas the no.7 cement involves polymerization of the monomer by adding a catalyst then applying the polymer when it is still soft resulting in welds of higher mechanical strengths.

The geometrical characteristics of the 3-dimensional standard channel are illustrated in Fig.3.3. If one of the plates is rotated by 180° the corrugations become parallel or interlocking, instead of crossing each other, resulting in a 2-dimensional channel with no contact between the plates. The equivalent diameters of the 3-dimensional and 2-dimensional channels would be the same if their volumes were equal. This was achieved and the 2-dimensional channel referred to as the "parallel pattern", with which only the original gasket was involved.

Fig.3.4 shows a diagram of the experimental rig. The set-up was flexible for reasons which will become evident, and the dashed lines enclose parts which were subjected to frequent changes. The diagram features UP-Flow in the channel; DOWN-Flow was also investigated in all the channels under consideration. The delivery of the Stuart Turner no.12 centrifugal pump* fluctuated, albeit insignificantly for most purposes. However, because of the sensitivity of pressure drop to flow in the range investigated and the high accuracy required in this work due to disparate results in the past, it was decided to rely on a constant-head tank. Nevertheless the feed pump was used to drive air out of the system or to circulate

---

* GHP 720/150 FT.HD. 10/45 [0.036 hp]

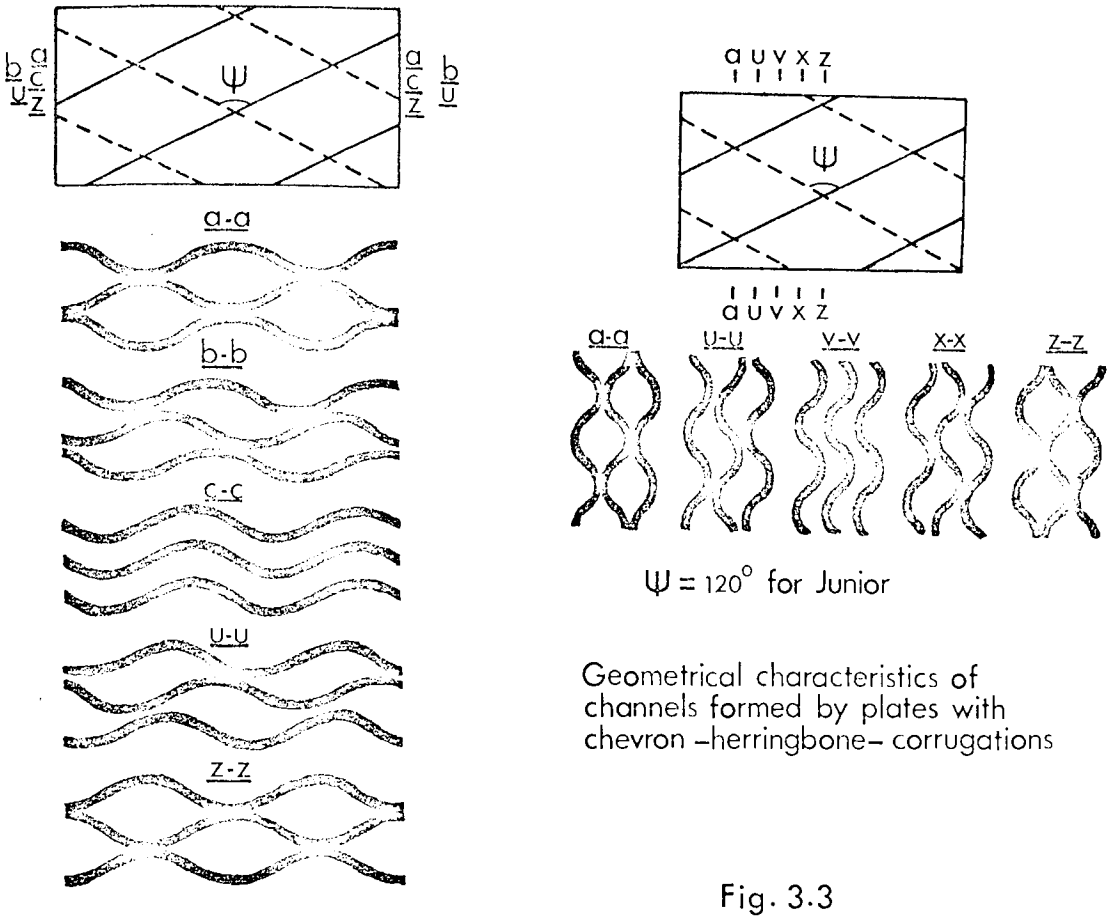

Geometrical characteristics of channels formed by plates with chevron –herringbone– corrugations

Fig. 3.3

the fluid when mixing was required. The differential pressure instruments were usually isolated before operating the feed pump. Physical limitations determined the available head,e.g. the height of the laboratory. To obtain maximum advantage from the available head it was decided to minimize energy losses in conduits leading to the channel. Another factor was that the fluid flow profile should be reasonably developed before entering the channel. The complexity of a permanent arrangement taking into account both UP-Flow and DOWN-Flow would unduly increase the resistance and substantial pipe lengths would be required to develop the flow. 15.875 mm 'QVF' pipes and fittings were mainly used in the set-up and flexible PVC tubes were introduced wherever necessary. The inlet and outlet pipe sections were arranged in a way making the replacement of one by the other an easy and quick task whenever it

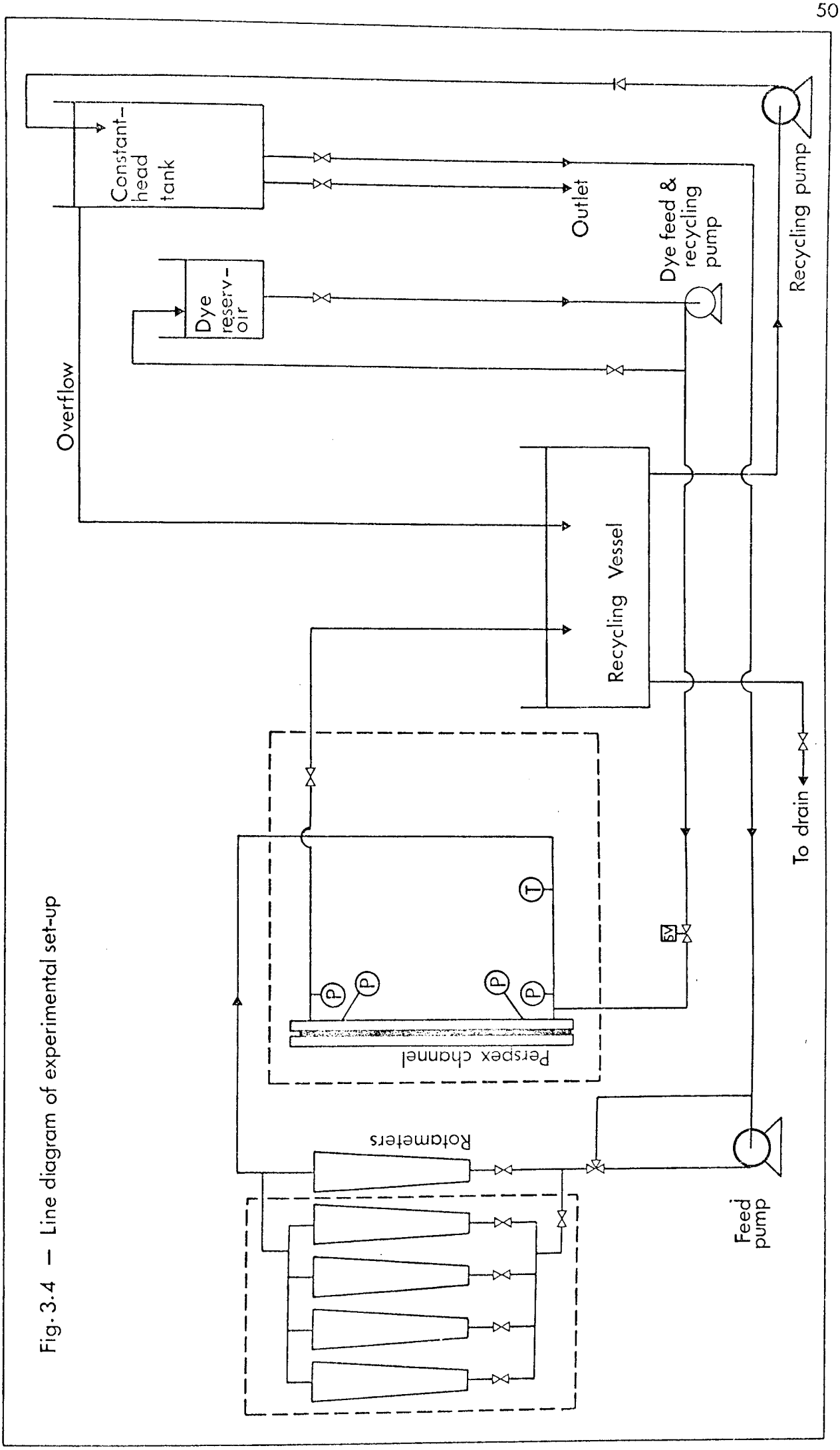

Fig. 3.4 — Line diagram of experimental set-up

was desired to reverse the direction of flow.

Flow rates of water were measured by various combinations of the 'Rotameter Manufacturing Co.' no.10 and no.7 rotameters. The no.10 rotameter with stainless steel float indicates a maximum flow rate of water of 2.0 litres/min and a minimum of 0.2 litres/min, whereas a ceramic float would render the maximum 0.9 litres/min and the minimum 0.075 litres/min. The maximum rate of water flow encountered was 7.955 litres/min in conjunction with the Gap 2 channel corresponding to a Re of nearly 5000. This rate was handled by 4 no.10 rotameters with ss floats. The no.7 rotameter measures a minimum of 0.04 litres/min and a maximum of 0.4 litres/min with a ceramic float, increasing to 0.1 litres/min and 1.0 litres/min if replaced by an ss float. For the four aqueous glycerol solutions and very low flow rates of water, a 'Fischer & Porter' FP-$\frac{1}{2}$-17-G-10 flowrator was used. Three different floats were employed namely: $\frac{1}{2}$-GUSVT-410, $\frac{1}{2}$-GSVT-45-A, and $\frac{1}{2}$-GSVT-44-A having viscosity immunity ceilings (VIC) of 2.2, 5.1, and 7.1 respectively. The flowrator is unaffected by viscosity if the ratio of the operating viscosity in centipoises to the square root of the density in g/cc is less than the float VIC. The flowrator was calibrated by direct weighing of effluent whenever the float or the system was changed. At low rates of flow the flowrator calibration becomes discontinuous. For such rates and lower, when the flowrator becomes out of range, the specific rate was determined by direct weighing of effluent at the same time the corresponding differential pressure measurement was recorded.

The use of viscosity-immune floats was thought to be simpler and cheaper than the alternative of maintaining the system at a constant temperature. A mercury-in-glass thermometer with 0.1°C divisions was used to indicate the temperature of the fluid

prior to it entering the channel.

Needle valves were used whenever fine control of the flow was necessary e.g. before the rotameters. In order to prevent air from getting into the system at low rates, back pressure was applied by a valve downstream in the channel outlet pipe. A solenoid valve was incorporated into the dye circuit in order to supply pulses of dye which was administered through a hypodermic tube. The most suitable dye for flow visualization proved to be methyl-soluble-blue.

All the vessels were assembled from standard 'QVF' pipe sections, hemispheres, and reducers. An overall picture of the experimental set-up could be seen in Fig.'s 3.5 and 3.6.

Apart from distilled water, the four aqueous glycerol solutions used in the experiments had the physical properties shown in Table 3-I.

Percentage Glycerol W/W	Dynamic Viscosity at 20°C; cp.	Density at 20°C g/mℓ
30.15	2.5152	1.0712
41.95 - 42.10	4.09655 - 4.1261	1.1026 - 1.1030
50.45	6.206	1.1255
65.45	16.08	1.16667

TABLE 3-I

Aqueous glycerol was chosen on three accounts. It is one of the most extensively examined systems and its physical properties are widely reported in the literature. It is chemically safe to use with respect to the perspex channel and experimental rig, and the operator. An organic chemical was available, to be used as manometer fluid, reasonably inexpensive, totally immiscible with the system, having a density fairly close to those of the aqueous glycerol solutions, and not prohibitively dangerous to handle.

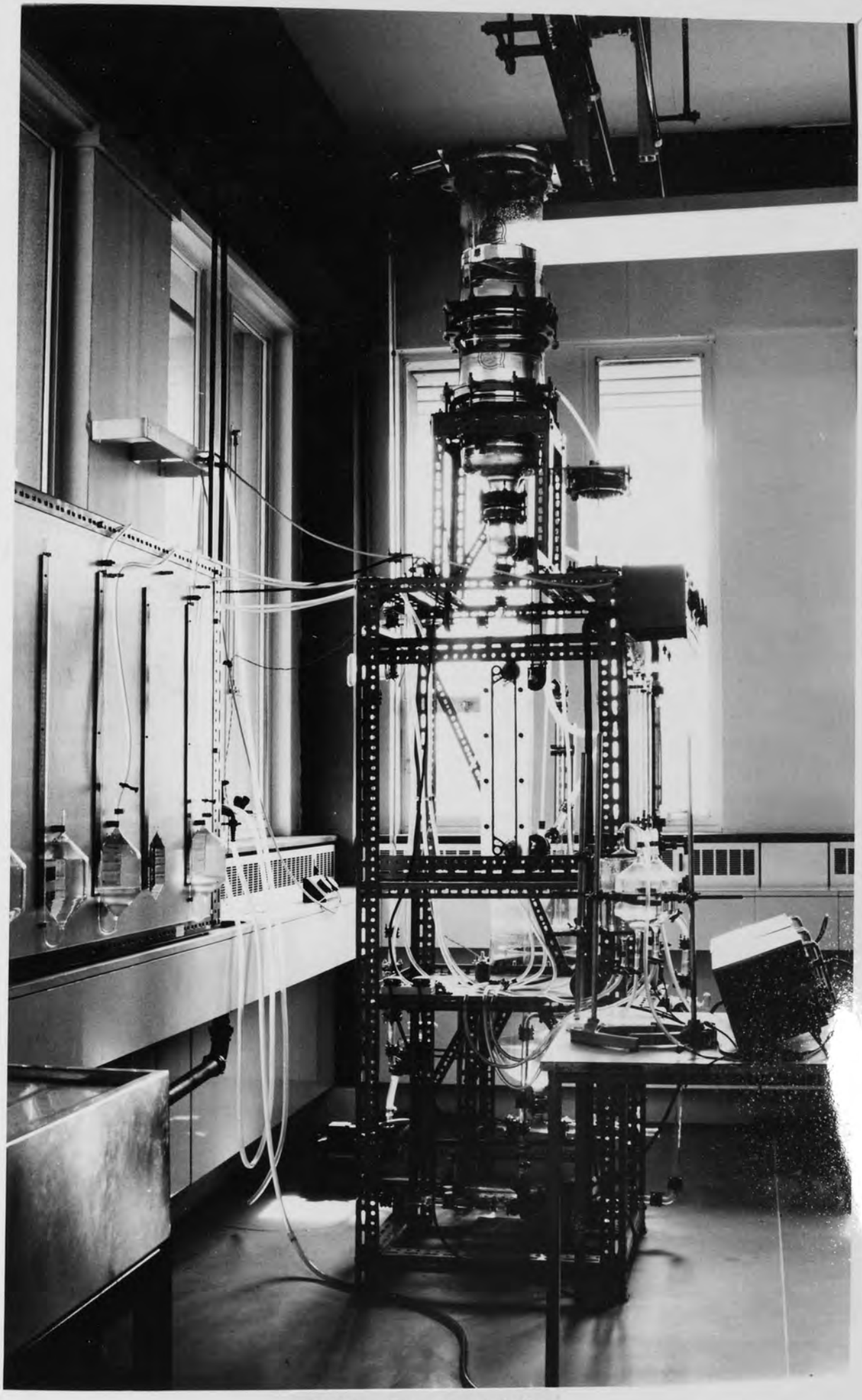

Fig. 3.5 — Experimental Rig

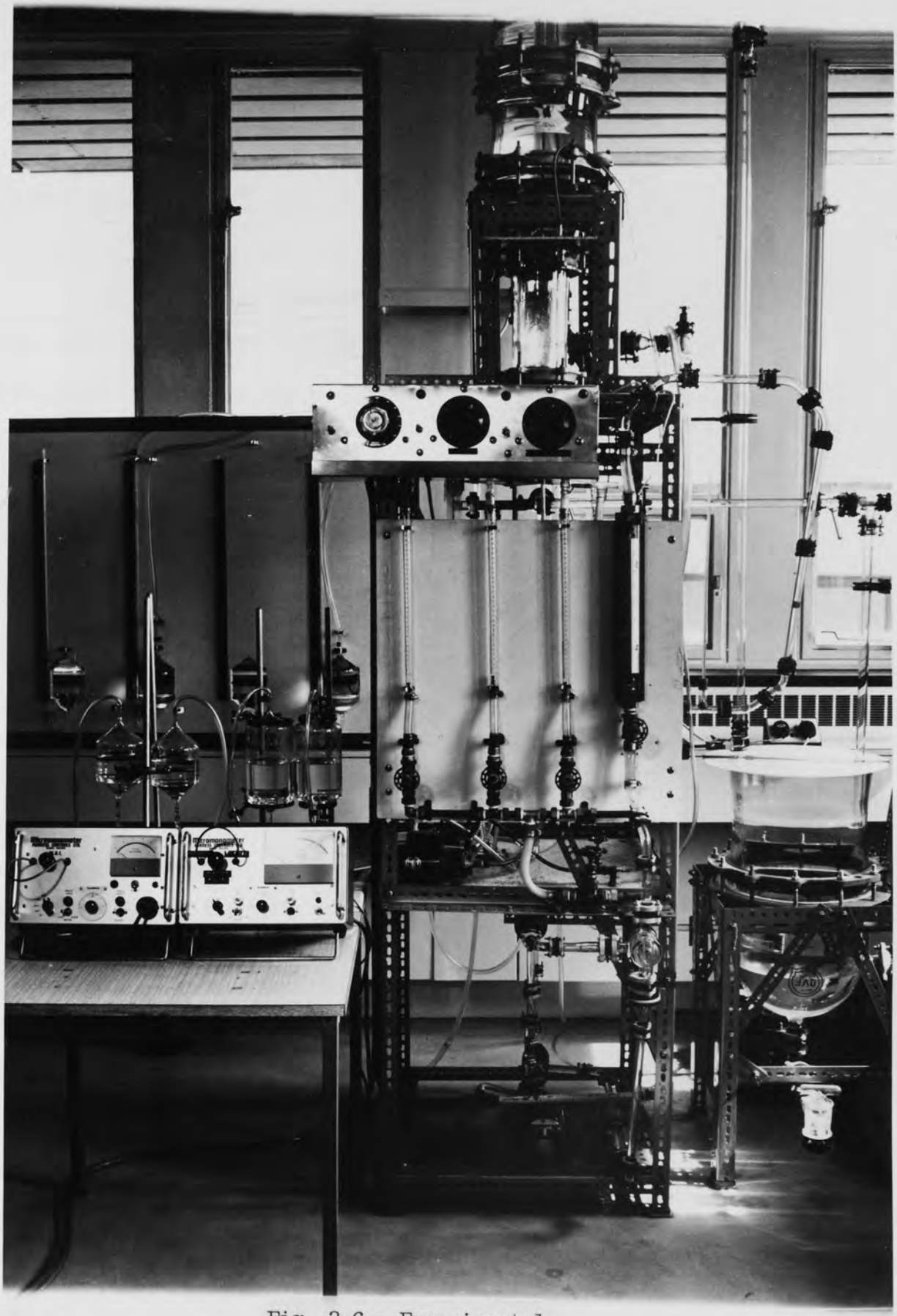

Fig. 3.6 - Experimental Rig

As far as this work is concerned, glycerol has one disadvantage, the fact that it is hygroscopic. However, this property becomes less significant as the concentration of glycerol in the solution decreases. On the other hand the evaporation of water gains significance as the solution is diluted. In fact these phenomena could cancel the effects of each other establishing equilibrium if the correct humidity is prevalent.

Chemically pure, highly concentrated, glycerol (ca. 99% W/W) and distilled water were used to prepare the desired solutions. After introducing a particular solution into the set-up it was further mixed for total consistency by operating the feed and recycling circuits. All the pumps were controlled through variable transformers (Variacs). Physical analyses were carried out on samples drawn from different locations in the rig . During such operations the differential pressure instruments were disconnected.

The two physical properties determined were primarily refractive index and secondarily density. Both properties were utilized to establish and check the concentrations of the different glycerol solutions from data available in the literature. Periodic refractive index measurements were conducted to detect changes in the concentration of any particular solution during the period of experimentation. Hence, the importance of an accurate determination of the refractive index cannot be over stressed. An 'ABBE 60' high accuracy refractometer was employed. This instrument indicates the refractive index value to five figures after the decimal point while the literature quotes four. Prior to each measurement the instrument was checked using freshly prepared distilled water. It was maintained at 20°C by a heating/cooling system. Accurate determination of the density was achieved by ensuring that the volume of the density bottle was at least 25 $m\ell$[11].

Viscosities were not measured through the use of visco-

meters, rather they were determined from the literature after the exact concentrations were established. It was thought that standard values would be more meaningful since density and refractive index are considerably easier to measure accurately than viscosity. Variation of viscosity with temperature was always taken into account. Since aqueous glycerol solutions viscosity data are available from 20°C to 30°C it is advisable to operate within this range, and in this work the temperature was either 20°C or slightly higher.

Fig.3.7 shows a diagram of the differential pressure measuring instruments, depicting UP-Flow situation. As can be seen there are four pressure tappings. Those at the inlet and exit pipes are about 6 cm away from the channel and consist of 3.797 mm ID stainless steel piezometer tubes. The other two are situated along the vertical centre line of the channel at the two points where the width available to flow ceases to be constant and starts narrowing. Each consist of 3.175 mm ID perspex tubes, and was made by drilling a 3.175 mm hole through the thickness of one perspex plate to the bottom of a valley on the corrugated side. A larger hole of 15.525 mm diameter was drilled half-way through the thickness of the plate starting from the flat side, to accommodate the perspex tube. Perspex cement no.7 was finally applied to secure the tube in position. This tapping is illustrated in Fig.3.8. That part of the channel between these two tappings is designated 'ribbed section' or simply 'ribs'. The 'entrance' and 'exit' include the 90° sharp turns plus the areas at the two ends of the channel where the width available to flow is variable. The tapping points for pressure drop measurements are indicated in Fig.3.7.

In addition to the instruments depicted, a well type inclined-tube manometer was used. However, satisfactory results

Fig. 3.7 – Schematic diagram of differential pressure measuring instruments

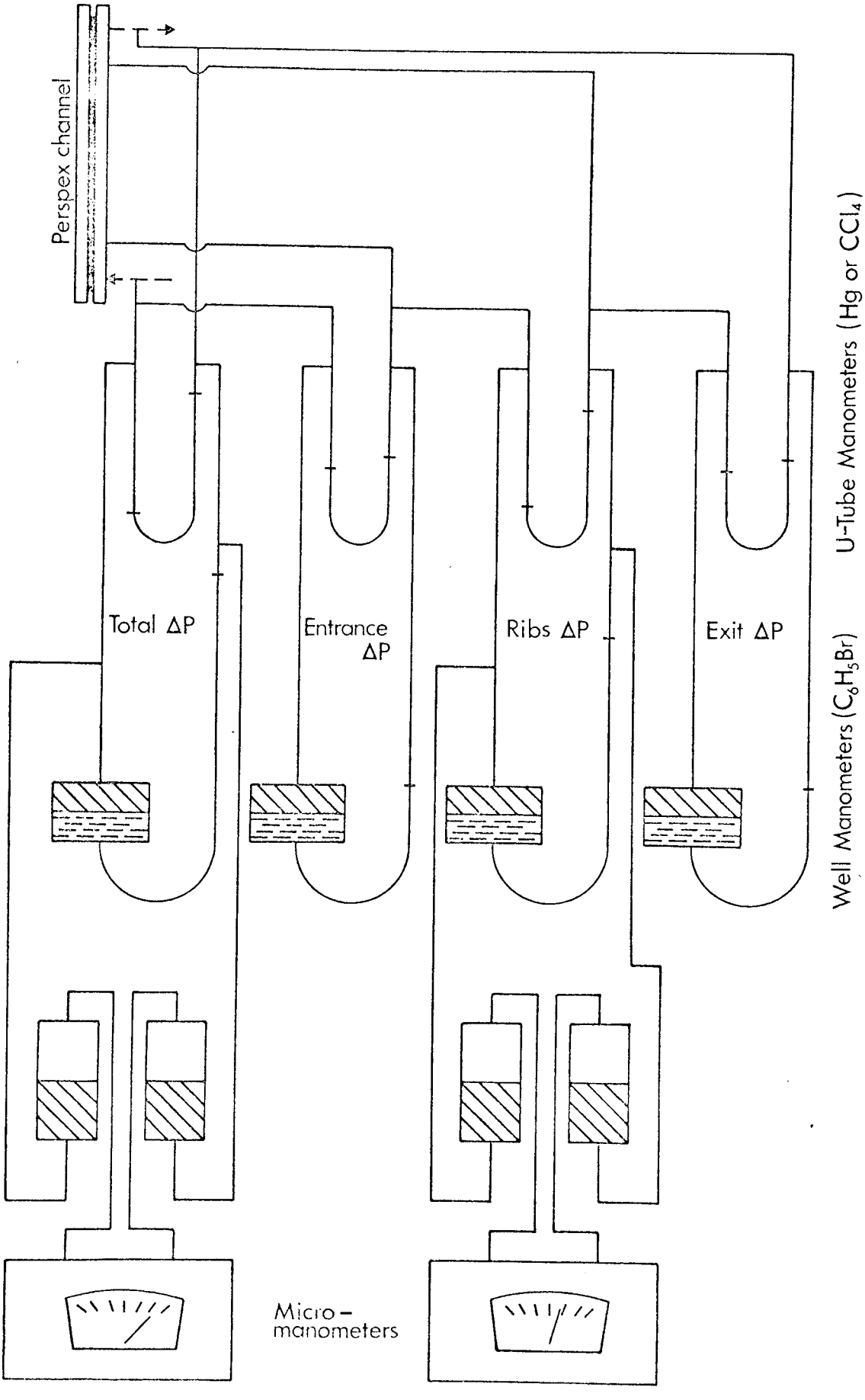

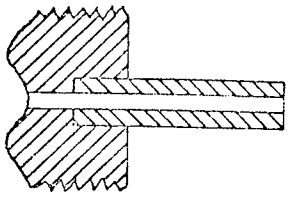

Fig. 3.8

Sectional-view of channel pressure tapping

were not obtained due to its peculiar behaviour. Unexpected behaviour was also noticed, under certain conditions, in conjunction with U-tube manometers containing $CC\ell_4$ and well manometers containing $CC\ell_4$ or C_6H_5Br. These aspects are discussed in Appendix A-2.0.

The area of the well in a well manometer should be at least 500 times larger than the area of the vertical leg in order that the change in the well fluid level becomes negligible[19]. Hence, only the change in the vertical leg fluid level need be considered when measuring the pressure drop.

$CC\ell_4$ has a specific gravity of 1.595 whereas that of C_6H_5Br is 1.495. Technical dyes, in very small quantities, were used to colour them since both are colourless. These were azobenzene and 4-O-Tolylazo-O-toluidine 2-Naphthol respectively. Bromobenzene was chosen because it is completely immiscible with aqueous glycerol, it must be pointed out that care should be taken in handling it for its vapour is quite harmful. The fact that both bromobenzene and carbon tetrachloride attack perspex chemically necessitated the use of a system of traps to protect the channel.

The two micromanometers employed were the 'MDC' type manufactured by 'Furness Controls Ltd.'. Because they were designed

to measure gas differential pressure, therefore a system of reservoirs based on Benedini's technique[9] had to be introduced to render them suitable for liquid differential pressure as seen in Fig.3.7. The MDC micromanometer has 5 ranges with a maximum of 100 mm Wg (981 N/m^2) at full scale deflection (FSD). The lowest range indicates a maximum of 1.0 mm Wg (9.81 N/m^2) at FSD. Since the scale has 100 divisions it is possible to measure pressure drops of the order of 0.01 mm Wg.

The measuring head of the MDC micromanometer consists of two symmetrically arranged cavities separated by a taught metal diaphragm. This diaphragm, together with a fixed electrode on either side, forms two capacitors which are part of the tuning capacities of two tuned circuits, both equally coupled to an R.F. oscillator. Movement of the diaphragm causes a variation in the capacitance between it and each adjacent electrode, thus unbalancing the voltage across the tuned circuits. These voltages are compared by a differential voltmeter, and the difference is amplified and is shown on a meter calibrated directly in pressure. Calibrations of the micromanometers were mechanical, done prior to experimentation.

There was considerable overlapping among the ranges of the different manometers which served as a check and made error analysis feasible. These aspects are considered in the Appendix.

Flexible and transparent PVC tubing (6.35 mm) was used as pressure leads. 'Union'-clips were employed to secure the PVC tubing to manometers, glass T-pieces, and pressure tappings. Screw-clips were extensively used with the PVC lines to isolate manometers.

The procedure for the operation of the rig was as follows:

(i) Having isolated the manometers, leakage in the channel was checked by putting the feed pump on maximum power. The key

(i) contd.

to the leakage problem was the proper fitting of the gasket and the application of equal stresses on the bolts. The best adhesive for fixing the gasket proved to be that supplied by the plate manufacturer (The APV Co.). A thin layer of it should be applied to the gasket groove. All adhesives contain chemicals which are likely to affect perspex in varying degrees, therefore care should be taken to confine it to the groove and it should be removed mechanically.

(ii) Air was driven out of the system utilising the feed pump.

(iii) The manometers and the pressure leads would then be filled with the consistent system ensuring no air remained.

(iv) With no-flow the manometers were zeroed or their no-flow readings recorded.

(v) The flow was then gradually increased relying on the constant-head tank only. Each manometer reaching its limit would be isolated. When all the manometers had been isolated, flow was increased to the maximum then brought gradually down connecting the different manometers as they came into range. Hence, pressure drop measurements were conducted with the flow increasing as well as with it decreasing. Temperature of fluid entering the channel was recorded before each measurement.

CHAPTER 4

RESULTS

4.0) RESULTS

The definitions of the dimensionless groups, variables, and parameters used in the graphs and empirical formulae are as follows:-

$$Re = \frac{\rho\ De\ u}{\mu} \tag{4.1}$$

$$De = \frac{4 \times \text{Channel Volume}}{\text{Developed Heat Transfer Area}} \tag{4.2}$$

$$u = \frac{\text{Volumetric Flow Rate}}{\text{Area of Flow}} \tag{4.3}$$

$$\text{Area of Flow} = \frac{\text{Channel Volume}}{\text{Channel Developed Length}} \tag{4.4}$$

The channel volume and developed length correspond to the developed heat transfer area. Both the developed length and the developed heat transfer area were quoted by the manufacturers.

The channel volume was determined by filling it with mercury to a certain level, then an exact amount of mercury was added and the apparent change in the level measured. To obtain the developed distance the Hg level travelled, the apparent change was multiplied by the ratio of developed to projected area. By simple proportionality the volume corresponding to the channel developed length was established. Details of this determination are given in Appendix A-3.0.

$$f_t = \frac{\Delta P_t\ De}{2\rho u^2 L} \tag{4.5}$$

$$f_r = \frac{\Delta P_r\ De}{2\rho u^2 L} \tag{4.6}$$

where the subscripts t and r refer to the 'total' and 'ribbed section' respectively; L is the channel developed length. The entrance and exit pressure drops are designated ΔP_{en} and ΔP_{ex} respectively, see Fig.3.7.

4.1) STANDARD CHANNEL

Table 4.I lists the important parameters:

Developed heat transfer area/plate	...	258.064 cm^2
Developed length	...	47.2 cm
Developed/projected area	...	1.18 -
Channel volume	...	49.776 cm^3
Equivalent diameter	...	0.386 cm
Area of flow	...	1.0546 cm^2

[TABLE 4.I]

Fig.'s 4.1 to 4.6 show the experimental data for the ribbed section (allowing for anomalous pressure drops, appendix A-2) for the various systems employed. Fig.4.7 shows the combined results apart from some points at less than Reynolds number of 5 where the extremely low peressure drop caused a high degree of scatter. The following empirical relationships are proposed to describe the data in Fig.4.7:

$$(3 < Re < 300) \qquad f_r = \frac{36.418}{Re} + 0.307 \qquad (4.7)$$

$$(300 \leq Re < 3000) \qquad f_r = 1.770\ Re^{-0.230} \qquad (4.8)$$

Fig.'s 4.8 to 4.15 show the corresponding results for the overall pressure drop including the contribution of the ports. Fig.4.16 is a composite of all the results apart again from some of the water results, at the lower end of the range, which were excluded. The equations best describing the results as seen in Fig.4.16 are as follows:

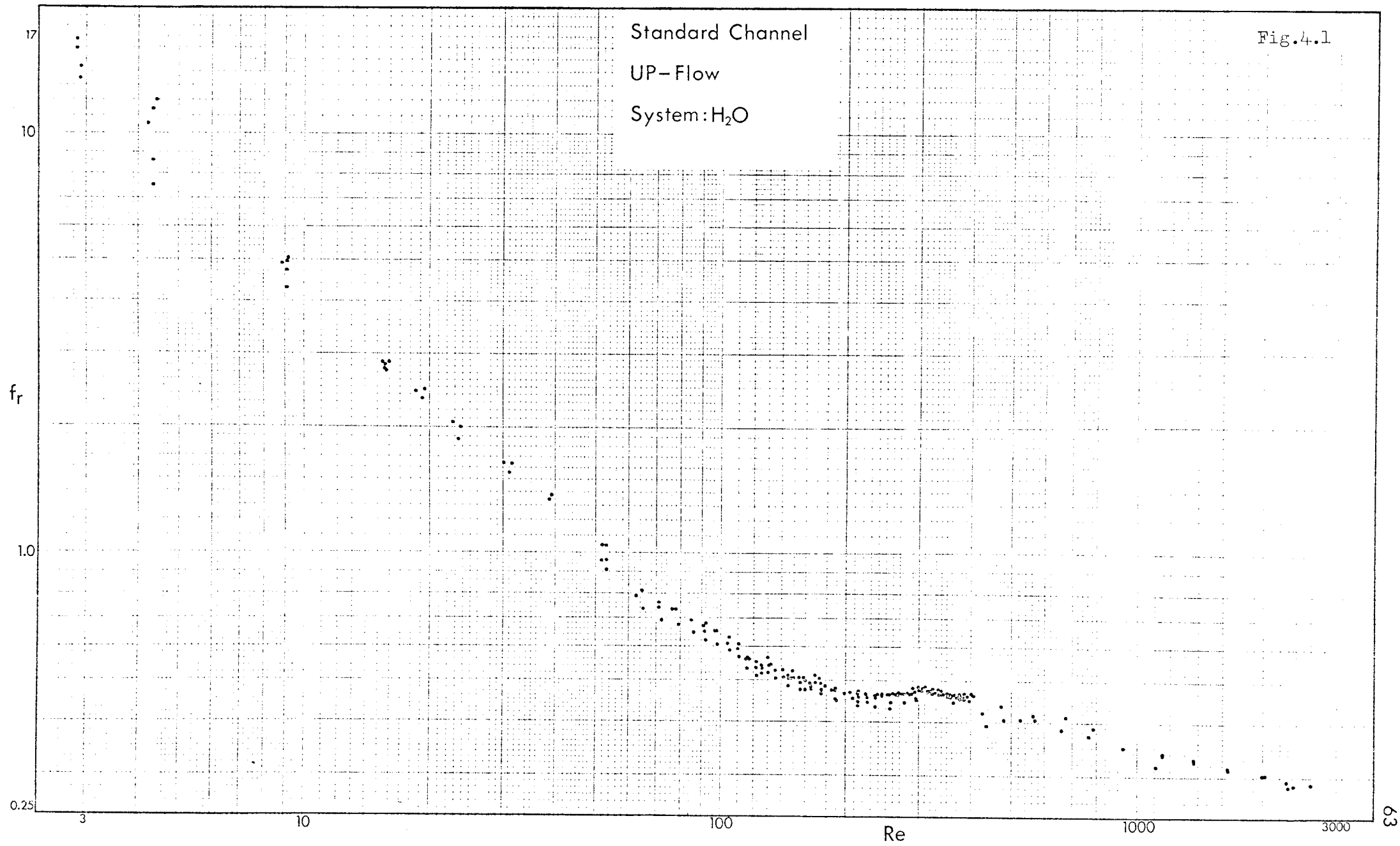
Standard Channel
UP – Flow
System : H_2O
Fig.4.1
17
10
1.0
0.25
f_r
3
10
100
1000
3000
Re

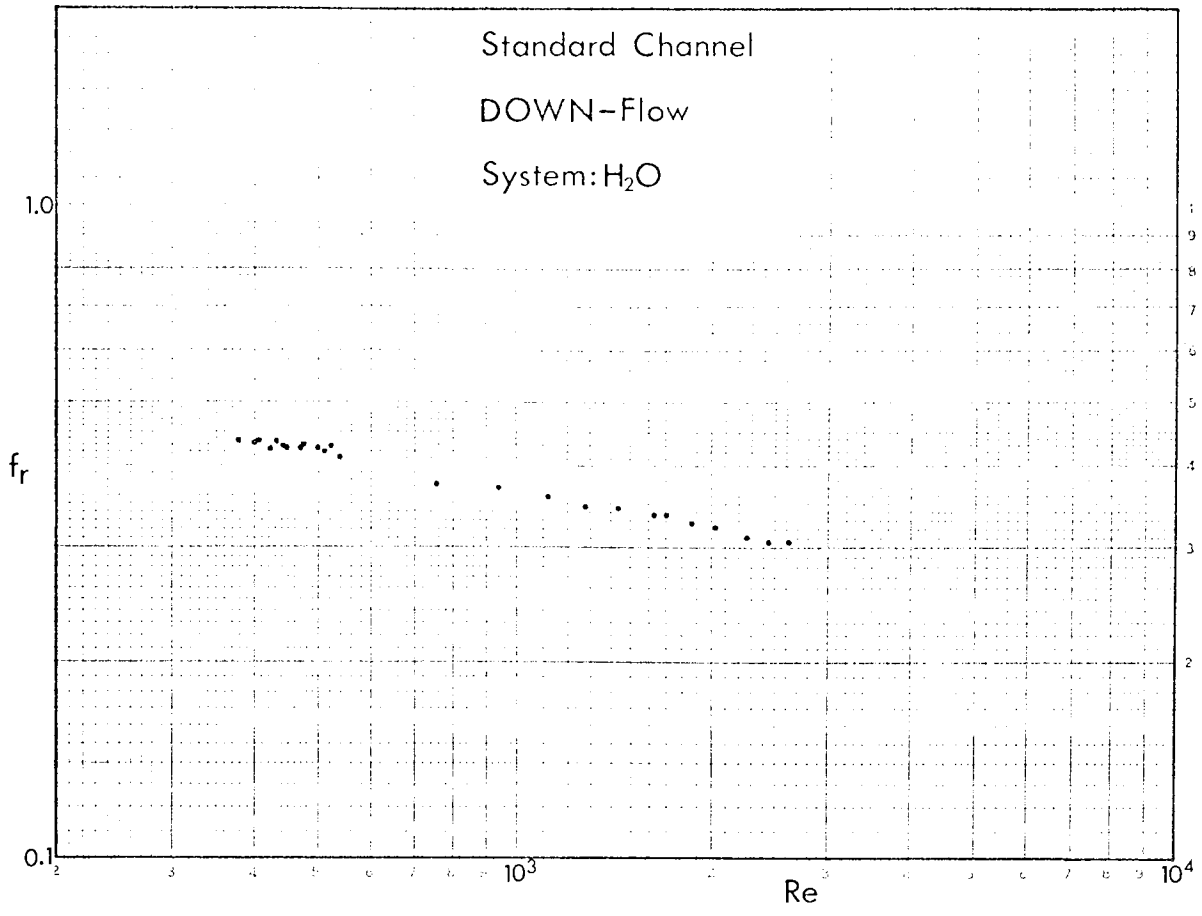

Fig.4.2

$$(3 \leq Re \leq 400) \qquad f_t = \frac{44.139}{Re} + 0.461 \qquad (4.9)$$

$$(400 \leq Re < 3000) \qquad f_t = 1.750\ Re^{-0.196} \qquad (4.10)$$

Fig.4.17 to 4.21 show the contributions of ribbed, entrance and exit sections to the channel total pressure drop. A common legend has been adopted for these figures (Table 4.II):

	Viscosity at 20°C (cp)	Direction of Flow
■	16.1	UP
□	16.1	DOWN
▲	6.2	UP
△	6.2	DOWN
●	4.1	UP
○	4.1	DOWN
◆	2.5	UP
◇	2.5	DOWN
▼	1.0	UP
▽	1.0	DOWN

TABLE 4-II

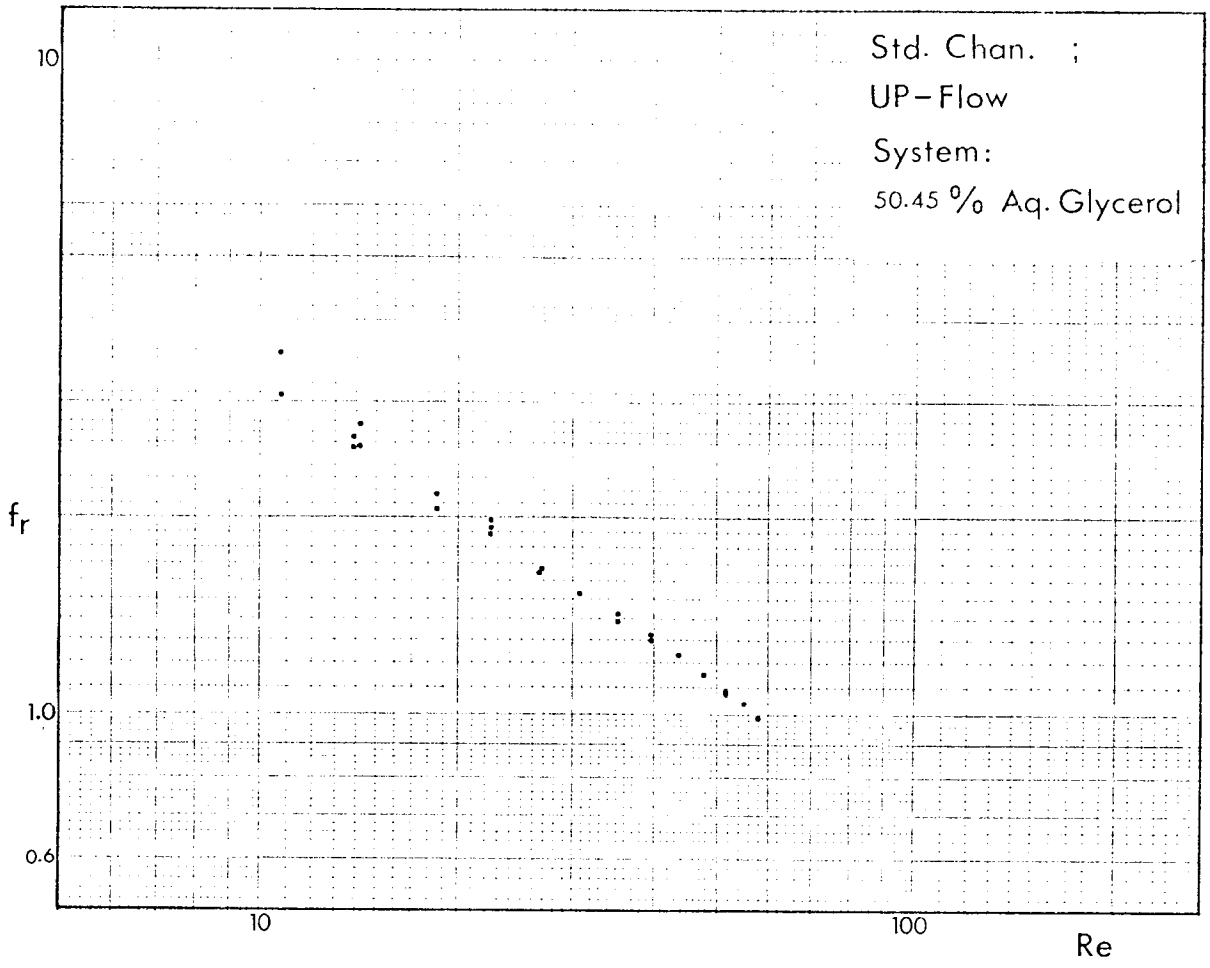
Std. Chan. ;
UP-Flow
System:
50.45 % Aq. Glycerol
10
1.0
0.6
f_r
10
100
Re

Fig.4.3

Fig.4.4

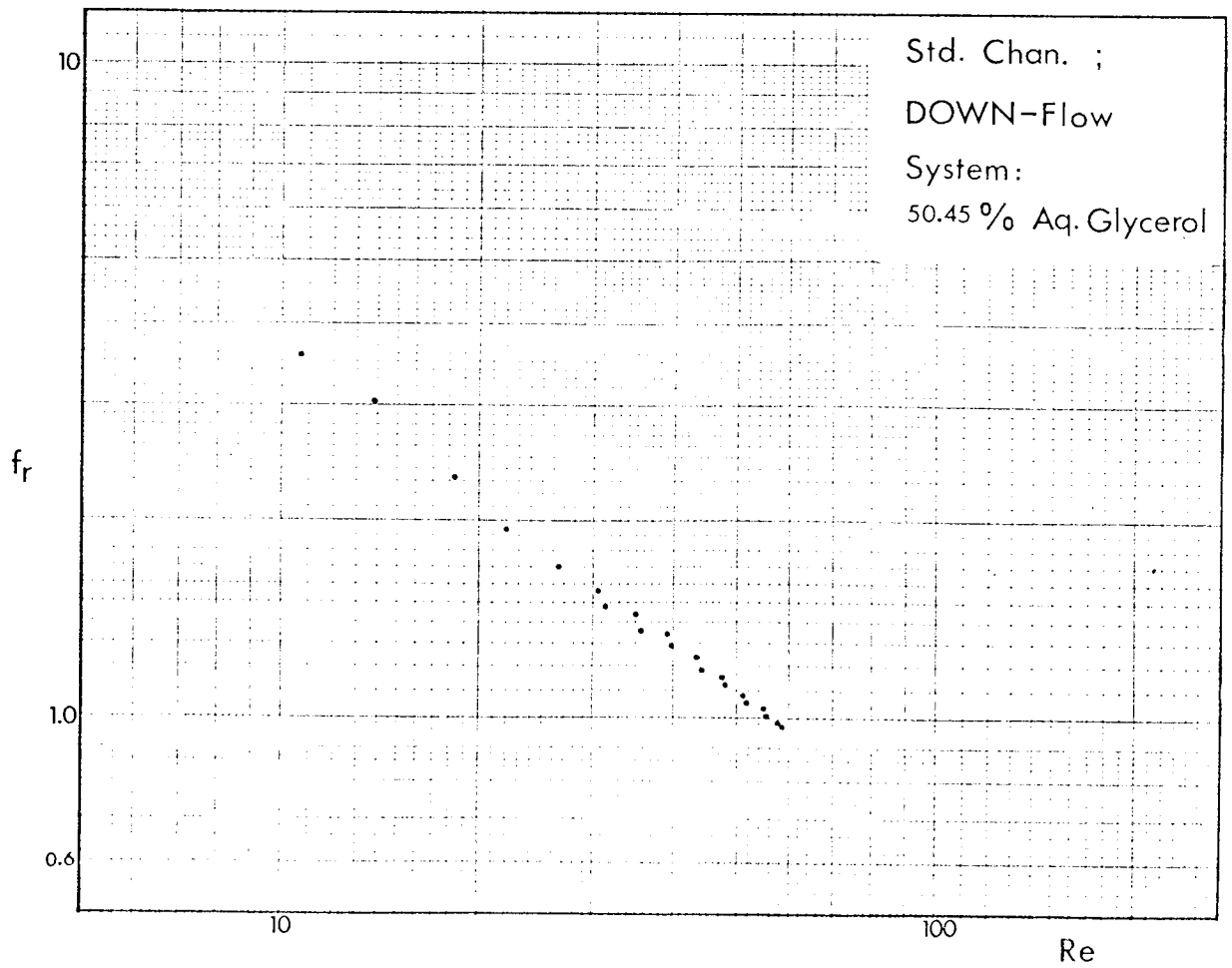
Std. Chan. ;
DOWN-Flow
System:
50.45 % Aq. Glycerol
10
1.0
0.6
f_r
10
100
Re

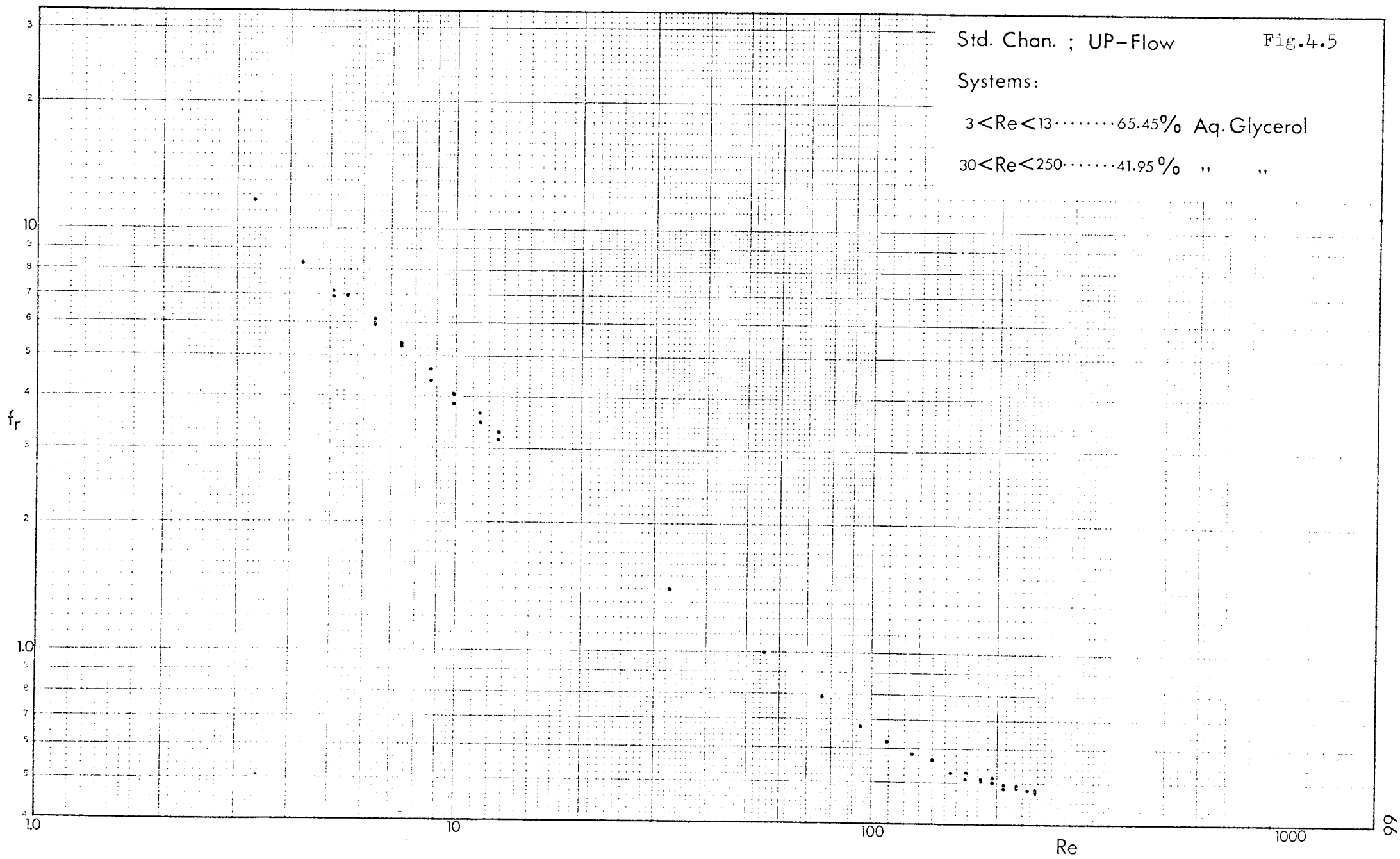
Std. Chan. ; UP-Flow
Fig.4.5
Systems:
3<Re<13·····65.45% Aq. Glycerol
30<Re<250·····41.95% ,, ,,
f_r
Re
1.0
10
100
1000

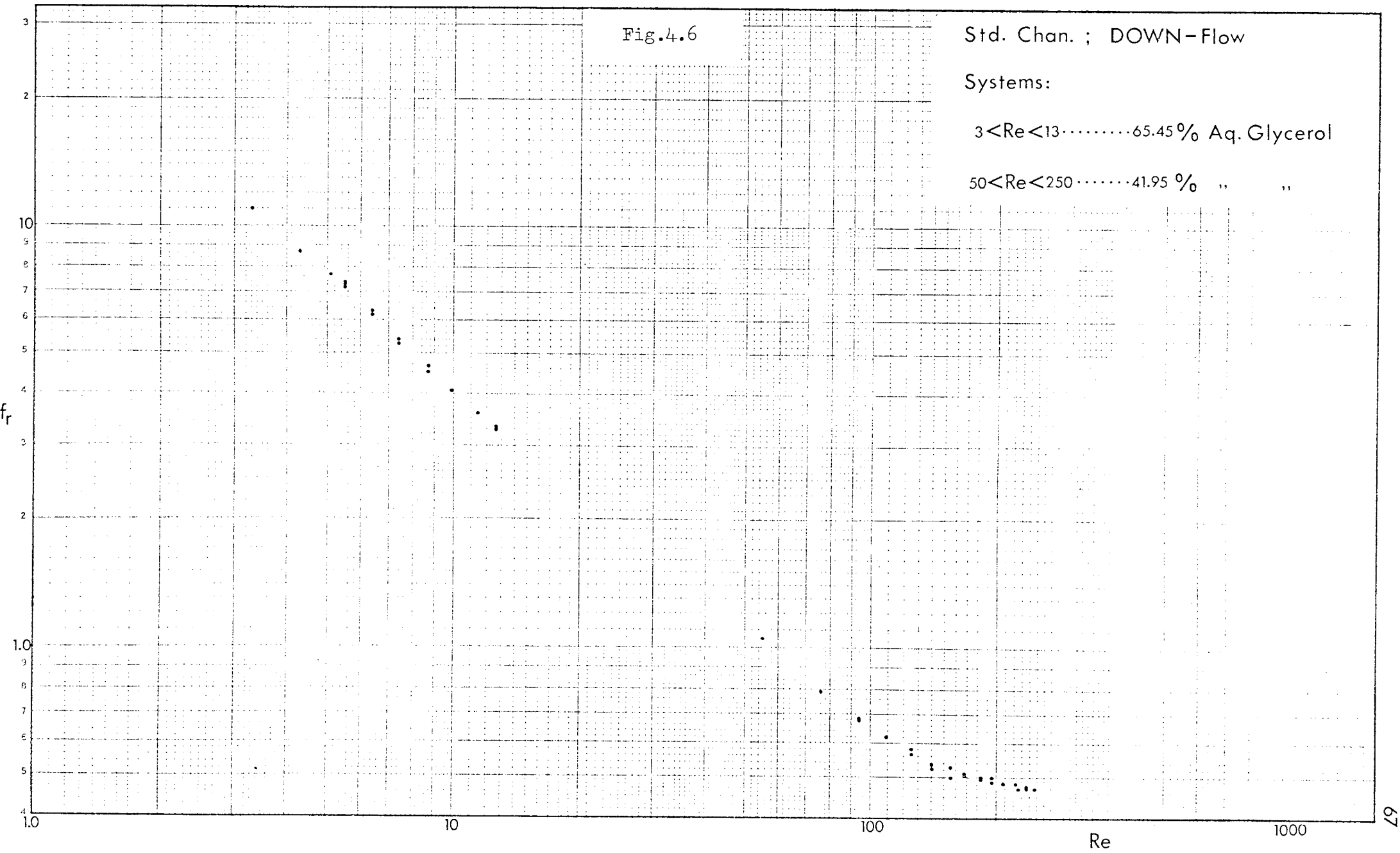
Fig.4.6
Std. Chan. ; DOWN-Flow
Systems:
3<Re<13·····65.45% Aq. Glycerol
50<Re<250·····41.95 % ,, ,,
f_r
Re
1.0
10
100
1000

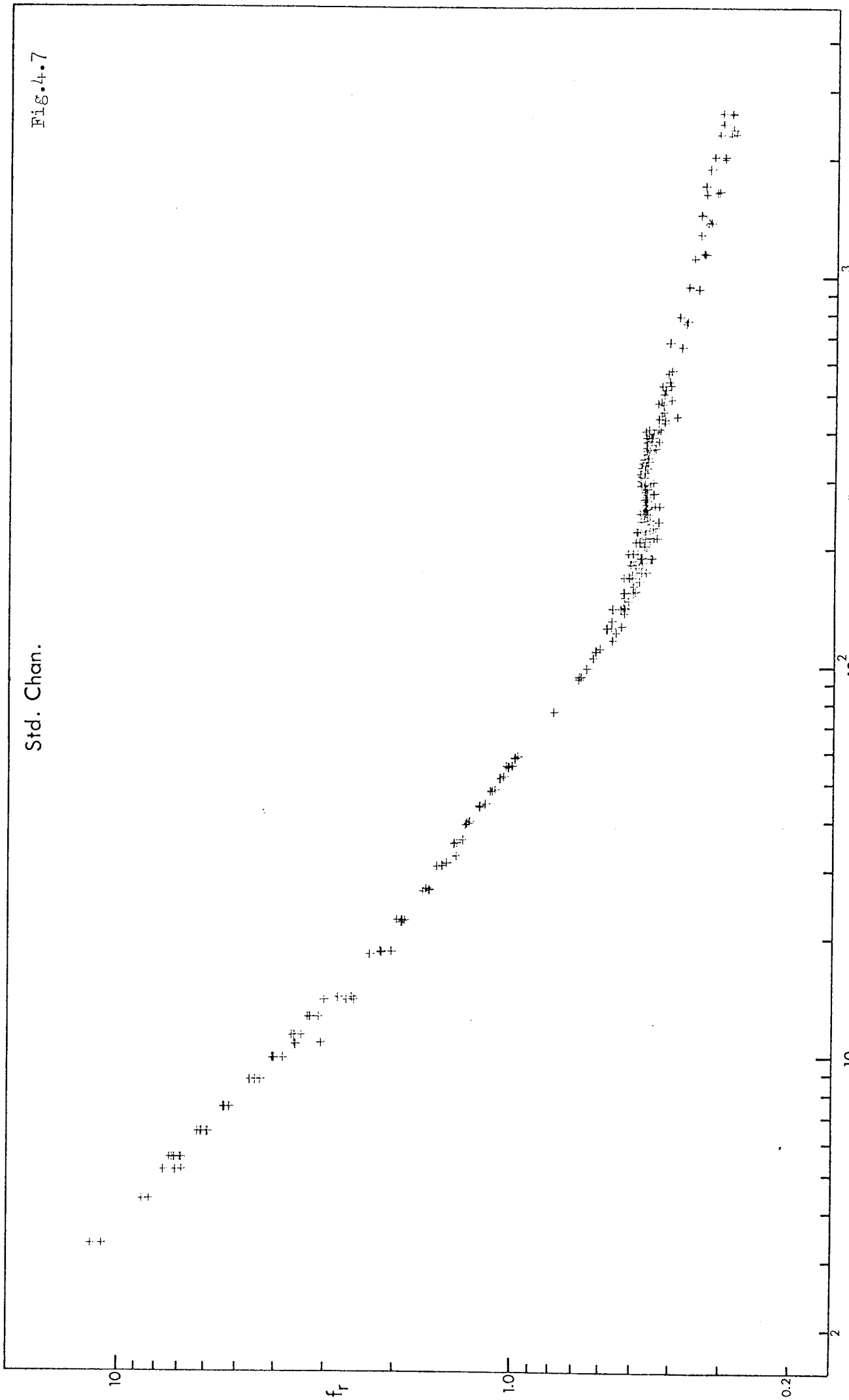

Fig.4.7

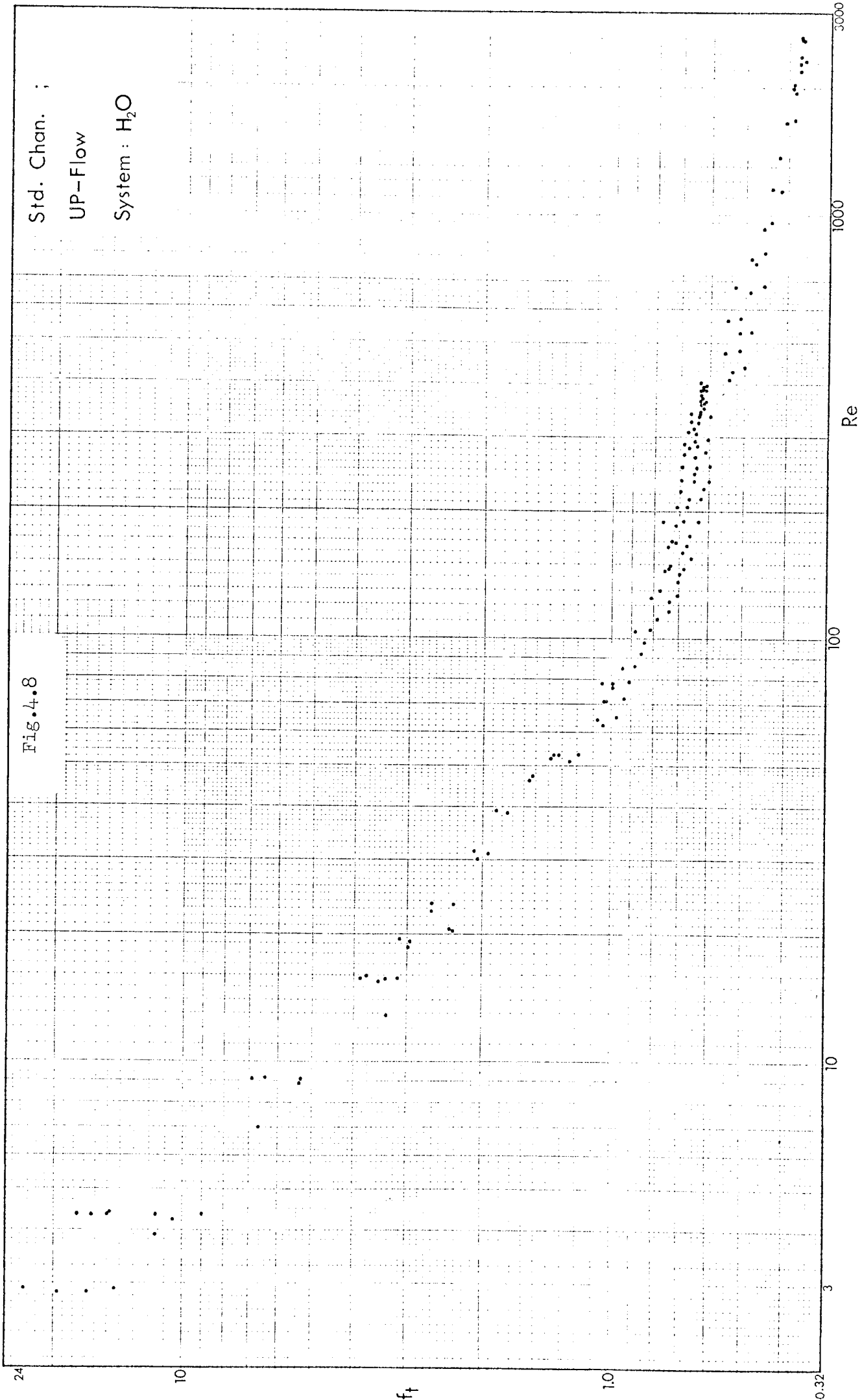
Std. Chan. ;
UP-Flow
System : H_2O
Fig.4.8
24
10
1.0
0.32
f_t
3
10
100
1000
3000
Re

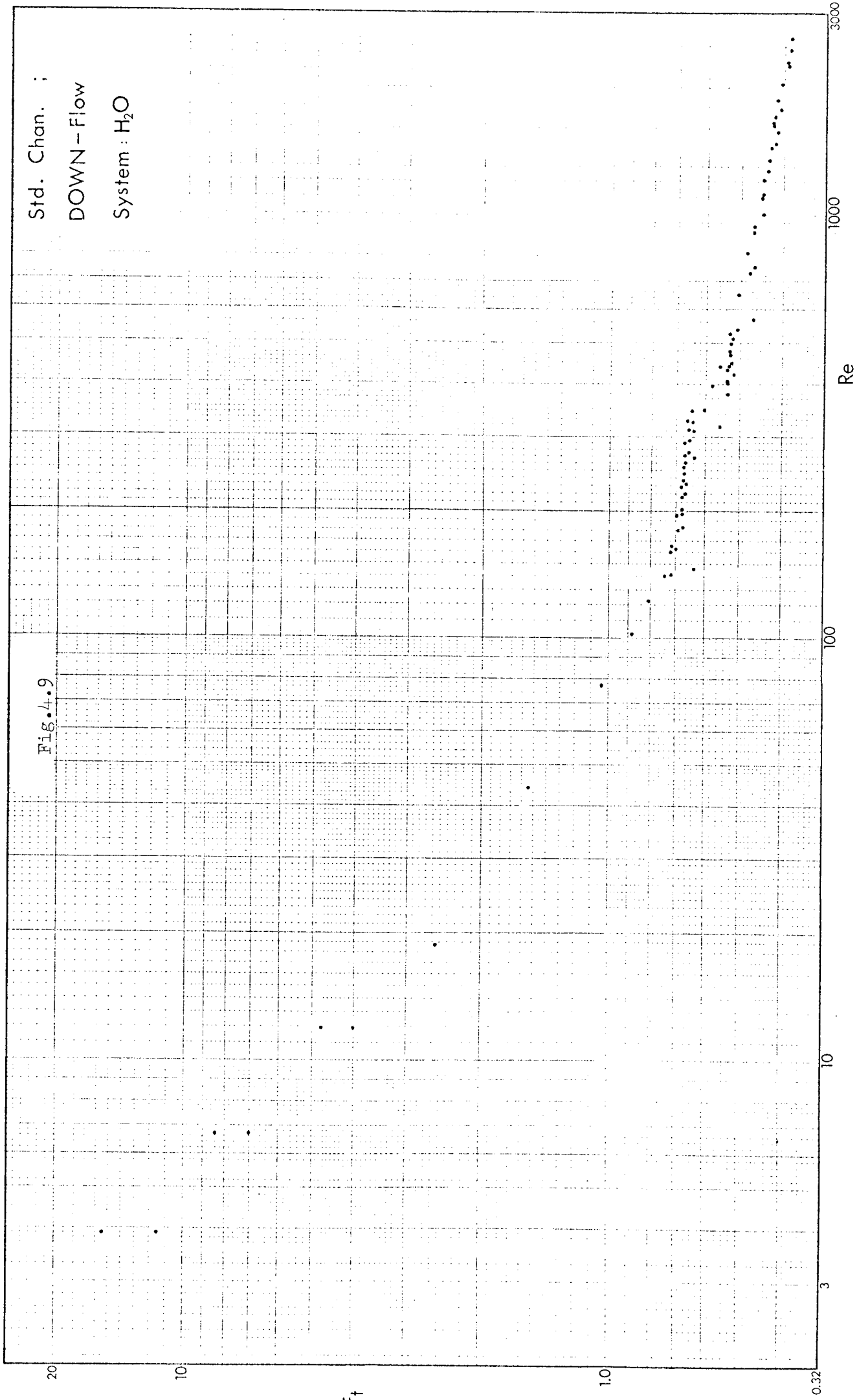
Std. Chan. ;
DOWN - Flow
System : H_2O
Fig. 4.9
20
10
1.0
0.32
3
10
100
1000
3000
Re

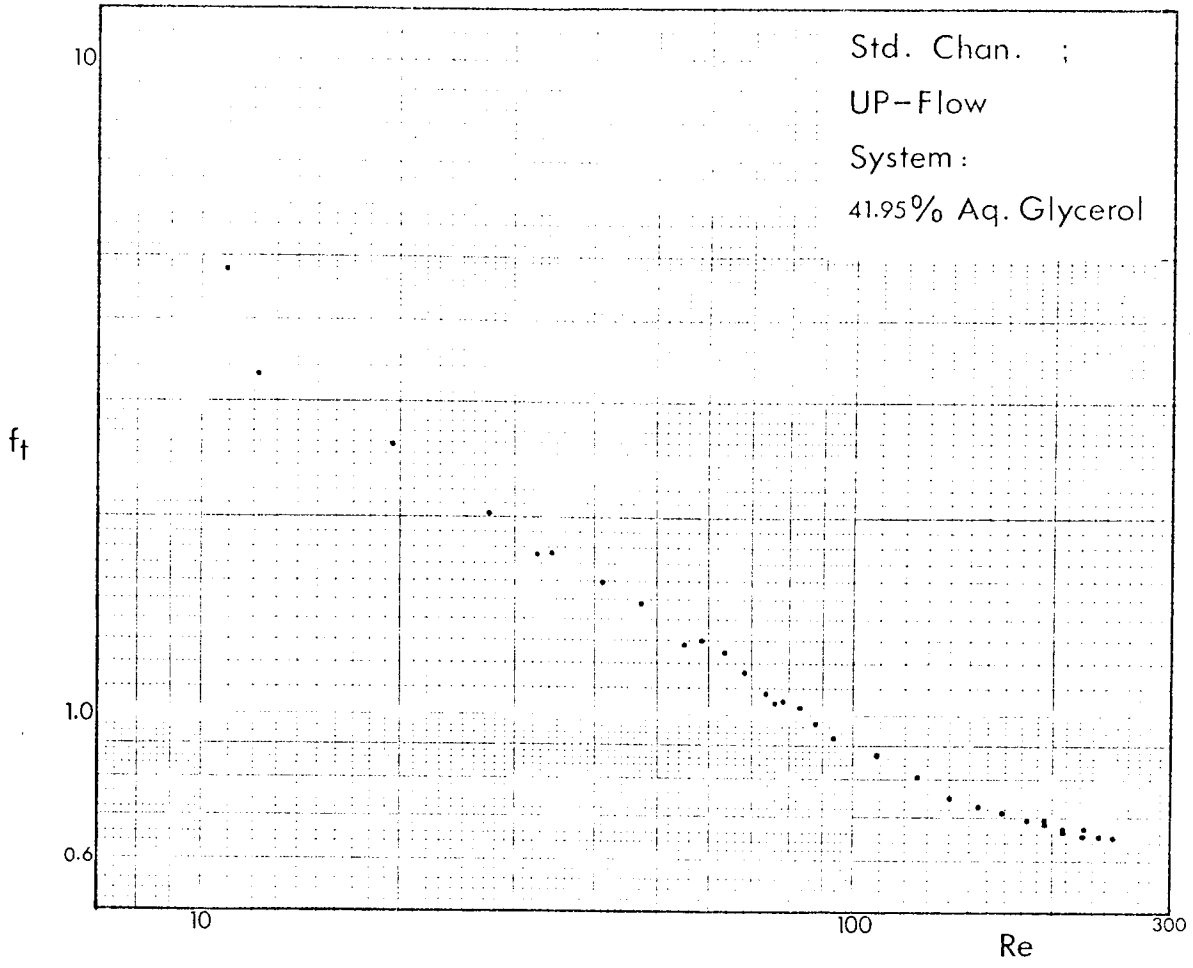

Fig.4.10

Fig.4.11

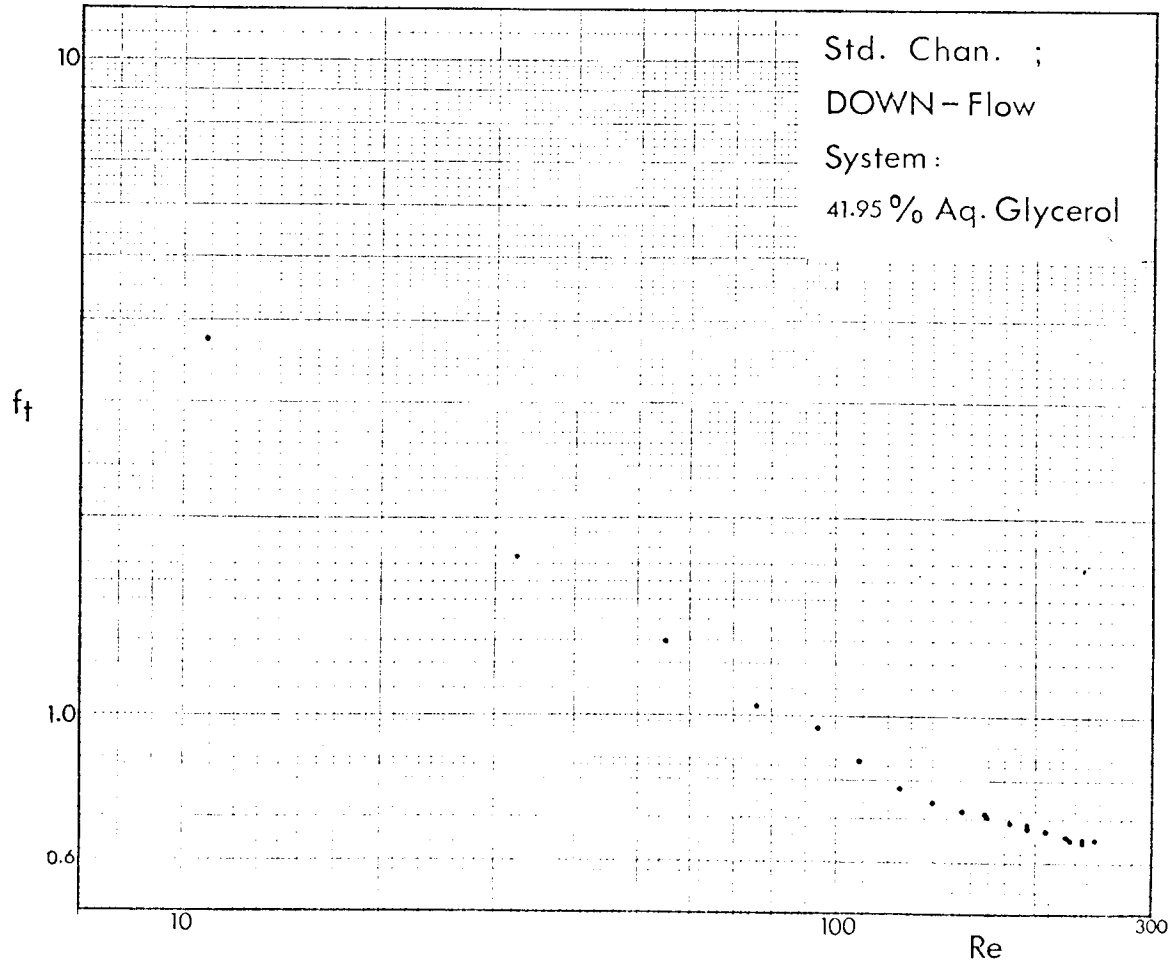

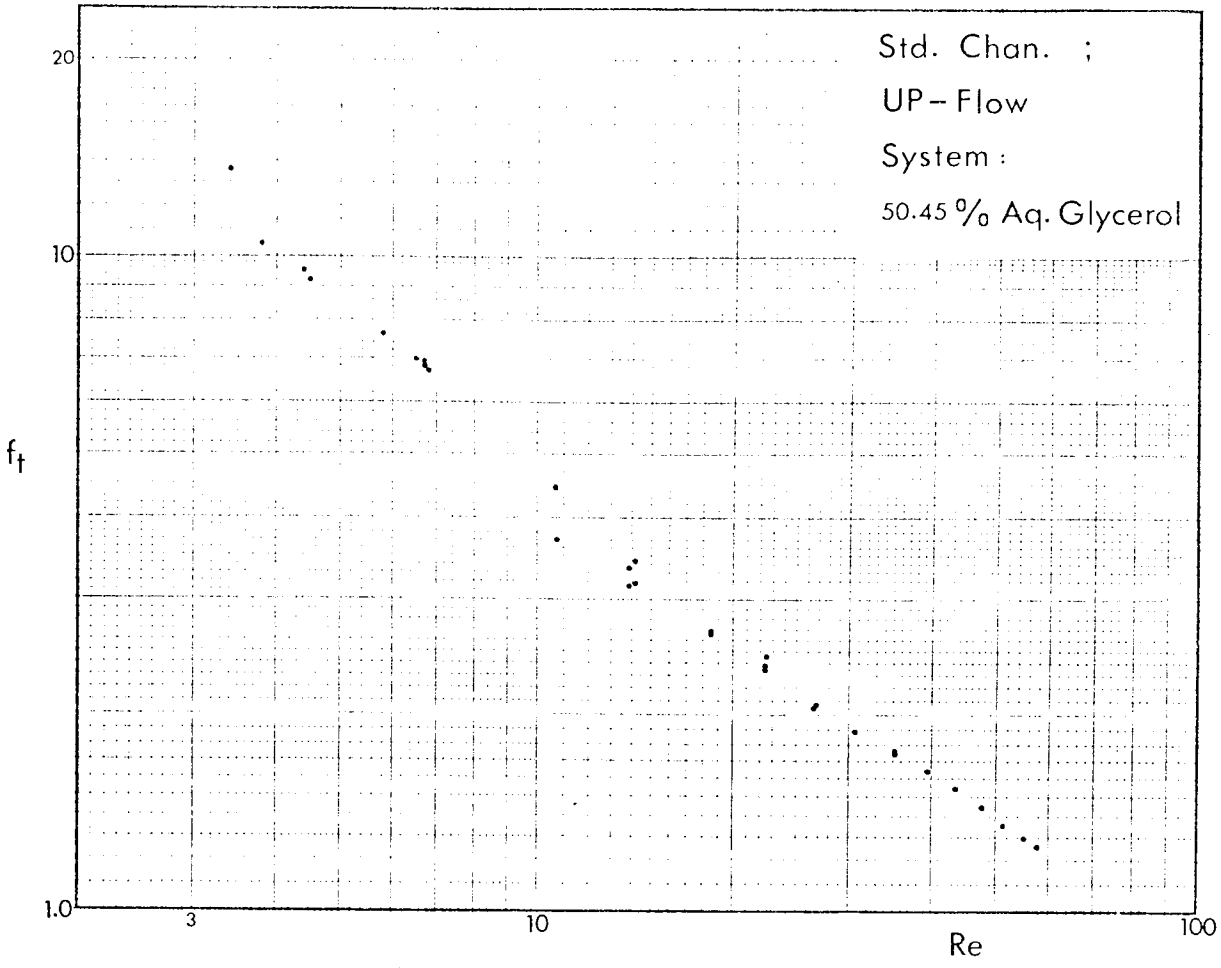

Fig.4.12

Fig.4.13

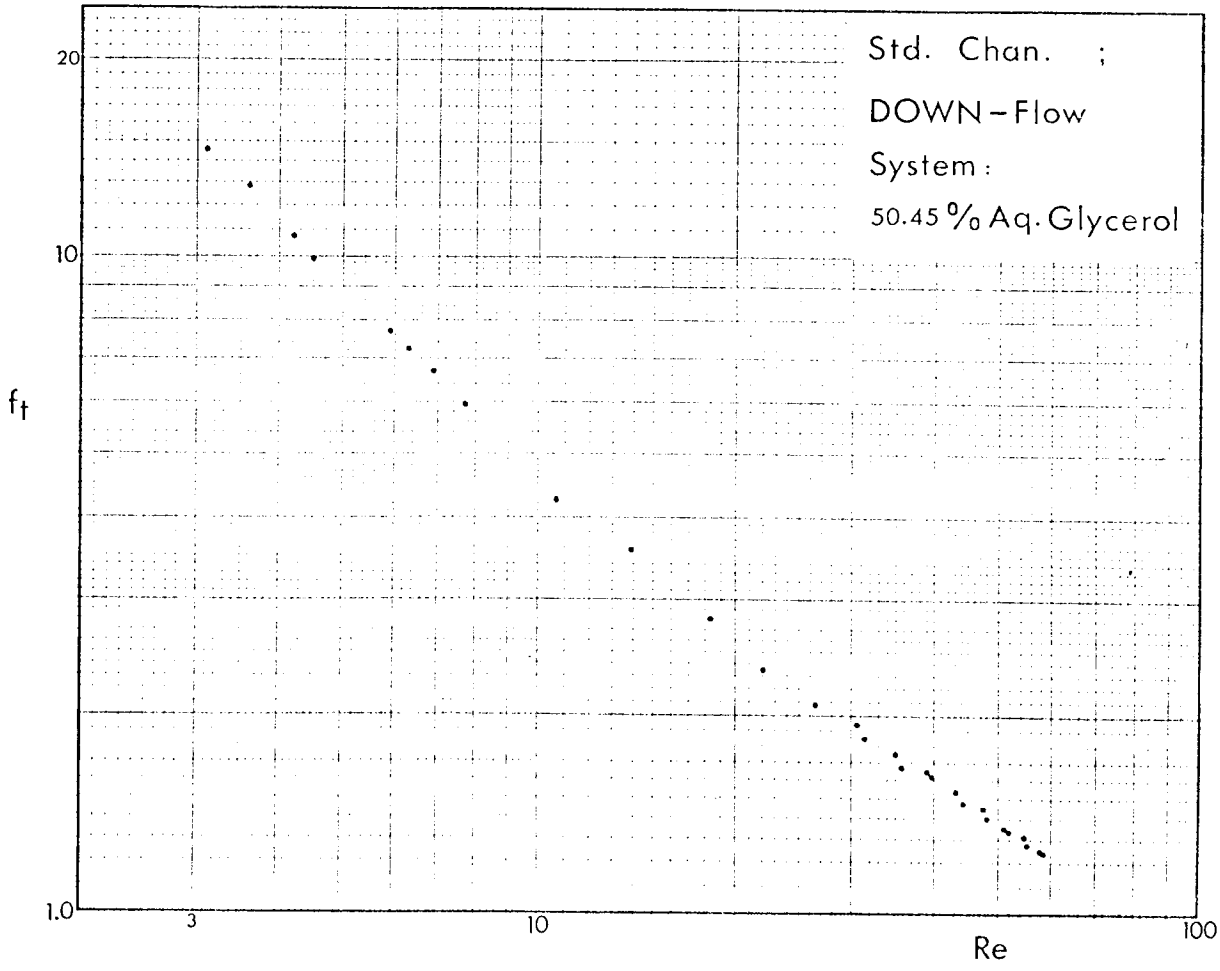

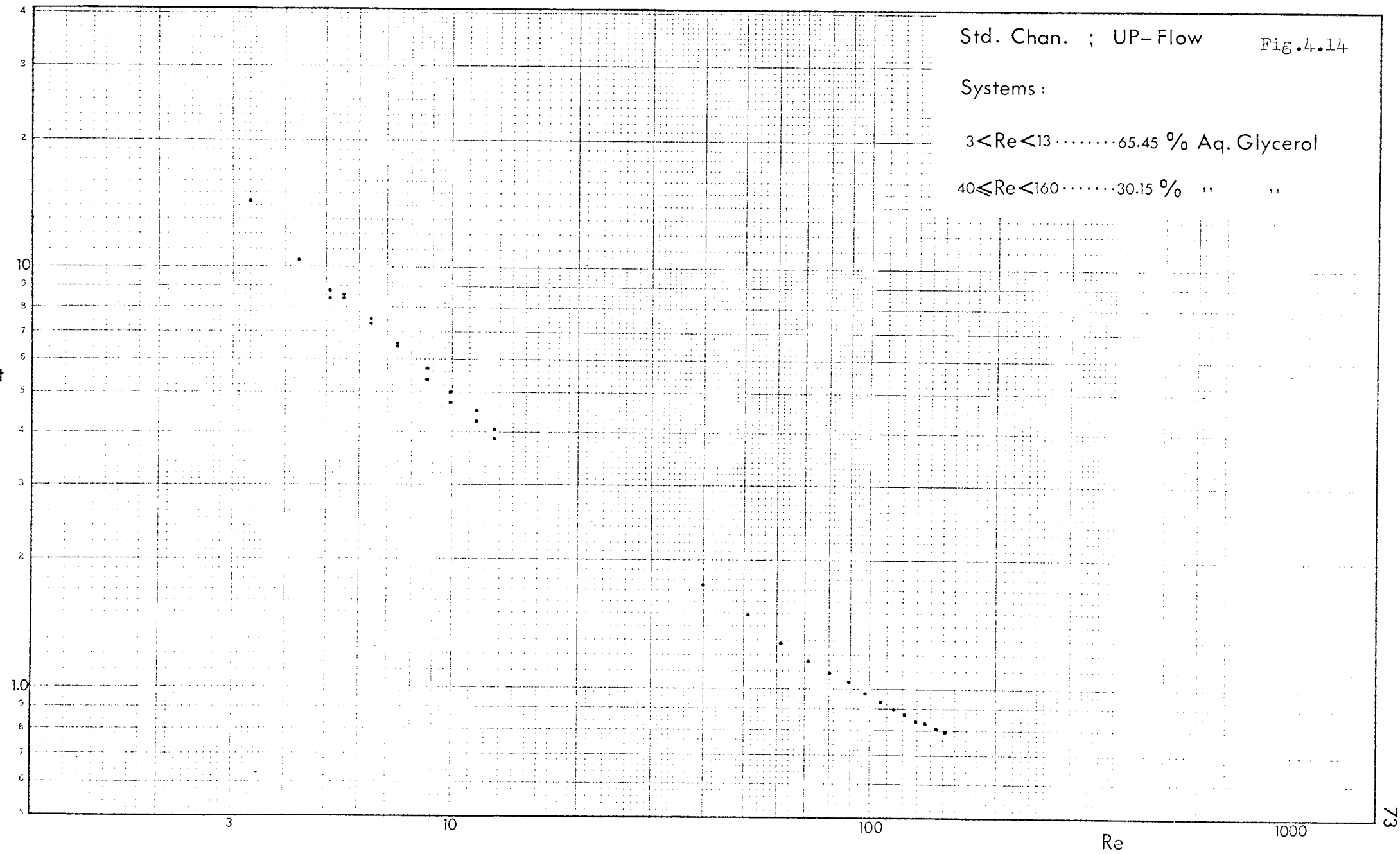
Std. Chan. ; UP-Flow
Fig.4.14
Systems :
3<Re<13 ·····65.45 % Aq. Glycerol
40≤Re<160 ·····30.15 % ,, ,,
10
1.0
3
10
100
1000
Re

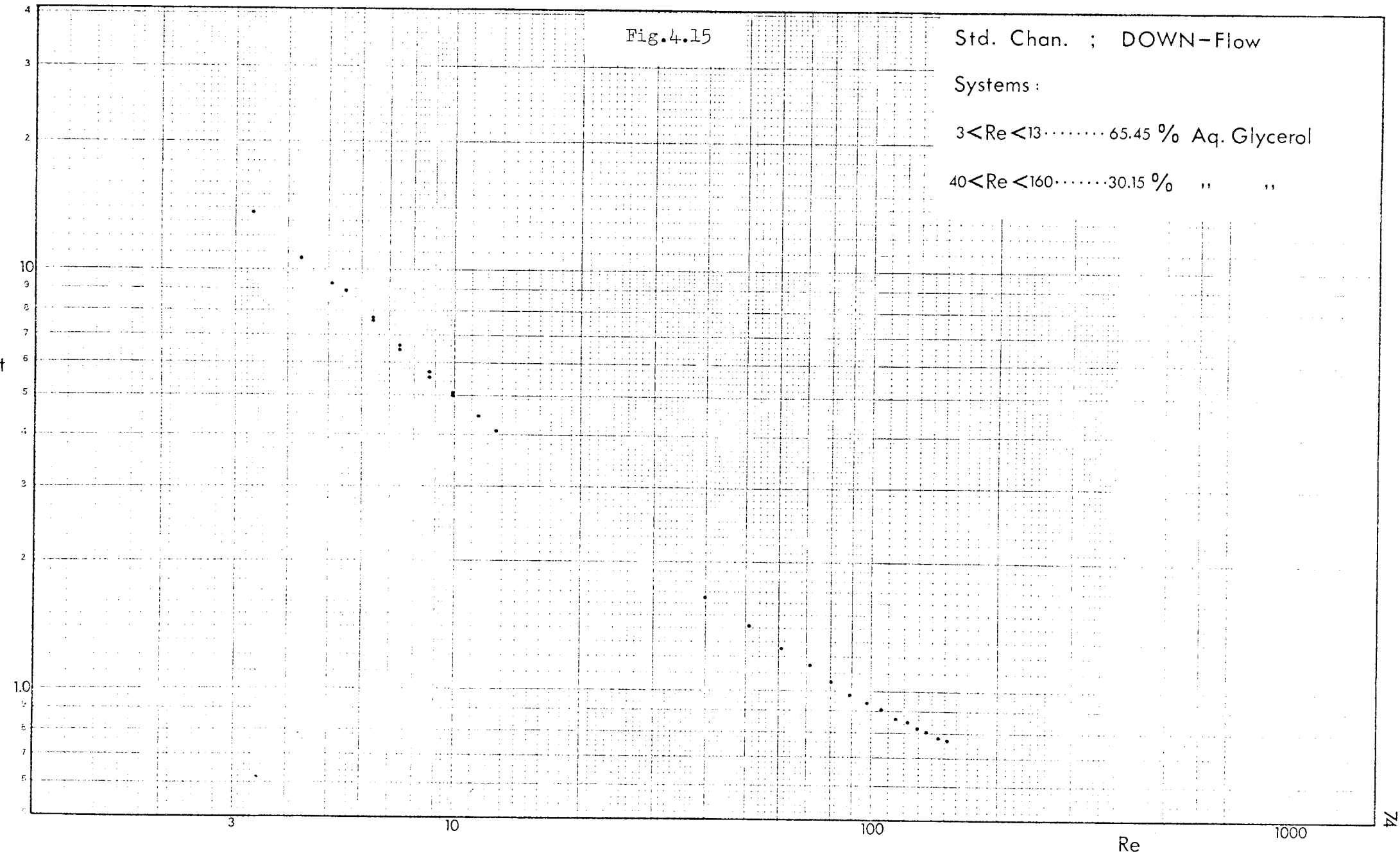
Fig.4.15
Std. Chan. ; DOWN-Flow
Systems :
3<Re<13 ..... 65.45 % Aq. Glycerol
40<Re<160 ..... 30.15 % ,, ,,
4
3
2
10
9
8
7
6
5
4
3
2
1.0
9
8
7
6
t
3
10
100
1000
Re

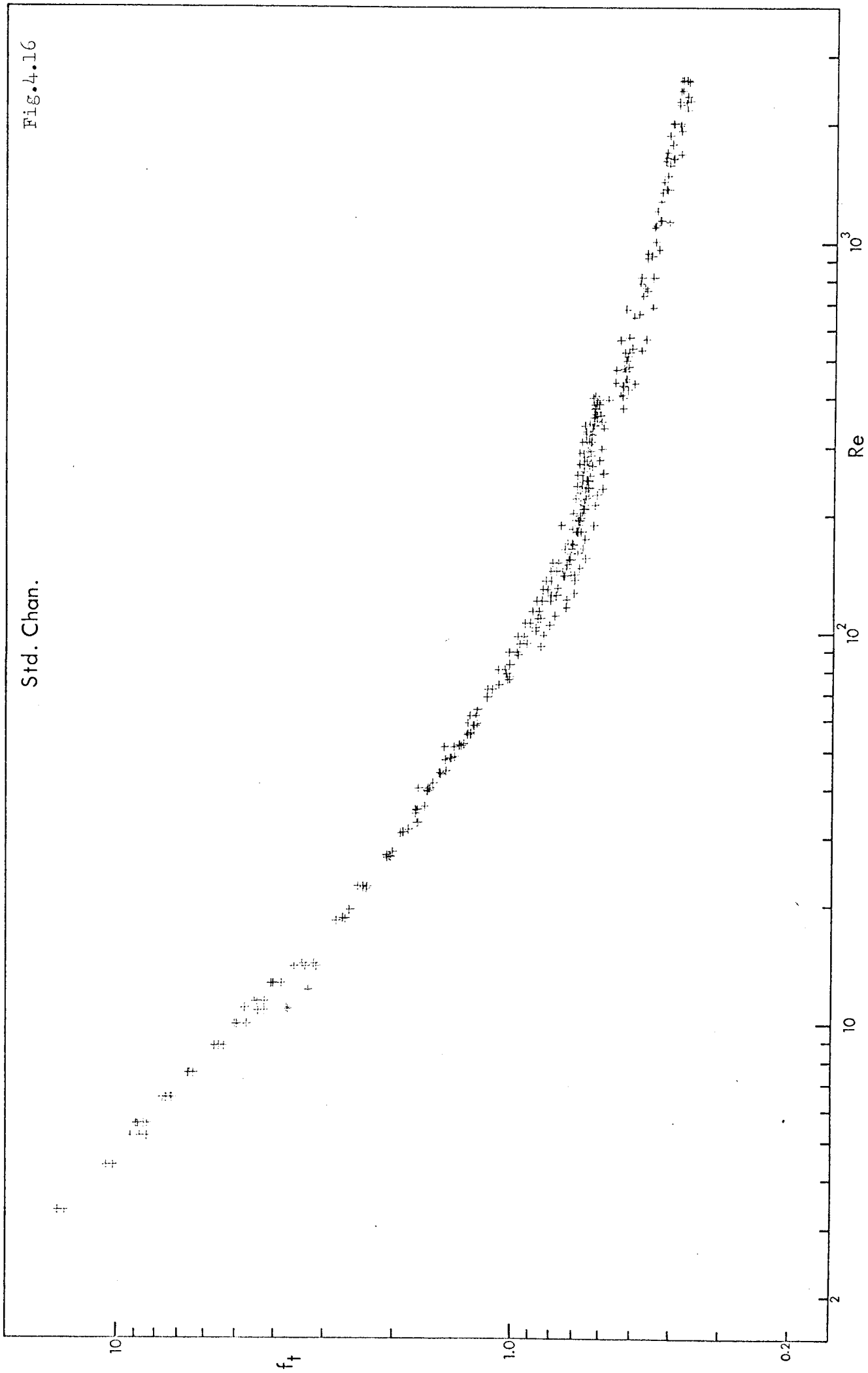

Fig.4.16

Graph Data Ref. 5531 Log 3 Cycles x mm, ½ and 1 cm

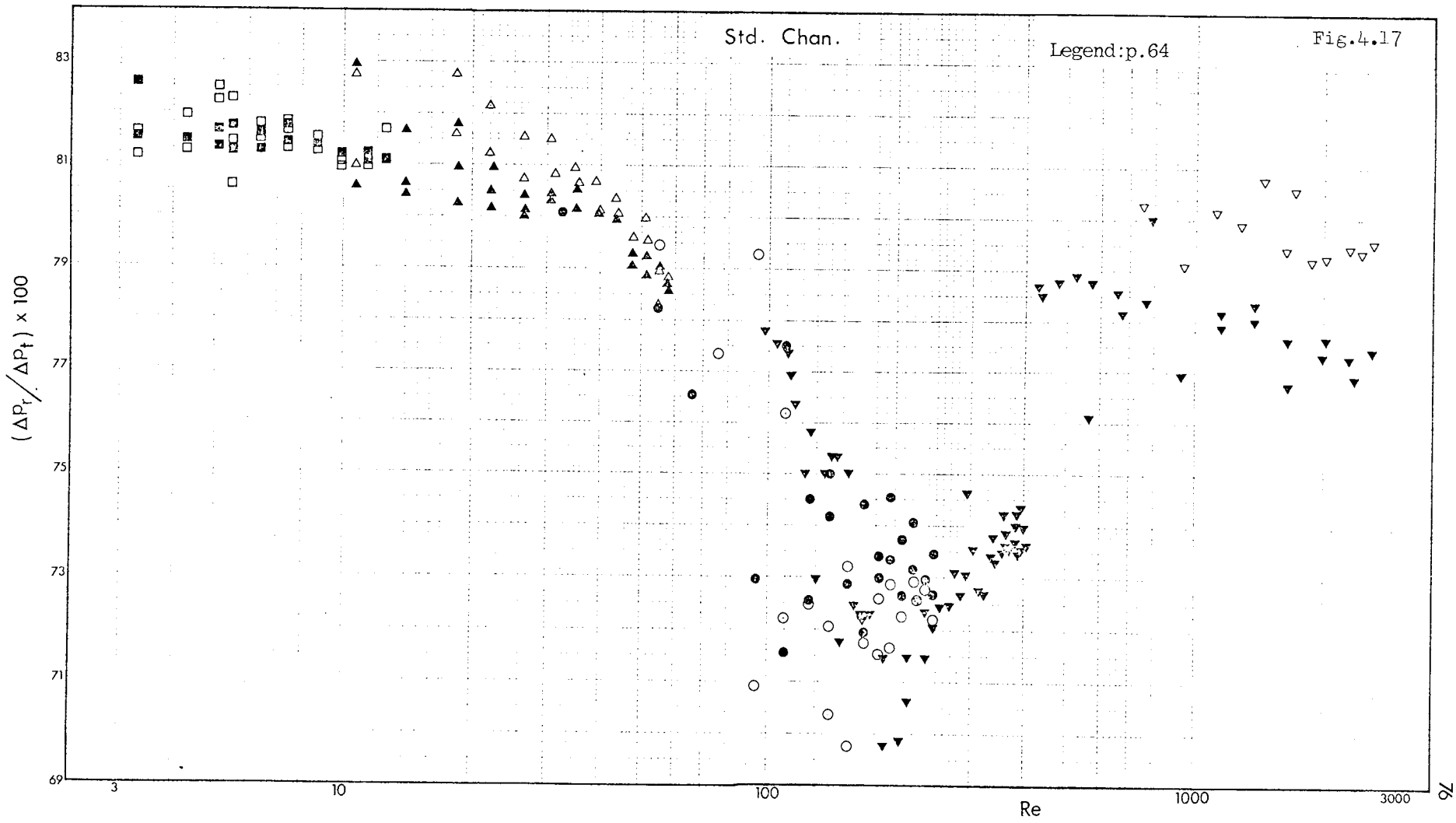

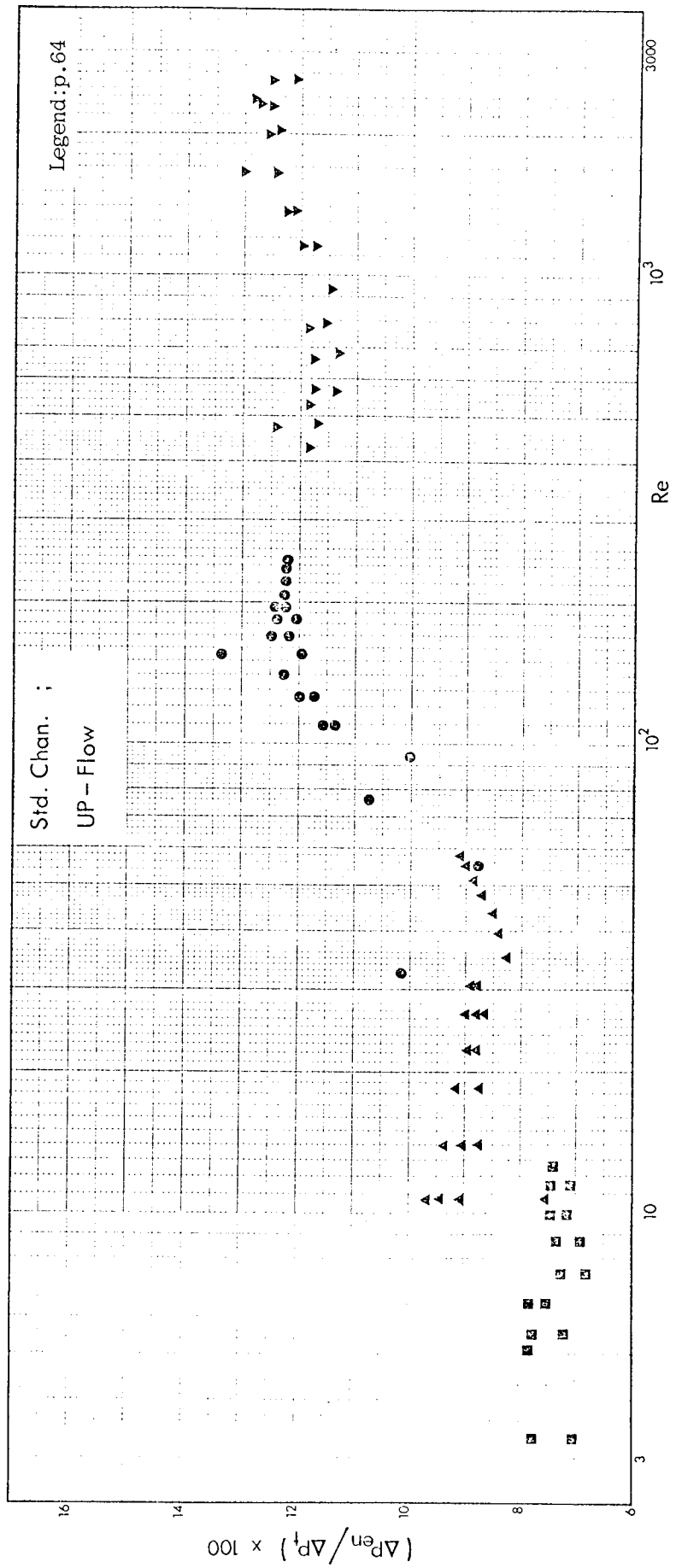
Legend:p.64
Std. Chan. ;
UP – Flow
$(\Delta P_{en}/\Delta P_t) \times 100$
Re
16
14
12
10
8
6
3
10
10^2
10^3
3000

Fig.4.18

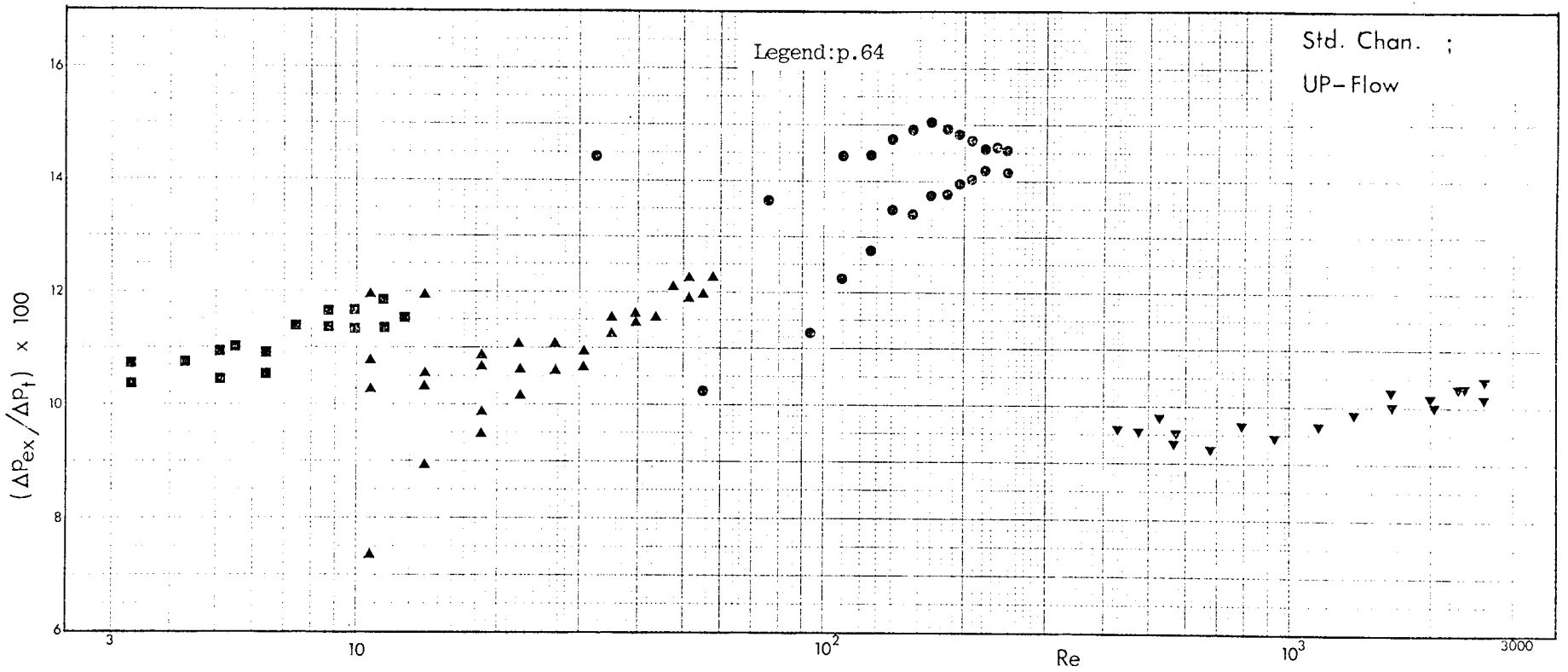
Legend:p.64
Std. Chan. ;
UP-Flow
$(\Delta P_{ex}/\Delta P_t) \times 100$
16
14
12
10
8
6
3
10
10^2
Re
10^3
3000

Fig.4.19

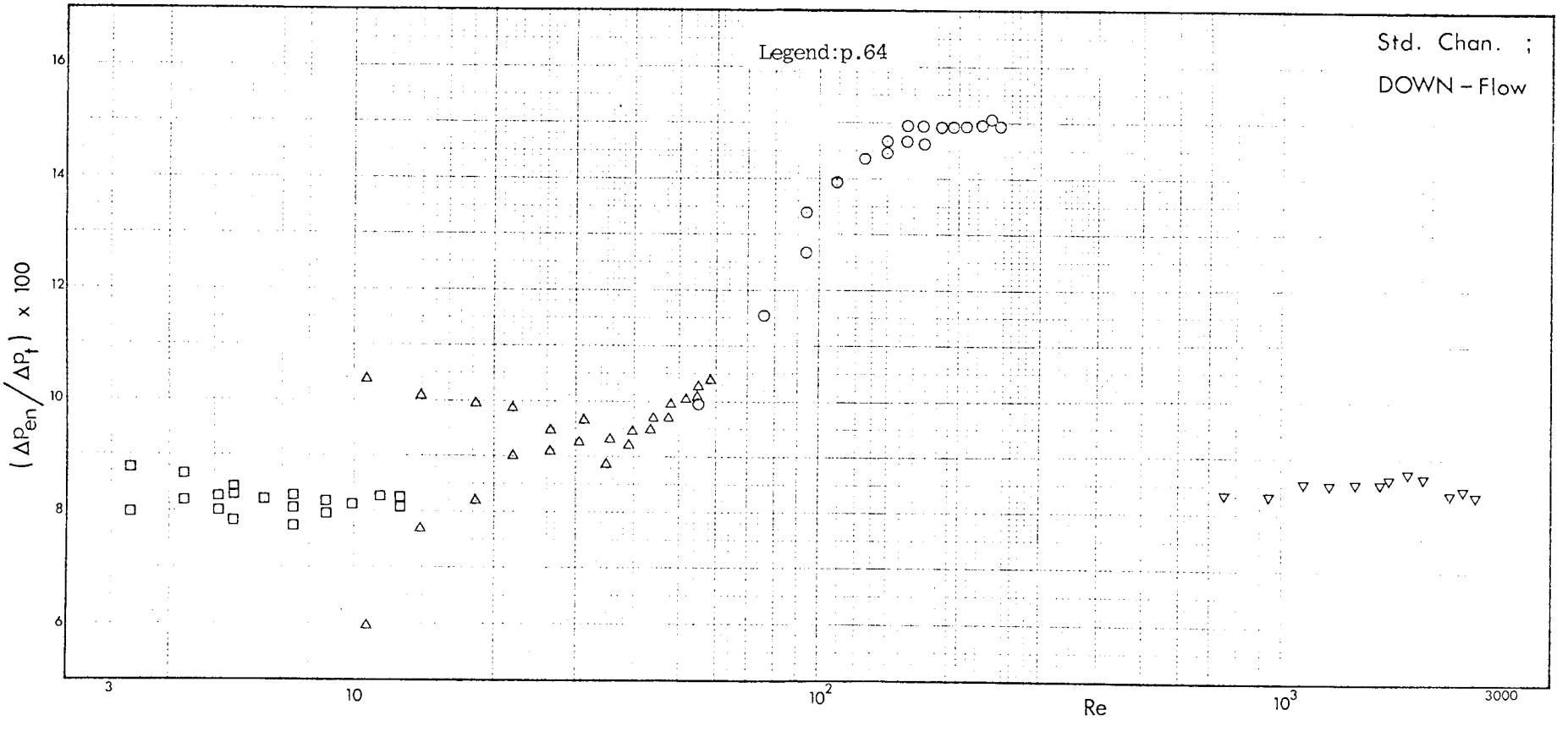

Fig.4.20

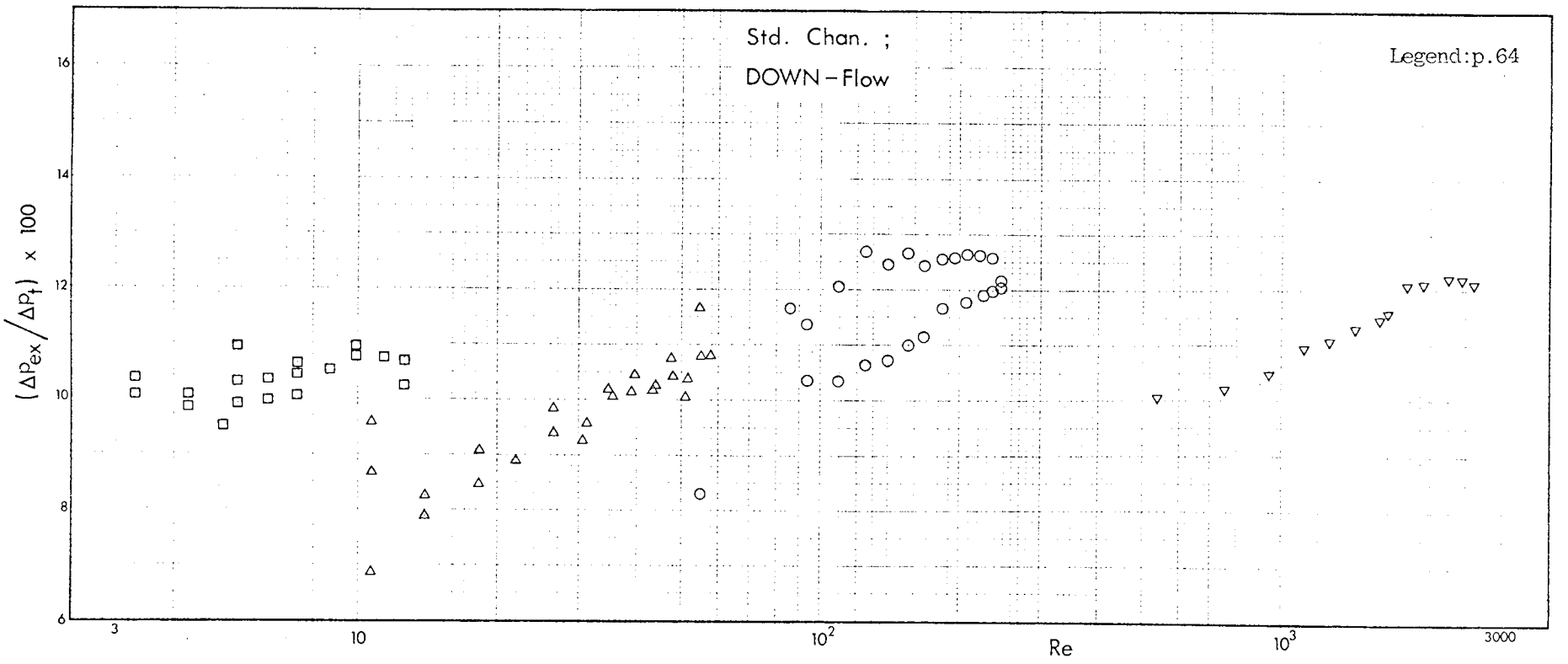
Std. Chan. ;
DOWN – Flow
Legend:p.64
$(\Delta P_{ex}/\Delta P_f) \times 100$
16
14
12
10
8
6
3
10
10^2
Re
10^3
3000

Fig.4.21

The very few cases where the individual contributions did not add up to approximately 100% resulted in the rejection of the least accurate components of the data.

The entrance in the case of UP-Flow is the lower port, however, it becomes the upper port when the flow direction is reversed. The exit, in turn, becomes upper or lower port in UP-Flow or DOWN-Flow respectively.

4.1.1) FLOW VISUALIZATION

Fig's 4.22 to 4.26 show the results of flow visualization experiments performed in conjunction with the standard channel. UP-Flow as well as DOWN-Flow situations were considered. 65.45% aq.gylcerol was the system used in the test depicted by Fig.4.22; water was employed in the rest. As can be seen, Fig.'s 4.22-4.24 involve single dye filaments whereas Fig.'s 4.25 and 4.26 depict velocity profiles as a result of injecting pulses of dye.

4.2) GAP 1 CHANNEL

The parameters differing from those of the standard channel and their values are as follows:

Channel volume	...	62.584 cm^3
Equivalent diameter	...	0.485 cm
Area of flow	...	1.3259 cm^2

[TABLE 4.III]

Details of the determination of the channel volume are given in Appendix A.3.0.

Fig.4.29 contains the results shown in Fig.'s 4.28 and 4.27. The following relationships are proposed to describe the data in Fig.4.29:

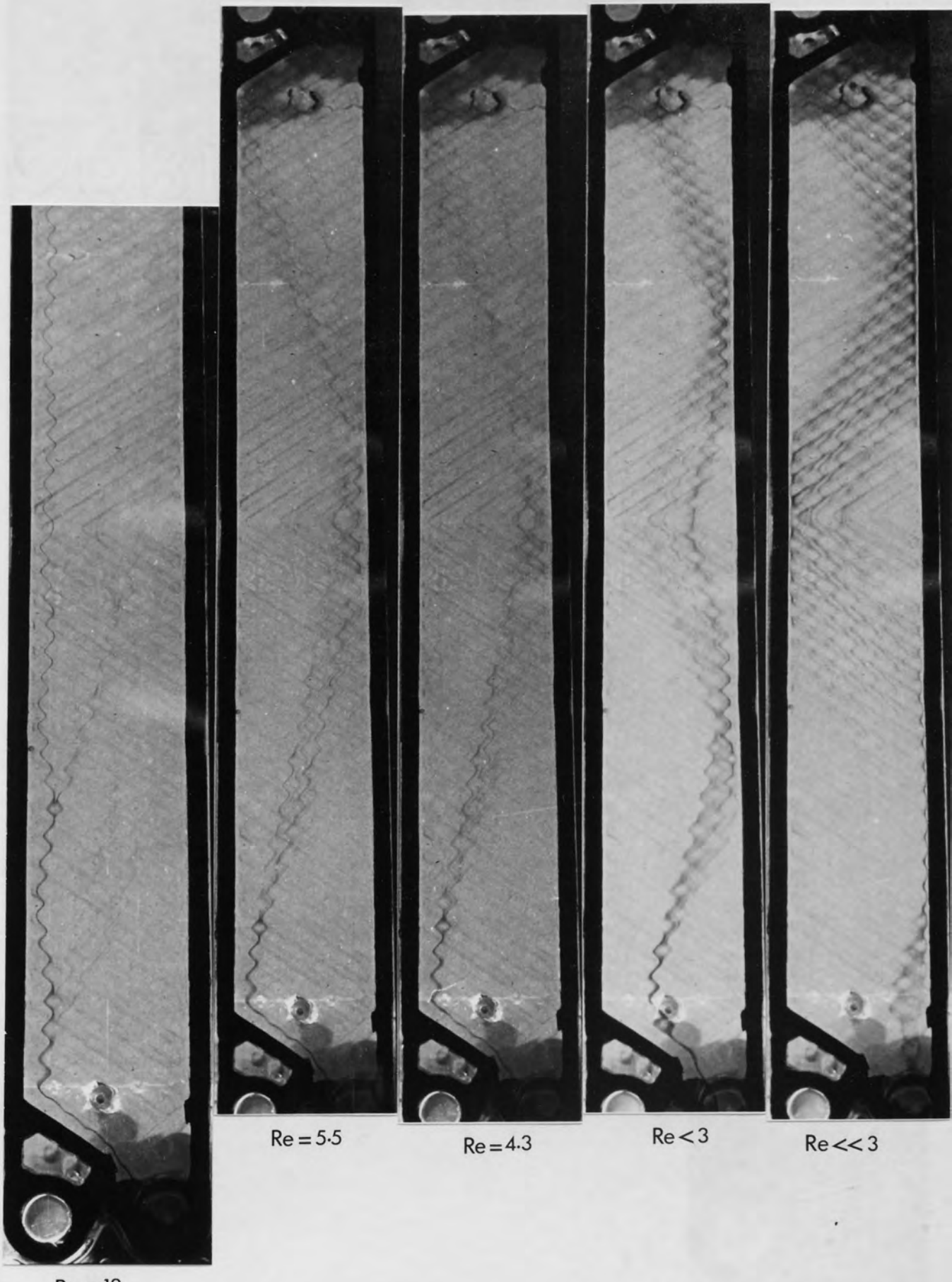

Fig. 4·22

Fig. 4.23

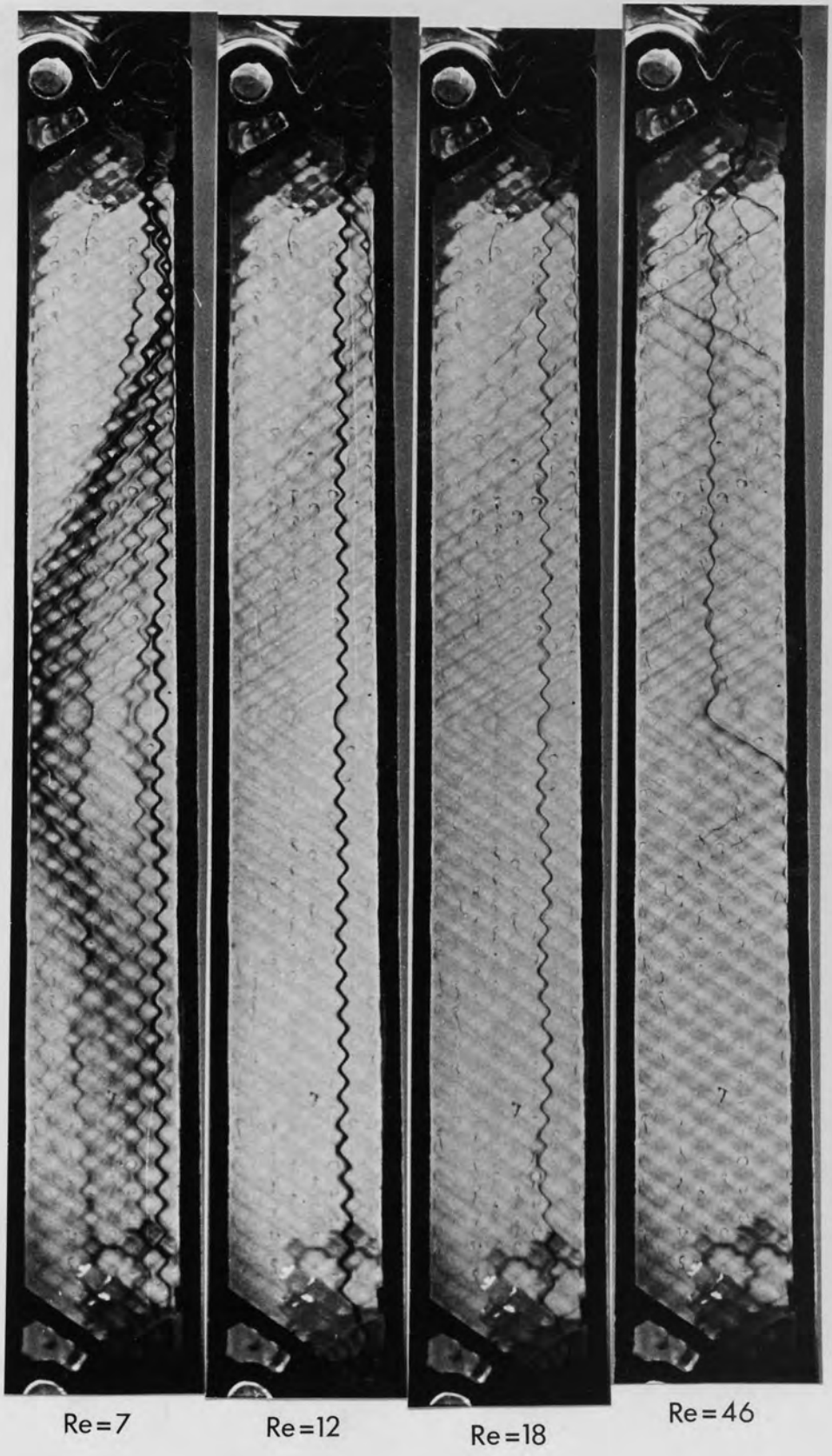

Fig. 4.24

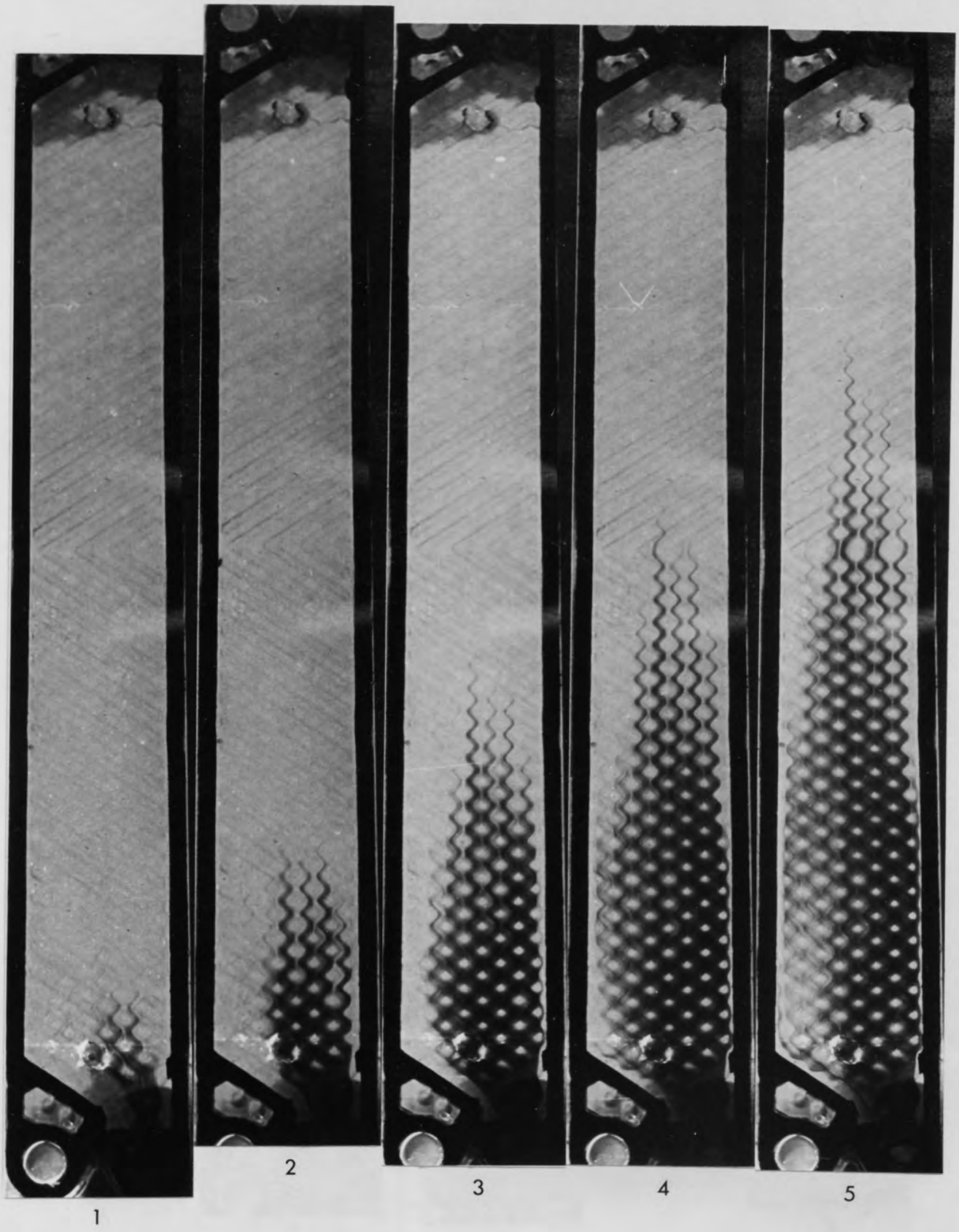

Re = 9.9

Fig. 4.25

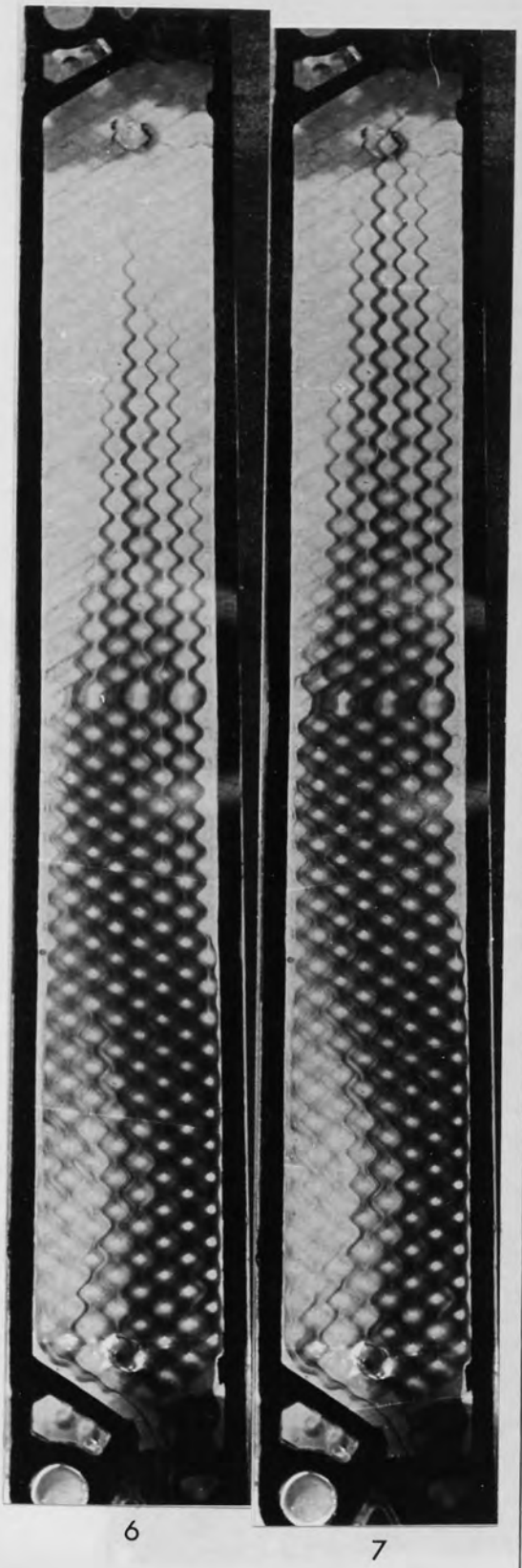

Re = 9.9

Fig. 4.25 (Contd.)

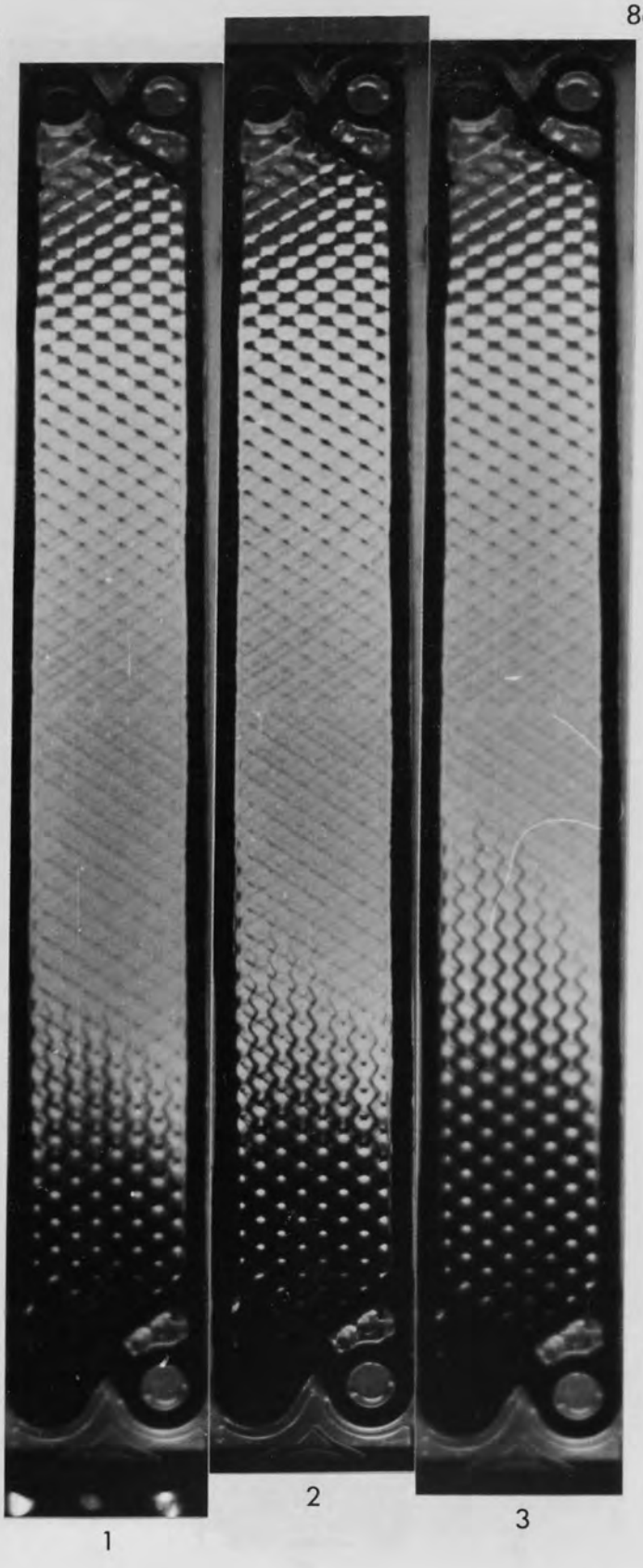

Re = 25

Fig. 4.26

Re = 25

Fig. 4.26 Contd.

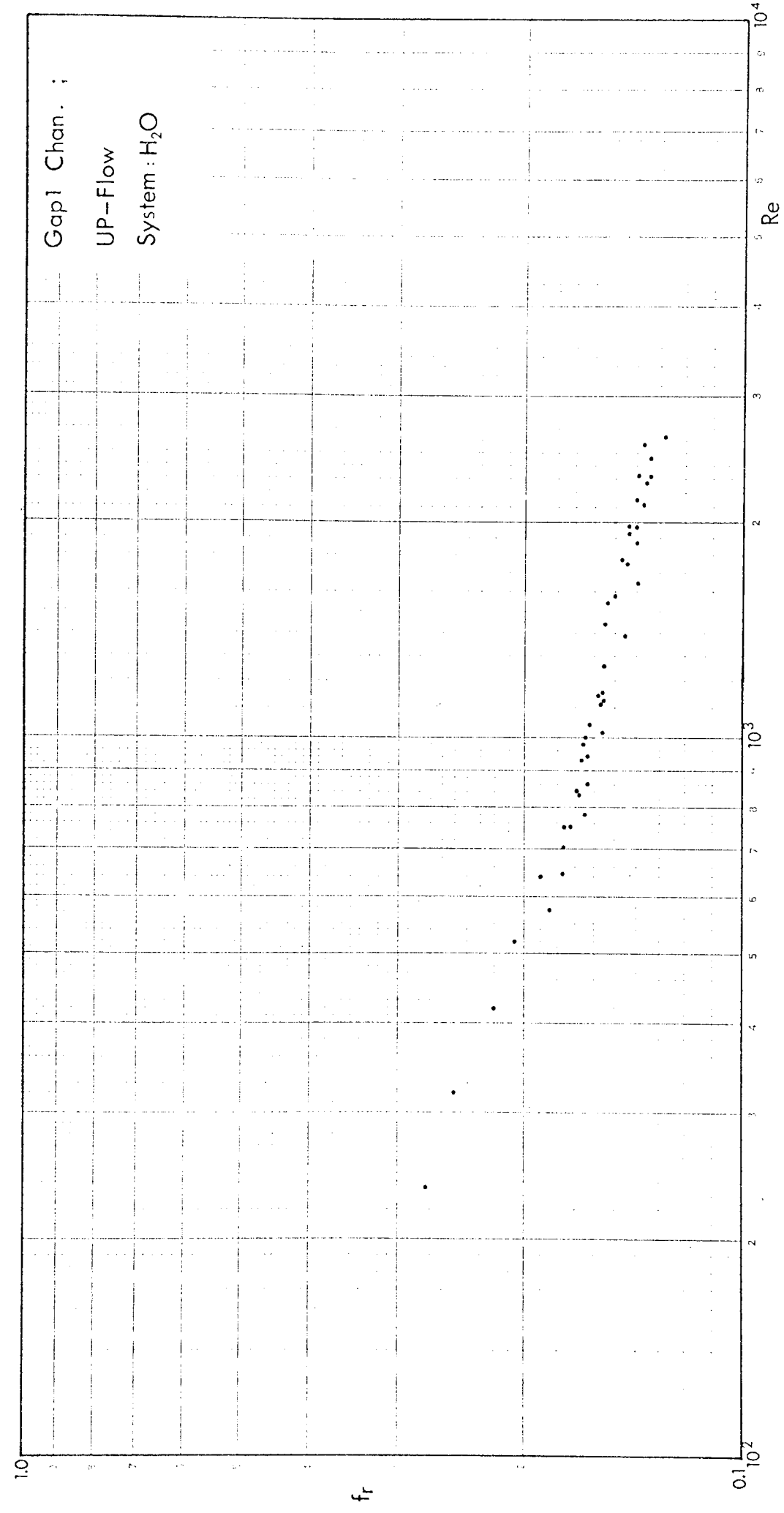

Fig.4.27

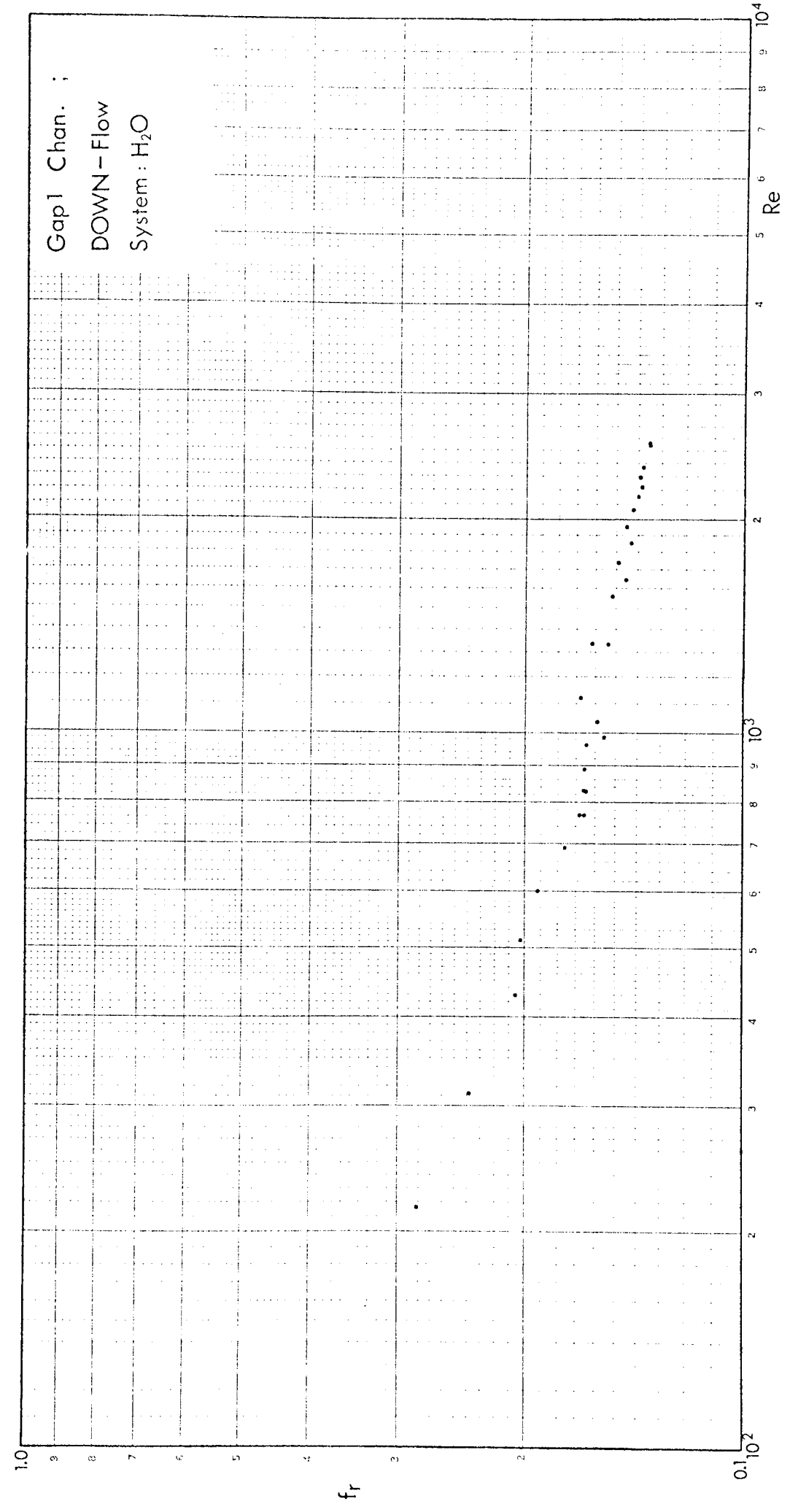

Fig.4.28

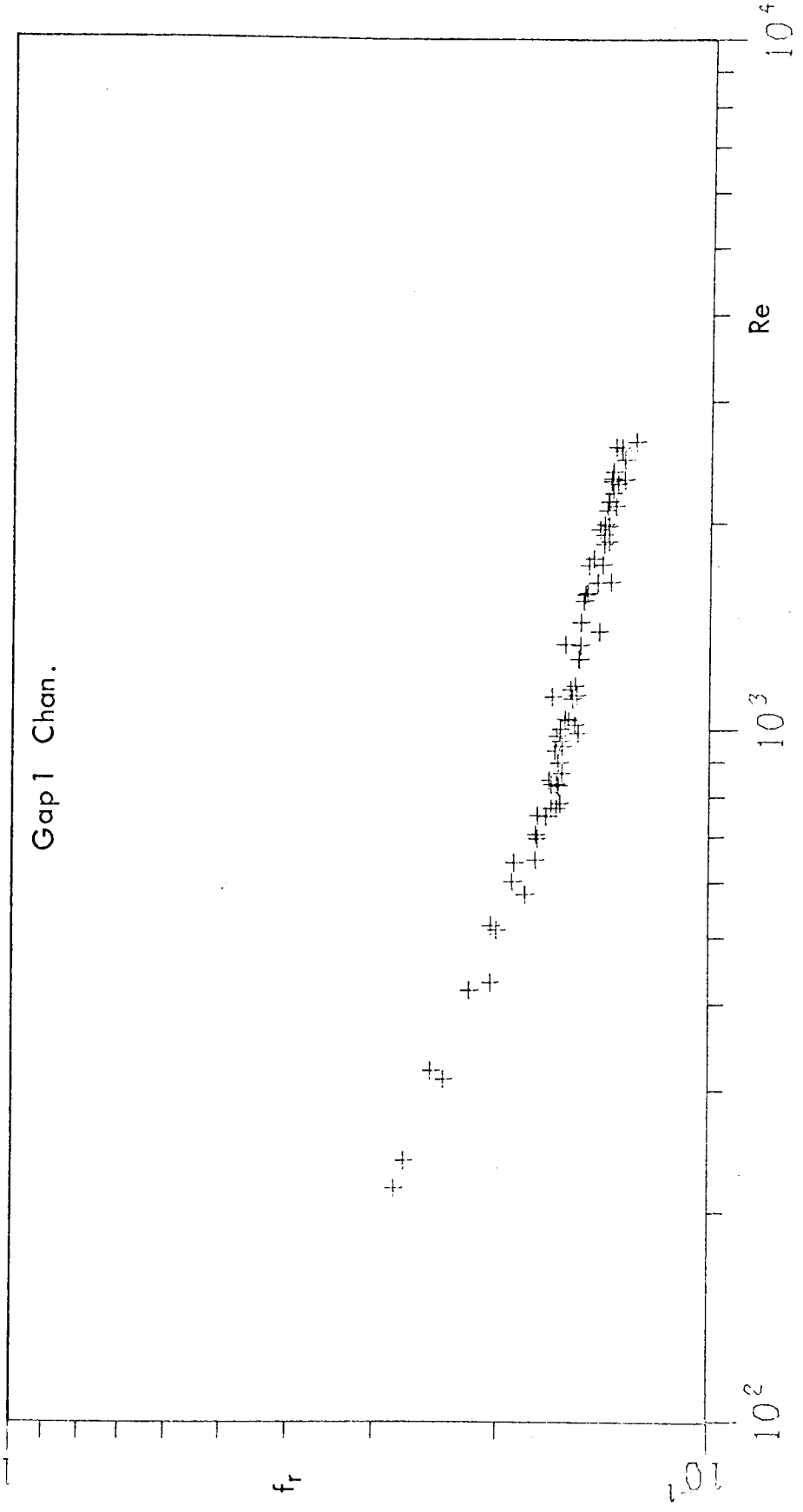

Fig.4.29

$$(210 < Re < 3000) \qquad f_r = \frac{36.644}{Re} + 0.123 \qquad (4.11)$$

$$(700 < Re < 3000) \qquad f_r = 0.614\, Re^{-0.194} \qquad (4.12)$$

The combined data of Fig.'s 4.30 and 4.31 could be seen in Fig.4.32. The following empirical equations were developed to describe the combined results:

$$(150 \leq Re < 3000) \qquad f_t = \frac{46.254}{Re} + 0.206 \qquad (4.13)$$

$$(750 \leq Re < 3000) \qquad f_t = 0.592\ Re^{-0.124} \qquad (4.14)$$

4.3) GAP 2 CHANNEL

The table below gives the relevant values of the volume, De, and the flow area:

Channel volume	...	88.392 cm^3
Equivalent diameter	...	0.685 cm
Area of flow	...	1.8727 cm

[TABLE 4.IV]

The results in Fig.'s 4.36 and 4.37 appear together in Fig.4.38, and the following models best describe the combined data:

$$(120 \leq Re < 5000) \qquad f_r = \frac{26.825}{Re} + 0.0564 \qquad (4.15)$$

$$(1400 < Re < 5000) \qquad f_r = 0.362\ Re^{-0.216} \qquad (4.16)$$

The relationships suggested for the data of Fig.'s 4.39 and 4.40 as shown in Fig.4.41 are:

$$(90 < Re < 5000) \qquad f_t = \frac{32.134}{Re} + 0.166 \qquad (4.17)$$

$$(1800 < Re < 5000) \qquad f_t = 0.471\ Re^{-0.128} \qquad (4.18)$$

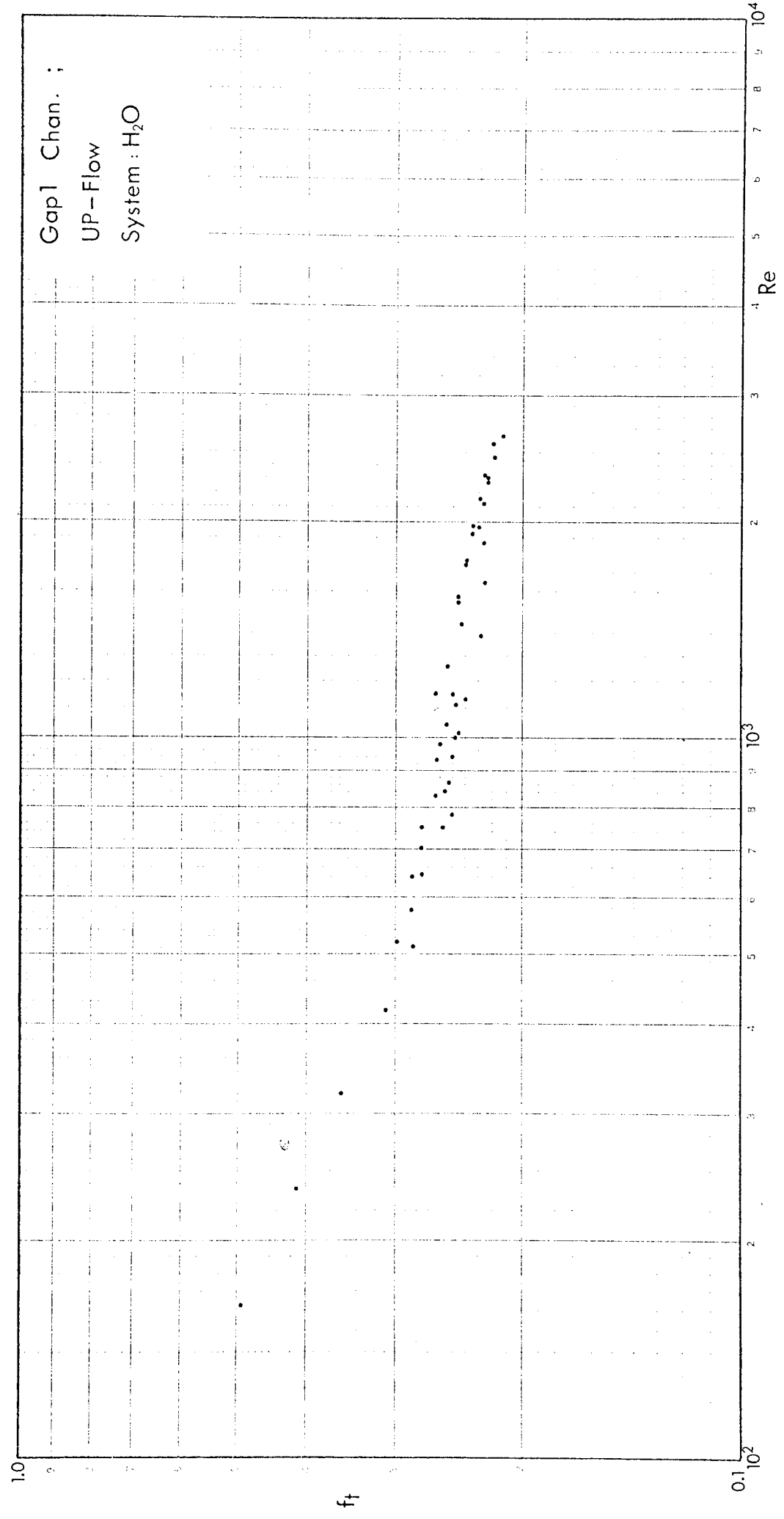

Fig.4.30

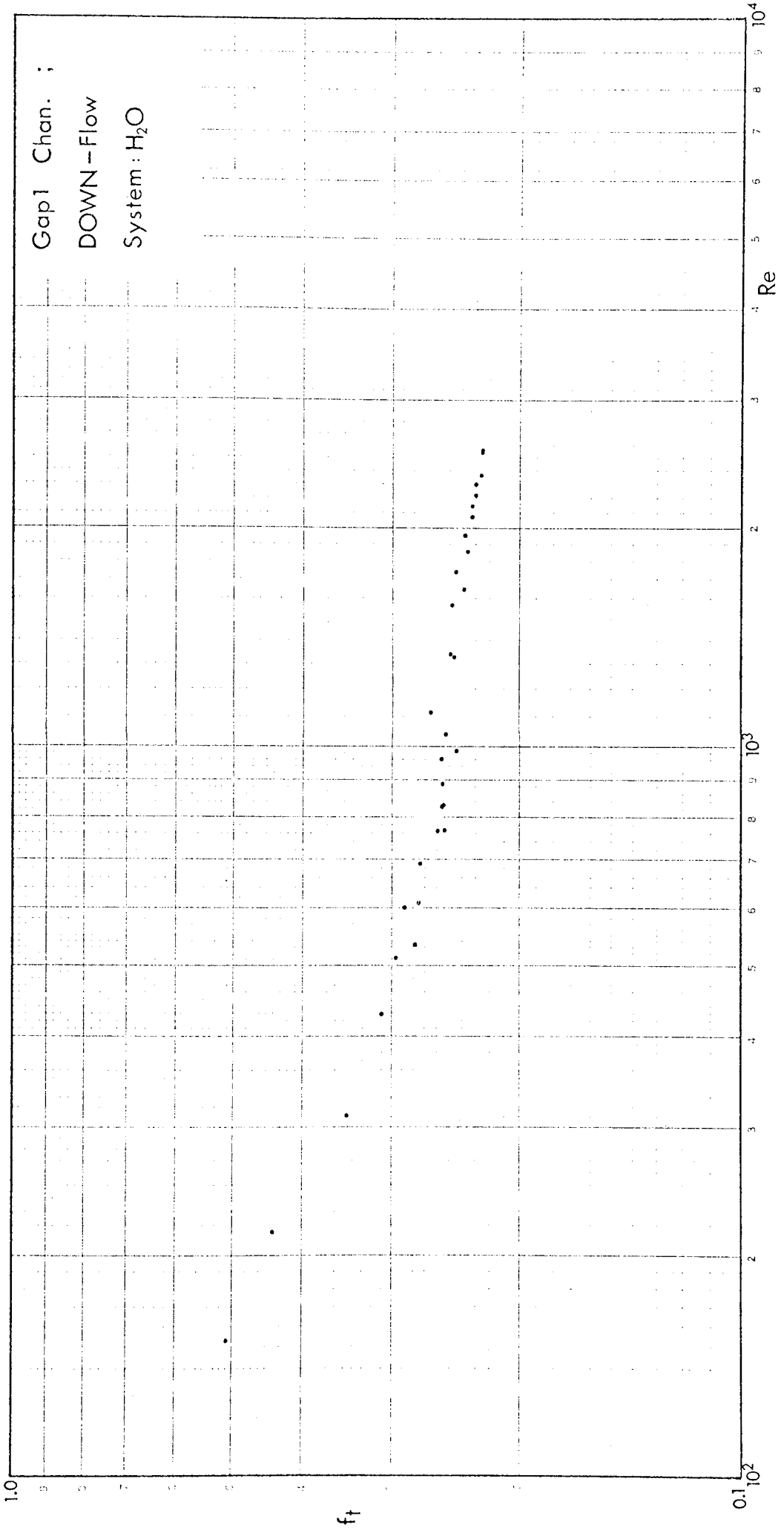

Fig.4.31

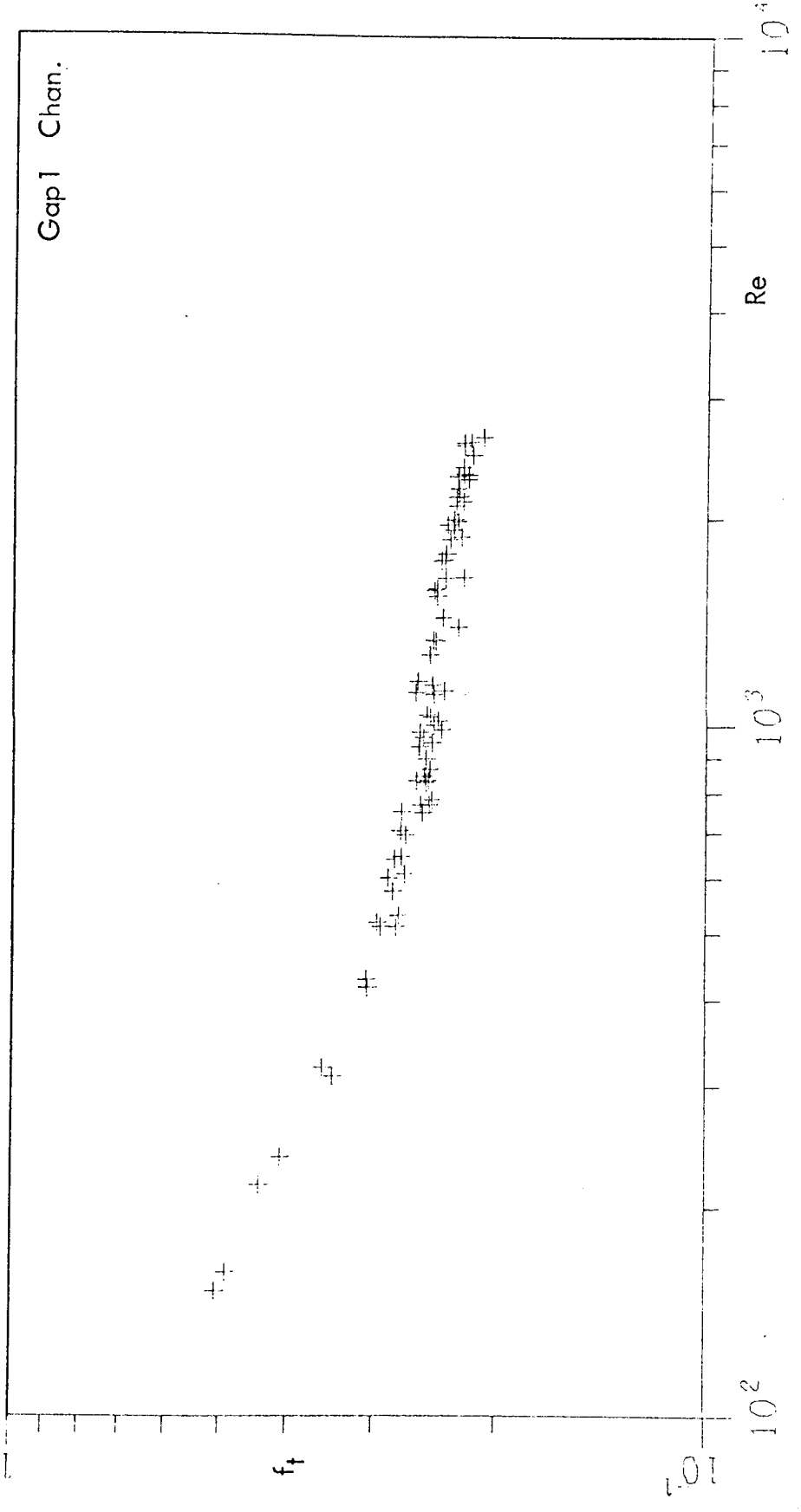

Fig.4.32

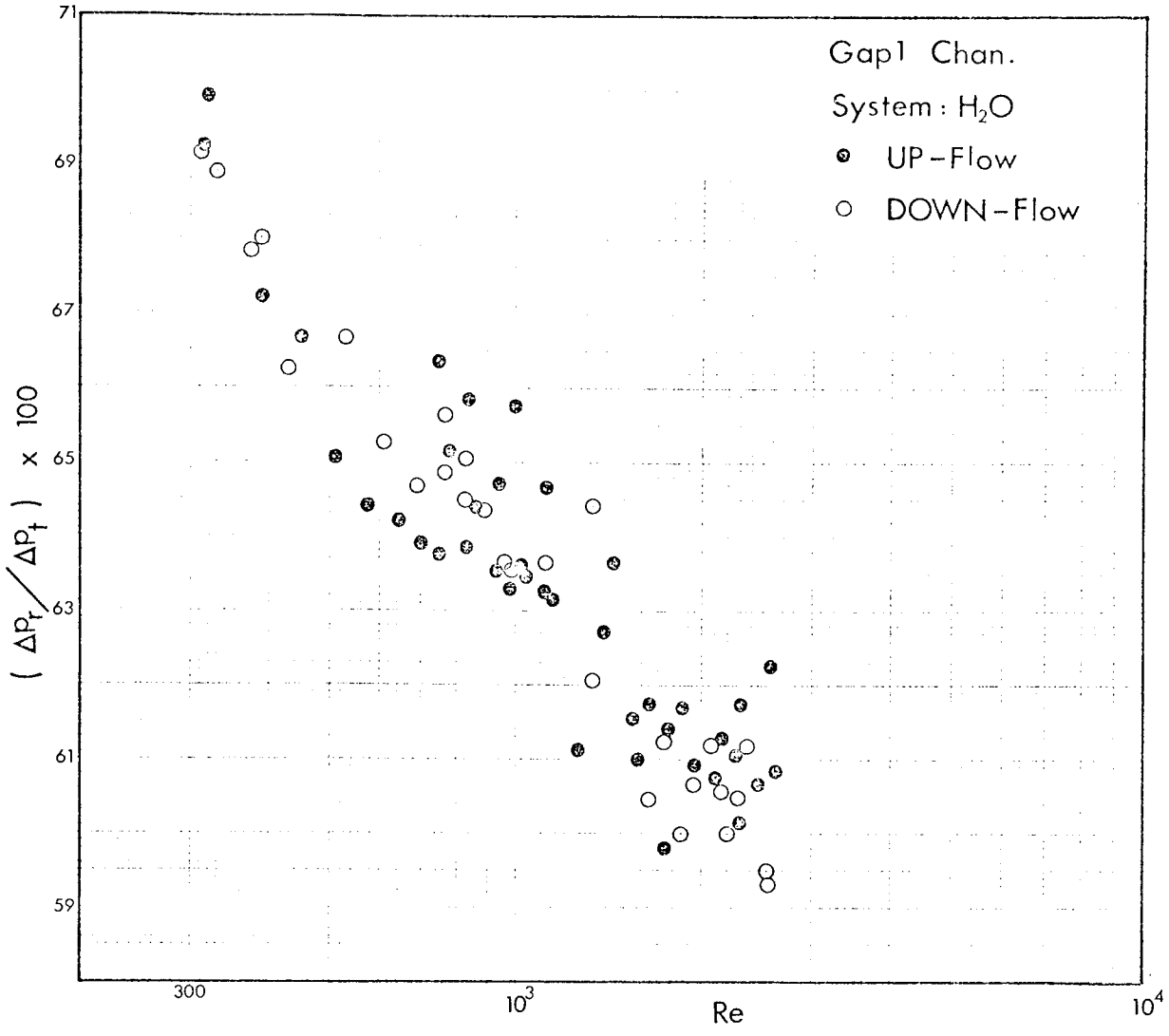

Fig.4.33

4.4) PARALLEL PATTERN CHANNEL

Fig.4.45 shows the results of the test conducted on the 2-dimensional parallel pattern channel. The data corresponding to Re ≥ 250 was correlated as follows:

$$f_t = 0.843\ Re^{-0.199} \qquad (4.19)$$

The channel parameters are the same as those of the standard channel mentioned earlier in Table 4.I.

The statistical aspects of all the empirical relationships reported in this chapter are presented in Appendix A-4.0.

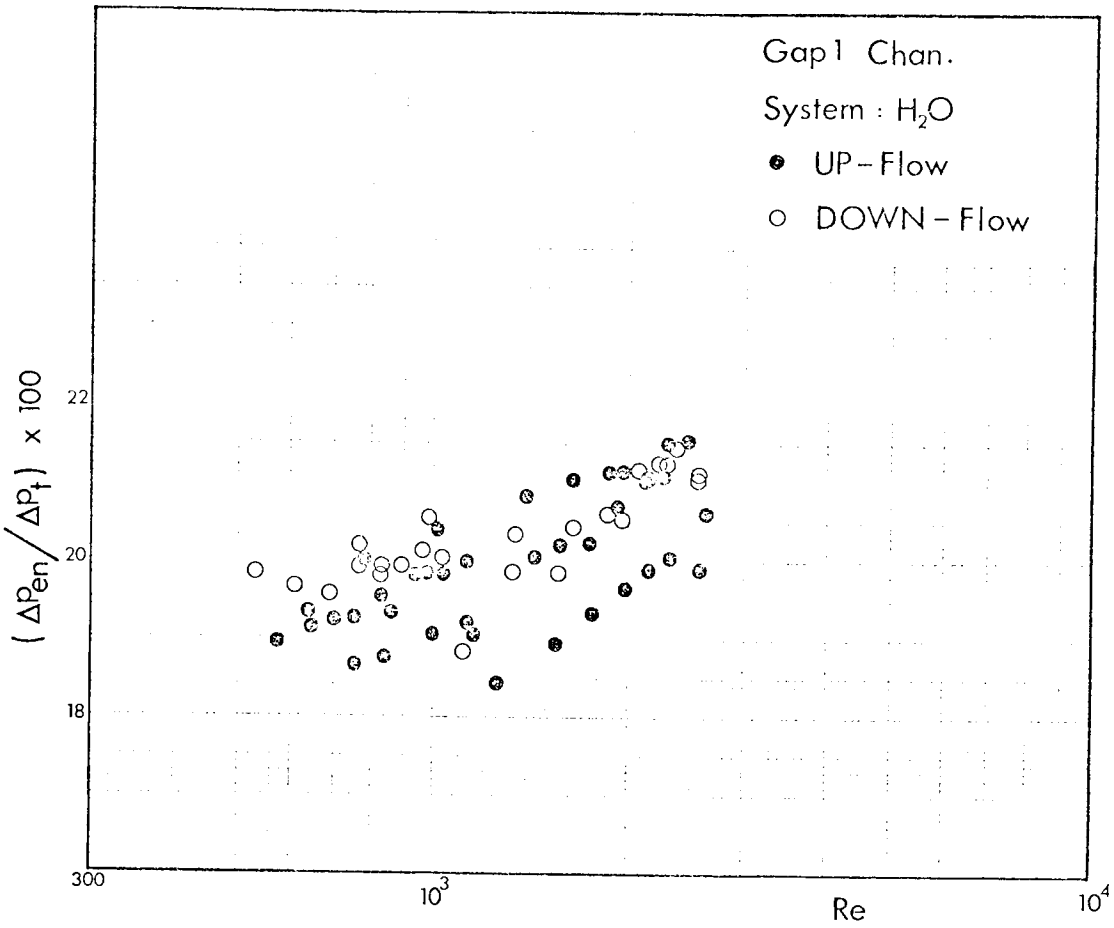

Fig.4.34

Fig.4.35

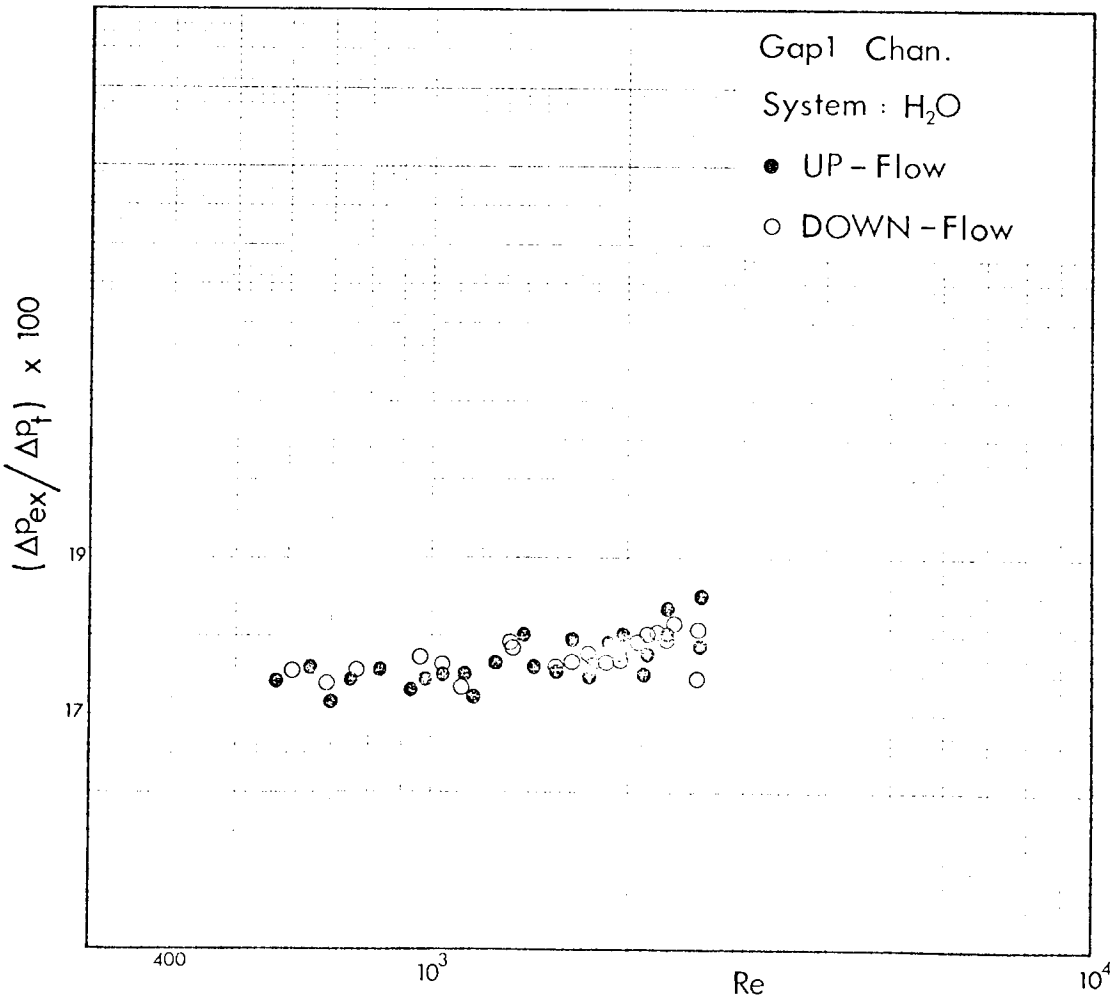

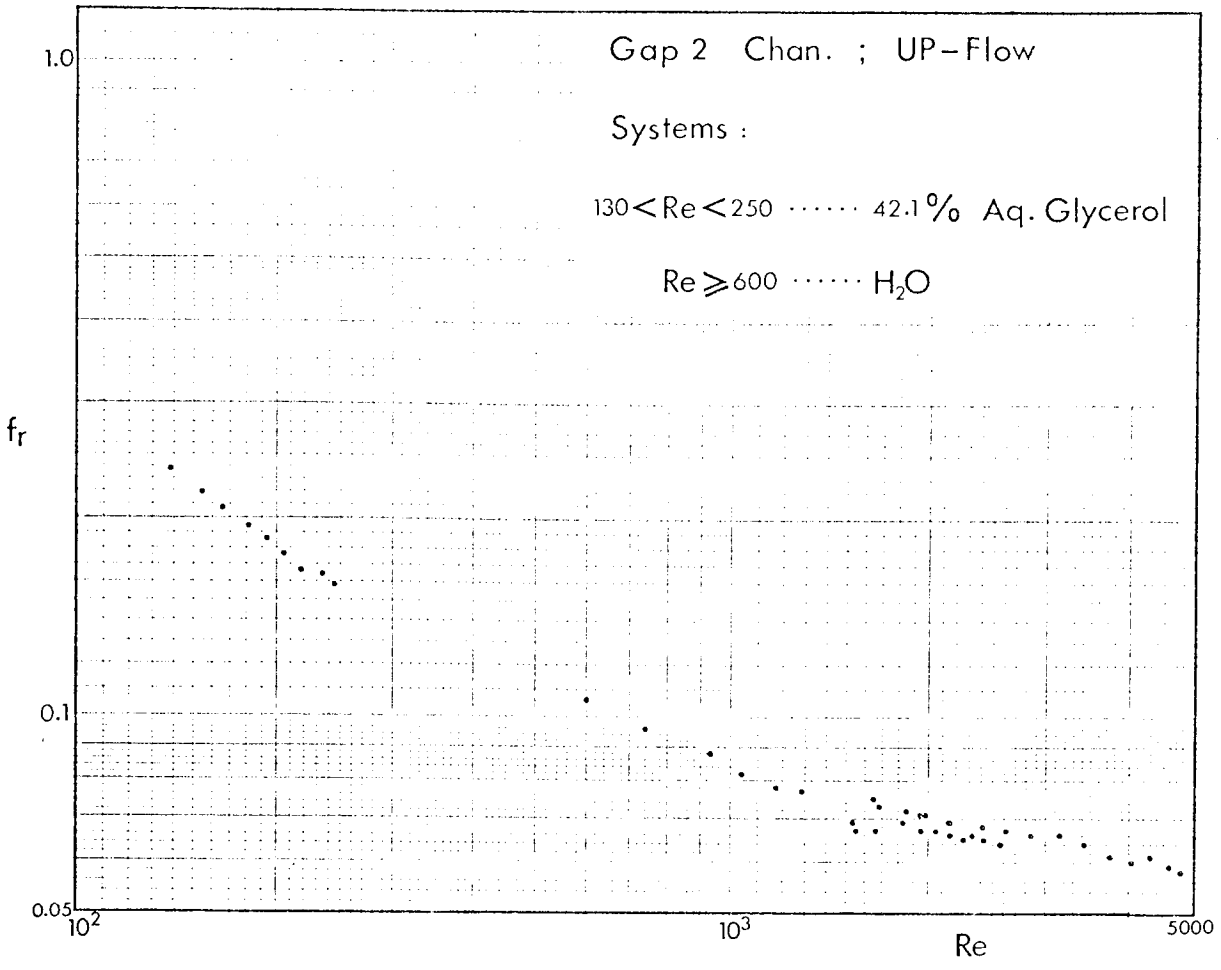

Fig.4.36

Fig.4.37

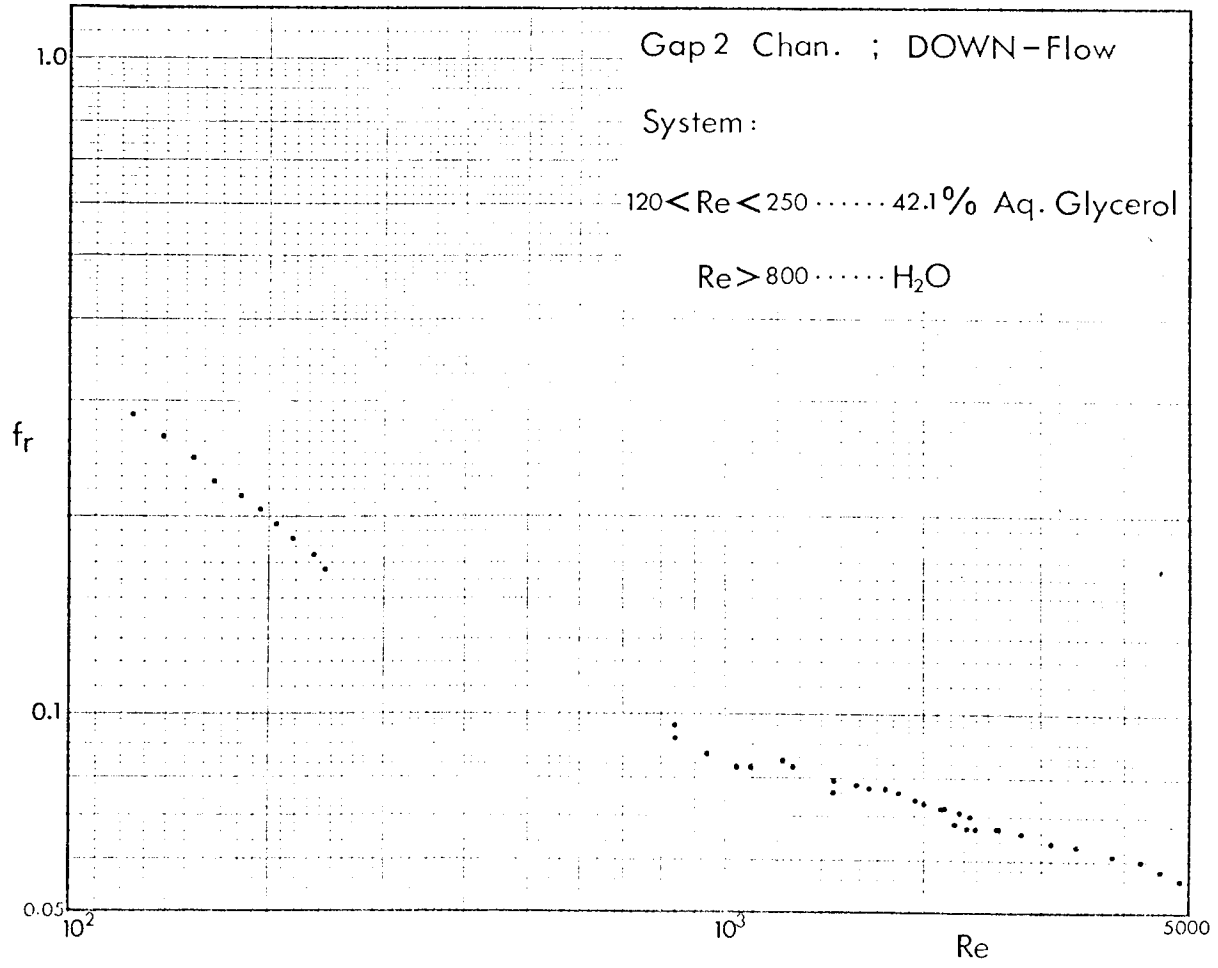

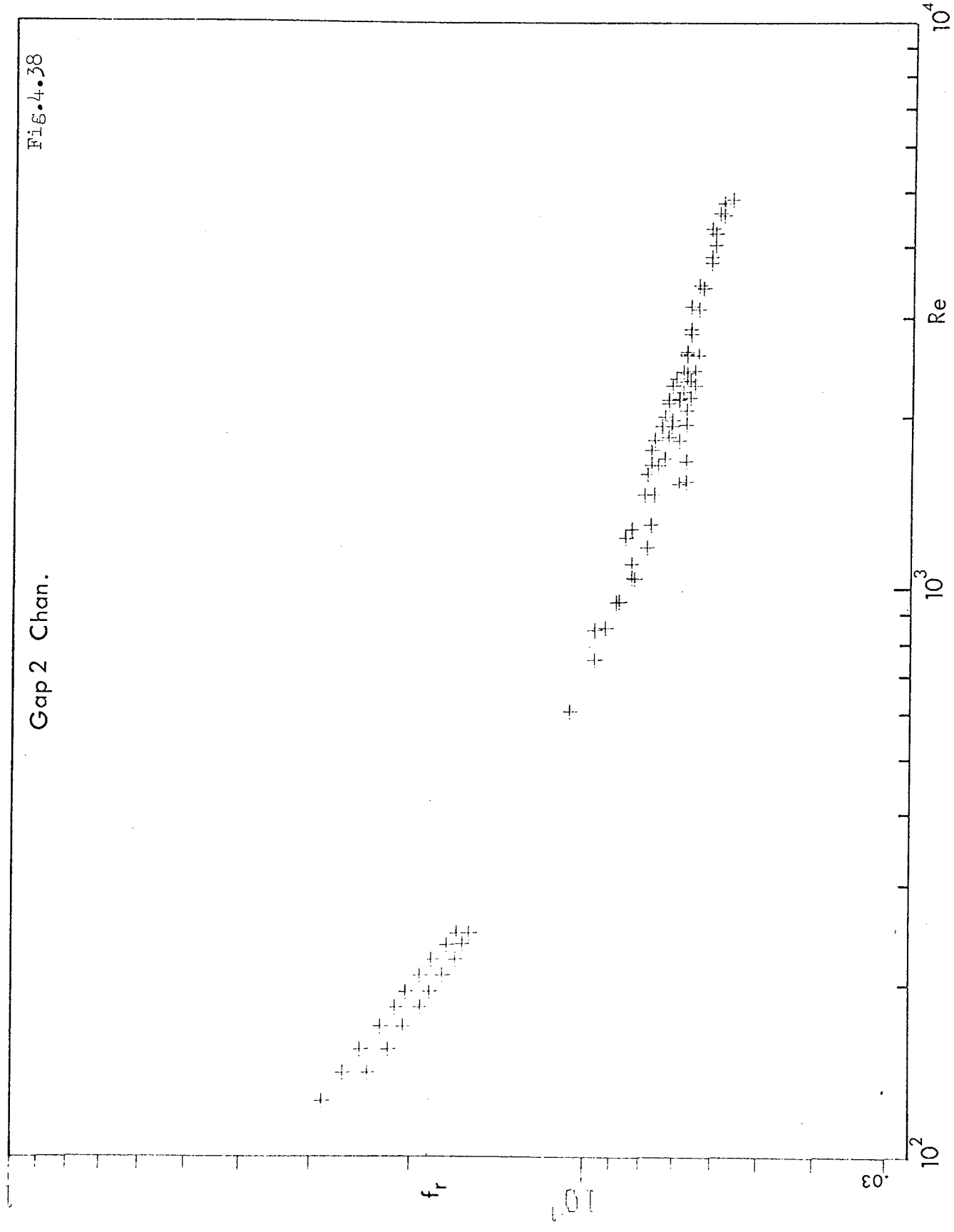

Fig.4.38

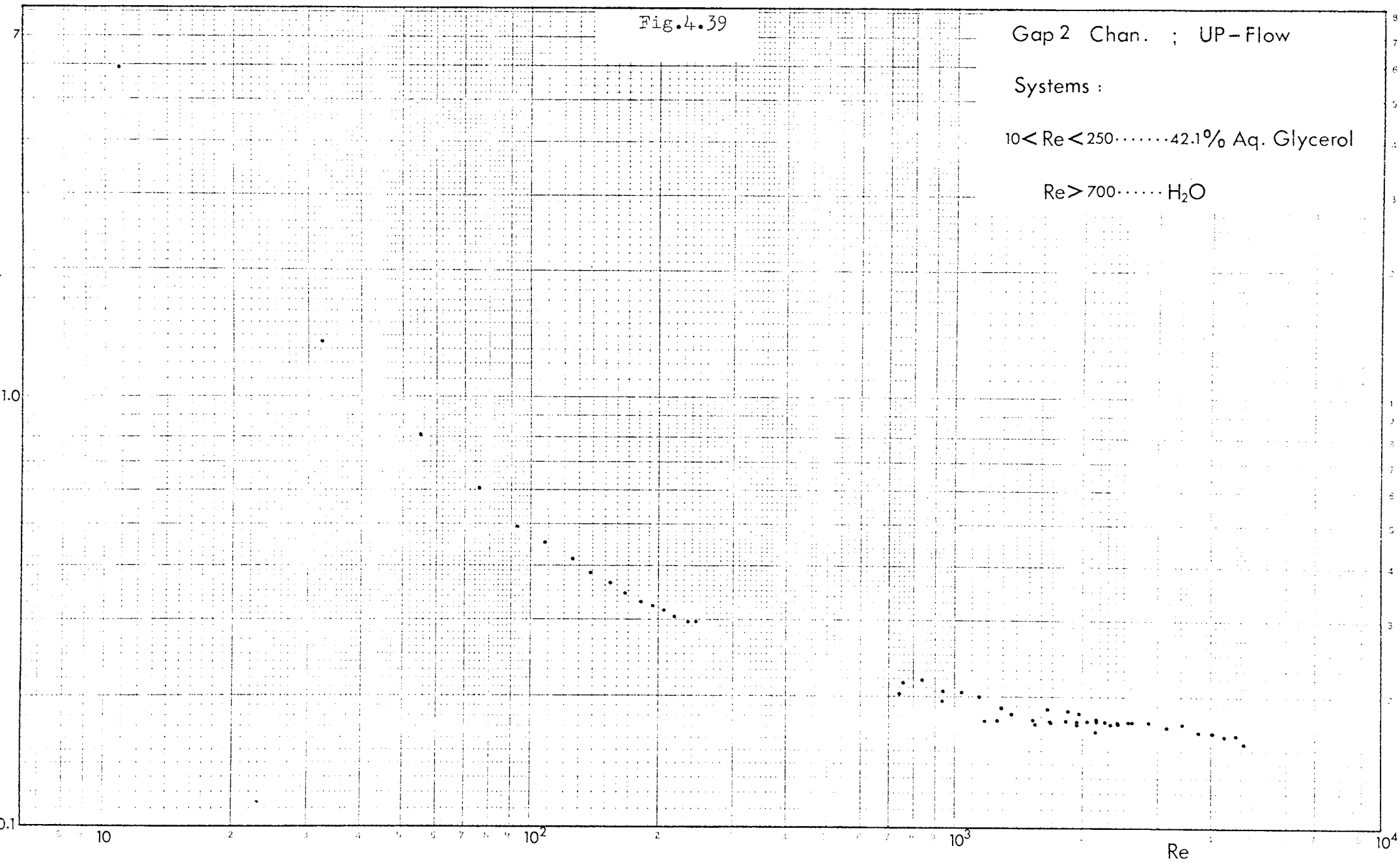
Fig.4.39
Gap 2 Chan. ; UP-Flow
Systems :
10< Re <250·····42.1% Aq. Glycerol
Re>700····· H_2O
1.0
0.1
10
10^2
10^3
10^4
Re

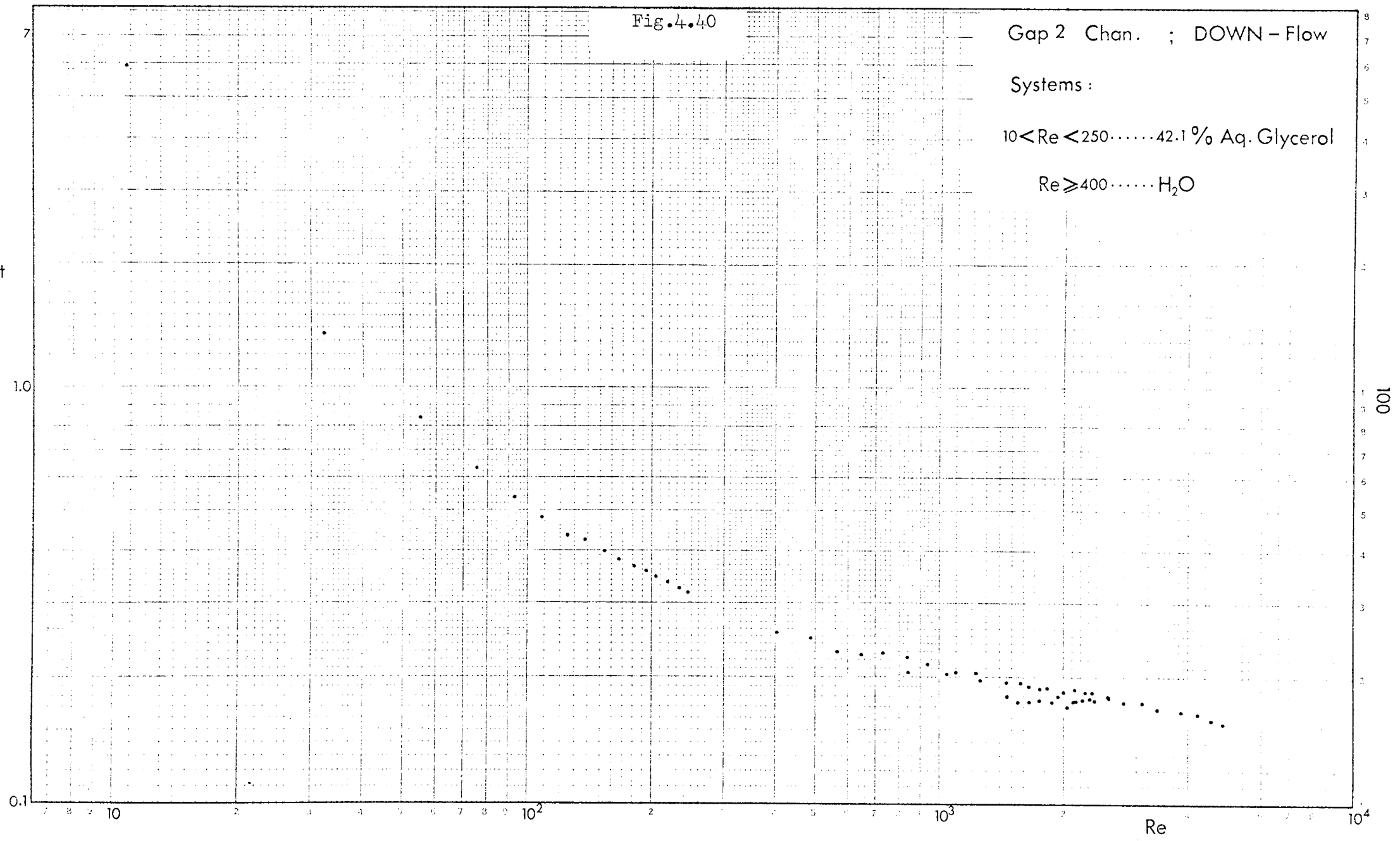
Fig.4.40
Gap 2 Chan. ; DOWN – Flow
Systems :
10 < Re < 250 ..... 42.1 % Aq. Glycerol
Re ≥ 400 ..... H_2O
f
7
1.0
0.1
10
10^2
10^3
10^4
Re
100

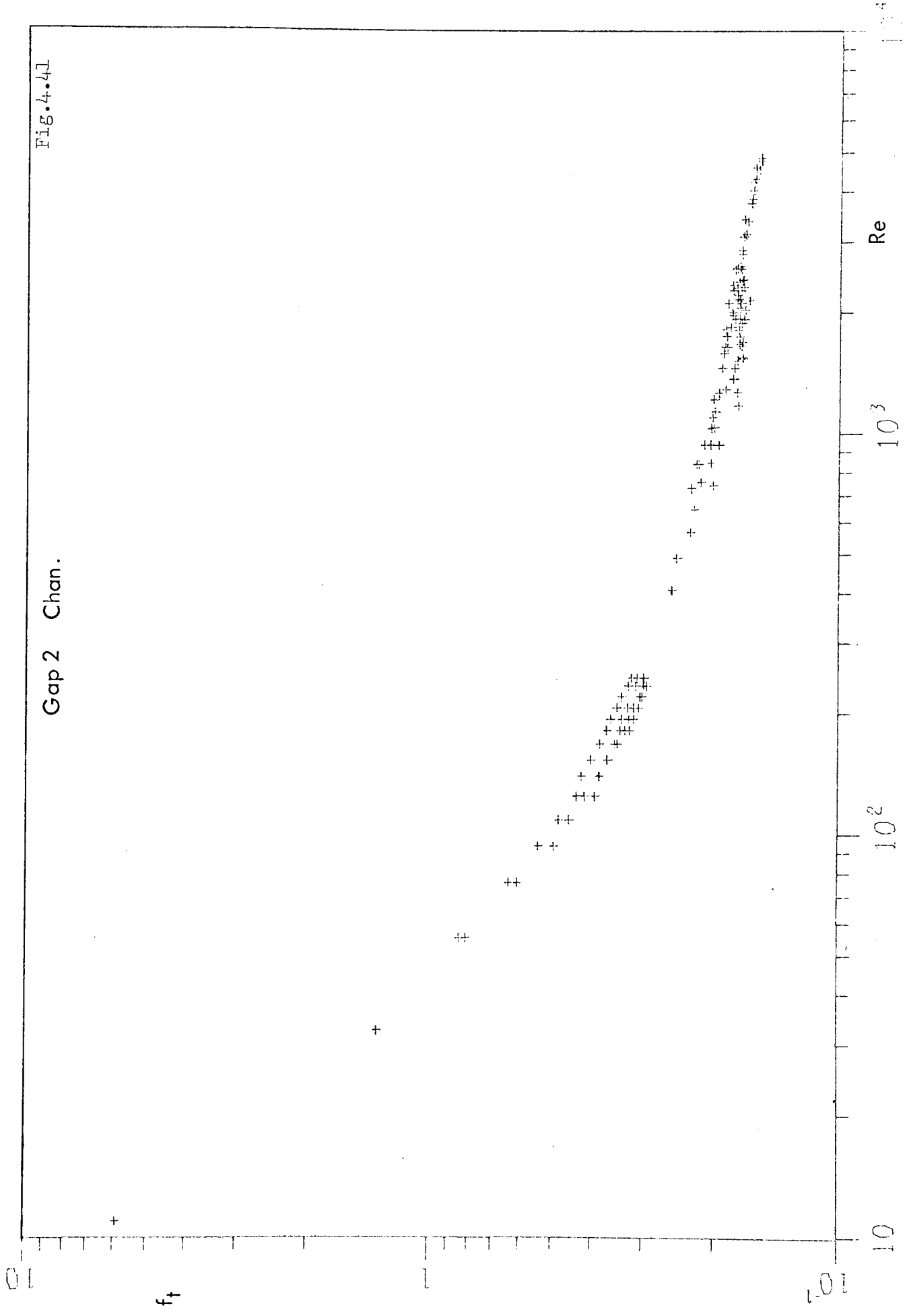

Fig.4.41

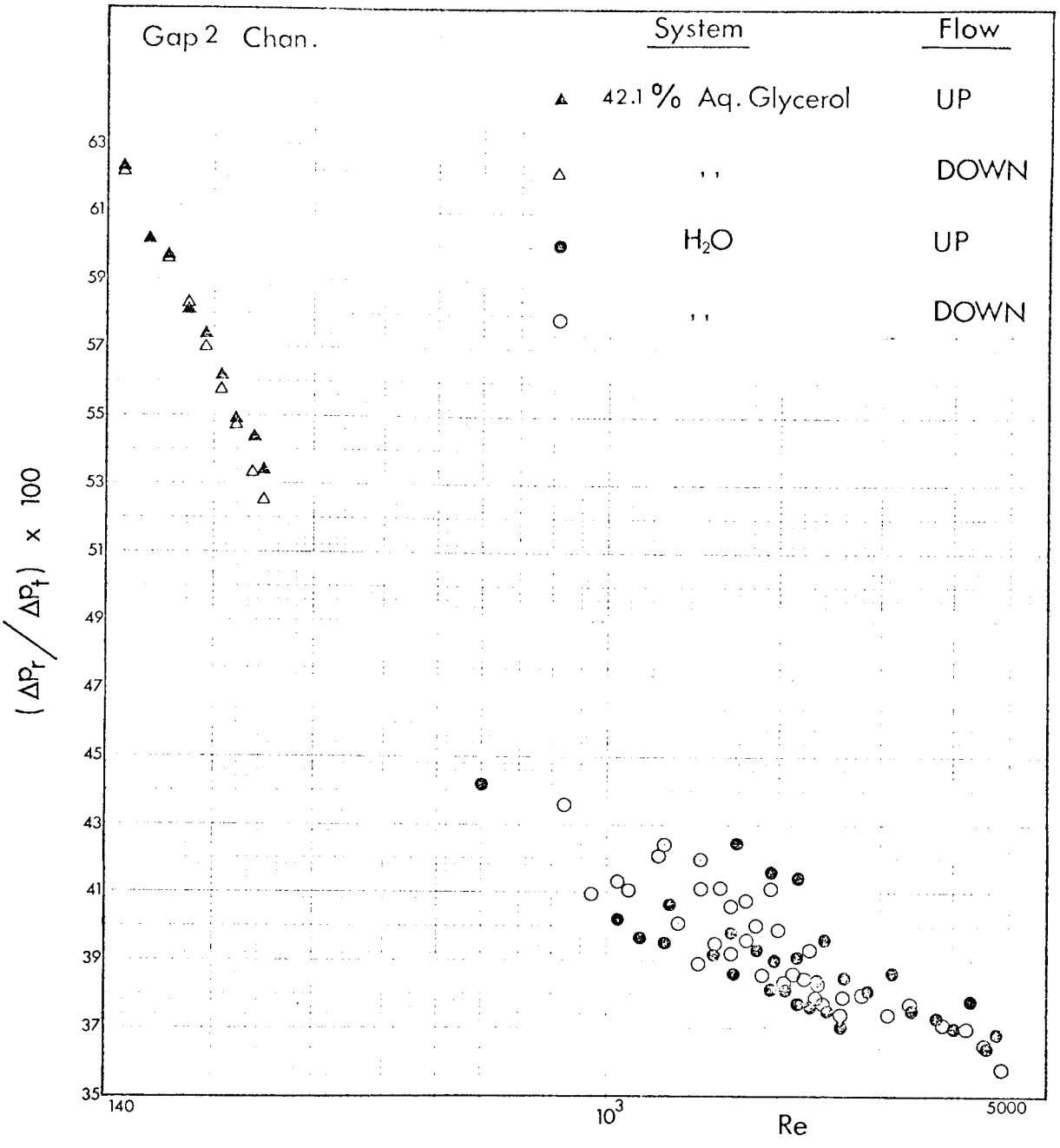
Gap 2 Chan.
System
Flow
42.1 % Aq. Glycerol
UP
,,
DOWN
H_2O
UP
,,
DOWN
$(\Delta P_r / \Delta P_t) \times 100$
63
61
59
57
55
53
51
49
47
45
43
41
39
37
35
140
10^3
5000
Re

Fig.4.42

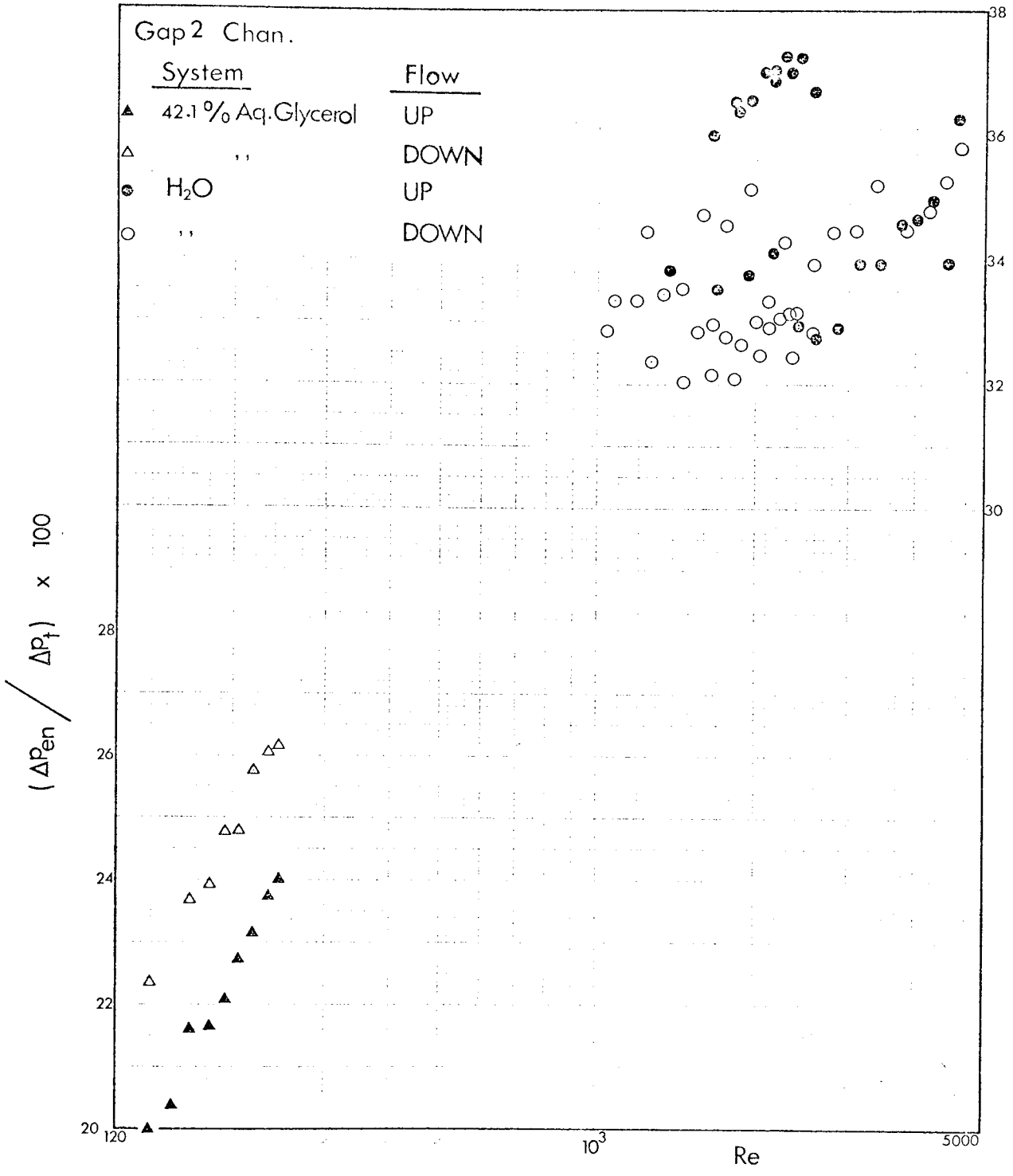
Gap 2 Chan.
System
Flow
42.1 % Aq. Glycerol
UP
,,
DOWN
H_2O
UP
,,
DOWN
$(\Delta p_{en} / \Delta p_t) \times 100$
20
22
24
26
28
30
32
34
36
38
120
10^3
5000
Re

Fig.4.43

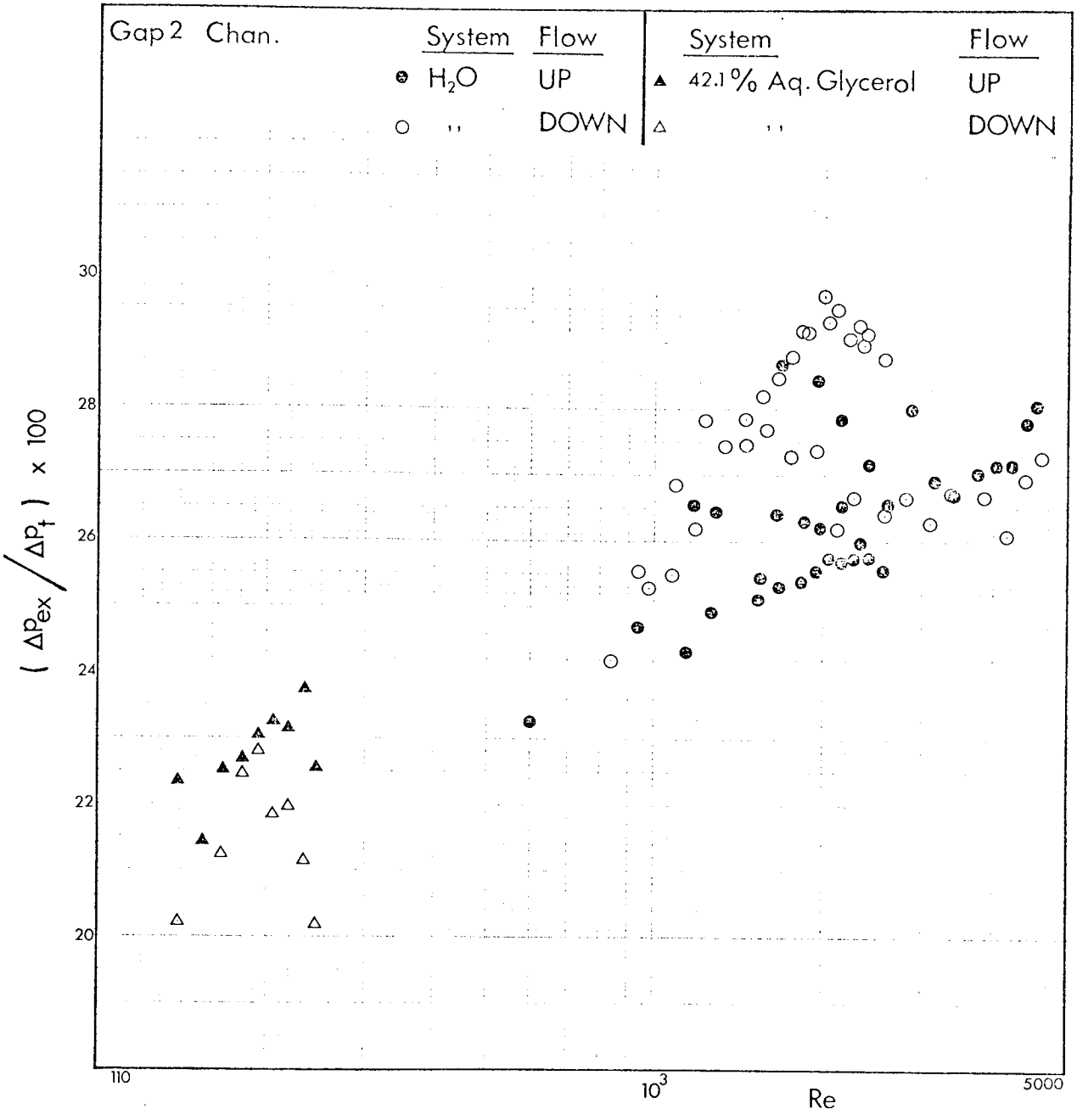
Gap 2 Chan.
System
Flow
H2O
UP
,,
DOWN
System
Flow
42.1% Aq. Glycerol
UP
,,
DOWN
(ΔPex / ΔPt) x 100
30
28
26
24
22
20
110
10^3
5000
Re

Fig.4.44

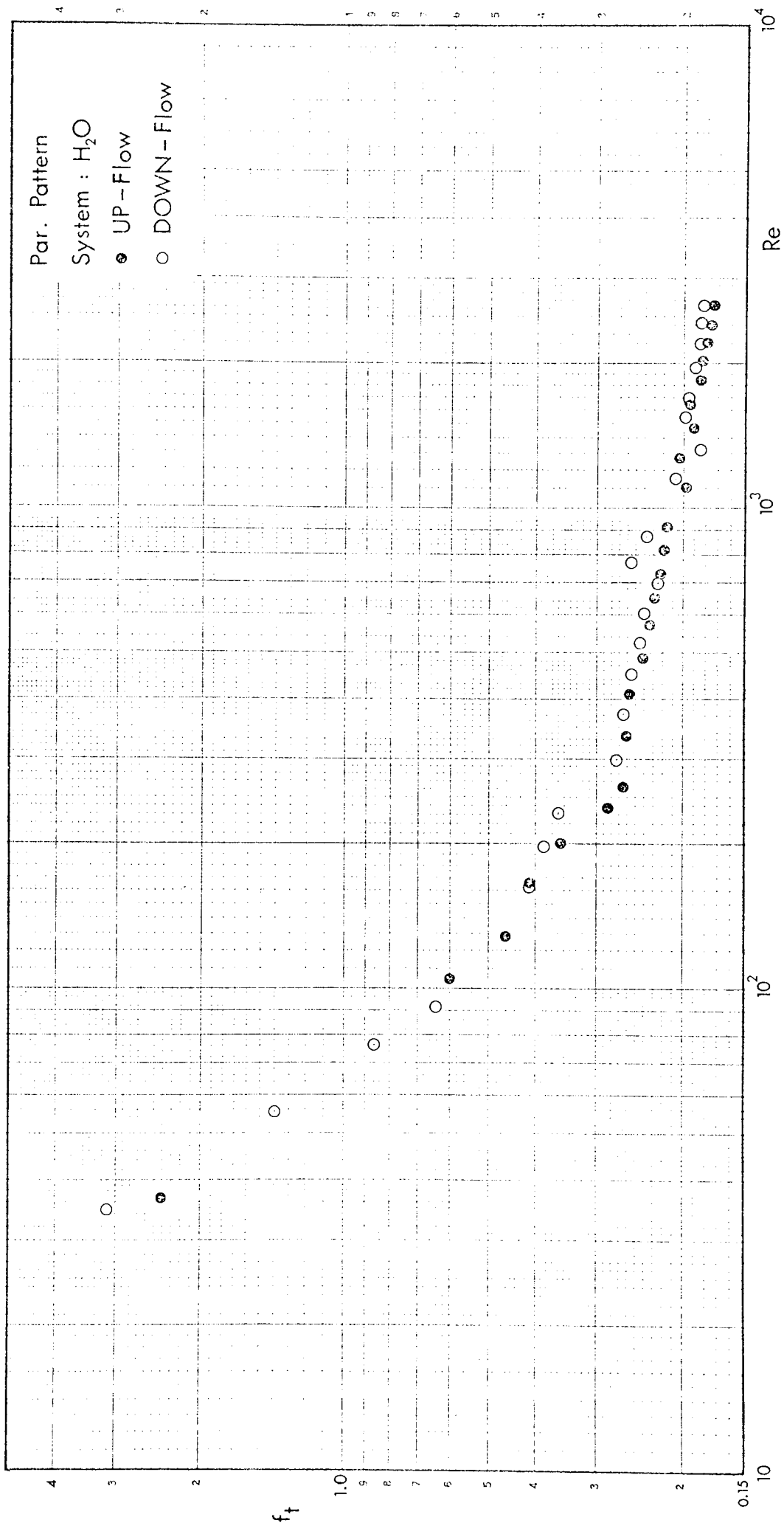
Par. Pattern
System : H_2O
● UP-Flow
○ DOWN-Flow
f_t
Re
4
3
2
1.0
0.15
10^2
10^3
10^4

Fig. 4.45

CHAPTER 5

DISCUSSION

5.0) DISCUSSION

5.1) DEFINITIONS AND ESTIMATIONS OF PARAMETERS

If comparisons between different plate heat exchangers are not envisaged and one is determining the performance of a particular exchanger solely to predict the performance of that heat exchanger with another fluid or another duty, then the choice of defintions of parameters can be totally arbitrary. However, definitions matter when comparisons are to be made with other types of plate. This situation becomes more critical in the case of 3-dimensional trough form plates. For instance, the plate projected area is important in an economic assessment, and is a significant factor in plate manufacture but it is irrelevant in considering plate performance. The comparison of one trough form with another in terms of their heat transfer and pressure drop characteristics must be based on the developed area, i.e. the concept of heat transfer coefficients and pressure gradients cannot be applied in a 3-dimensional geometry using 2-dimensional and one-dimensional terms. Furthermore, the basic nature of the present work also demands special considerations for the definitions and estimations of the relevant parameters.

The equivalent diameter as defined by equation (4.2) is really an equivalent to the equivalent diameter which is:

$$De = \frac{4 \times \text{Flow area}}{\text{Wetted Perimeter}} \qquad (5.1)$$

The concept of equivalent diameter as expressed by equation (5.1) is empirical and has no theoretical justification and in some geometries (e.g. annuli) with laminar flow it has been shown to lead to errors[10]. Nevertheless, because the flow channels in a PHE are complex and an analysis of the performance, based on the equations of motion and energy, is impossible the use of equivalent diameter enables us to envisage the flow between plates as flow in

a straight pipe of diameter De.

For channels, made from 2-dimensional flat plates, in which the plate gap b is negligible in comparison with the plate width W, equation (5.1) could be reduced to:

$$De = \frac{4Wb}{2W+2b} = \frac{4Wb}{2W} = 2b \qquad (5.2)$$

Equation (5.2) was applied not only to 2-dimensional trough form plates but also to 3-dimensional ones until Parrott[30] suggested the definition given by equation (2.10) for the 3-dimensional plates.

Even in some recent works on 3-dimensional plates the fluid velocity and pressure gradient are still being based on a 2-dimensional plate flow area (cf. equations (2.11), (4.3), and (4.4)) and a projected channel length respectively.

The developed heat transfer area of a plate is a little less than the wetted plate area, the difference depends on the particular plate design. Therefore when considering equation (5.1) it can be deduced that it is the wetted surface which should have been used in equation (4.2) rather than the developed heat transfer area. This is not so because the plate developed length used corresponds to the developed heat transfer area, which were both available. In any case the difference between the two areas is rather small in the APV Junior plate.

The perspex model made direct volume determination possible and therefore strict adherence to the definitions given at the beginning of Chapter 4 was achieved.

5.2) STANDARD CHANNEL RIBBED SECTION

Fig.4.7 reveals that up to a Reynolds number of about 12 the ribbed section friction factor f_r is inversely proportional to the Reynolds number. The slope of virtually minus one signifies

laminar flow, being analogous to the Hagen-Poiseuille equation for developed laminar flow in tubes. However, Cattell[13] and Parrott[30] indicate that recent studies at the APV Co. into the local flow behaviour of water within the channels of a pressed form showed evidence of separated flow extending into the laminar region. On this evidence, the notion of continuous boundary layer in laminar flow is invalid and therefore casts doubt on the assumption of true 'laminar' flow in PHE's prompting the use of the term 'viscous flow'.

As Re increases, the hydraulic entry length is increased causing change in the velocity profile - the transition region. However, the extremely gradual nature of this change, as indicated by Fig.4.7, implies only a limited level of turbulence up to a Reynolds number of 100. This may be termed the 'quasi-viscous' part of the transition region where the mechanism is basically controlled by laminar boundary layer(s) subjected to separation. The degree of turbulence seems to increase rapidly beyond a Reynolds number of 100 until the friction factor becomes virtually constant and independent of Re in the range $200 \leq Re \leq 300$. In the $100 < Re \leq 300$ 'quasi-turbulent' part of the transition region the separated boundary layer(s) have probably become partially laminar and partially turbulent. The independence of transition flow from flow history, i.e. as Re is experimentally increased from viscous through transition to turbulent flow and back again the friction factor follows a unique path without hysterisis, supports the theory that a PHE channel acts as an entrance region which reacts immediately to changes in flow rate[13].

The high concentration of data points in the Re range 150 to 400 resulted from the unexpected shape of the curve obtained from the initial work. Since the kink had not been reported elsewhere, all other published work indicated a smooth curve in this region, it was considered necessary to pay particular attention to this area.

A large number of runs were therefore carried out under very carefully controlled conditions to ensure that the results presented in Fig.4.7 were genuine and repeatable.

The apparent discontinuity at Re = 300 is probably the result of change in the boundary layer(s) from partially laminar/partially turbulent to completely turbulent and therefore the start of the turbulent region. It may be interesting to note that the ribbed section friction factor/Reynolds number relationship bears striking resemblance to the drag coefficient/Reynolds number relationship of a circular disc with the flat side perpendicular to flow[32] to the extent that the discontinuity occurs at almost the same Reynolds number. The drag on such an object is totally due to normal stress with virtually no tangential stress. It is, however, difficult to visualise the complex geometry of the PHE channel with its continually changing shape to be equivalent to that of a flat disc.

Fig.4.7 shows no secondary viscosity effect, i.e. the friction factor seems to be a function of Reynolds number only. Parrott[30] revealed that for 2-dimensional trough forms the transition region is given by a family of f-Re curves whose parameter is viscosity, with a low viscosity fluid giving rise to a higher friction factor - pressure drop - than a more viscous one at the same Reynolds number. This is explained by the fact that in a 2-dimensional geometry, expansion and contraction of the fluid elements is not experienced and changes of direction are only accompanied by changes in momentum of the fluid boundary layer, which are a function of viscosity. In a 3-dimensional geometry, however, the fluid flows through a series of cavities of varying cross-section, where alternate expansion and contraction of the fluid elements takes place. Hence, energy loss is mainly due to eddy

effects which are only dependent on Re.

The direction of flow does not seem to have any effect on the friction factor/Reynolds number relationship. This is borne out by Fig.'s 4.1-4.7.

If a single best-fit Ergun type model is employed to correlate all the data of Fig.4.7 on the lines suggested by Edwards et al.[20] then it will be as follows:

$$(3 < Re < 3000) \qquad f_r = \frac{36.329}{Re} + 0.319 \qquad (5.3)$$

Equation (5.3) could be re-arranged in the following manner:

$$f_r - 0.319 = \frac{36.329}{Re} \qquad (5.4)$$

Taking the logs of both sides:

$$\log(f_r - 0.319) = \log 36.329 - \log Re \qquad (5.5)$$

If the model expressed by equation (5.3) holds then a plot of $\log (f_r - 0.319)$ vs. log Re should produce a straight line with a slope of minus one. The result is shown in Fig.5.1. It is evident that equation (5.3) holds reasonably well only up to a Reynolds number of about 220. The discontinuity in the data is rather dramatically illustrated in the figure, followed by points indicating the failure of the Ergun type model. Consequently it was decided to fit an Ergun type relationship for the data in the range $3 < Re < 300$, equation (4.7), and a straight-line model for the data in the range $300 \leq Re < 3000$, equation (4.8).

It must be pointed out though that equation (4.7) is not really the best model for the data in the range $200 \leq Re < 300$ since it represents a shallow curve and the friction factor is virtually constant (average $f_r = 0.465$) or has a slightly increasing tendency with increasing Re in this range. In fact, the curve represented by equation (4.7) cuts through the data in the $200 \leq Re < 300$ range predicting a slightly higher pressure drop

Fig. 5.1

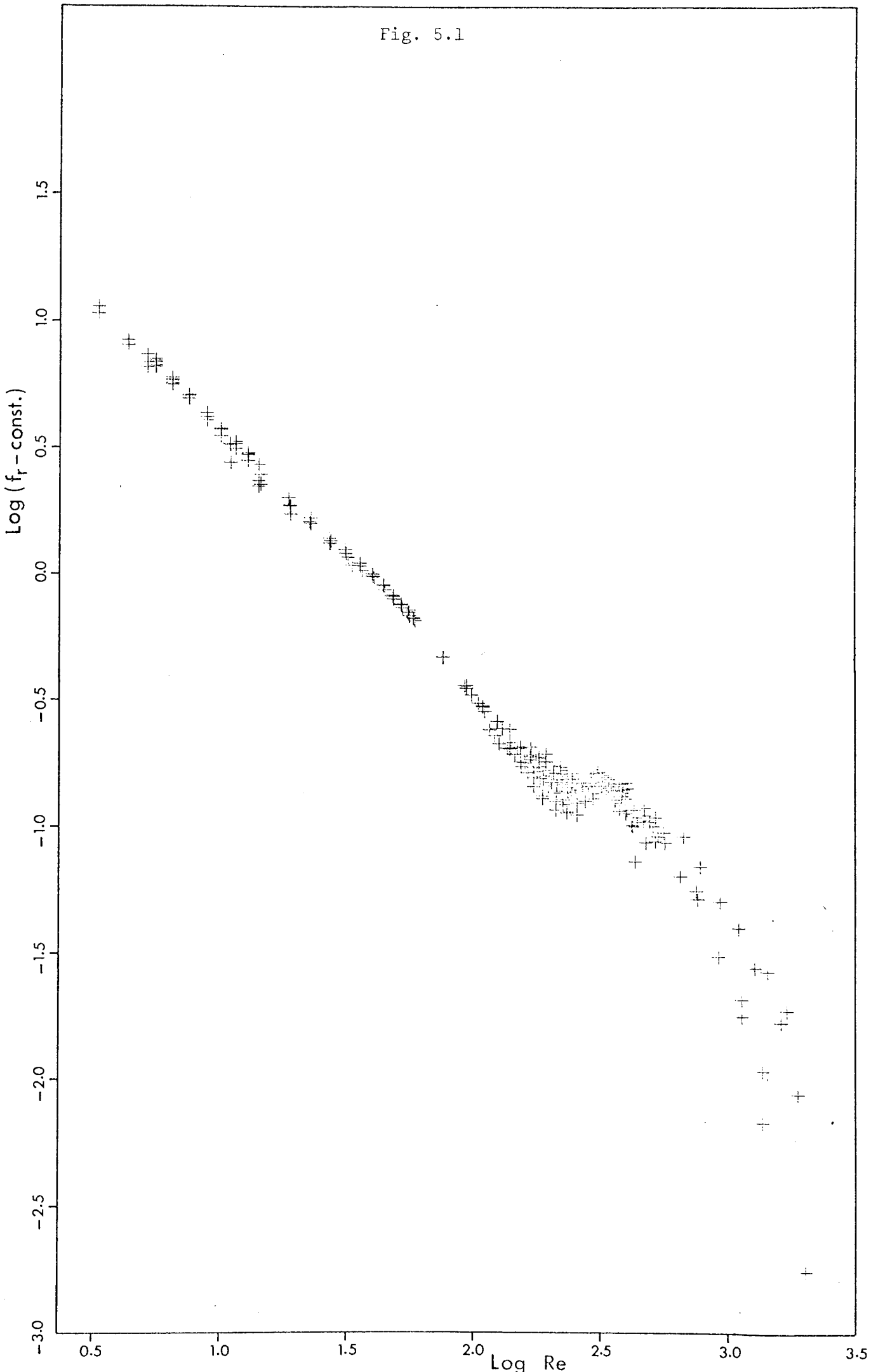

and a slightly lower one at the beginning and end of this range respectively. The standard percentage error of estimate (root mean square value of percentage error), a measure of the data scatter about an empirical model, pertaining to equation (4.8) is 2.79 which is 3-times less than the value of 8.58 resulting from equation (5.3) in the range Re ≥ 300.

The plastic model employed in this work represents an end channel of a single-pass U arrangement (Fig.1.1) and it may be argued that the discontinuity at Re = 300 could be due to the disturbance the fluid is subjected to, at the entrance to the channel. However, the data of Savostin and Tikhonov[33] on specimens B-4 and B-5 (Fig.2.4) suggests that the observed discontinuity is characteristic of the hydrodynamic behaviour in this geometry since the entrance effect was accounted for and removed (equation (2.29)). It is interesting to note the effect of the angle ψ between the corrugations of adjacent plates on the Reynolds number at which the kink occurs (120° for the Junior and 66° for B-4).

5.3) THE STANDARD CHANNEL

The inclusion of the entrance and exit pressure losses in the pressure drop used to calculate the resistance coefficient f_t seems to have had a significant effect on the hydrodynamic characteristics as could be seen in Fig.4.16. In addition to the higher friction factor, the discontinuity at Re = 300 has become insignificant and almost unnoticeable. Instead, a marked discontinuity appears to take place at a Reynolds number of 400.

The resistance to flow in this case is due to the two sharp 90° changes in flow direction and the possible flow separation at the edges of the two ports, in addition to flow separations which occur at the numerous changes of direction in the tortuous flow passage and of course frictional losses. Furthermore, an additional

disturbance results from the variable flow area in the regions of the two ports giving rise to a constantly changing velocity profile.

The data of Fig.4.16 run parallel to those of Fig.4.7 in the viscous region, i.e. up to Re of about 12, however the gap between the two sets increases gradually in the transition region reaching a maximum just before the discontinuity at Re of 300. The two sets of data become closer at Re ≥ 300 with the difference between them starting to increase very gradually at the end of the range.

Apart from the foregone discrepancies, the two sets of data are similar and the comments on the ribbed section results apply here as well. This is confirmed by Fig.'s 4.8-4.16.

Equations (4.9) and (4.10) are a reasonably accurate way of describing the data of Fig.4.16. A more accurate description for the data in the range covered by equation (4.9) would be achieved by fitting a Hagen-Poiseuille type relationship for the data in the viscous region up to an Re of 12, namely:

$$f_t = \frac{46.85}{Re} \qquad (5.6)$$

and an Ergun type model for the data over the range $12 \leq Re \leq 400$ which would be very similar to equation (4.9) itself. However, the marginal increase in accuracy is more than offset by the use of two equations instead of one. The other extreme would be to describe all the data by a single Ergun type equation, namely:

$$(3 \leq Re < 3000) \quad f_t = \frac{44.142}{Re} + 0.446 \qquad (5.7)$$

This equation, clearly, is very similar to equation (4.9) and therefore it is the range corresponding to Re > 400, the fully-turbulent region, which will be at a disadvantage because of its use.

Equation (4.10) indicates a smaller slope for the standard channel data corresponding to Re ≥ 400 (-0.196) than that pertaining

to the ribbed section data in the range Re ≥ 300 (-0.230) pointed out by equation (4.8). This suggests that the entrance and exit inclusion has lessened the dependence of the friction factor on Reynolds number implying higher levels of turbulence.

5.4) ANALYSIS OF STANDARD CHANNEL PRESSURE DROP

In spite of the scatter in the data of Fig.4.17, the variation in the percentage contribution of the ribbed section, to the standard channel total pressure drop, with Reynolds number is clearly revealed. This contribution seems to be almost constant in the viscous region at about 81.5%. It then gradually decreases to 80% at a Reynolds number of just over 40. The decline in the ribbed section contribution becomes rapid as Re is increased to more than 45 and reaches a recorded minimum of about 70% at a Reynolds number of around 200. The turning point takes place at Re = 300 beyond which the contribution increases and seems to stabilise with an average of about 78.5% at Re > 1000. The Reynolds number at which the contribution terminates its descent corresponds to the point at which the discontinuity in the f_r vs. Re relationship was observed (Fig.4.7).

The general trend given by Fig.'s 4.18-4.21 regarding the entrance and exit contributions, to the total pressure drop of the standard channel, is that it is constant in the viscous region, increases to a maximum in the transition region, followed by discontinuity, it then becomes stabilised in the fully-turbulent region. However, it is evident that discrepancies exist among the four graphs. In the viscous region the contribution of the entrance (Fig.'s 4.18 and 4.20) averages about 8% which is lower than the 11% average contribution of the exit (Fig.'s 4.19 and 4.21). It is important to note that the terms entrance and exit refer to different ports depending on the direction of flow. In the transition region up to

a Reynolds number of about 70 the entrance (or exit) contribution trend seems to be independent of the flow direction and therefore whether the port is the upper or lower one, in spite of the scatter in the data, i.e. in the range $10 < Re < 70$ Fig.4.18 is similar to Fig.4.20and Fig.4.19 is similar to Fig.4.21. However, in the remainder of the transition region it appears that the location of the port becomes more important, i.e. in the range $70 < Re < 300$ Fig.4.18 is similar to Fig.4.21 and Fig.4.19 is similar to Fig.4.20. The upper port contributes more than the lower one and the maximum recorded was 15% of the channel total pressure drop at a Reynolds number of about 200. In the turbulent region, the average port contributions in Fig.'s 4.18-4.21 are 12%, 10%, 8.5%, and 11% of the total pressure drop respectively.

Small physical differences in the gasket around the ports could be expected to have an effect on the pressure drop. Another effect could be expected from the changes in shape of the flow channel: i.e. entrance is from a circular pipe into a rectangular duct which increases in cross-sectional area into the contoured surface section of the PHE channel proper, while the exit has the reverse description. Flow in the pipe leading to the entrance was generally fully developed during experimental work whereas flow in the pipe at the exit was disturbed due to the geometry of the port.

In order to utilise the available pressure drop productively to generate the maximum heat transfer coefficient it follows that as much of this pressure drop as practicable should be consumed in the ribbed section and that the losses in the ports be kept to a minimum. The foregone analysis of the contributions of the ribbed section and the ports suggests that the quasi-turbulent part of the transition region does not appear to be conducive to the productive utilisation of the pressure drop in comparison with other flow regions. This argument, at this stage, applies only to the single model-channel.

5.5) STANDARD CHANNEL FLOW VISUALISATION

Observations with dye can be misleading and are only qualitative. It was still felt worthwhile to include photographs showing the dye behaviour because some upheld the trends suggested by the quantitative experimental results and the others may be of use to other workers. Thus it is considered that the dye results should not be over influential yet at the same time they should not be disregarded. It is emphasised that the dye filaments were obtained by injecting the dye with as low a velocity as possible through a hypodermic tube, or when a pulse of dye was involved by the very rapid opening and closing of the solenoid valve.

Fig.4.22 depicts the behaviour of a dye filament as the flow rate is gradually decreased from one corresponding to a Reynolds number of about 12 to a rate corresponding to Re $\ll$ 3. Therefore, the viscous region is involved here. The medium is 65.45% aqueous glycerol and the direction of flow is upward. The sequence starts with the dye filament travelling "straight" up the channel. The word "straight" in the context of the channel geometry is in practice a sinusoidal line. Two minor splits occur at the lower half of the channel, but otherwise the filament remains intact. It must be stressed that the dye flow was left unpurturbed as the flow rate was decreased. The filament shifts from the left side of the channel to the right side and the "straight" path becomes a unimode curve at Re of about 5.5 and 4.3. Diffusion of the dye is also observed. This is due to the increasing residence or hold-up time. The unimode path becomes bimode when the flow corresponds to Re of less than 3 and greater diffusion of the dye takes place. As it enters the channel, the filament keeps shifting towards the right side and in the last frame of the set it is travelling alongside the gasket in the lower right side of the channel.

In Fig.4.23 the medium is water instead of aqueous

glycerol, i.e. the viscosity is 16-times lower, but the direction of flow remains upward. Hence for the same Reynolds number the flow rate of water is roughly 16-fold higher than that of the aqueous glycerol because the variation in the density is very small. The starting flow rate corresponds to a Reynolds number of about 4 and was gradually increased to a rate corresponding to $Re \approx 46$, therefore covering both viscous as well as transitional flow. In the first frame the dye filament is travelling up the left side of the channel in the tiny recess adjacent to the gasket formed by the termination of the corrugations on the side furthest from the inlet port. The filament could be seen clearly in the exit region of the channel leaving the recess. This path, obviously, offers the least resistance to flow. Diffusion of the dye is evident. As Re increases, more dye splits from the filament flowing back and forth across the channel in a zig-zag manner. However, the 4th frame shows that at a Reynolds number of about 18 a substantial amount of dye is still flowing in the filament next to the left side of the gasket. The last frame is typical of transitional flow with part of the dye going "straight" up and other part going up zigzagging across the channel. It also appears that in the transition region the flow in the channel is viscous at the beginning then becoming turbulent downstream. The extent of each regime depends on the Reynolds number. This may explain the gradual and extensive transition region as observed in the friction factor - Reynolds number plot.

Fig.4.24 shows a sequence similar to that of Fig.4.23 except that the flow direction is downward instead of upward. These photographs show the dye filament travelling down the right-hand side of the channel near the edge adjacent to the inlet port. Apart from this difference the comments on Fig.4.23 apply here as well, i.e. more cross flow as Re increases rendering the filament fainter until it disappears altogether. The last frame corresponding to a

Reynolds number of about 46 is very similar to the one in Fig.4.23 confirming the existence of "straight" and cross or zigzagging viscous flow followed by turbulence downstream.

At higher Reynolds number, flow visualization is not possible because of the immediate dispersion of the dye.

The 7-frame sequence in Fig.4.25 shows the development of the velocity profile in the viscous region at a Reynolds number of about 10. The system is 65.45% aqueous glycerol and the flow direction is upward. The effect of the 90° sharp change in flow direction from a circular pipe to the channel, followed by convergence and then divergence as the flow area increases to a maximum at the end of the entrance is clearly there. At the beginning of the ribbed section the velocity profile is almost flat, then the parabolic profile starts developing gradually. However, it takes more than one-half the channel length before the profile is fully developed (cf. 4th, 5th, and 6th frames).

In Fig.4.26 the medium is water and the upward flow corresponds to a Reynolds number of about 25, i.e. quasi-viscous flow. In this case, the disturbance due to the port is obviously greater. The fact that both ports are on the same side of the channel (vertical flow) is causing the fluid to travel faster in the ports side. These factors are evidently affecting the development of the velocity profile as could be established from the 8-frame sequence. It therefore seems that the whole plate length lies within the entry length required for the velocity profile to be fully-developed.

It should be noted that at higher Reynolds numbers the main factors contributing to flow disturbances are the geometry of the plate and the 90° sharp turn plus the entrance region, in which case the positioning of the two ports on one side or on opposite sides becomes of minor importance[4].

5.6) GAP 1 CHANNEL RIBBED SECTION

In the gap 1 channel there is no contact between the plates and the equivalent diameter is 1.256 times that of the standard channel. Water was the only medium used in this channel and pressure drop data were obtained in the range $200 < Re < 3000$ with respect to the ribbed section. No significant difference was observed between UP-flow and DOWN-flow as could be established from Fig.'s 4.27-4.29. The first thing to be noticed about the ribbed section data of Fig.4.29 is the disappearance of the discontinuity observed at Re = 300 in the standard channel ribbed section f_r-Re relationship. Instead there is a marked change of slope at a Reynolds number of just over 700, probably indicating the start of the fully-turbulent regime. At a given Re, the friction factor has evidently become lower than the one relevant to the standard channel ribbed section (Fig.4.7). Hence, the f_r-Re relationship corresponding to fully-turbulent flow, for instance, is lower and to the right of the corresponding one in Fig.4.7.

Equation (4.12) indicates less dependence of f_r on Re (slope of -0.194) than the case with the standard channel (slope of -0.23) pointed out by equation (4.8). All the results of Fig.4.29 could also be correlated in a single Ergun type equation, namely equation (4.11). It may be interesting to note that the first term in the right-hand side of equation (4.11), accounting for the viscous forces dominant in the viscous region is very similar to the corresponding one in equation (4.7), pertaining to the standard channel ribbed section, whereas the second term, which is the turbulent contribution to the pressure drop becoming important at higher Reynolds numbers, is only 40% of the corresponding term in equation (4.7). This suggests that the effect of the loss of contact between the plates becomes more pronounced as Re increases,

i.e. the gap between the data of Fig.'s 4.7 and 4.29 increases with Re, highlighting the importance of contact between the plates in the attainment of high heat transfer coefficient/ pressure drop in the turbulent region.

5.7) THE GAP 1 CHANNEL

The inclusion of the two port regions (Fig.'s 4.30-4.32) does not seem to have altered the nature of the friction factor-Reynolds number interaction to the extent observed with the standard channel. Nevertheless, the f_t-Re relationship as shown in Fig.4.32 is quite different from that between f_r and Re in Fig.4.29. In this case the results follow a shallow curve over the range $150 < Re \leq 750$, then the resistance factor f_t becomes virtually constant (ca. 0.255) between Re of 750 and about 1030. At higher Re, f_t becomes dependent on Re again and follows a straight-line relationship.

Although the gap between the data of Fig.4.32 and that of Fig.4.16 pertaining to the standard channel increases with Re in a similar manner to the one between the data of Fig.'s 4.29 and 4.7, the rate of increase in the difference between the f_t's is much slower than that between the f_r's as Re is increased. This suggests an increasingly significant effect of the entrance and exit on the total pressure drop of the channel after losing contact between the two plates.

The slope of the data in the range $Re \geq 750$ as indicated by equation (4.14), i.e. (-0.124), is smaller than that relevant to the data of the ribbed section over the same Re range as pointed out by equation (4.12), i.e. (-0.194). This confirms the same trend observed with the standard channel, however, the change in the slope is greater in this case owing to greater port contributions to the channel total pressure drop.

Due to its nature, all the data of Fig.4.32 could also be correlated in a single Ergun type model, namely equation (4.13). Equation (4.13) is similar to equation (4.9) of the standard channel in its viscous contribution term, but the turbulent contribution term is only 45% of the corresponding one in equation (4.9) which is roughly the position of the equations pertaining to the ribbed section.

5.8) ANALYSIS OF GAP 1 CHANNEL PRESSURE DROP

The contribution of the ribbed section to the gap 1 channel total pressure drop decreases rapidly as Re increases as could be seen in Fig.4.33. At a Reynolds number of 300 the percentage contribution is roughly similar to that of the standard channel ribbed section, however the loss of contact between the plates not only has lowered its magnitude but has also reversed its variation trend with increasing Re, at Re > 300. The decline in the ribbed section percentage contribution is about twice as much as the increase in that contribution when there was contact between the plates over the same range of 300 < Re < 3000 (cf. Fig.4.17).

The port contribution results of Fig.'s 4.34 and 4.35 show on the whole less scatter than those of the standard channel ports. The data are also more readily classified as belonging to the entrance or exit whether the port in question is the upper or lower one, i.e. independent of flow direction. It should be stressed here that in the case of the gap 1 channel a new gasket, thicker than the original one, was employed. This gives more weight to the suggestion that the gasket may be responsible for the discrepancies noticed between the results of the upper port and those of the lower port in the standard channel.

The entrance contribution is a little higher than that of the exit with the difference between them increasing with increasing

Re because the entrance contribution is rising at a faster rate than that of the exit as could be seen in Fig.'s 4.34 and 4.35.

5.9) GAP 2 CHANNEL RIBBED SECTION.

In this case the gap between the two plates was further increased rendering the equivalent diameter to be 1.775 times that of the standard channel or 1.412 times that of the gap 1 channel. Although there is a gap between the data of aqueous glycerol and those of water in Fig.4.38, the relationship between f_r and Re appears to follow a shallow curve which becomes a straight line at higher Re without any noticeable discontinuity. The fully-turbulent regime probably starts at a Reynolds number of about 1400 where there is a marked change of slope. Hence the increase in De has shifted the flow regions, in the friction factor-Reynolds number relationship, further to the right in addition to the lowering in the values of the resistance factor.

The slope of the data in the fully-turbulent region (-0.216) indicated by equation (4.16) is closer to that of the standard channel ribbed section Re $\geq$ 300 data than to the slope of the gap 1 channel ribbed section results in the fully-turbulent region by a ratio of 1:1.5. In other words the loss of contact between the plates reduces the dependence of the friction factor on Re, however this trend is reversed as the equivalent diameter is further increased by increasing the gap between the two plates.

Equation (4.15) describes the f_r-Re relationship reasonably accurately over the whole range of Fig.4.38. Comparing it with equation (4.7) of the standard channel ribbed section it could be seen that the drop in the turbulent contribution to the pressure drop is far greater than that in the viscous contribution since the constant in the first term is about 74% of the corresponding one in equation (4.7) whereas the second term is only 18% of the

turbulent contribution in equation (4.7). On the other hand, when equation (4.15) is compared with equation (4.11) pertaining to the gap 1 channel ribbed section it is found that whereas the relationship between the respective viscous contributions is similar to the aforementioned one with the standard channel, the turbulent contribution to the pressure drop is about 46% of the corresponding one in equation (4.11). This, again, highlights the effect of the contact between the plates in the degree of turbulence attained.

5.10) THE GAP 2 CHANNEL

The region between the aqueous glycerol and water results is narrower in the case of the channel total pressure drop as could be seen in Fig.4.41 giving more weight to the assumption that the friction factor-Reynolds number relationship follows a continuous shallow curve which becomes a straight line at higher Re.

Equation (4.18) indicates a slope, for the data in the fully-turbulent region, which is very similar to that of the gap 1 channel results in the turbulent region as pointed out by equation (4.14) but significantly smaller than the slope of the standard channel Re $\geq$ 400 results (eq. (4.10)). This is indicative of considerable port contributions since it has already been pointed out in section 5.9 that the slope of the ribbed section data in the turbulent region is closer to that of the standard channel ribbed section than the slope of the gap 1 f_r-Re results in the turbulent region. The substantial port contributions in the turbulent region is also manifested by the magnitude by which the slope of the friction factor-Reynolds number data diminishes after the inclusion of the entrance and exit, cf. equations (4.16) and (4.18) respectively. This decrease in slope is 1.25 times the corresponding one in the gap 1 channel but 2.6 times the decrease in slope in the standard channel.

Because of the small number of data points over the

range 10 < Re < 90 in Fig.4.41, it was decided to exclude them from the attempt to correlate all the data in a single Ergun type equation. The result was equation (4.17) which describes the f_t-Re relationship fairly accurately over all but the very end of the specified range, i.e. a slightly higher f_t is predicted at Re > 4000. When equation (4.17) is compared with equation (4.9) of the standard channel it becomes evident that the viscous contribution term is about 73% of the corresponding one in equation (4.9) which is the relationship between the viscous terms of the two respective ribbed section Ergun type equations, (4.15) and (4.7), as pointed out in the previous section. The turbulent contribution term in equation (4.17) is 36% of the corresponding one in equation (4.9) whereas the turbulent contribution term in equation (4.15) pertaining to the ribbed section was shown to be only 18% of the corresponding term in equation (4.7) of the standard channel ribbed section. This demonstrates the diminishing role of the ribbed section and the major role played by the two ports in the turbulent region.

5.11) ANALYSIS OF GAP 2 CHANNEL PRESSURE DROP

Fig.4.42 shows the percentage contribution of the ribbed section to the channel total pressure drop over the Reynolds number range 130 < Re < 5000. It is evident that the ribbed section contribution experiences a major decline over the range covered. The rate of decline is almost 4 times as great at the lower end of the range as it is at higher Re. Over the common Re range, 300 < Re < 3000, the drop in the contribution is 1.27 times that observed with the gap 1 channel.

The contributions of the entrance and exit are revealed in Fig.'s 4.43 and 4.44 respectively. It is clear that the two ports account for over 40% of the pressure drop at the beginning of the range rising to become 67% of the total pressure drop. It

could also be seen that the percentage contribution of the entrance is equal to that of the exit at the start of the range, however the entrance contribution rises at a faster rate than the exit when Re increases so that at the high-Re end of the range the entrance contributes significantly more than the exit. It also appears that whereas the rate of increase of the exit contribution is constant, that of the entrance is not and is higher at low Re. The degree of scatter in the data of Fig.'s 4.43 and 4.44 is noticeably greater than that observed in the gap 1 port contribution results (Fig.'s 4.34 and 4.35). It must be stressed that different gaskets were used in the two channels.

In spite of differences between the contribution results of the gap 1 and gap 2 channels, it is evident that their trends are similar and are very different from those of the standard channel.

5.12) THE PARALLEL PATTERN

Fig.4.45 indicates that in this 2-dimensional channel viscous flow extends up to a Reynolds number of 100 followed by a short transition region, turbulent flow appears to begin at a Reynolds number of about 250. No attempt was made to correlate the results in the viscous region because of the small number of data points and the difficulties of measuring small pressure drops associated with water.

The slope of the line best describing the data in the turbulent region, equation (4.19), is virtually the same as that corresponding to the standard channel results in the Re $\geq$ 400 range, equation (4.10), i.e. the degree of dependence of f_t on Re is the same in the turbulent regions of the two channels. The resistance factor, or pressure drop, in the parallel pattern channel is only about one-half that of the standard channel at the same Re in the

turbulent regime. It should be emphasized that both channels have the same equivalent diameter, but one is 2-dimensional while the other is 3-dimensional.

The relative positions of the lines representing equations (4.10) and (4.19), in addition to those corresponding to equations (4.14) and (4.18) of the gap 1 and gap 2 channels respectively could be seen in Fig.5.2.

5.13) COMPARISON WITH THE WORK OF EDWARDS et al.[20]

In this section the hydrodynamic behaviour of the standard channel and its ribbed section represented by equations (4.9)/(4.10) and (4.7)/(4.8) respectively will be compared with equation (2.12) developed by Edwards et al.[20] whose work was reviewed in Chapter 2 pp.26-27.

Since discrepancies exist in the definitions/values of such parameters as the channel length, equivalent diameter, and area of flow, between this work and that of Edwards et al., equations (4.7)-(4.10) had to be transformed thereby bringing them in line with equation (2.12). Details of these transformations are given in Appendix A-5.0. The transformed equations (4.7)-(4.10) are respectively as follows:

$$f_r = \frac{30.769}{Re} + 0.298 \qquad (5.8)$$

$$f_r = 1.663\ Re^{-0.230} \qquad (5.9)$$

$$f_t = \frac{37.292}{Re} + 0.447 \qquad (5.10)$$

$$f_t = 1.652\ Re^{-0.196} \qquad (5.11)$$

It should be stressed that this comparison applies to the common range of $3 \leq Re \leq 10^3$. In equation (5.10) the viscous contribution to the pressure drop, represented by the first right-hand side term, is similar to the corresponding one in equation (2.12)

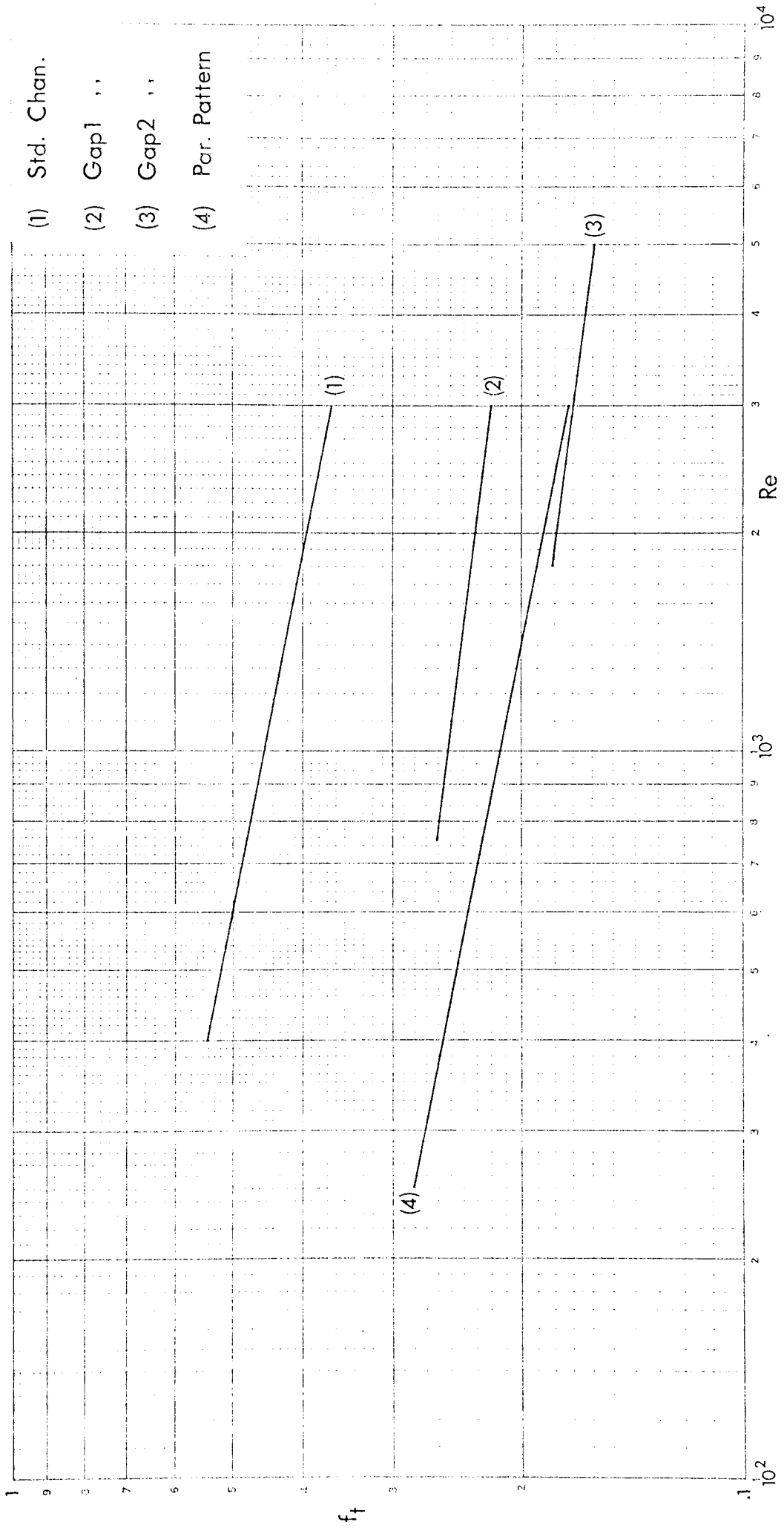
(1) Std. Chan.
(2) Gap1 ''
(3) Gap2 ''
(4) Par. Pattern
(1)
(2)
(3)
(4)
f_f
Re
1
.9
.8
.7
.6
.5
.4
.3
.2
.1
10^2
10^3
10^4

Fig.5.2

although slightly higher, however the turbulent contribution is only 56% of the one in the Edwards equation.

Fig.5.3 contains the graphical forms of equation (2.12) and equations (5.8)-(5.11). There is evidence of reasonable agreement between curves a and b up to Re of 20. However, the difference between the two curves becomes more than 10% of the friction factor as predicted by equation (2.12) at a Reynolds number of 25 and continues to increase with Re. At a Reynolds number of 1000 the standard channel resistance coefficient is only 51% of that predicted by the Edwards equation.

It must be borne in mind that curve a in Fig.5.3 is relevant to a pack of APV Junior metal plates. The pressure drop of a plate pack constitutes the following:

1 - Pressure loss in inlet and exit manifolds.

2 - Entrance pressure drop.

3 - Ribbed section pressure drop.

4 - Exit pressure drop.

5 - Cross-over pressure drop (when more than one pass is involved).

The contribution of each of the above-mentioned factors depends on the plate arrangement used and the nature of flow. In the single plastic channel of the present work factors (1) and (5) are irrelevant , factors (2) and (4) require some elaboration. The single plastic channel represents an "end channel" in a pack where the effect of the entrance and exit are more pronounced in comparison with the other channels within a pass. In the former the fluid experiences the 90° sharp turn whereas in the latter only part of the fluid in the inlet manifold enters the channel depending on its pressure, the entrance and exit could therefore be thought of as T-junctions instead of 90° sharp elbows.

Another important point is the fact that the Reynolds

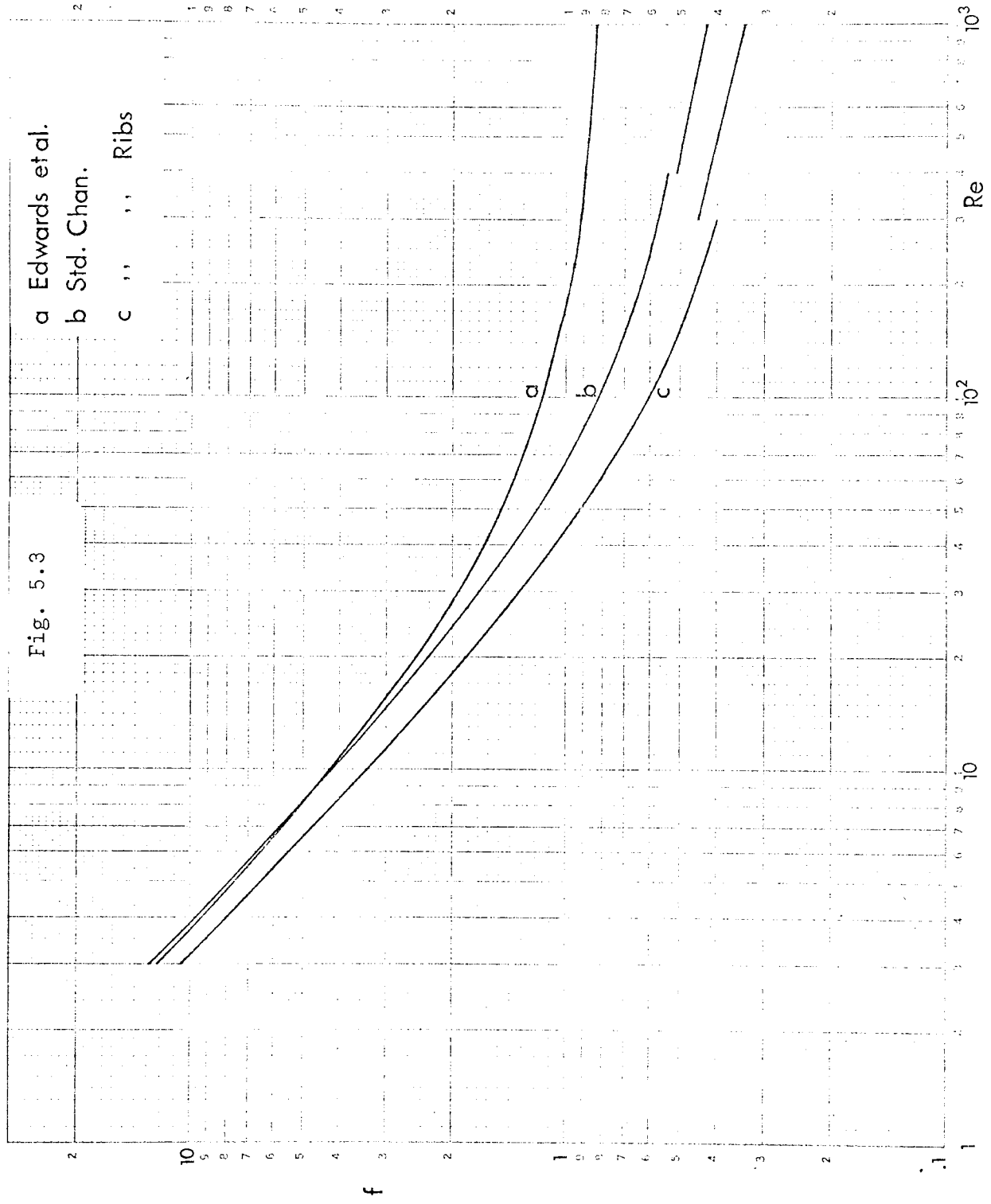

Fig. 5.3

number is based on the flow in one channel, therefore at a given Re the flow rate in each channel of a single pass pack should be equal to that in the single plastic channel. It follows that the manifolds of the pack must handle a flow rate that is considerably higher depending on the number of channels used. Since the pressure drop used in the pack resistance coefficient f is measured across the whole exchanger it includes the energy loss in the two very rough manifolds. The pressure loss in the manifolds must depend on the following:

1 - Size of the ports, i.e. diameter of the manifolds.

2 - Number of plates used, i.e. length of the manifolds.

3 - Flow rate and properties of fluid.

Edwards et al.[20] used a single pass of 12 channels and 2 passes of 12 channels per pass and found that the data for the two cases fell together concluding that manifold losses were negligible. The fact that their data for the single pass and two-pass plate arrangements fell together indicates only that the effect of the cross-over pressure drop from one pass to the other is insignificant in comparison with the other 4 causes of pressure loss.

The reasonable agreement between curves a and b in Fig.5.3 in the viscous and quasi-viscous flow regimes suggests that the pressure loss in the inlet and exit manifolds and the various entrances and exits in the pack is equivalent to the pressure drop in the entrance and exit of the plastic model. The increasing gap between curves a and b on the other hand demonstrates the significance of the pressure loss in the two manifolds in the quasi-turbulent and turbulent regions. Comparison between curves a and c renders untenable the assumption of Edwards et al. that their results represent the flow between corrugated plates. Furthermore, the substantially lower dependence of the friction factor f on Re in the

quasi-turbulent and turbulent regions of curve a in comparison with the respective regions of curves b or c may lead to the wrong assumption of higher pressure drop/heat transfer coefficient in the channels than actually is the case.

It was pointed out in Chapter 2 that Ellison[21] reported variations in the f vs. Re relationship when the number of plates in the single pass U-arrangement pack was changed. The difference diminishes gradually as the Reynolds number is decreased.

One way of assessing heat transfer surfaces/heat exchangers is by plotting the film heat transfer coefficient against the energy absorbed per unit heat transfer area. Cattell[14] compared plots of the above-mentioned variables pertaining to basic heat transfer surfaces and overall plate performance noting the effect of parasitic losses and unproductive pressure drop in lowering the performance of the overall plate case. He then points out that care must be taken so that the reduction in performance is not exaggerated by excessive pressure losses or mal-distribution.

CHAPTER 6

CONCLUSIONS

6.0) CONCLUSIONS

1) Hydrodynamic characteristics of 3-dimensional PHE channels can be studied using polymethylmethacrylate replicas, of the metal plates, produced by expertly casting perspex from a liquid form at low temperature. This approach solves the problems of air pockets and/or contact between the plates inherent in tests on packs of metal plates in addition to facilitating flow visualisation and/or pressure drop measurements of parts of a single channel without sacrificing the exact geometrical characteristics of the metal plates.

2) The reliable measurement of small liquid differential pressures is a formidable task. Straightforward application of the well type inclined-tube manometer should be avoided. It could however be applied in conjunction with Benedini's technique which could also be used to adapt any reliable gas micromanometer for liquid pressure drop measurements (Appendix A-2.1). U-tube manometers employing coloured $CC\ell_4$ develop serious errors at the lower ends of their ranges, therefore readings should not be considered below a certain value (Appendix A-2.2). Readings of well type manometers using coloured $C_6H_5Br/CC\ell_4$ should be taken with the flow medium replacing the manometer fluid in the limb; readings obtained with the manometer fluid replacing the flow medium should only be considered when in agreement with the corresponding ones obtained in the above-mentioned opposite manner (Appendix A-2.3).

3) Hydrodynamically there is no difference between UP-flow and DOWN-flow in 3-dimensional PHE channels. Therefore the results of Ellison[21] in the viscous region must have been erroneous probably due to the presence of air pockets in channels with DOWN-flow.

4) The results of Fig.4.7 represent the basic flow behaviour between corrugated plates of the 3-dimensional chevron type. In this geometry, viscous flow exists up to a Reynolds number of about 12 followed by a very gradual and predictable transition region over the range $12 < Re < 300$. The degree of turbulence is very limited in the range $12 < Re < 100$ and the flow is quasi-viscous. Over the remainder of the transition region the level of turbulence increases substantially and the flow is quasi-turbulent. There are no secondary viscosity effects. The termination of the transition region and the setting-in of fully-turbulent flow is marked by a characteristic kink at Re of 300.

5) The friction factor-Reynolds number relationship pertaining to flow between corrugated plates of the herringbone pattern over the range investigated cannot be described satisfactorily by a single Ergun type equation as suggested by Edwards et al.[20]. A minimum of two models are required, equations (4.7) and (4.8), the first of which is an Ergun type relationship covering both the viscous and the transition regions.

6) The entrance and exit have a significant and variable effect on the standard channel total pressure drop. Between them, the two port regions contribute from a minimum of about 18.5% to a maximum of about 30% of the channel total pressure drop over the range investigated. The quasi-turbulent part of the transition region is the zone where the ports effect is most pronounced, influencing not only the magnitude of the friction factor but also the nature of its interaction with Re thereby resulting in a different discontinuity at a Reynolds number of 400, Fig.4.16. The inclusion of the two port regions reduce the slope of the friction factor-Reynolds number curve, pertaining

6) contd.

to the ribbed section, by a magnitude commensurate with their contribution, e.g. in the turbulent region the standard channel f-Re curve slope is diminished by 15%, cf. equations (4.8) and (4.10); for the gap 1 channel the slope reduction is 36%, cf. equations (4.12) and (4.14); the gap 2 channel experiences a slope change of the order of 41%, cf. equations (4.16) and (4.18). The smaller slope would infer higher levels of turbulence and heat transfer coefficients than actually is the case in the ribbed or heat transfer section.

7) The contribution of the ribbed section is at its highest in the viscous region, accounting for about 81.5% of the standard channel total pressure drop. In the transition region, the relative effect of the ribbed section undergoes a major decline to a recorded minimum of less than 70%. This trend reverses itself at a Reynolds number of 300 which corresponds to the point at which the kink occurs in the f_r-Re plot, Fig.4.7. At Re > 1000 the average ribbed section contribution becomes about 78.5%, Fig.4.17. The range 100 < Re < 400, in which the ribbed section contribution is at its lowest, is not conducive to the productive utilisation of the available pressure drop in comparison with other flow regions.

8) The physical contact between the plates is a cardinal factor in the hydrodynamic characteristics of the standard channel. This is not only so in the context of the values of the friction factor — pressure drop — attained, but also with respect to the discontinuities in the f_r-Re and f_t-Re relationships, the extent of flow regions, and the contributions of the ribbed section and the two port regions. Fig.6.1 presents a quantitative account of the fall-off in performance if the plates are not tightened correctly, i.e. with no contact between

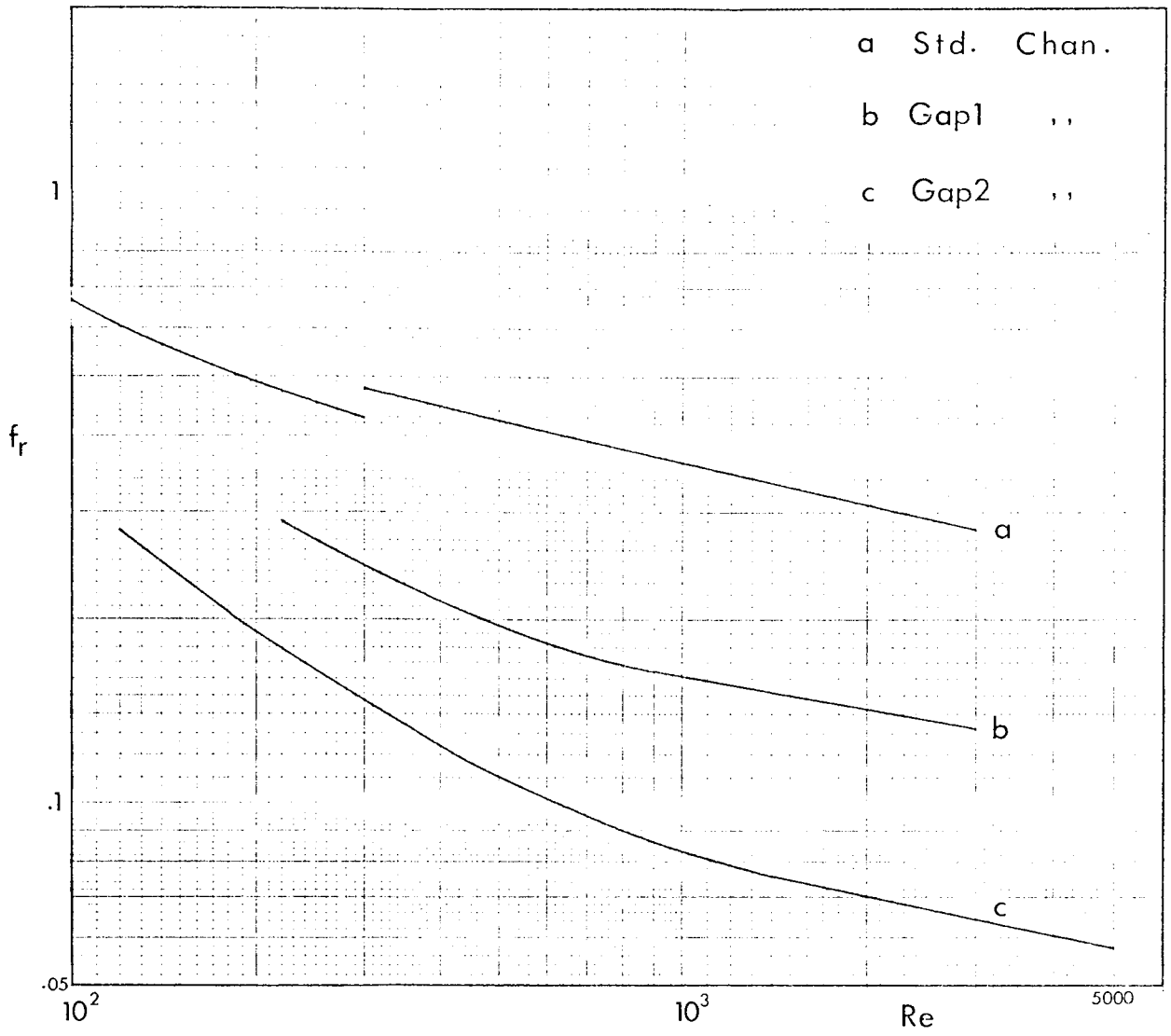

Fig. 6.1

plates. The equivalent diameter corresponding to plot a is 80% of that relevant to curve b or 56% of the equivalent diameter pretaining to curve c. The decline in the hydrodynamic performance due to the loss of contact is a minimum in the viscous region (curve b would merge with curve a at Re < 20, cf. first term on right-hand side of equation (4.7) accounting for the viscous contribution to the pressure drop with its counterpart in equation (4.11)) however it increases with Re becoming substantial in the turbulent region. Contact between the chevron corrugated plates results in unique ribbed section, entrance, or exit contribution/Reynolds number relationships (Fig.'s 4.17-4.21); severance of the physical contact leads to different trends which are sustained with

8) contd.

further increase in the gap between the plates (Fig.'s 4.33-4.35 and Fig.'s 4.42-4.44).

9) Flow visualisation with coloured dyes can be notoriously misleading and must not be employed without prior knowledge of the hydrodynamic characteristics, i.e. they should be used to uphold or explain known behaviour rather than to establish flow characteristics. The gradual and extensive transition region is the result of two modes of flow occurring simultaneously in the channel, viscous flow initially followed by turbulence further downstream with the extent of each mode depending on the Reynolds number (Fig.'s 4.23 and 4.24). At a Reynolds number of 10, more than one-half the channel length is required for the flow to be fully-developed due to the disturbance at the entrance region (Fig.4.25). In the transition region the disturbance caused by the entrance and the position of the two ports on the same side of the channel renders the whole channel length within the entry length required for the flow to be fully-developed (Fig.4.26).

10) 2-dimensional channels made from chevron corrugated plates (by rotating one of them by 180°) and having the same equivalent diameter as the 3-dimensional channels would generate a pressure drop which is about $\frac{1}{2}$ as much as that generated by the 3-dimensional channel at the same Reynolds number in the turbulent region (Fig.5.2).

11) The data of Edwards et al.[20], pertaining to a pack of metal plates, do not represent flow between corrugated plates only, rather they are the result of pressure losses in the manifolds, entrance, ribbed section, and exit. The effect of extraneous pressure losses increases with Re becoming dominant in the turbulent region even with relatively small

11) contd.

number of channels per pass, e.g. with only 12 channels (13 plates) the pressure loss utilised productively to enhance heat transfer in the ribbed section is only 41% of that consumed by the pack at Re of 1000, cf. curves a and c in Fig.5.3. The magnitude of parasitic pressure losses can also be appreciated by comparing the slope of the f-Re turbulent region relationship belonging to the pack with the (-0.23) value pertaining to the ribbed section, i.e. the greater is the drop in the slope the bigger is the effect of extraneous losses, e.g. there is 70% reduction in slope between curves c and a over the Re > 400 range in Fig.5.3. Since the APV Junior PHE is designed to accommodate up to 152 plates, extrinsic pressure losses will be unduly high if the machine is to be operated in the quasi-turbulent transition or turbulent regions. The obvious solution to such a problem is to enlarge the ports, however the argument against this has been that by doing so the plates will become wider, and shorter if the plate area is to remain constant. Because of distribution problems across the plate width available for flow, the practice has been to set the minimum possible plate width to keep the two ports sufficiently far apart to allow all standard flanges to be connected without interference. Furthermore, the θ value of a plate depends on the configuration into which it is pressed and on the plate length. It therefore appears that the only way to maintain the plate width and length at desirable values and enlarge the ports is to abandon the rectangular shape of the plate in the port regions, i.e. to increase the overall plate width beyond the ribbed section to accommodate larger ports. This will not only rectify the problem

11) contd.

of extraneous pressure losses but will also contribute to the solution of the problem of fluid distribution amongst those channels in a pass with the likelihood of "dead" areas caused by fluid starvation. However, there may be economic arguments against a non-rectangular overall plate shape when very expensive metals are involved. It remains to be seen whether the operational advantages gained can offset the economic disadvantages.

7.0) RECOMMENDATIONS FOR FUTURE WORK

1 - The feasibility of employing a laser Doppler velocimeter to measure point velocities in the perspex channel should be investigated. If successful, this method could supersede flow visualisation, through the use of technical dyes, as a reliable and accurate way to establish velocity profiles and to study flow distribution especially in the quasi-turbulent transition and turbulent regions where dye flow visualisation is not possible because of immediate dispersion.

2 - The effect of heat flux on hydrodynamic characteristics should be studied using a modified system to form a two channel pack. A perspex plate could be used on the cold fluid side to allow visual observation and the fitting of multiple pressure tappings. The hot side could be a channel containing hot liquid, condensing vapour, or a specially fabricated, electrically heated plate to provide a constant heat flux. The effect of changes in physical properties should be examined with a view to defining a caloric temperature at which the properties could be evaluated so that the established isothermal f-Re relationships could be directly applied.

3 - The effects of the chevron angle and depth of corrugations on the hydrodynamic characteristics should be examined especially in the transition and viscous regions.

4 - The depth of the cross-corrugated form is small, in most respects an advantage. However, this means that flow velocities in the entrance region of the plate form can be excessive causing high unproductive pressure losses and mal-distribution of flow, thereby reducing the effectiveness of the plate form. Hence, the effect of depth of corrugations, geometry of the entrance region, and the plate width available for flow on flow distribution/

4 - contd.

unproductive pressure losses should be investigated.

APPENDICES

Appendix A-1.0

Transformation of the friction factor and Reynolds number relevant to the results of Emerson[22]

$$\phi = \frac{\text{Developed Heat Transfer Area}}{\text{Projected Heat Transfer Area}} = \frac{0.12 \quad m^2}{0.0983 \ m^2} = 1.22$$

applying equation (2.10) for the equivalent diameter:

$$De = \frac{2b}{\phi} = \frac{2 \times 0.294 \text{ cm}}{1.22} = 0.482 \text{ cm.}$$

$$\text{Project Plate Length} = \frac{\text{Projected Heat Transfer Area}}{\text{Plate Width Available for Flow}}$$

$$= \frac{983 \ cm^2}{21.5 \text{ cm}} = 45.7 \text{ cm.}$$

Developed Plate Length = $(45.7)(\phi)$ = 55.78 cm.

Let the subscripts (n) and (o) denote new and old respectively.

$$Re_o = \frac{(\rho)(2b)(u)}{\mu} \quad ; \quad De_o = 2b \text{ according to Emerson.}$$

The linear velocity u is based on equation (2.11) and no transformation is required.

$$Re_n = \frac{(\rho)(2b/\phi)(u)}{\mu} = \frac{(\rho)(2b/1.22)(u)}{\mu}$$

$$\therefore \quad Re_n = 0.82 \ Re_o$$

Plate length L used by Emerson is 60.5 cm which is the projected distance between the centres of the inlet and outlet ports.

$$L_n = \frac{55.78}{60.5} \ L_o = 0.922 \ L_o$$

$$f_o = \frac{\Delta P)(2b)}{2(\rho)(u^2)(L_o)} \quad ; \quad f_n = \frac{(\Delta P)(2b/1.22)}{2(\rho)(u^2)(0.922 \ L_o)}$$

$$\therefore \ f_n = \frac{0.82}{0.922} \ \frac{(\Delta P)(2b)}{2(\rho)(u^2) \ (L_o)}$$

$$\therefore \quad f_n = 0.889 \ f_o$$

APPENDIX A-2.0

A-2.0 Behaviour of Manometers

In this section, unexpected aspects of manometer behaviour as observed during experimentations will be discussed.

A-2.1 The Well Type Inclined-Tube Manometer

This type of manometer has been widely used to measure small differential pressures of gases in general and air in particular, hence it is sometimes referred to as an air type manometer. The liquids usually employed are alcohol, kerosene (paraffin oil), or other petroleum fractions with specific gravity range of 0.7-0.9.

Theoretically there is no reason why this instrument should not be used to measure liquid differential pressures provided a suitable manometer fluid is employed. Standard textbooks or even specialized ones on instrumentation certainly do not advise against it, see for instance Eckman[19].

In the present work an attempt was made to measure small water pressure drops pertaining to the entrance/exit regions using a well type inclined-tube manometer which employed $CC\ell_4$ or C_6H_5Br. The angle of inclination of the limb was 6° with a sine of 0.1. This attempt proved to be a complete failure owing to the following:

(i) The manometer fluid indicated different zero readings at different times.

(ii) Although the water flow rate in the channel remained constant the manometer reading varied with time to the extent that it eventually indicated an entrance pressure drop which was higher than the channel total pressure drop.

(iii) The meniscus sharpness and parabolic profile did not persist making exact determination of the manometer reading difficult.

The failure of the inclined-tube manometer to measure accurately liquid differential pressures has been recently reported

by Preston[31] who attributed it to zero creep caused by change of temperature and surface tensions effects. Furthermore, in a more recent paper, Weihs and Sumer[38] call attention to the long measurement rise-time of the inclined-tube manometer. They pointed out that in actual experiments movement of the meniscus was still noticeable after 5 minutes ascribing it to the slow response time of the system and to thermal expansion effects.

In his paper Preston[31] describes a system based upon Benedini's technique[9] of using an air manometer in conjunction with a reservoir to measure small liquid pressures accurately. The Preston arrangement consists basically of a standard air type manometer connected to two reservoirs providing large water-air interfaces, the air trapped between them and the manometer transfers the liquid pressure to the manometer. Surface tension effects and zero creep (temperature changes) effects are thereby greatly reduced. In the Weihs and Sumer[38] arrangement the well type inclined-tube manometer of the Preston arrangement is replaced by a simple U-tube manometer. This system was claimed to result in faster response time, without loss in accuracy, in addition to being simpler in construction.

In the present work Benedini's technique was used in conjunction with a sophisticated micromanometer as described in Chapter 3, however the Preston and Weihs systems offer accurate and cheap alternatives and are strongly recommended for small liquid differential pressures.

A-2.2 U-Tube Manometer Employing $CC\ell_4$

Carbon tetrachloride is widely used in U-tube manometers to measure water differential pressures too small to be indicated by mercury. This was done in the present work, however it was observed that serious errors arose at the lower end of the manometer

range probably due to surface tension effects.

The manometer was a new 50 cm standard one with an ID of 4 mm and the $CC\ell_4$ was chemically pure. As mentioned in Chapter 3 a small amount of dye was used to colour the $CC\ell_4$. It must be pointed out that prior to its use the manometer was cleaned with distilled water but no agents were used to affect the surface energy. Table A-2I reveals the nature and magnitude of the errors:

	Manometer Reading, cm $CC\ell_4$	Re	f_t^*	f_t^{**}	% Error $\frac{f_t^* - f_t^{**}}{f_t^{**}} \times 100$
First Run, UP-Flow	3.4	115.9	0.908	0.842	+ 7.8%
	2.5	79.3	1.425	1.018	+ 40 %
	1.8	48.8	2.710	1.365	+ 98 %
Second Run, DOWN-Flow	3.2	97.6	1.205	0.913	+ 32 %
	3.05	73.2	2.041	1.064	+ 92 %
	2.3	42.7	4.523	1.495	+202 %
	1.7	24.4	10.239	2.270	+ 351 %

* Friction factor based on manometer reading

** " " calculated from equation (4.9)

TABLE A-2-I

The experiments from which the U-tube manometer $CC\ell_4$ readings were taken were conducted starting with the maximum flow rate. The magnitude of error increases as the manometer reading becomes smaller reaching colossal proportions at the end of the range. It is also evident that the manometer behaviour is not consistent in this range, i.e. the manometer reading at the same flow rate is different in different runs.

The conclusion to be drawn from the foregoing is that the minimum reliable reading of a 4 mm ID U-tube manometer employing

$CC\ell_4$ is 4 cm.

A-2.3 Well Type Manometer Employing C_6H_5Br

The well manometer examined had a limb with an ID of 4 mm and again only distilled water was used to clean it prior to its use. The bromobenzene used was chemically pure to which a little amount of suitable dye was added as pointed out in Chapter 3.

The behaviour of this type of manometer would be best discussed in conjunction with Fig.A-2.1. In this experiment the medium flowing in the channel was distilled water and the direction of flow was upward. The standard channel ribbed section pressure drop was measured by a micromanometer of the kind, and in the way, described in Chapter 3 and a well type manometer containing coloured C_6H_5Br. Initially the flow was set at such a rate so that the well manometer limb was filled with bromobenzene, then the flow rate was gradually decreased so that the flow medium, water, replaced the manometer fluid in the limb. Pressure drop measurements were taken from both instruments. The second run was conducted starting from zero flow, i.e. with the C_6H_5Br replacing the water in the limb.

As could be seen in Fig.A-2.1 (a) the micromanometer behaviour was reasonably consistent over the two runs, however the well manometer indicated a lower pressure drop in the second run than it did in the first run up to a certain point beyond which the instrument became consistent, Fig.A-2.1 (b). Since there is reasonable agreement between the well manometer readings when the water replaced the bromobenzene (first run) and those of the micromanometer (average deviation based on the well manometer was $\pm$ 2.5% over the entire range) it was decided that the lower pressure drop readings of the well manometer when the C_6H_5Br replaced the water in the limb (second run) were erroneous probably due to surface tension effects.

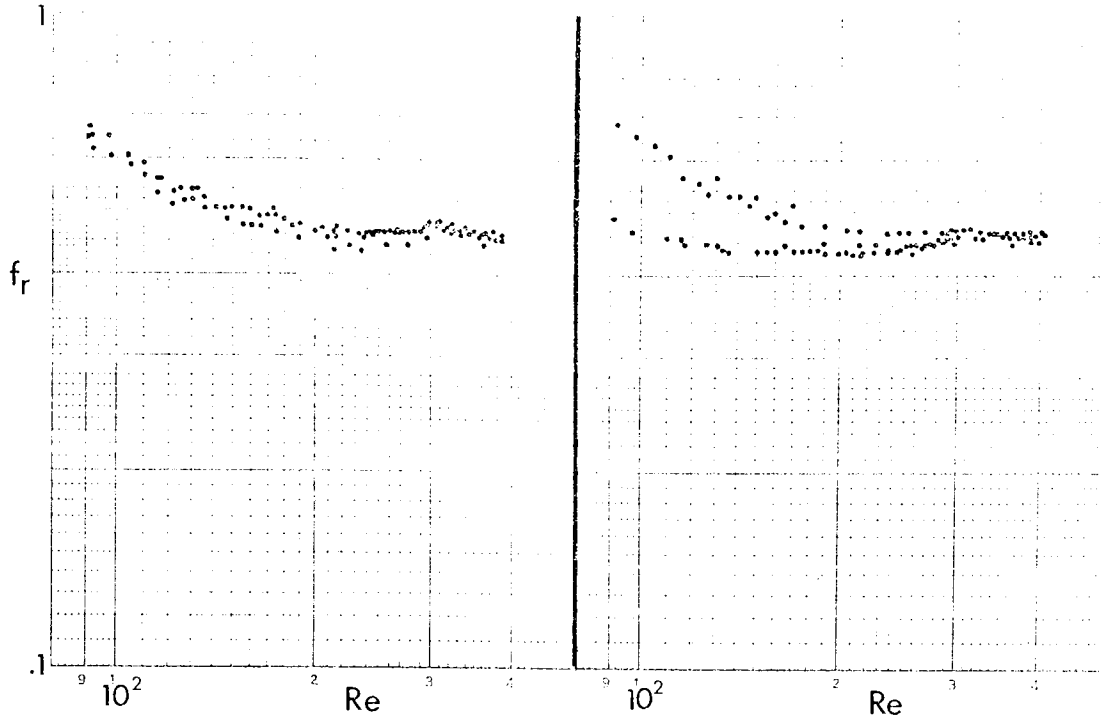

(a) Micromanometer (b) Well Manometer

Fig. A-2.1

The minimum length of the bromobenzene column recorded was 1.60 cm in the first run, becoming only 1.15 cm in the second run at the same flow rate resulting in -28% error. This error diminishes gradually as the manometer reading increases becoming less than -10% at 4 cm of C_6H_5Br and at 7 cm C_6H_5Br could be considered virtually non-existent. A similar behaviour of the well type manometer was also observed when the manometer fluid was $CC\ell_4$.

As a result of these findings it was decided to take as a standard, well manometer readings with the flow rate decreasing, i.e. with the flow medium replacing the manometer fluid in the limb than vice versa. Pressure drop measurements in the case of increasing flow rate, i.e. manometer fluid replacing flow medium, were taken into account only when in agreement with the ones obtained in the opposite manner, otherwise they were rejcted for being erroneously low.

Appendix A-3.0

Determination of Channel Volume

A-3.1 Standard Channel

Volume of Hg introduced = 25 cm^3.

Apparent change in Hg level = 20.09 cm.

Developed change in Hg level = $(20.09)(\phi)$

= $(20.09)(1.18)$ = 23.706 cm.

Plate Developed Length = 47.2 cm.

$\therefore$ Channel Volume (Corresponding to Heat Transfer Area):

$$\frac{(25\ cm^3)(47.2\ cm)}{23.706\ cm} = 49.776\ cm^3.$$

A-3.2 Gap 1 Channel

Total Volume (Corresponding to Wetted Area and measured by water) = 67.6 cm^3.

Channel Volume (Corresponding to Heat Transfer Area) =

$$(67.6)\left(\frac{\text{Std.Chan.Volume Corresponding to Heat Transfer Area}}{\text{Std.Chan.Total Volume Corresponding to Wetted Area}}\right)$$

$$= (67.6)\left(\frac{49.776}{53.76}\right) = 62.584\ cm^3.$$

A-3.3 Gap 2 Channel

Total Volume (Corresponding to Wetted Area and measured by water) = 95.5 cm^2

Channel Volume (Corresponding to Heat Transfer Area) =

$$(95.5)\left(\frac{49.776}{53.76}\right) = 88.392\ cm^2$$

APPENDIX A-4.0 STATISTICAL CHARACTERISTICS OF DEVELOPED EMPIRICAL EQUATIONS

The simple-nonlinear regression analysis was performed by the University Computer Centre Application Program UA16. This program calculates the regression coefficients and comparative data for each of six curve types (which include the two types used in this work), based on a least squares fit. It also does an analysis of variance to find 95% confidence limits.

Equation (4.7)

224 Individual Data Points (IDP); Coefficient of Correlation = 0.998575

Root Mean Square (R.M.S.) Value of Percentage Error = $\pm$ 5.042504

* Dispersion. F_c is the critical F value at 99% confidence level.

Source	Degrees of Freedom	Sum of Squares	Mean of Squares	F	F_c
Regression	1	992.695263	992.695263	77734	6.63
Residual	222	2.835003	0.012770*		
Total	223	995.530266			

Equation (4.8)

95 IDP; Coefficient of Correlation = 0.984496

R.M.S. Value of Percentage Error = ± 2.789503

Source	Degrees of Freedom	Sum of Squares	Mean of Squares	F	F_c
Regression	1	0.345610	0.345610	2790	6.96
Residual	93	0.011517	0.000124*		
Total	94	0.357127			

Equation (4.9)

291 IDP; Coefficient of Correlation = 0.998102

R.M.S. Value of Percentage Error = ± 5.465593

Source	Degrees of Freedom	Sum of Squares	Mean of Squares	F	F_c
Regression	1	1403.295834	1403.295834	75918	6.63
Residual	289	5.341915	0.018484*		
Total	290	1408.637749			

Equation (4.10)

80 IDP; Coefficient of Correlation = 0.971366

R.M.S. Value of Percentage Error = ± 3.050435

Source	Degrees of Freedom	Sum of Squares	Mean of Squares	F	F_c
Regression	1	0.258857	0.258857	1182	7.01
Residual	78	0.017068	0.000219*		
Total	79	0.275925			

Equation (4.11)

73 IDP; Coefficient of Correlation = 0.987515

R.M.S. Value of Percentage Error = ± 2.776398

Source	Degrees of Freedom	Sum of Squares	Mean of Squares	F	F_c
Regression	1	0.065182	0.065182	2790	7.04
Residual	71	0.001659	0.000023*		
Total	72	0.066840			

Equation (4.12)

60 IDP; Coefficient of Correlation = 0.961943

R.M.S. Value of Percentage Error = ± 2.250439

Source	Degrees of Freedom	Sum of Squares	Mean of Squares	F	F_c
Regression	1	0.008612	0.008612	697	7.10
Residual	58	0.000716	0.000012*		
Total	59	0.009329			

Equation (4.13)

78 IDP; Coefficient of Correlation = 0.990020

R.M.S. Value of Percentage Error = ± 2.889989

Source	Degrees of Freedom	Sum of Squares	Mean of Squares	F	F_c
Regression	1	0.223975	0.223975	3750	7.02
Residual	76	0.004538	0.000060*		
Total	77	0.228513			

Equation (4.14)

58 IDP; Coefficient of Correlation = 0.887906

R.M.S. Value of Percentage Error = ± 2.547580

Source	Degrees of Freedom	Sum of Squares	Mean of Squares	F	F_c
Regression	1	0.008004	0.008004	202	7.13
Residual	56	0.002215	0.000040*		
Total	57	0.010219			

Equation (4.15)

84 IDP; Coefficient of Correlation = 0.995524

R.M.S. Value of Percentage Error = ± 4.447056

Source	Degrees of Freedom	Sum of Squares	Mean of Squares	F	F_c
Regression	1	0.281000	0.281000	9008	7.00
Residual	82	0.002558	0.000031*		
Total	83	0.283558			

Equation (4.16)

52 IDP; Coefficient of Correlation = 0.893811

R.M.S. Value of Percentage Error = ± 3.589746

Source	Degrees of Freedom	Sum of Squares	Mean of Squares	F	F_c
Regression	1	0.001204	0.001204	176	7.20
Residual	50	0.000341	0.000007*		
Total	51	0.001545			

Equation (4.17)

120 IDP; Coefficient of Correlation = 0.997308

R.M.S. Value of Percentage Error = ± 4.800580

Source	Degrees of Freedom	Sum of Squares	Mean of Squares	F	F_c
Regression	1	0.937250	0.937250	6281	6.86
Residual	118	0.017606	0.000149*		
Total	119	0.954856			

Equation (4.18)

45 IDP; Coefficient of Correlation = 0.834221

R.M.S. Value of Percentage Error = ± 2.489434

Source	Degrees of Freedom	Sum of Squares	Mean of Squares	F	F_c
Regression	1	0.001834	0.001834	91	7.28
Residual	43	0.000865	0.000020*		
Total	44	0.002699			

Equation (4.19)

34 IDP; Coefficient of Correlation = 0.964968

R.M.S. Value of Percentage Error = ± 3.774380

Source	Degrees of Freedom	Sum of Squares	Mean of Squares	F	F_c
Regression	1	0.029847	0.029847	414	7.51
Residual	32	0.002302	0.000072*		
Total	33	0.032149			

Appendix A-5.0

Transformation of friction factor and Reynolds number to bring equations (4.7)-(4.10) of the standard channel and its ribbed section in line with equation (2.12) of Edwards et al.[20]

Let the subscript B denote relevance to the work of Edwards et al.

$$\frac{De}{De_B} = \frac{0.386 \text{ cm}}{0.343 \text{ cm}} = 1.125$$

$$\frac{(\text{Flow Area})_B}{\text{Flow Area}} = \frac{10.759 \times 10^{-5} \text{ m}^2}{10.546 \times 10^{-5} \text{m}^2} = 1.020$$

$$\therefore \frac{\text{Velocity}}{(\text{Velocity})_B} = 1.020$$

$$Re = (1.125)(1.02)\ Re_B$$

$$\therefore Re = 1.148\ Re_B$$

$$\text{or } Re_B = 0.871\ Re$$

$$\frac{L}{L_B} = \frac{47.2 \text{ cm}}{45 \text{ cm}}$$

$$f = \frac{(\Delta P)\ (De)}{2(\rho)(u^2)(L)} = \frac{(1.125)(45)}{(1.02)^2(47.2)} \frac{(\Delta P)(De_B)}{2(\rho)(u_B^2)(L_B)}$$

$$f = 1.031\ f_B$$

$$\text{or } f_B = 0.970\ f$$

Appendix A-6.0 Tabulated Results

Standard Channel

Fluid: Water

UP-Flow

u, m/s	Re	ΔP_t, N/m^2	f_t
0.67008	2586.5	40670	0.370
0.61477	2373.0	34610	0.374
0.56736	2190.0	29420	0.374
0.50098	1933.8	23730	0.387
0.43618	1683.7	18050	0.388
0.29237	1128.5	8652	0.414
0.24970	963.8	6675	0.438
0.21177	817.4	4944	0.451
0.17700	683.2	3461	0.452
0.13749	530.7	2225	0.481
0.10589	408.7	1483	0.541
0.08692	335.5	1101	0.596
0.06638	256.2	641.6	0.595
0.03793	146.4	259.0	0.736
0.09721	340.6	1534	0.664
0.09279	325.1	1391	0.661
0.08790	308.7	1271	0.673
0.08226	289.4	1131	0.684
0.07712	271.5	993.0	0.684
0.07213	254.0	880.0	0.692
0.06740	238.0	769.4	0.693
0.06266	221.2	668.6	0.697
0.05727	202.8	567.8	0.709
0.05210	184.8	472.0	0.712
0.04615	164.1	386.0	0.742

0.04036	143.8	299.9	0.754
0.03461	124.1	236.0	0.807
0.02871	103.1	177.0	0.879
0.02178	78.5	120.5	1.040

DOWN-Flow

u, m/s	Re	ΔP_t, N/m^2	f_t
0.67482	2604.8	43140	0.387
0.63373	2446.2	38190	0.389
0.58474	2257.1	32760	0.392
0.52469	2025.3	27320	0.406
0.46305	1787.4	21380	0.408
0.42828	1653.2	18910	0.422
0.40932	1580.0	16930	0.413
0.38403	1482.4	15080	0.418
0.34926	1348.2	12860	0.431
0.31291	1207.9	10630	0.444
0.28447	1098.0	8900	0.450
0.26076	1006.5	7416	0.446
0.23706	915.0	6428	0.468
0.21177	817.4	5315	0.485
0.18965	732.0	4203	0.478
0.16752	646.6	3461	0.504
0.14698	567.3	2472	0.468
0.11379	439.2	1766	0.558
0.10272	396.5	1495	0.579
0.09008	347.7	1195	0.602
0.08218	317.2	918.2	0.556
0.06954	268.4	753.4	0.637
0.06005	231.8	582.7	0.661

0.05057	195.2	435.6	0.696
0.04267	164.7	317.8	0.714
0.03793	146.4	223.7	0.636
0.09718	324.0	1484	0.643
0.09722	344.1	1490	0.645
0.09277	309.6	1344	0.639
0.09280	328.4	1386	0.659
0.08787	293.7	1233	0.654
0.08790	310.7	1241	0.658
0.08224	276.3	1083	0.656
0.08226	290.4	1106	0.669
0.07709	259.7	967.9	0.666
0.07712	271.5	968.5	0.667
0.07212	244.2	852.5	0.671
0.07213	253.7	852.9	0.671
0.06738	228.9	754.3	0.680
0.06740	236.7	747.2	0.673
0.06265	214.7	651.1	0.679
0.06266	219.8	639.1	0.666
0.05726	197.0	543.1	0.678
0.05727	200.6	543.2	0.678
0.05210	179.9	457.1	0.689
0.05210	182.1	447.3	0.675
0.04614	160.0	373.5	0.718
0.04615	161.3	363.7	0.699
0.04036	140.3	294.9	0.741
0.04036	140.7	285.1	0.716
0.03461	120.9	235.9	0.806
0.02871	101.1	177.0	0.879
0.02177	76.9	118.0	1.019

UP-Flow

u, m/s	Re	ΔP_t, N/m^2	ΔP_{en}, N/m^2	ΔP_{ex}, N/m^2	ΔP_r, N/m^2	f_t	f_r
0.67403	2601.8	41530	5191	4202	32136	0.374	0.289
0.61524	2374.8	34730	4449	3584	26696	0.375	0.288
0.59754	2306.5	32140	4079	3337	24723	0.368	0.283
0.51726	1996.6	25590	3214	2596	19780	0.391	0.302
0.42670	1647.1	18050	2349	1854	13847	0.405	0.311
0.35638	1375.6	13100	1583	1283	10258	0.422	0.330
0.29632	1143.8	9332	1095	900.5	7293	0.435	0.340
0.24022	927.2	6428	735.8	606.3	4945	0.455	0.350
0.20387	786.9	4944	570.9	476.7	3955	0.486	0.389
0.17542	677.1	3955	447.3	364.9	3090	0.526	0.411
0.14618	564.3	2843	323.7	264.9	2163	0.544	0.414
0.12248	472.8	2039	253.0	194.2	1606	0.556	0.438
0.11300	436.2	1560	185.4	150.1	1224	0.500	0.392
0.11078	427.6	1601	188.4	153.0	1260	0.533	0.420
0.12485	481.9	1966	229.6	188.4	1548	0.516	0.406
0.13623	525.8	2343	276.7	229.6	1848	0.516	0.407

0.14856	573.4	2784	326.7	264.9	2192	0.516	0.406
0.17036	657.6	3461	406.2		2719	0.488	0.383
0.19881	767.4	4573	541.4		3584	0.473	0.371
0.29506	1138.9	9209	1104	835.8	7169	0.433	0.337
0.35527	1371.3	12920	1581	1280	10076	0.418	0.326
0.42512	1641.0	17920	2225	1792	13903	0.406	0.315
0.52247	2016.7	25960	3214	2596	20150	0.389	0.302
0.59375	2291.9	32630	4079	3337	25214	0.378	0.292
0.67640	2610.9	41900	5067	4388	32445	0.374	0.290

Down-Flow

u, m/s	Re	ΔP_t, N/m^2	ΔP_{en}, N/m^2	ΔP_{ex}, N/m^2	ΔP_r, N/m^2	f_t	f_r
0.67656	2611.5	42890	3584	5191	34114	0.383	0.305
0.63579	2454.1	38010	3214	4635	30161	0.384	0.305
0.59501	2296.7	33930	2843	4141	26946	0.392	0.311
0.52263	2017.4	27070	2349	3275	21446	0.405	0.321
0.48707	1880.1	24040	2101	2905	19034	0.414	0.328
0.44172	1705.0	20020	1730	2318	16127	0.420	0.338

0.42070	1623.9	18290	1565	2095	14521	0.423	0.336
0.37139	1433.6	14460	1236	1633	11679	0.429	0.346
0.33141	1279.2	11680	994.7	1292	9332	0.435	0.347
0.28715	1108.4	9023	771.0	985.9	7231	0.447	0.359
0.24369	940.7	6798	565.1	712.2	5377	0.468	0.370
0.19597	756.4	4388	365.0	447.4	3523	0.467	0.375
0.13939	538.0	2407	211.9	241.3	1954	0.507	0.411

UP-Flow

u, m/s	Re	ΔP_t, N/m^2	ΔP_{en}, N/m^2	ΔP_{ex}, N/m^2	ΔP_r, N/m^2	f_t	f_r
0.10114	390.4	1551			1233	0.620	0.493
0.09277	358.1	1318			1047	0.626	0.498
0.07317	282.4	871.1			697.5	0.665	0.533
0.04899	189.1	447.3			359.0	0.762	0.612
0.04393	169.6	344.3			282.5	0.729	0.599

u, m/s	Re	ΔP_t, N/m^2	ΔP_r, N/m^2	f_t	f_r
0.09736	405.2	1447	1065	0.626	0.461
0.09648	397.0	1387	1020	0.611	0.449
0.09372	385.6	1311	966.1	0.612	0.451
0.09293	386.8	1309	961.4	0.621	0.456
0.09083	378.1	1257	926.8	0.625	0.460
0.08889	370.0	1200	882.5	0.623	0.458
0.08801	362.1	1148	845.3	0.608	0.447
0.08575	356.9	1134	833.2	0.632	0.465
0.08237	342.9	1043	764.2	0.630	0.462
0.08033	334.4	1001	734.6	0.636	0.467
0.07722	322.2	929.4	675.4	0.639	0.464
0.07520	313.7	894.8	650.8	0.649	0.472
0.07320	305.4	838.1	616.3	0.641	0.471
0.07223	296.5	766.4	571.7	0.602	0.449
0.07025	293.1	776.5	567.0	0.645	0.471
0.06835	285.2	729.7	530.0	0.640	0.465
0.06749	277.0	677.7	495.3	0.610	0.446
0.06441	268.7	653.3	473.3	0.646	0.468
0.06274	257.0	571.7	414.0	0.595	0.431
0.06042	252.6	571.9	414.2	0.642	0.465
0.05837	244.1	537.4	387.0	0.647	0.466
0.05734	234.9	480.5	347.5	0.599	0.433
0.05628	235.9	500.5	357.5	0.648	0.463
0.05522	226.2	458.3	332.7	0.616	0.447
0.05216	213.2	414.0	295.7	0.624	0.445
0.05086	213.2	419.1	295.8	0.664	0.469
0.04848	203.7	384.6	268.7	0.671	0.469
0.04620	188.8	327.7	234.1	0.629	0.449
0.04507	189.3	339.3	236.7	0.685	0.478

u, m/s	Re	ΔP_t, N/m^2	ΔP_r, N/m^2	f_t	f_r
0.04268	174.0	293.2	211.9	0.660	0.477
0.04042	169.4	283.5	204.6	0.711	0.513
0.03908	164.9	249.0	180.0	0.669	0.483
0.03794	160.1	241.6	175.1	0.688	0.499
0.03680	155.3	217.0	162.7	0.657	0.493
0.03565	149.4	226.8	162.7	0.732	0.525
0.03467	146.6	199.7	150.4	0.681	0.513
0.03337	141.2	189.9	143.0	0.699	0.526
0.03223	136.3	177.5	133.2	0.701	0.525
0.03109	130.3	182.4	133.1	0.774	0.565
0.02986	126.3	152.9	115.9	0.703	0.533
0.02875	121.6	148.0	111.0	0.734	0.550
0.02748	116.2	135.6	103.6	0.736	0.562
0.02615	110.6	130.7	101.1	0.784	0.606
0.02472	104.6	120.8	93.7	0.811	0.629
0.02329	98.3	111.0	86.3	0.838	0.652
0.02181	92.3	98.6	78.9	0.850	0.680
0.08237	340.5	1043	769.0	0.630	0.465
0.08465	350.7	1082	803.5	0.619	0.460
0.08684	359.8	1136	843.0	0.618	0.458
0.08801	363.8	1188	877.4	0.629	0.464
0.09083	375.4	1262	934.1	0.627	0.464
0.09292	385.9	1309	971.2	0.621	0.461
0.09373	386.6	1353	1001	0.631	0.467
0.09468	392.3	1353	1006	0.619	0.460
0.09735	401.5	1466	1084	0.634	0.469

u, m/s	Re	ΔP_r , N/m^2	f_r
0.09293	386.8	951.3	0.452
0.09083	378.1	912.1	0.453
0.08889	370.0	882.7	0.458
0.08801	362.1	838.6	0.444
0.08575	356.9	823.8	0.459
0.08237	342.9	765.0	0.462
0.08033	334.4	725.8	0.461
0.07722	322.2	676.7	0.465
0.07520	313.7	647.3	0.469
0.07320	305.4	622.8	0.476
0.07223	296.5	576.7	0.455
0.07025	293.1	568.8	0.472
0.06835	285.2	529.6	0.465
0.06749	277.0	495.3	0.446
0.06441	268.7	470.8	0.465
0.06274	257.0	426.6	0.444
0.06042	252.6	411.9	0.463
0.05837	244.1	382.5	0.460
0.05734	234.9	348.2	0.434
0.05628	235.9	353.1	0.457
0.05522	226.2	328.6	0.442
0.05216	213.2	289.3	0.436
0.05086	213.2	294.2	0.466
0.04849	203.7	269.7	0.470
0.04620	188.8	235.4	0.452
0.04507	189.3	235.4	0.475
0.04268	174.0	206.0	0.464

u, m/s	Re	ΔP_t , N/m^2	f_t
0.02030	85.9	88.3	0.878
0.01873	79.2	77.8	0.909
0.01711	72.2	66.7	0.934
0.01540	65.0	56.2	0.971
0.01263	53.2	46.4	1.193
0.00920	38.8	36.0	1.742
0.00737	31.0	25.5	1.926
0.00558	23.5	17.6	2.324
0.00454	19.1	14.8	2.940
0.00375	15.8	10.8	3.152
0.00217	9.11	6.08	5.306
0.00104	4.34	2.35	8.986
0.00069	2.91	1.68	14.191
0.00069	2.84	1.96	16.700
0.00069	2.84	2.30	19.622
0.00104	4.23	2.75	10.487
0.00104	4.42	3.87	14.787
0.00217	8.86	6.13	5.350
0.00217	9.17	7.36	6.417
0.00374	15.3	12.0	3.497
0.00375	16.0	12.8	3.725
0.00454	18.6	15.0	2.980
0.00455	19.4	15.7	3.115
0.00558	22.8	19.9	2.622
0.00558	23.8	19.9	2.620
0.00737	30.1	27.0	2.037
0.00737	31.4	27.8	2.096
0.00920	39.1	38.0	1.842
0.01262	51.5	48.1	1.236

u , m/s	Re	ΔP_t , N/m^2	f_t
0.01263	53.2	53.0	1.362
0.01262	51.9	53.9	1.388
0.01540	62.5	59.8	1.034
0.01540	64.4	62.3	1.076
0.01711	71.2	72.6	1.016
0.01873	78.1	84.6	0.989
0.01872	76.5	84.8	0.992
0.02030	84.7	94.6	0.942
0.01263	53.2	51.0	1.312
0.00375	15.7	13.2	3.869
0.00217	9.09	7.85	6.846
0.00104	4.34	4.61	17.598
0.00104	4.34	4.22	16.100
0.00104	4.34	3.04	11.607
0.00375	15.7	11.6	3.381
0.00217	9.09	7.94	6.932
0.00104	4.34	3.92	14.977
0.00069	2.91	2.75	23.374
0.01711	71.2	73.1	1.023

u , m/s	Re	ΔP_r , N/m^2	f_r
0.04145	174.1	206.0	0.491
0.04269	179.3	215.8	0.485
0.04383	184.1	222.6	0.475
0.04507	189.3	235.4	0.475
0.04620	189.2	250.1	0.480
0.04744	198.8	255.0	0.465
0.04849	203.2	269.7	0.470

u , m/s	Re	ΔP_r , N/m^2	f_r
0.04968	208.7	274.6	0.456
0.05086	213.7	289.3	0.458
0.05217	214.6	313.8	0.473
0.05310	223.6	313.8	0.456
0.05418	222.9	333.5	0.466
0.05524	232.6	343.3	0.461
0.05629	237.5	353.1	0.457
0.05736	242.1	372.7	0.464
0.05838	246.4	387.4	0.466
0.05942	250.8	402.1	0.467
0.06042	255.0	411.9	0.463
0.06152	259.6	431.5	0.468
0.06276	264.9	446.2	0.464
0.06342	267.6	461.0	0.470
0.06442	272.5	470.8	0.465
0.06542	276.7	485.5	0.465
0.06646	281.1	505.1	0.469
0.06751	285.5	519.8	0.468
0.06836	288.5	534.5	0.469
0.06931	292.5	549.2	0.469
0.07025	290.4	578.7	0.481
0.07131	300.9	588.5	0.474
0.07223	298.6	608.1	0.478
0.07224	299.3	613.0	0.482
0.07419	307.4	647.3	0.482
0.07519	311.5	666.9	0.484
0.07722	319.2	686.5	0.472
0.07823	323.4	716.0	0.480
0.07928	328.5	720.9	0.470

u , m/s	Re	ΔP_r , N/m^2	f_r
0.08032	332.0	750.3	0.477
0.08237	340.5	784.6	0.474
0.08465	350.7	818.9	0.468
0.08684	359.8	853.3	0.464
0.08801	363.8	882.7	0.467
0.09083	375.4	941.5	0.468
0.09292	385.9	971.0	0.461
0.04145	172.1	210.9	0.503
0.05735	239.3	372.7	0.464

DOWN-Flow

u, m/s	Re	ΔP_t , N/m^2	ΔP_r, N/m^2	f_t	f_r
0.09783	377.6	1248	1018	0.533	0.435
0.10399	401.4	1413	1142	0.534	0.432
0.10510	405.7	1448	1177	0.536	0.436
0.10905	420.9	1507	1224	0.518	0.421
0.11157	430.7	1630	1327	0.536	0.436
0.11426	441.0	1683	1365	0.527	0.428
0.11600	447.8	1722	1395	0.523	0.424
0.12153	469.1	1901	1536	0.526	0.425
0.12359	477.0	1984	1607	0.531	0.430
0.12912	498.4	2137	1731	0.524	0.424
0.13291	513.0	2248	1815	0.520	0.420
0.13575	524.0	2378	1931	0.528	0.428

Fluid: 30.15% Aq.Glycerol

UP--Flow

u , m/s	Re	ΔP_t , N/m^2	f_t
0.09202	151.3	1765	0.796
0.08764	144.1	1622	0.806
0.08281	136.1	1490	0.830
0.07854	129.1	1360	0.841
0.07352	120.9	1236	0.873
0.06910	113.6	1121	0.896
0.06433	105.8	1011	0.932
0.05941	97.7	901.5	0.975
0.05424	89.2	790.0	1.025
0.04885	80.3	679.4	1.087
0.04356	71.6	575.5	1.157
0.03722	61.2	466.1	1.284
0.03096	50.9	374.4	1.491
0.02420	39.8	265.0	1.728
DOWN--Flow			
0.09202	151.3	1709	0.770
0.08764	144.1	1569	0.780
0.08281	136.1	1444	0.804
0.07854	129.1	1322	0.818
0.07352	120.9	1199	0.847
0.06910	113.6	1078	0.862
0.06433	105.8	980.1	0.904
0.05941	97.7	867.6	0.938
0.05424	89.2	753.0	0.977
0.04885	80.3	652.0	1.043
0.04356	71.6	559.5	1.125
0.03722	61.2	450.1	1.240
0.03096	50.9	353.3	1.407
0.02420	39.8	250.3	1.632

Fluid: 41.95% Aq. Glycerol

UP-Flow

υ, m/s	Re	ΔP_t, N/m^2	ΔP_{en}, N/m^2	ΔP_{ex}, N/m^2	ΔP_r, N/m^2	f_t	f_r
0.23691	246.1	9931	1218	1444	7295	0.656	0.482
0.23691	246.1	9869	1201	1398	7172	0.652	0.474
0.22631	235.1	9072	1109	1325	6620	0.657	0.479
0.21287	221.2	8214	1002	1197	6007	0.672	0.492
0.21287	221.2	8030	986.3	1138	5946	0.657	0.487
0.20000	207.8	7233	888.9	1064	5333	0.671	0.494
0.20000	207.8	7172	877.2	1006	5210	0.665	0.483
0.18695	194.2	6498	807.0	962.9	4843	0.689	0.514
0.18695	194.2	6436	787.5	898.6	4720	0.683	0.501
0.17551	182.3	5762	713.4	859.6	4230	0.694	0.509
0.17551	182.3	5762	693.9	793.3	4205	0.694	0.506
0.16226	168.6	5027	627.7	756.3	3739	0.708	0.527
0.16226	168.6	5027	612.1	690.0	3617	0.708	0.509
0.14827	154.0	4291	573.1	639.4	3126	0.724	0.527
0.14827	154.0	4291	512.7	575.0	3126	0.724	0.527

0.13479	140.0	3678	452.2	541.9	2758	0.751	0.563
0.12011	124.8	3126	374.3	452.2	2268	0.804	0.583
0.12011	124.8				2256		0.580
0.10488	109.0	2575	298.2	372.3	1842	0.868	0.621
0.09015	93.7	2023	202.7	228.1	1476	0.923	0.673
0.07313	76.0	1487	159.8	202.7	1138	1.031	0.789
0.05317	55.2	931.7	81.9	95.5	729.0	1.283	0.999
0.03126	32.5	460.0	46.8	66.3	368.4	1.746	1.398

Down-Flow

u, m/s	Re	ΔP_t, N/m^2	ΔP_{en}, N/m^2	ΔP_{ex}, N/m^2	ΔP_r, N/m^2	f_t	f_r
0.23691	246.1	9832	1466	1197	7099	0.650	0.469
0.23691	246.1	9832	1470	1183	7099	0.650	0.469
0.22631	235.1	8974	1353	1129	6547	0.650	0.474
0.22631	235.1	8913	1341	1068	6486	0.645	0.470
0.21629	224.7	8177	1218	972.7	5934	0.648	0.470
0.21287	221.2	8055	1209	1016	5873	0.659	0.481
0.20000	207.8	7197	1080	908.3	5198	0.667	0.482

u, m/s	Re	ΔP_t, N/m^2	ΔP_{en}, N/m^2	ΔP_{ex}, N/m^2	ΔP_r, N/m^2	f_t	f_r
0.20000	207.8	7197	1068	847.9	5198	0.667	0.482
0.18695	194.2	6461	966.8	812.8	4708	0.686	0.500
0.18695	194.2	6400	953.2		4585	0.679	0.487
0.17551	182.3	5725	853.8	717.3	4156	0.689	0.500
0.17551	182.3	5725	853.8	666.6	4095	0.689	0.493
0.16168	168.0	4990	744.6	619.9	3604	0.708	0.511
0.16226	168.6	4990	729.0	555.5	3580	0.703	0.504
0.14827	154.0	4254	635.5	538.0	3114	0.718	0.525
0.14827	154.0	4254	623.8	467.8	2967	0.718	0.500
0.13479	140.0	3641	534.1	454.2	2624	0.743	0.535
0.13479	140.0	3641	526.3	389.8	2562	0.743	0.523
0.12011	124.8	3028	436.6	384.0	2256	0.778	0.580
0.12011	124.8	3028	432.7	321.6	2195	0.778	0.564
0.10488	109.0	2538	354.8	306.0	1832	0.856	0.618
0.10488	109.0				1840		0.620
0.09015	93.7	2109	267.0	239.8	1495	0.962	0.682
0.09015	93.7				1478		0.674

u, m/s	Re	ΔP_t, N/m^2	ΔP_{en}, N/m^2	ΔP_{ex}, N/m^2	ΔP_r, N/m^2	f_t	f_r
0.07313	76.0	1472	169.6	171.5	1138	1.021	0.789
0.05317	55.2	939.5	93.6	78.0	746.6	1.295	1.038
0.03126	32.5	456.1				1.731	
0.01051	10.9	111.1				3.728	

Fluid: 42.1% Aq. Glycerol

UP-Flow

u, m/s	Re	ΔP_t, N/m^2	f_t
0.08503	87.7	1895	0.971
0.08045	83.0	1778	1.018
0.07612	78.5	1622	1.038
0.07124	73.5	1484	1.084
0.06615	68.3	1369	1.160
0.06151	63.5	1254	1.229
0.05682	58.6	1129	1.297

u, m/s	Re	ΔP_t, N/m^2	f_t
0.05315	54.8	975.6	1.280
0.04578	47.2	837.3	1.481
0.03979	41.1	679.6	1.591
0.03321	34.3	523.8	1.761
0.02644	27.3	379.7	2.013
0.01883	19.4	247.3	2.586
0.01176	12.1	122.7	3.289

Fluid: 50.45% Aq. Glycerol

UP-Flow

u, m/s	Re	ΔP_t, N/m^2	ΔP_{en}, N/m^2	ΔP_{ex}, N/m^2	ΔP_r, N/m^2	f_t	f_r
0.08214	57.7	2337	211.8	286.0	1839	1.258	0.990
0.07776	54.8	2162	194.2	257.7	1710	1.299	1.027
0.07288	51.4	1991	176.5	236.8	1578	1.362	1.079
0.06757	47.7	1798	157.4	219.2	1422	1.431	1.131
0.06184	43.6	1611	136.8	186.5	1288	1.531	1.223
0.05586	39.4	1407	117.7	163.4	1126	1.638	1.311
0.04979	35.1	1198	98.6	134.7	964.4	1.755	1.413
0.04356	30.7	986.4	87.8	105.1	793.6	1.889	1.520
0.03774	26.5	797.2	71.6	84.5	641.1	2.033	1.635
0.03774	26.8	817.4	73.6	89.9	653.9	2.085	1.668
0.03143	22.1	648.4	56.9	71.7	519.8	2.386	1.912
0.03143	22.3	668.6	59.8	70.6	538.2	2.460	1.980
0.02603	18.4	494.1	43.2	46.9	404.1	2.649	2.166
0.02603	18.5	501.5	46.1	49.4	406.0	2.688	2.176
0.01988	13.9	341.7	30.9	35.2	275.5	3.140	2.532

u, m/s	Re	ΔP_t, N/m^2	ΔP_{en}, N/m^2	ΔP_{ex}, N/m^2	ΔP_r, N/m^2	f_t	f_r
0.01988	14.1	371.1	34.8	33.2	303.1	3.410	2.785
0.01525	10.7	282.9	21.3	33.8	227.8	4.420	3.559
0.01525	10.8	237.0	23.0	17.5	196.6	3.702	3.071
0.01988	13.9	363.7	31.9	43.4	288.4	3.342	2.650
0.01988	14.1	347.2	31.4	36.6	279.2	3.191	2.566
0.02603	18.5		43.2	50.5	380.2		2.038
0.03143	22.2	635.6	56.9	64.4	514.3	2.338	1.892
0.03143	22.3	648.4	57.4	69.4	521.7	2.386	1.919
0.03774	26.6	802.7	70.6	89.2	642.9	2.047	1.640
0.03774	26.8	815.6	70.6	91.0	653.9	2.080	1.668
0.04356	30.7	988.3	86.8	107.9	793.6	1.892	1.520
0.04979	35.1	1185	98.6	136.6	949.7	1.736	1.392
0.05586	39.4	1392	117.7	159.7	1115	1.621	1.298
0.06184	43.6	1604	136.8	184.6	1282	1.524	1.218
0.06757	47.7	1809	157.4	217.3	1435	1.440	1.142
0.07288	51.4	1991	176.5	244.1	1571	1.362	1.074
0.07776	54.8	2160	194.2	259.5	1707	1.298	1.025

0.08214	57.9	2331	213.3	286.3	1831	1.255	0.986

Down-Flow

u, m/s	Re	ΔP_t, N/m^2	ΔP_{en}, N/m^2	ΔP_{ex}, N/m^2	ΔP_r, N/m^2	f_t	f_r
0.08214	57.7	2318	239.8	250.7	1828	1.248	0.984
0.07776	54.7	2175	219.2	252.9	1703	1.307	1.023
0.07288	51.2	1973	197.1	197.8	1578	1.350	1.079
0.06757	47.5	1806	175.1	194.2	1436	1.437	1.143
0.06184	43.3	1598	151.5	162.6	1284	1.518	1.220
0.05586	39.1	1407	129.5	142.4	1135	1.638	1.322
0.04979	34.9	1196	105.9	121.9	968.1	1.752	1.419
0.04356	30.6	1003	92.7	92.8	817.4	1.921	1.565
0.03774	26.4	815.6	74.0	76.6	665.0	2.080	1.696
0.03143	22.0	637.4	57.4	56.5	523.5	2.345	1.926
0.02603	18.2	521.7	42.7	47.4	431.7	2.797	2.314
0.01988	13.9	389.4	29.9	30.7	328.8	3.579	3.022
0.01525	10.7	271.9	16.2	26.1	229.6	4.247	3.587
0.04356	31.2	957.0	92.2	91.5	773.3	1.833	1.481

0.04979	35.7	1139	105.9	114.5	918.5	1.669	1.346
0.05586	39.8	1385	130.9	144.6	1110	1.613	1.292
0.06184	44.1	1549	150.1	158.5	1240	1.471	1.178
0.06757	48.0	1760	175.1	183.1	1402	1.400	1.115
0.07288	51.8	1938	195.7	201.1	1541	1.326	1.054
0.07776	55.3	2120	217.7	228.6	1673	1.274	1.005
0.08214	58.4	2289	238.3	246.6	1804	1.232	0.971

Fluid: 65.45% Aq. Glycerol

UP-Flow

u, m/s	Re	ΔP_f, N/m^2	ΔP_{en}, N/m^2	ΔP_{ex}, N/m^2	ΔP_r, N/m^2	f_t	f_r
0.04498	12.6	2333	170.7	270.2	1892	4.042	3.278
0.04024	11.3	2076	147.1	246.0	1683	4.494	3.643
0.03540	9.9	1785	128.0	208.2	1449	4.994	4.054
0.03093	8.7	1554	107.4	181.0	1266	5.694	4.638
0.02657	7.4	1321	89.7	150.9	1080	6.557	5.362
0.02290	6.4	1095	82.4	119.7	892.7	7.316	5.966
0.01962	5.5	925.8	66.7	102.3	756.8	8.429	6.891

u, m/s	Re	ΔP_t, N/m^2	ΔP_{en}, N/m^2	ΔP_{ex}, N/m^2	ΔP_r, N/m^2	f_t	f_r
0.01827	5.1	800.9	63.3	83.7	653.9	8.412	6.869
0.01187	3.3	569.4	40.2	59.0	470.3	14.163	11.696
0.01544	4.3		53.9	74.6	565.8		8.323
0.01827	5.1	835.8	64.7	91.4	679.7	8.779	7.139
0.01962	5.5	940.5	73.1	103.3	764.2	8.563	6.958
0.02290	6.4	1089	85.3	118.6	885.4	7.279	5.917
0.02290	6.4	1121	87.8	118.0	914.8	7.488	6.113
0.02657	7.4	1295	94.2	146.5	1054	6.429	5.235
0.03093	8.7	1464	107.4	166.3	1190	5.365	4.362
0.03540	9.9	1684	125.0	190.9	1369	4.711	3.828
0.04024	11.3	1956	145.6	221.7	1589	4.235	3.440
0.04498	12.6	2221	166.2	254.4	1800	3.847	3.119
Down-Flow							
0.04498	12.6	2364	192.7	253.7	1918	4.096	3.322
0.04498	12.6	2348	189.8	240.1	1918	4.067	3.322
0.03540	9.9	1804	145.6	197.9	1460	5.045	4.085
0.03093	8.7	1552	123.6	163.0	1266	5.688	4.638

υ, m/s	Re	ΔP_t, N/m^2	ΔP_{en}, N/m^2	ΔP_{ex}, N/m^2	ΔP_r, N/m^2	f_t	f_r
0.02657	7.4	1332	110.3	134.0	1087	6.612	5.399
0.02657	7.4	1334	103.0	139.5	1091	6.621	5.417
0.02290	6.4	1150	94.6	114.8	940.5	7.685	6.285
0.02290	6.4	1132	92.2	117.2	922.1	7.562	6.162
0.01962	5.5	975.4	82.4	106.8	786.2	8.881	7.158
0.01962	5.5	984.6	77.0	97.5	810.1	8.965	7.376
0.01827	5.1	881.7	70.6	83.7	727.4	9.261	7.640
0.01187	3.3	547.4	43.2	56.0	440.9	13.615	10.965
0.01544	4.3		62.8	73.2	589.7		8.674
0.01962	5.5	969.9	80.4	99.6	789.9	8.831	7.192
0.01962	5.5	980.9	82.4	101.3	797.2	8.931	7.259
0.02657	7.4	1297	104.5	138.0	1054	6.439	5.235
0.03093	8.7	1510	123.6	159.3	1227	5.533	4.496
0.03540	9.9	1784	145.6	192.3	1446	4.989	4.043
0.04024	11.3	2046	169.2	220.2	1657	4.430	3.587
0.04498	12.6	2335	192.7	248.1	1894	4.045	3.281

Gap 1 Channel

Fluid: Water

UP-Flow

u, m/s	Re	ΔP_t, N/m^2	ΔP_{en}, N/m^2	ΔP_{ex}, N/m^2	ΔP_r, N/m^2	f_t	f_r
0.53197	2580.0	12110	2410	2163	7540	0.220	0.137
0.54001	2619.1	11990	2472	2225	7293	0.211	0.128
0.50859	2466.6	11000	2372	2031	6675	0.219	0.133
0.47741	2315.4	10010	2007	1804	6180	0.226	0.139
0.47578	2307.5	9765	2101	1792	5871	0.222	0.133
0.46912	2275.2	9518	2007	1713	5809	0.222	0.136
0.44398	2153.3	8776	1745	1560	5377	0.229	0.140
0.43543	2111.8	8343	1754	1460	5068	0.226	0.137
0.40966	1986.8	7602	1495	1348	4635	0.233	0.142
0.40727	1975.3	7416	1569	1336	4512	0.230	0.140
0.39608	1921.0	7107	1471	1265	4326	0.233	0.142
0.38716	1877.7	6613	1398	1183	4079	0.227	0.140
0.36604	1775.3	6242	1207	1101	3832	0.239	0.147

u, m/s	Re	ΔP_t, N/m^2	ΔP_{en}, N/m^2	ΔP_{ex}, N/m^2	ΔP_r, N/m^2	f_t	f_r
0.35850	1738.7	5995	1213	1048	3585	0.240	0.143
0.32557	1579.0	5068	1024	888.8	3090	0.246	0.150
0.33788	1638.7	5006	1054	897.6	3090	0.225	0.139
0.31714	1538.1	4821	912.3	844.6	2967	0.246	0.152
0.29515	1431.5	4079	818.2	718.1	2596	0.241	0.153
0.28597	1387.0	3646	759.3	656.3	2287	0.229	0.144
0.26070	1264.4	3337	615.1	588.6	2039	0.252	0.154
0.23883	1158.3	2905	553.3	500.3	1730	0.262	0.156
0.23619	1145.5	2713	541.5	473.8	1713	0.250	0.158
0.22840	1107.7	2513	503.3	441.4	1589	0.248	0.157
0.23116	1121.1	2499	479.7		1616	0.240	0.155
0.21357	1035.8	2254	447.7	394.4	1430	0.254	0.161
0.20891	1013.2	2078	423.8		1321	0.245	0.156
0.20175	978.5	2060	409.1	359.0	1304	0.260	0.165
0.20615	999.8	2054	391.4		1351	0.248	0.163
0.19182	930.3	1872	370.8	323.7	1189	0.261	0.166
0.19446	943.1	1842	364.9		1192	0.250	0.162

u, m/s	Re	ΔP_t, N/m^2	ΔP_{en}, N/m^2	ΔP_{ex}, N/m^2	ΔP_r, N/m^2	f_t	f_r
0.17824	864.5	1554	300.2		1001	0.251	0.162
0.17384	843.1	1507	282.5		991.8	0.256	0.169
0.17158	832.2	1507	294.3	264.9	962.4	0.263	0.168
0.15461	749.9	1283	247.2	223.7	818.2	0.276	0.176
0.16115	781.6	1265	253.1		824.0	0.250	0.163
0.15436	748.6	1198	223.7		794.6	0.258	0.171
0.14506	703.5	1133	217.8	194.2	724.0	0.277	0.177
0.13199	640.1	959.4	185.4		644.5	0.283	0.190
0.13324	646.2	953.5	182.5	167.8	612.1	0.276	0.177
0.11854	574.9	777.0	147.1	135.4	500.3	0.284	0.183
0.10697	518.8	665.1			456.2	0.299	0.205
0.10534	510.9	606.3				0.281	
0.08623	418.2	447.3			317.8	0.309	0.220
0.06599	320.1	303.1			211.9	0.358	0.250
0.04890	237.2	191.3			126.5	0.411	0.272
0.03331	161.6	105.9				0.491	

Down-Flow

u, m/s	Re	ΔP_t, N/m^2	ΔP_{en}, N/m^2	ΔP_{ex}, N/m^2	ΔP_r, N/m^2	f_t	f_r
0.52970	2569.1	12300	2596	2225	7293	0.225	0.134
0.52480	2545.3	12050	2534	2101	7169	0.225	0.134
0.48923	2372.8	10510	2254	1907	6428	0.226	0.138
0.47326	2295.3	10010	2128	1795	6057	0.230	0.139
0.45554	2209.4	9270	1972	1672	5562	0.230	0.138
0.44209	2144.1	8776	1848	1580	5315	0.231	0.140
0.42902	2080.7	8282	1754	1483	5068	0.231	0.141
0.40363	1957.6	7540	1548	1333	4573	0.238	0.144
0.38439	1864.3	6798	1401	1201	4079	0.236	0.142
0.35749	1733.8	6057	1224	1077	3708	0.243	0.149
0.33776	1638.1	5315	1086	938.8	3214	0.239	0.145
0.32393	1571.1	5068	1007	891.7	3090	0.248	0.151
0.27403	1329.0	3646	741.6	650.4	2349	0.249	0.161
0.27302	1324.2	3585	712.2	641.6	2225	0.247	0.153
0.22991	1115.0	2719	512.1	470.9	1730	0.264	0.168
0.21231	1029.7	2204	441.4	388.5	1398	0.251	0.159
0.19810	960.8	1960	394.4	347.3	1248	0.257	0.163

u, m/s	Re	ΔP_t, N/m^2	ΔP_{en}, N/m^2	ΔP_{ex}, N/m^2	ΔP_r, N/m^2	f_t	f_r
0.20338	986.4	1945	400.2		1236	0.242	0.154
0.18415	893.1	1683	335.5		1083	0.255	0.164
0.17133	831.0	1448	288.4	276.6	941.8	0.253	0.165
0.17045	826.7	1442	285.5	253.1	930.0	0.255	0.164
0.15801	766.3	1257	250.2	220.7	815.2	0.259	0.168
0.15813	766.9	1224	247.2	235.4	803.4	0.252	0.165
0.14292	693.2	1083	211.9	188.4	700.4	0.272	0.176
0.12382	600.5	859.4		173.6	570.9	0.288	0.191
0.12558	609.0	838.8	164.8	147.1		0.273	
0.10961	531.6	653.3	129.5	117.7		0.279	
0.10559	512.1	641.6			435.6	0.296	0.201
0.08837	428.6	470.9			312.0	0.310	0.205
0.06411	310.9	276.6			191.3	0.346	0.239
0.04462	216.4	170.7			108.9	0.440	0.281
0.03130	151.8	97.1				0.509	

Gap 2 Channel

Fluid: Water

UP-Flow

u, m/s	Re	ΔP_t, N/m^2	ΔP_{en}, N/m^2	ΔP_{ex}, N/m^2	ΔP_r, N/m^2	f_t	f_r
0.69931	4776.3	10570	3832	2967	3894	0.156	0.058
0.67077	4581.4	10010	3399	2781	3646	0.161	0.059
0.62974	4301.1	8838	3090	2401	3337	0.161	0.061
0.58960	4027.0	7849	2719	2131	2905	0.163	0.060
0.54901	3749.8	6860	2372	1854	2560	0.165	0.061
0.50040	3417.7	5933	2013	1583	2225	0.171	0.064
0.45892	3134.5	4944	1678	1330	1907	0.170	0.066
0.41923	2863.3	4203	1383	1177	1601	0.173	0.066
0.38177	2607.5	3523	1154	935.9	1357	0.175	0.067
0.35233	2406.4	2967	977.1	806.4	1174	0.173	0.068
0.31398	2144.5	2260	771.1	629.8	935.9	0.166	0.069
0.28231	1928.2	1884	635.7	535.6	782.8	0.171	0.071
0.24752	1690.6	1457	488.5	417.9	618.0	0.172	0.073
0.20070	1370.8	1009	341.4			0.181	

0.16591	1133.2	759.3				0.200	
0.15119	1032.6	644.5			259.0	0.204	0.082
0.13737	938.2	535.6				0.205	
0.12265	837.7	456.2				0.219	
0.11061	755.4	364.9				0.216	

Down-Flow

u, m/s	Re	ΔP_t, N/m^2	ΔP_{en}, N/m^2	ΔP_{ex}, N/m^2	ΔP_r, N/m^2	f_t	f_r
0.70957	4846.4	10880	3894	2967	3894	0.156	0.056
0.66453	4538.7	9641	3399	2596	3523	0.158	0.058
0.61770	4218.9	8529	2967	2225	3152	0.162	0.060
0.56195	3838.1	7169	2472	1913	2658	0.164	0.061
0.49416	3375.1	5686	2001	1519	2143	0.168	0.063
0.45313	3094.9	4882	1683	1283	1825	0.172	0.064
0.40987	2799.4	4017	1383	1071	1524	0.173	0.066
0.37865	2586.2	3523	1195	930.0	1336	0.178	0.067
0.33271	2272.4	2781	953.5	741.6	1092	0.182	0.071
0.30907	2111.0	2472	824.0	647.5	950.6	0.187	0.072

u, m/s	Re	ΔP_t, N/m^2	ΔP_{en}, N/m^2	ΔP_{ex}, N/m^2	ΔP_r, N/m^2	f_t	f_r
0.28231	1928.2	1978	694.5	541.5	812.3	0.180	0.074
0.25600	1748.5	1704	588.6	465.0	694.5	0.188	0.077
0.23236	1587.0	1424	494.4	394.4	585.7	0.191	0.078
0.21363	1459.1	1136		312.0	476.8	0.180	0.076
0.17840	1218.4	888.8	306.1	247.2	373.8	0.202	0.085
0.16056	1096.6	724.0		194.2	297.2	0.203	0.083
0.13737	938.2	553.3		141.3	226.6	0.212	0.087
0.12265	837.7	459.1			200.1	0.221	0.096
0.10677	729.2	359.0				0.228	
0.09455	645.8	276.6				0.224	
0.08295	566.6	217.8				0.229	
0.07136	487.4	173.6				0.247	
0.05932	405.1	123.6				0.254	
UP-Flow							
0.37412	2570.2	3337	1224	853.5	1236	0.174	0.064
0.35133	2413.7	2922	1089	753.4	1095	0.172	0.065
0.33697	2315.0	2672	988.8	694.5	1027	0.171	0.066

u, m/s	Re	ΔP_t, N/m^2	ΔP_{en}, N/m^2	ΔP_{ex}, N/m^2	ΔP_r, N/m^2	f_t	f_r
0.33058	2271.1	2607	971.2	671.0	980.0	0.174	0.065
0.31515	2165.1	2384	882.9	612.1	897.6	0.175	0.066
0.31427	2159.0	2396	882.9	635.7	935.9	0.177	0.069
0.29910	2054.8	2148	794.6	553.3	818.2	0.175	0.067
0.28749	1975.0	2066	753.4	541.5	806.4	0.182	0.071
0.28181	1936.1	1913	700.4	488.5	729.9	0.175	0.067
0.26780	1839.8	1813	659.2	476.8	712.2	0.184	0.072
0.26417	1814.8	1692	618.0	429.7	665.1	0.176	0.069
0.24297	1669.2	1419		359.0	547.4	0.175	0.067
0.23889	1641.2	1471	529.7	388.5	585.7	0.188	0.075
0.22355	1535.8	1180		300.2	462.1	0.172	0.067
0.22151	1521.8	1195		300.2	467.9	0.177	0.069
0.18737	1287.2	912.3		241.3	370.8	0.189	0.077
0.18462	1268.4	827.0		206.0		0.177	
0.17106	1175.2	709.3		188.4	312.0	0.176	0.078
0.13630	936.3	500.3		123.6	223.7	0.196	0.088
0.10792	741.4	323.7			153.0	0.202	0.096
0.08752	601.3				111.8		0.106

Down- Flow

u, m/s	Re	ΔP_t, N/m^2	ΔP_{en}, N/m^2	ΔP_{ex}, N/m^2	ΔP_r, N/m^2	f_t	f_r
0.37377	2567.8	3461	1136	994.7	1295	0.180	0.067
0.34779	2389.3	2931	971.2	853.5	1107	0.176	0.067
0.34060	2340.0	2905	941.8	841.7	1112	0.182	0.070
0.33599	2308.3	2755	912.3	806.4	1045	0.178	0.067
0.32172	2210.2	2510	829.9	729.9	965.3	0.177	0.068
0.31170	2141.4	2334	794.6	718.1	956.5	0.175	0.072
0.30726	2110.9	2254	741.6	665.1		0.174	
0.29591	2032.9	2048	665.1	600.4		0.170	
0.29148	2002.5	2140	706.3	635.7	853.5	0.183	0.073
0.27419	1883.7	1786	582.7	520.9		0.173	
0.26452	1817.3	1816	582.7	529.7	726.9	0.189	0.076
0.25415	1746.0	1554	509.1	447.3		0.175	
0.24058	1652.8	1374	453.2	391.4		0.173	
0.23951	1645.5	1501	482.7		609.2	0.190	0.077
0.22550	1549.2	1201	394.4	338.4		0.172	
0.21211	1457.2	1195	382.6		491.5	0.193	0.079

0.18383	1262.9	909.4	294.3		385.5	0.196	0.083
0.15075	1035.6	626.9	206.0		259.0	0.201	0.083
0.12282	843.7	423.8			191.3	0.204	0.092

Fluid: 42.1% Aq. Glycerol

UP-Flow

u, m/s	Re	ΔP_t, N/m^2	ΔP_{en}, N/m^2	ΔP_{ex}, N/m^2	ΔP_r, N/m^2	f_t	f_r
0.13293	244.1	794.5	190.8	179.2	424.5	0.297	0.158
0.13293	244.1	791.8				0.296	
0.12730	233.8	730.2	173.3	173.3	397.2	0.297	0.162
0.12699	233.2	712.7				0.292	
0.11944	219.4	656.2	151.9	151.9	360.2	0.303	0.167
0.11944	219.4	648.4				0.300	
0.11222	206.1	599.8	136.3	139.4	336.9	0.314	0.176
0.11222	206.1	582.2				0.305	
0.10490	192.7	537.5	118.8	123.8	308.4	0.322	0.185
0.10490	192.7	523.8				0.314	
0.09848	180.9	485.7	105.2	110.2	282.4	0.330	0.192

u, m/s	Re	ΔP_t, N/m^2	ΔP_{en}, N/m^2	ΔP_{ex}, N/m^2	ΔP_r, N/m^2	f_t	f_r
0.09848	180.9	471.2				0.321	
0.09105	167.2	432.3	93.5	97.4	258.2	0.344	0.206
0.08320	152.8	381.7	77.9	81.8	229.8	0.364	0.219
0.07564	138.9	331.0	66.2	74.0	206.4	0.382	0.238
0.06740	123.8	284.3				0.413	
0.05885	108.1	236.8				0.451	
0.05058	92.9	190.8				0.492	
0.04103	75.4	153.8				0.603	
0.02983	54.8	109.0				0.808	
0.01754	32.2	62.3				1.337	
0.00590	10.8	31.2				5.908	
Down-Flow							
0.13293	244.1	849.0	222.0	171.4	445.9	0.317	0.166
0.13293	244.1	825.6				0.308	
0.12699	233.2	792.5	206.4	167.5	422.6	0.324	0.173
0.12699	233.2	757.5				0.310	
0.11944	219.4	726.3	186.9	159.7	397.2	0.336	0.184

u, m/s	Re	ΔP_t, N/m^2	ΔP_{en}, N/m^2	ΔP_{ex}, N/m^2	ΔP_r, N/m^2	f_t	f_r
0.11222	206.1	660.1	163.6	144.1	368.0	0.346	0.193
0.11222	206.1	621.2				0.325	
0.10490	192.7	597.8	148.0	136.3	340.8	0.358	0.204
0.10490	192.7	560.8				0.336	
0.09848	180.9	537.5	128.5	120.7	313.5	0.366	0.213
0.09848	180.9	498.5				0.339	
0.09105	167.2	477.1	112.9	101.3	284.3	0.380	0.226
0.09105	167.2	440.1				0.350	
0.08320	152.8	418.7	97.4	89.6	257.0	0.399	0.245
0.08320	152.8	381.7				0.364	
0.07564	138.9	366.1	81.8	74.0	227.8	0.422	0.263
0.07564	138.9	329.1				0.380	
0.06740	123.8	297.9			196.7	0.433	0.286
0.06740	123.8	268.7				0.390	
0.05885	108.1	251.2				0.479	
0.05058	92.9	208.4				0.537	
0.04103	75.4	161.6				0.633	

u , m/s	Re	ΔP_t , N/m^2	f_t
0.02983	54.8	112.9	0.837
0.01754	32.2	62.3	1.337
0.00590	10.8	31.2	5.908
Parallel Pattern Channel			
Fluid : Water			
UP-Flow			
0.68114	2629.2	19650	0.173
0.62267	2403.5	16810	0.177
0.57210	2208.3	14340	0.179
0.52152	2013.1	12110	0.182
0.47411	1830.1	10140	0.184
0.42354	1634.9	8405	0.192
0.37929	1464.1	6675	0.190
0.33188	1281.1	5439	0.202
0.28605	1104.1	3955	0.198
0.23706	915.0	2967	0.216
0.21177	817.4	2401	0.219
0.18965	732.0	1942	0.221
0.16910	652.7	1595	0.228
0.14698	567.3	1236	0.234
0.12643	488.0	941.8	0.241
0.10589	408.7	706.3	0.258
0.08692	335.5	482.7	0.261
0.06796	262.3	300.2	0.266
DOWN-Flow			
0.67640	2610.9	20390	0.182
0.62583	2415.7	17550	0.183

u , m/s	Re	ΔP_t , N/m^2	f_t
0.56894	2196.1	14710	0.186
0.51125	1973.4	12110	0.190
0.43935	1695.9	9270	0.196
0.39667	1531.2	7664	0.199
0.33978	1311.6	5191	0.184
0.29553	1140.7	4450	0.208
0.22599	872.3	2967	0.238
0.19913	768.6	2472	0.255
0.18095	698.5	1813	0.226
0.15646	603.9	1436	0.240
0.13591	524.6	1107	0.245
0.11695	451.4	847.6	0.253
0.09640	372.1	600.4	0.264
0.07744	298.9	400.2	0.273

Appendix A-7.0 Computation

The data presented in Appendix A-6.0 were quoted from print-out's of Fortran IV programs run on the University ICL 1900 computer. The program which processed the standard channel data when 50.45% and 65.45% aqueous glycerol solutions were employed is presented here as an example (pp.196-202). Its relative complexity and length are due to the multiplicity of manometers used, pressure drop measurements of the ribbed section, each of the two ports, as well as the channel total, and UP-Flow in addition to DOWN-Flow situations. Hence, readings of various manometers were directly fed without pre-adjustments. A sample of print-out results from another program (standard channel 41.95% aq.glycerol data) is also presented on pages 203 and 204. The last column on page 204 is the summation of the percentage contributions and can be regarded as a measure of accuracy.

Fig.'s 4.7, 4.16, 4.29, 4.32, 4.38, and 4.41 were plotted by the computer graph plotter. Standard sub-routines were used for this purpose.

```
0012                    TRACE 1
0013                    READ FROM (CR)
0001                    MASTER GLYCE2
0002                    REAL MU,MFLOW
0003                    DIMENSION MFLOW(172),TODP(172),MU(115),ENDP(106),RBDP(106)
0004                    DIMENSION VELO(172),TPD(172),RE(172)
0005                    READ (1,10) MFLOW,TODP,MU,ENDP,RBDP
0006                 10 FORMAT (669F0.0)
COMMENT 178      IS THIS LARGE A REPEAT COUNT INTENDED AT ABOUT COLUMN 16, LINE 0006

0007                    WRITE (2,19)
0008                 19 FORMAT (1H1,27X,'AQUEOUS GLYCEROL 50.45% BY WEIGHT'//)
0009                    WRITE (2,20)
0010                 20 FORMAT      (5X,'UPWARD FLUID MOVEMENT :'//5X,'              VELOCITY
0011                   1    REYNOLDS    PRESSURE DROP     EULER      FRICTION'//7X,'
0012                   2METERS       NUMBER      NEWTON/METER2       NO.         FACTOR')
0013                    DATA AREA,RHO,DE,CLEN/10.546E-5,1125.5,3.86E-3,0.472/
0014                    DO 29 I=1,65
0015                    VELO(I)=MFLOW(I)/(AREA*RHO)
0016                    RE(I)=(RHO*DE*VELO(I))/(MU(I)*(10.0**(-3.0)))
0017                    IF ((I.GT.0.AND.I.LT.9).OR.I.GT.57) GO TO 50
0018                    IF (I.GT.8.AND.I.LT.29) GO TO 50



0019                    IF (I.GT.28.AND.I.LT.38) GO TO 40
0020                    IF (I.GT.37.AND.I.LT.58) GO TO 60
0021                 30 IF (MOD(I,2).EQ.0) GO TO 40
0022                 50 TPD(I)=TODP(I)*3.745*9.81
0023                    GO TO 80
0024                 40 TPD(I)=TODP(I)*9.80768
0025                    GO TO 80
0026                 60 IF (MOD(I,2).EQ.0) GO TO 50
0027                    GO TO 40
0028                 80 EU=TPD(I)/(RHO*(VELO(I)**2.0))
0029                    FANN=(TPD(I)*DE)/(2.0*RHO*(VELO(I)**2.0)*CLEN)
0030                    WRITE (2,90) VELO(I),RE(I),TPD(I),EU,FANN
```

```
0031          90 FORMAT (/17X,F7.5,5X,F6.1,5X,E10.4,5X,F6.1,5X,F6.3)
0032          29 CONTINUE
0033             WRITE (2,100)
0034         100 FORMAT (/////5X,'ENTRANCE DELTAP PERCENT OF   EXIT DELTAP PERCENT
0035            1OF   RIBS DELTAP PERCENT OF   REYNOLDS   RIBS'//7X,'NEWTONPERM2
0036            2 TOTAL       NEWTONPERM2   TOTAL       NEWTONPERM2   TOTAL        NUM
0037            3BER  FRICTION   EUEN   EUEX')
0038             K=0
0039             N=18
0040             DO 110 I=1,36
0041             ENP=ENDP(I)*9.80768
0042             RBP=RBDP(I)*3.745*9.81
0043             IF (I.GT.9.AND.I.LT.19) GO TO 120
0044             IF (I.GT.18.AND.I.LT.29) GO TO 130
0045             IF (I.GT.28) GO TO 131
0046             ENC=(ENP/TPD(I))*100.0
0047             RBC=(RBP/TPD(I))*100.0
0048             EXP=TPD(I)-(RBP+ENP)
0049             EXC=(EXP/TPD(I))*100.0
0050             VEL=VELO(I)
0051             REAN=(RHO*DE)/(2.0*RHO*(VEL**2.0)*CLEN)
0052             EUEN=ENP/(RHO*(VEL**2.0))
0053             EUEX=EXP/(RHO*(VEL**2.0))
0054             REY=RE(I)
0055             GO TO 132
0056         120 K=K+1
0057             ENC=(ENP/TPD(I+K))*100.0
0058             RBC=(RBP/TPD(I+K))*100.0
0059             EXP=TPD(I+K)-(RBP+ENP)
0060             EXC=(EXP/TPD(I+K))*100.0
0061             VEL=VELO(I+K)
0062             REAN=(RHO*DE)/(2.0*RHO*(VEL**2.0)*CLEN)
0063             EUEN=ENP/(RHO*(VEL**2.0))
0064             EUEX=EXP/(RHO*(VEL**2.0))
0065             REY=RE(I+K)
0066             GO TO 132
0067         130 K=K+1
```

```
0068                ENC=(ENP/TPD(I+N))*100.0
0069                RBC=(RBP/TPD(I+N))*100.0
0070                EXP=TPD(I+N)-(RBP+ENP)
0071                EXC=(EXP/TPD(I+N))*100.0
0072                VEL=VELO(I+N)
0073                RFAN=(RBP*DE)/(2.0*RHO*(VEL**2.0)*CLEN)
0074                EUEN=ENP/(RHO*(VEL**2.0))
0075                EUEX=EXP/(RHO*(VEL**2.0))
0076                REY=RE(I+N)
0077                GO TO 132
0078           131  ENC=(ENP/TPD(I+29))*100.0
0079                RBC=(RBP/TPD(I+29))*100.0
0080                EXP=TPD(I+29)-(RBP+ENP)
0081                EXC=(EXP/TPD(I+29))*100.0



0082                VEL=VELO(I+29)
0083                RFAN=(RBP*DE)/(2.0*RHO*(VEL**2.0)*CLEN)
0084                EUEN=ENP/(RHO*(VEL**2.0))
0085                EUEX=EXP/(RHO*(VEL**2.0))
0086                REY=RE(I+29)
0087           132  WRITE (2,140) ENP,ENC,EXP,EXC,RBP,RBC,REY,RFAN,EUEN,EUEX
0088           110  CONTINUE
0089           140  FORMAT (//7X,E10.4,5X,F6.3,6X,E10.4,3X,F6.3,6X,E10.4,3X,F6.3,7X,F5.
                  1 1,4X,F5.3,5X,F7.3,4X,F5.2,2X,F5.2)
0091                WRITE (2,19)
0092                WRITE (2,160)
0093           160  FORMAT      (5X,'DOWNWARD FLUID MOVEMENT :'//5X,'              VELOCI
                  1TY    REYNOLDS    PRESSURE DROP     EULER       FRICTION'/7X,'
                  2  MBERS       NUMBER      NEWTONPERM2        NO.          FACTOR')
0096                DO 170 I=66,113
0097                VELO(I)=MFLOW(I)/(AREA*RHO)
0098                RE(I)=(RHO*DE*VELO(I))/(MU(I)*(10.0**(-3.0)))
0099                IF ((I.GT.65.AND.I.LT.74).OR.I.EQ.97.OR.I.GT.105) GO TO 180
0100                IF ((I.GT.73.AND.I.LT.84).OR.I.GT.97.AND.I.LT.106) GO TO 181
0101                IF (I.GT.83.AND.I.LT.93) GO TO 182
```

```
      IF (I.GT.92.AND.I.LT.97) GO TO 185
181   IF (MOD(I,2).EQ.0) GO TO 180
182   TPD(I)=TODP(I)*9.80768
      GO TO 190
180   TPD(I)=TODP(I)*3.745*9.81
      GO TO 190
185   IF (MOD(I,2).EQ.0) GO TO 182
      GO TO 180
190   EU=TPD(I)/(RHO*(VELO(I)**2.0))
      FANN=(TPD(I)*DE)/(2.0*RHO*(VELO(I)**2.0)*CLEN)
      WRITE (2,90) VELO(I),RE(I),TPD(I),EU,FANN
170   CONTINUE
      WRITE (2,100)
      K=29
      J=42
      N=45
      DO 200 I=37,63
      ENP=ENDP(I)*9.80768
      RBP=RBDP(I)*3.745*9.81
      IF (I.GT.45.AND.I.LT.50) GO TO 210
      IF (I.EQ.50.OR.I.EQ.51) GO TO 220
      IF (I.GT.51.AND.I.LT.56) GO TO 230
      IF (I.GT.55) GO TO 240
      ENC=(ENP/TPD(I+29))*100.0
      RBC=(RBP/TPD(I+29))*100.0
      EXP=TPD(I+29)-(RBP+ENP)
      EXC=(EXP/TPD(I+29))*100.0
      VEL=VELO(I+29)
      RFAN=(RBP*DE)/(2.0*RHO*(VEL**2.0)*CLEN)
      EUEN=ENP/(RHO*(VEL**2.0))
      EUEX=EXP/(RHO*(VEL**2.0))
      REY=RE(I+29)
      GO TO 250
210   K=K+1
      ENC=(ENP/TPD(I+K))*100.0
      RBC=(RBP/TPD(I+K))*100.0
      EXP=TPD(I+K)-(RBP+ENP)
      EXC=(EXP/TPD(I+K))*100.0
      VEL=VELO(I+K)
      RFAN=(RBP*DE)/(2.0*RHO*(VEL**2.0)*CLEN)
      EUEN=ENP/(RHO*(VEL**2.0))
      EUEX=EXP/(RHO*(VEL**2.0))
      REY=RE(I+K)



      GO TO 250
220   J=J+1
      ENC=(ENP/TPD(I+J))*100.0
      RBC=(RBP/TPD(I+J))*100.0
      EXP=TPD(I+J)-(RBP+ENP)
      EXC=(EXP/TPD(I+J))*100.0
      VEL=VELO(I+J)
      RFAN=(RBP*DE)/(2.0*RHO*(VEL**2.0)*CLEN)
      EUEN=ENP/(RHO*(VEL**2.0))
      EUEX=EXP/(RHO*(VEL**2.0))
      REY=RE(I+J)
      GO TO 250
230   N=N+1
      ENC=(ENP/TPD(I+N))*100.0
      RBC=(RBP/TPD(I+N))*100.0
      EXP=TPD(I+N)-(RBP+ENP)
      EXC=(EXP/TPD(I+N))*100.0
```

```
      VEL=VELO(I+N)
      REAN=(RBP*DE)/(2.0*RHO*(VEL**2.0)*CLEN)
      EUEN=ENP/(RHO*(VEL**2.0))
      EUEX=EXP/(RHO*(VEL**2.0))
      REY=RE(I+N)
      GO TO 250
240   ENC=(ENP/TPD(I+50))*100.0
      RBC=(RBP/TPD(I+50))*100.0
      EXP=TPD(I+50)-(RBP+ENP)
      EXC=(EXP/TPD(I+50))*100.0
      VEL=VELO(I+50)
      REAN=(RBP*DE)/(2.0*RHO*(VEL**2.0)*CLEN)
      EUEN=ENP/(RHO*(VEL**2.0))
      EUEX=EXP/(RHO*(VEL**2.0))
      REY=RE(I+50)
250   WRITE (2,140) ENP,ENC,EXP,EXC,RBP,RBC,REY,REAN,EUEN,EUEX
200   CONTINUE
      WRITE (2,260)
260   FORMAT (1H1,27X,'AQUEOUS GLYCEROL 65.45% BY WEIGHT'//)
      WRITE (2,20)
      RHO=1166.67
      VIS=16.08E-3
      DO 270 I=114,139
      VELO(I)=MFLOW(I)/(AREA*RHO)
      RE(I)=(RHO*DE*VELO(I))/VIS
      IF ((I.GT.113.AND.I.LT.121).OR.I.GT.132) GO TO 280
      IF (I.GT.120.AND.I.LT.133)GO TO 290
290   IF (MOD(I,2).EQ.0) GO TO 300
280   TPD(I)=TODP(I)*3.745*9.81
      GO TO 320
300   TPD(I)=TODP(I)*9.80768
320   EU=TPD(I)/(RHO*(VELO(I)**2.0))
      FANN=(TPD(I)*DE)/(2.0*RHO*(VELO(I)**2.0)*CLEN)
      WRITE (2,90) VELO(I),RE(I),TPD(I),EU,FANN
270   CONTINUE
      WRITE (2,100)
      K=50
      DO 310 I=64,83
      ENP=ENDP(I)*9.80768
      RBP=RBDP(I)*3.745*9.81
      IF (I.GT.71.AND.I.LT.78) GO TO 330
      IF (I.GT.77) GO TO 340
      ENC=(ENP/TPD(I+50))*100.0
      RBC=(RBP/TPD(I+50))*100.0
      EXP=TPD(I+50)-(RBP+ENP)
      EXC=(EXP/TPD(I+50))*100.0



      VEL=VELO(I+50)
      REAN=(RBP*DE)/(2.0*RHO*(VEL**2.0)*CLEN)
      EUEN=ENP/(RHO*(VEL**2.0))
      EUEX=EXP/(RHO*(VEL**2.0))
      REY=RE(I+50)
      GO TO 350
330   K=K+1
      ENC=(ENP/TPD(I+K))*100.0
      RBC=(RBP/TPD(I+K))*100.0
      EXP=TPD(I+K)-(RBP+ENP)
      EXC=(EXP/TPD(I+K))*100.0
      VEL=VELO(I+K)
      REAN=(RBP*DE)/(2.0*RHO*(VEL**2.0)*CLEN)
      EUEN=ENP/(RHO*(VEL**2.0))
```

```
0222            EUEX=EXP/(RHO*(VEL**2.0))
0223            REY=RE(I+K)
0224            GO TO 350
0225        340 ENC=(ENP/TPD(I+56))*100.0
0226            RBC=(RBP/TPD(I+56))*100.0
0227            EXP=TPD(I+56)-(RBP+ENP)
0228            EXC=(EXP/TPD(I+56))*100.0
0229            VEL=VELO(I+56)
0230            RFAN=(RBP*DE)/(2.0*RHO*(VEL**2.0)*CLEN)
0231            EUEN=ENP/(RHO*(VEL**2.0))
0232            EUEX=EXP/(RHO*(VEL**2.0))
0233            REY=RE(I+56)
0234        350 WRITE (2,140) ENP,ENC,EXP,EXC,RBP,RBC,REY,RFAN,EUEN,EUEX
0235        310 CONTINUE
0236            WRITE (2,260)
0237            WRITE (2,160)
0238            DO 360 I=140,172
0239            VELO(I)=MFLOW(I)/(AREA*RHO)
0240            RE(I)=(RHO*DE*VELO(I))/VIS
0241            IF((I.GT.139.AND.I.LT.154.AND..NOT.I.EQ.150).OR.I.GT.167) GO TO 5
0242            IF (I.EQ.150) GO TO 6
0243            IF (I.GT.153.AND.I.LT.168) GO TO 7
0244          7 IF (TODP(I,2).EQ.0) GO TO 5
0245          6 TPD(I)=TODP(I)*9.80768
0246            GO TO 370
0247          5 TPD(I)=TODP(I)*3.745*9.81
0248        370 EU=TPD(I)/(RHO*(VELO(I)**2.0))
0249            FANN=(TPD(I)*DE)/(2.0*RHO*(VELO(I)**2.0)*CLEN)
0250            WRITE (2,90) VELO(I),RE(I),TPD(I),EU,FANN
0251        360 CONTINUE
0252            WRITE (2,100)
0253            K=53
0254            DO 380 I=84,106
0255            ENP=ENDP(I)*9.80768
0256            RBP=RSDP(I)*3.745*9.81
0257            IF (I.EQ.94) GO TO 15
0258            IF (I.GT.94.AND.I.LT.102) GO TO 16
```

```
      IF (I.GT.101) GO TO 17
      ENC=(ENP/TPD(I+56))*100.0
      RBC=(RBP/TPD(I+56))*100.0
      EXP=TPD(I+56)-(RBP+ENP)
      EXC=(EXP/TPD(I+56))*100.0
      VEL=VELO(I+56)
      RFAN=(RBP*DE)/(2.0*RHO*(VEL**2.0)*CLEN)
      EUEN=ENP/(RHO*(VEL**2.0))
      EUEX=EXP/(RHO*(VEL**2.0))
      REY=RE(I+56)
      GO TO 390
   15 ENC=(ENP/TPD(I+57))*100.0


      RBC=(RBP/TPD(I+57))*100.0
      EXP=TPD(I+57)-(RBP+ENP)
      EXC=(EXP/TPD(I+57))*100.0
      VEL=VELO(I+57)
      RFAN=(RBP*DE)/(2.0*RHO*(VEL**2.0)*CLEN)
      EUEN=ENP/(RHO*(VEL**2.0))
      EUEX=EXP/(RHO*(VEL**2.0))
      REY=RE(I+57)
      GO TO 390
   16 K=K+1
      ENC=(ENP/TPD(I+K))*100.0
      RBC=(RBP/TPD(I+K))*100.0
      EXP=TPD(I+K)-(RBP+ENP)
      EXC=(EXP/TPD(I+K))*100.0
      VEL=VELO(I+K)
      RFAN=(RBP*DE)/(2.0*RHO*(VEL**2.0)*CLEN)
      EUEN=ENP/(RHO*(VEL**2.0))
      EUEX=EXP/(RHO*(VEL**2.0))
      REY=RE(I+K)
      GO TO 390
   17 ENC=(ENP/TPD(I+66))*100.0
      RBC=(RBP/TPD(I+66))*100.0
      EXP=TPD(I+56)-(RBP+ENP)
      EXC=(EXP/TPD(I+66))*100.0
      VEL=VELO(I+66)
      RFAN=(RBP*DE)/(2.0*RHO*(VEL**2.0)*CLEN)
      EUEN=ENP/(RHO*(VEL**2.0))
      EUEX=EXP/(RHO*(VEL**2.0))
      REY=RE(I+66)
  390 WRITE (2,140) ENP,ENC,EXP,EXC,RFP,RBC,REY,RFAN,EUEN,EUEX
  380 CONTINUE
      STOP
      END

LENGTH  2313, NAME  GLYCP2          - COMMENTS

      FINISH

ION -  NO ERRORS   1 COMMENT

        41 BUCKETS USED
```

DOWNWARD FLUID MOVEMENT :

VELOCITY MPERS	REYNOLDS NUMBER	PRESSURE DROP NEWTONPERM2	EULER NO.	FRICTION FACTOR
0.23691	246.1	0.9832E 04	158.9	0.650
0.23691	246.1	0.9832E 04	158.9	0.650
0.22631	235.1	0.8974E 04	158.9	0.650
0.22631	235.1	0.8913E 04	157.8	0.645
0.21629	224.7	0.8177E 04	158.5	0.648
0.21287	221.2	0.8055E 04	161.2	0.659
0.20000	207.8	0.7197E 04	163.2	0.667
0.20000	207.8	0.7197E 04	163.2	0.667
0.18695	194.2	0.6461E 04	167.7	0.686
0.18695	194.2	0.6400E 04	166.1	0.679
0.17551	182.3	0.5725E 04	168.6	0.689
0.17551	182.3	0.5725E 04	168.6	0.689
0.16168	168.0	0.4990E 04	173.1	0.708
0.16226	168.6	0.4990E 04	171.9	0.703
0.14827	154.0	0.4254E 04	175.5	0.718
0.14827	154.0	0.4254E 04	175.5	0.718
0.13479	140.0	0.3641E 04	181.8	0.743

ENTRANCE DELTAP NEWTONPERM2	PERCENT OF TOTAL	EXIT DELTAP NEWTONPERM2	PERCENT OF TOTAL	RIBS DELTAP NEWTONPERM2	PERCENT OF TOTAL	REYNOLDS NUMBER	RIBS FRICTION	
0.1218E 04	12.268	0.1444E 04	14.545	0.7295E 04	73.457	246.1	0.482	100.270
0.1201E 04	12.166	0.1398E 04	14.161	0.7172E 04	72.671	246.1	0.474	98.998
0.1109E 04	12.225	0.1325E 04	14.610	0.6620E 04	72.973	235.1	0.479	99.808
0.1002E 04	12.197	0.1197E 04	14.570	0.6007E 04	73.154	221.2	0.492	99.902
0.9063E 03	12.283	0.1138E 04	14.176	0.5946E 04	74.046	221.2	0.487	100.504
0.8659E 03	12.268	0.1064E 04	14.714	0.5333E 04	73.729	207.8	0.494	100.731
0.8772E 03	12.250	0.1006E 04	14.024	0.5210E 04	72.650	207.8	0.483	98.904
0.8070E 03	12.419	0.9629E 03	14.819	0.4843E 04	74.528	194.2	0.514	101.767
0.7675E 03	12.235	0.8986E 03	13.961	0.4720E 04	73.333	194.2	0.501	99.529
0.7134E 03	12.381	0.8596E 03	14.918	0.4230E 04	73.404	182.5	0.509	100.704
0.6939E 03	12.043	0.7933E 03	13.768	0.4205E 04	72.979	182.3	0.506	98.790
0.6477E 03	12.467	0.7563E 03	15.046	0.3759E 04	74.390	168.6	0.527	101.925
0.6121E 03	12.177	0.6900E 03	13.728	0.3617E 04	71.951	168.6	0.509	97.855
0.5731E 03	13.355	0.6394E 03	14.900	0.3126E 04	72.857	154.0	0.527	101.112
0.5127E 03	11.947	0.5750E 03	13.401	0.3126E 04	72.857	154.0	0.527	98.205
0.4522E 03	12.295	0.5419E 03	14.733	0.2758E 04	75.000	140.0	0.563	102.029

REFERENCES

(1) Ahlstrom,S., and Rylander,L. "The Central Cooling Concept", Chemical Processing, December 1971.

(2) The Alfa-Laval Co. "Thermal Handbook", Alfa-Laval AB, Lund, Sweden, 1969.

(3) The Alfa-Laval Co. "Heat Exchanger Guide",Alfa-Laval AB, Lund, Sweden, December 1969.

(4) The Alfa-Laval Co. "Alfa-Flex - the story of a new generation of heat exchangers", Publication No. PC 60515 E, Alfa-Laval AB, Lund, Sweden, 1972.

(5) The APV Co. "PARAFLOW SEMINAR : principles of plate heat transfer".

(6) Belcher,A.J. "Accommodation of Varying θ Values (Number of Theoretical Heat Transfer Units) Within a Given Plate Heat Exchanger". Paper presented at the Conference on Recent Developments in High Duty Heat Exchangers, Inst.of Mechanical Eng., London, 12th October 1972.

(7) Beloborodov,V.G. and Volgin,B.P. "A Study of Convectional Heat Exchange and Resistances in Narrow Channels of Sinuous and Variable Cross-Section", Industry of Fertilisers and Sulphuric Acid - Technical and Economical Information, NIUIF - Moscow, 1967.

(8) Beloborodov,V.G. and Volgin,B.P. "Heat Transfer and Pressure Drop in Heat Transfer Equipment and Slot Channels of Varying Cross-Section", International Chemical Engineering, Vol.11, No.2, April 1971.

(9) Benedini, M. "Readings of Small Pressure Differences in Liquids", Journal of Scientific Instruments, Vol.44, 1967.

(10) Bird,R.B., Stewart,W.E., and Lightfoot,E.N. "Transport Phenomena", John Wiley & Sons,Inc., 1960. P.204.

(11) British Standards 2621-5.

(12) Buonopane,R.A. and Troupe,R.A. "A Study of the Effects of Internal Rib and Channel Geometry in Rectangular Channels", AIChE Journal, Vol.15, No.4, July 1969.

(13) Cattell,G.S. "Heat Transfer in Plate Heat Exchangers with Laminar Flow". Paper presented at the International Symposium on Heat and Mass Transfer Problems in Food Engineering, Wageningen, the Netherlands, 24-27 October 1972.

(14) Cattell,G.S. "The Thermal Aspect of Plate Heat Exchanger Design for Turbulent Flow". Paper presented at the Conference on Heat Transfer and the Design and Operation of Heat Exchangers, Witwatersrand University, Johannesburg, South Africa, 17-19 April 1974.

(15) Clark,D.F. "Plate Heat Exchanger Design and Recent Development", The Chemical Engineer, May 1974.

(16) Cooper,A. "The Condensation of Steam in Plate Heat Exchangers". Paper presented at the 14th National Heat Transfer Conference, AIChE-A.S.M.E, Atlanta, Georgia, USA, 5-8 August 1973.

(17) Cooper,A. "Recover More Heat with Plate Heat Exchangers", The Chemical Engineer, May 1974.

(18) Dahlgren,A.I. and Jenssen,S.K. "Comparison of Heat Exchange Surfaces", Chemical and Process Engineering: Heat Transfer Survey, August 1970.

(19) Eckman,D.P. "Industrial Instrumentation", John Wiley & Sons, 1950.

(20) Edwards,M.F., Changal Vaie,A.A,, and Parrott,D.L. "Heat Transfer and Pressure Drop of a Plate Heat Exchanger Using Newtonian and Non-Newtonian Liquids", The Chemical Engineer, May 1974.

(21) Ellison,F.J. "Pressure Drop Characteristics of an APV Junior Paraflow Plate Heat Exchanger",B.Sc.Project, Aston University, January 1972.

(22) Emerson,W.H. "The Thermal and Hydrodynamic Performance of a Plate Heat Exchanger: IV A Rosenblad Exchanger", National Engineering Laboratory Report No.286, Ministry of Technology, April 1967.

(23) Ergun,S. "Fluid Flow Through Packed Columns", Chemical Engineering Progress, Vol.48, No.2,February 1952.

(24) Flack,P.H. "The Feasibility of Plate Heat Exchangers", Chemical and Process Engineering, August 1964.

(25) Jones,W.H. and Usher,J.D. "Plate Heat Exchangers in Chemical Engineering: A Comparative Study". Paper presented to the 4th Congress of the European Federation of Chemical Engineers, London, June 1966.

(26) Kays,W.M. and London,A.L. "Compact Heat Exchangers", McGraw Hill, 1964.

(27) Kovalenko,L.M. "Plate-Type Heat Exchangers", Plastinchatyye Teploobmenniki Khimicheskoye Mashinostroyenie, Vol.2, 1961.

(28) Marriott,J. "Where and How to Use Plate Heat Exchangers", Chemical Engineering, 5th April 1971.

(29) Okada,K., Ono,M.,Tomimura,T.,Okuma,T., Konno,H., and Ohtani,S. "Design and Heat Transfer Characteristics of New Plate Heat Exchangers", Heat Transfer - Japanese Research, Vol.1, No.1, January-March 1972.

(30) Parrott,D.L. "Heat Transfer in Plate Heat Exchangers at Low Reynolds Number". Paper presented at the 14th National Heat Transfer Conference, AIChE-A.S.M.E., Atlanta, Georgia, U.S.A., 5-8 August 1973.

(31) Preston,J.H. "The Measurement of Pressure in Low Velocity Water Flows", Journal of Physics E: Scientific Instruments,Vol.5, 1972.

(32) Rouse,H. and Howe,J.W. "Basic Fluid Mechanics", John Wiley & Sons, New York, 1953.

(33) Savostin,A.F. and Tikhonov,A.M. "Investigation of the Characteristics of Plate-Type Heating Surfaces", Teploenergetika, 17, (9), 1970.

(34) Shaoul,E.E. "Characteristics of an APV Junior Paraflow Plate Heat Exchanger", M.Sc.Dissertation, Aston University, September 1971.

(35) Usher,J.D. "The Plate Heat Exchanger". Paper presented to the Meeting on Compact Heat Exchangers, the National Engineering Laboratory, Glasgow, 22nd October 1969.

(36) Usher,J.D. "Current Trends in Plate Heat Exchanger Design". Paper presented at the Conference on Recent Developments in Compact High Duty Heat Exchangers, the Institute of Mechanical Engineers, London, 12th October 1972.

(37) Watson,E.L.,Mckillop,A.A.,Dunkley,W.L., and Perry,R.L. "Plate Heat Exchangers - Flow Characteristics", Industrial and Engineering Chemistry, Volume 52, No.9, September 1960.

(38) Weihs,D. and Sumer,M. "Measurement of Extremely Small Pressure Differences in Water", Journal of Physics E: Scientific Instruments, Volume 6, 1973.

(39) Wilkinson,W.L. "Flow Distribution in Plate Heat Exchangers", The Chemical Engineer, May 1974.